Investigating groundwater derived nutrient fluxes within Tauranga harbour, New Zealand

A thesis

submitted in fulfilment

of the requirements for the degree

of

Doctor of Philosophy in Earth Science

at

The University of Waikato

by

BENJAMIN THOMAS STEWART

THE UNIVERSITY OF
WAIKATO
Te Whare Wānanga o Waikato

2021

ABSTRACT

Submarine groundwater discharge (SGD) is one of the key pathways that connects land and ocean, delivering freshwater, nutrients, carbon, metals, and other chemical constituents to coastal waters. In New Zealand, local Māori have had a strong cultural connection to this natural process for centuries. Recently, it has been recognised that this process is important in global hydrological and biogeochemical cycles. Due to the large coastline to land area ratio, steep topography, permeable sediments and high rainfall, oceanic islands, may have the potential for disproportionally large SGD fluxes into the ocean compared to river inputs. Since SGD is driven under different timescales and processes (saline porewater through sediments and fresh groundwater from aquifers), it can provide a continual source of nutrients to coastal water bodies. This has previously received very little attention in New Zealand despite its potential importance, mainly due to the difficulty in measuring this diffuse process.

Regional system scale studies among oceanic islands are poorly quantified and understood, especially in the South Pacific region. Population increases have placed added stresses on hydrological cycles and subsequent land use changes, particularly agriculture, have resulted in excess nutrient loading and nitrogen pollution in coastal systems. Radium isotopes were used to quantify SGD and related nutrient fluxes into Tauranga Harbour, a coastal lagoon system, on the largely volcanic North Island of New Zealand. A ^{226}Ra mass balance quantified SGD fluxes at the harbour scale, resulting in a range of SGD flux rates between 0.53 cm d^{-1} and 3.09 x10^{6} m^{3} d^{-1}. When compared to other freshwater discharges (rivers and streams) into the harbour this was between ~1 – 2.8 times greater in flow. SGD inputs were also calculated to be ~5 times (for nitrogen) and ~8 times (for phosphorus) greater than the input from surrounding rivers and streams. Over the past decades the harbour has suffered reduced water quality and has inter-annual macro-algal blooms of Ulva spp. (sea lettuce). Harbour waters had a N:P ratio of ~17:1 with a positive relationship between radium isotopes (assumed groundwater related) and N:P ratios. This demonstrated that SGD has major implications for primary production, including recurrent algal bloom events which commonly occur in the harbour.

While higher loads of inorganic and organic nitrogen from surrounding water catchments are important for water quality, the physical processes that control estuarine flushing, such as tides, wind, rainfall, and freshwater discharge are equally as important. To better understand

how future changes in climate over the coming century will impact coastal systems a numerical model was developed and combined with machine learning techniques to 'emulate' dilution rates based on time series of historical hydro-metrological data. A 22-year hind cast revealed the spatial variability of flushing times over short term 'event' and long range inter annual timescales. A significant relationship (r^2 0.43 p =<0.001) between flushing rates and the southern oscillation index (SOI) was also established, highlighting direct and indirect implications of climate on water quality by altering flushing rates, nutrient availability, storage and transport across different regions. Using these data driven tools will be important into the future for monitoring water movement and 'estuarine forecasting'.

Finally, I present a study that assessed the effects of spring-neap tidal variations on estuarine connectivity over multiple spatial scales. Being a tidally dominated system, variations in tidal amplitudes can alter the movement of water and associated chemical exchanges between the harbours sub estuaries and coastal shelf. A combination of numerical modelling and artificial tracer experiments were used together with field-based measurements of naturally occurring radioactive tracers (radium). The modelled flushing times across all harbour regions (~4 – 20 days) agreed well with calculated apparent Ra ages. The average apparent radium water ages were revealed to be younger on spring tide at the harbour scale, suggesting tidal pumping of radium rich water from sub regions. Waters at the harbour scale were also well mixed from other sub regions. Nutrients and other chemical constituents varied substantially with the tide and were up to 4 times greater at the sub estuary scale on ebb tides. This demonstrated the important role of spring-neap tidal cycles in water transport, mixing and biogeochemical behaviour within sensitive coastal lagoon systems.

ACKNOWLEDGEMENTS

I would like to give a huge thankyou to my chief supervisor Karin Bryan for giving me the opportunity to undertake my PhD under her supervision. Your enthusiasm and love for science is truly infectious and I am grateful for having such a motivated, supportive, and helpful mentor. Thank you for your patience throughout the process and inspiring me to achieve my best. I would also like to thank Conrad Pilditch for his encouragement and ability to bring things in perspective.

To Isaac Santos, thank you for all your inspiration and support over the years and encouraging me to take my own path. You provided me with a solid base in which to grow and develop. To everyone back home at SCU, thank you for all your support over the years and great catch ups when I come back home. A big thankyou to Christian Winter for hosting me in Bremen, Germany and for your help and guidance in learning new modelling skills (numerical). To everyone part of the INTERCOAST program and friends in Germany, thank you for the fun times and great memories over the years.

I would like to thank Caine Taiapa and Hayden Murray for providing access to traditional Māori land on Matakana Island during sampling and their guidance in communicating with the Whanau. A huge thankyou to Chris Battershill for your encouragement, support, and opportunities you have provided over the years. I really appreciate you giving me the space and resources to undertake my research in Tauranga Harbour. A big shout out to everyone I worked with at the field station, looking forward to seeing you guys at the new building in the future! To Dirk Immenga, David Culliford and Dudley Bell, thank you for being exceptional skippers and technicians during my field campaigns over the years. It is a pleasure to work with you guys. Thank you to all the university administration and technical staff who have also assisted me, UoW for the “Terry Healy scholarship award”, the MBIE for INTERCOAST funding and the BoPRC for project funding.

I would like to acknowledge and give a special thank you to Jonno Rau, Dr Alex Port and all my friends I have met here in New Zealand (everyone in Raglan, Tauranga and the Tron). I am grateful for your friendships, awesome times together and understanding over the past years while I completed this PhD and I am looking forward to spending more time with everyone.

A special thankyou to Mariana for your love, kindness, and support over the years. I am very lucky to have had you by my side during this process. Your strength, determination, and attitude of never giving up has inspired me. Thank you for your help, awesome music, laughs and força! to help get me across the finish line. To Ze, Cleide, and Nat thank you for your warm welcome and time spent together while in Brazil.

Finally, to my family and friends in Australia and Germany. Thank you for all your support, unconditional love, and encouragement during this journey. You have always been there when I need the most and I love you all so much. Thankyou Martin and Mariana Kues, Jan and Sofie Bahrs, Renate Schnock, and all my family in Witzhelden. Thanks Mum and Dad, for all your love, encouragement and always believing in me. To the support from my big brothers Andrew and Mark for making me tough and always being there for me and my big sister Mish, for sparking my curiosity and interest in science. Looking forward to seeing you all again soon and celebrate!

TABLE OF CONTENTS

LIST OF FIGURES

LIST OF TABLES

CHAPTER 1 GENERAL INTRODUCTION

1.1 Background

Coastal oceans of the world are known to have high biogeochemical activity relative to their surface area. These include coastal systems such as estuaries, mangrove waters, salt marsh waters and marginal seas. These highly productive and dynamic environments receive large inputs of nutrients from the land and exchange large amounts of matter and energy with the open ocean (Borges, 2004). These ecosystems are influenced by seasonal variability in hydrology as well as short-term episodic events such as droughts, storms, and floods (Pearl *et al.* 2006).

Hydrologic forces such as surface water discharges (rivers and streams), groundwater and atmospheric deposition are important sources of nutrient inputs into estuaries that vary temporally and spatially (Lampman et al., 1999). The concentration of nutrients delivered with surface waters and ground water throughout the world is increasing substantially with time (Conley, 2000). Accelerating human population growth is altering the major biogeochemical cycles of the world, with land use changes occurring in sensitive catchment areas, including increased agricultural practices and coastal development (van der Strijk and Kroeze, 2010). This is resulting in a significant increase in bioactive nutrients such as nitrogen (N) and phosphorus (P) with consequential reduction of water quality (Pereira Coutinho *et al.* 2012, Seitzinger et al., 2005; Vitousek et al., 1997).

Coastal eutrophication events, which is an excess in the supply of organic matter, are well documented globally and can threaten natural systems with harmful algal blooms, loss of biodiversity and anoxic or hypoxic waters (Nixon, 1995; Michel et al. 2000). Algal growth is the primary biological response to nutrient enrichment in aquatic environments (Devlin *et al.* 2011). It is the dissolved inorganic forms of nitrogen (DIN), namely nitrate + nitrite (NO_x) and ammonium (NH_4^+), and the dissolved inorganic phosphorus (DIP) species, phosphorus (PO_4^{-3}), that are most readily available for assimilation by algae. The increased algal production associated with eutrophication generally takes the form of phytoplankton blooms or macro algae blooms, depending on the environment and climatic region (Davis & Koop 2006). This also affects the cycling of carbon (C), N and P as well as water quality parameters such as dissolved oxygen (DO) and pH (Pearl *et al.* 2006). Nutrient point sources such as surface water

inputs into estuaries from major rivers and creeks have been the main focus of investigations, with relatively precise estimates of discharge rates and nutrient loading, however large anomalies in nutrient over-enrichment exist.

While not visible or as obvious as surface water inputs such as rivers and creeks, Submarine groundwater discharge (SGD), which includes both recirculated saline and fresh terrestrial groundwater (Figure 1.1), discharges directly into the coastal ocean in processes occurring over differing time and spatial scales (Burnett & Dulaiova, 2003). These diffuse processes could explain widespread chemical anomalies (Santos et al., 2012). The drivers of seawater recirculation (or porewater advection) in permeable sediments can include wave action, tides, currents and bio-irrigation, while deeper freshwater flows are often driven by hydraulic gradients, convection and tidal pumping. Mixing between fresh meteoric water and sea water produces brackish saline water in many coastal aquifers. The mixing zone or 'subterranean estuary' (STE) is the area where ground water derived from land mixes with sea water that has entered the aquifer through a free connection to the sea (Moore, 1999). These STEs are characterized by intense biogeochemical reactions that influence the transfer of nutrients, carbon, metals and other dissolved species to the coastal zone in a manner similar to that of surface estuaries (Charette et al., 2006).

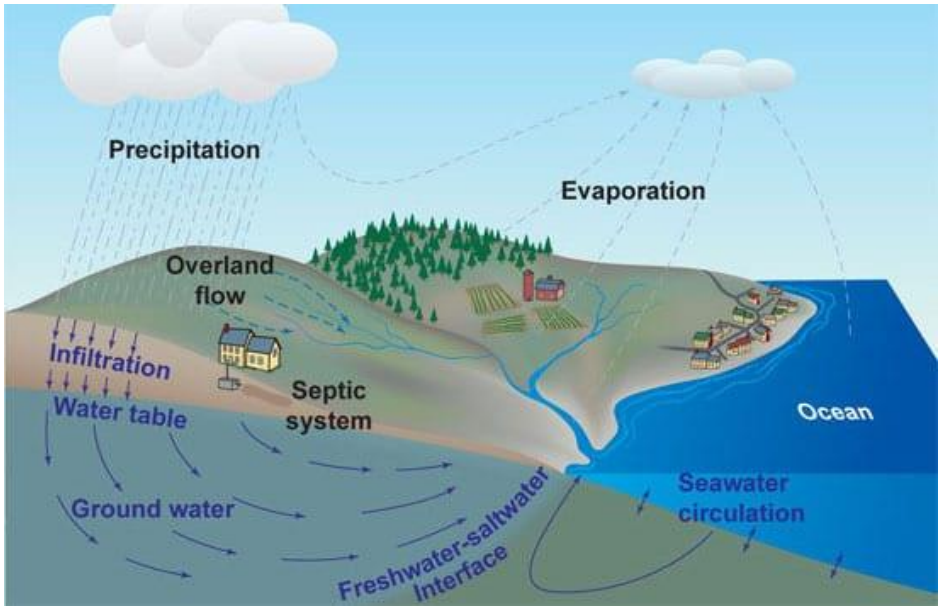

Figure 1.1 Conceptual diagram of submarine groundwater discharge (SGD) between the land and ocean. (WHOI, Mulligan and Charette, 2005, adapted from Heath, 1998).

Groundwater flows directly into the ocean wherever an aquifer is connected to the sea. However, coastal aquifers are almost always arranged in a complex matrix of confined, semi-confined and unconfined systems. Further to this is the variable nature of coastal sediments, dispersion of springs and tidal pumping which many simple hydrologic models do not take into consideration (Swarzenski, 2007; Charette et al., 2006). While this exchange of groundwater between the land and sea is now being considered as a major part of the hydrological cycle, its importance in the biogeochemical flux of materials into coastal waters has only in recent times received serious attention as new and more refined techniques are being investigated (Slomp & Cappellen, 2004; Moore, 2010).

Using modern radionuclide techniques has allowed groundwater discharges to be studied over large spatial and temporal scales (Charrete et al., 2006, Swarsenski, 2007). The application of naturally occurring geochemical isotope tracers can enable integrated estimations that have not been possible by non-nuclear methods (Moore, 1999; Charette et al., 2006). Radium (Ra) and its quartet of isotopes (^{223}Ra, ^{224}Ra, ^{226}Ra, & ^{228}Ra) have so far proven to be powerful tools in quantifying the fluxes of submarine groundwater discharge into the sea (Moore, 1996; Moore, et al., 2006; Garcia-Orellana, 2010). Radium lies in the decay series of its parent chemical elements 238 & 235-uranium (U) and 232-thorium (Th). Both elements U and Th are ubiquitous and occur naturally across many geologic formations. Water-rock ion exchange processes in brackish to saline waters release dissolved Ra into solution via desorption. Once mixed in coastal ocean waters Ra behaves conservatively where it decays naturally at different rates dependent on its isotope; the decay rate of the four Ra isotopes are: ^{224}Ra (half-life=3.7 days), ^{223}Ra (half-life=11.4 days), ^{228}Ra (half-life = 5.75 years), ^{226}Ra (half-life = 1600 years) (Moore, 2011; Charette et al., 2006; Dulaiova et al., 2006; Peterson et al., 2008; Beck and Lueck, 2014). These differing radioactive decay constants can be used to establish and trace SGD processes occurring over a broad range of spatial and temporal scales (Swarsenski, 2007). One of the desirable characteristics of using an isotopic tracer for SGD is that it has a unique fingerprint or dominant source in groundwater. Contributions via other pathways (e.g., river water) are generally small and/or easily quantifiable (Charette et al., 2006). Using these natural tracers to establish SGD sources and fluxes requires the knowledge of the terrestrial groundwater end-member radium

concentration as well as water residence times in the system being investigated (Moore et al., 2006).

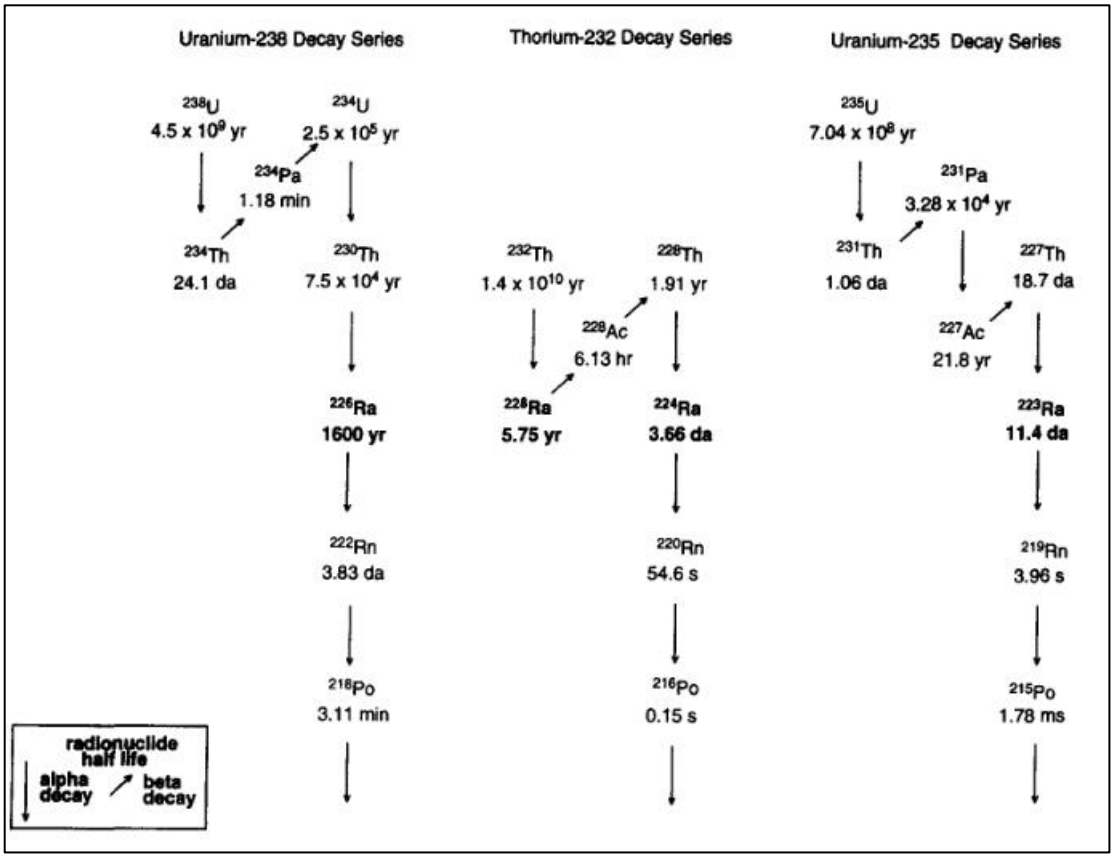

Figure 1.2 Illustration of radium isotopes in the uranium and thorium decay series, including their relative half-lives and the transformation of the different radionuclides in each series (Moore, 1996).

Residence times (the time it takes for a water parcel to leave a system through an outlet) are important in providing a timescale for water mixing processes as well as the accumulation and transport of materials within coastal systems (Monsen et al., 2002). Flushing time (a bulk or integrative parameter that describes the general exchange characteristics) and water ages (the time a water parcel has spent since entering an estuary through one of its boundaries) also explain important measures of water movement (Monsen et al., 2002; Sheldon and Alber, 2002). Circulation models that are based on monitoring of river discharge, tides, weather conditions, and salinity distribution have traditionally been used to evaluate the residence time of water within estuaries (Dulaiova and Burnett 2008). However, "Radium water ages" can also be applied and reflect the time elapsed since water samples have become enriched in Ra and isolated from its source, which is assumed to be groundwater discharge (Moore et

al., 2000a). Using Ra derived water ages is useful in assessing the relationships between different water circulation processes and ecological effects, such as primary productivity (Tomasky-Holmes et al., 2013). The use of radium models has been applied in various coastal settings worldwide (Garcia-Orellana et al., 2021). The main limitation in their application has historically been in being able to constrain the highly variable groundwater endmember concentrations. The underlying source assumptions used in the application of radium isotopes in coastal settings are well presented in the reviews by Charette et al., 2008 and Garcia-Orellana et al., 2021.

Climate drivers have a unique control on all measures of water movement by controlling important hydrological forces and wind patterns, which ultimately effect biogeochemical cycles and ecological functioning. Predicted changes in climate and associated shifts in temperature, wind and rainfall patterns are expected to modify the functioning of coastal systems over the next century (Schindler 2006). The El Niño -Southern Oscillation (ENSO), which is the largest global-scale climate oscillation, effects vast regions across the world, including New Zealand. These interannual swings between Pacific Ocean surface water warming (El Niño) and cooling (La Niña) develop over seasonal cycles (Timmermann et al., 2018), and can significantly disturb regional hydrology and impact water quality through the increased probability of extreme events (storms, floods and droughts).Understanding these interactions will allow management plans to better target the cause of water quality issues, including the occurrence of problematic algae blooms, especially with respect to predicted changes associated with future climate scenarios.

1.2 Thesis Questions and Aims

To address some key knowledge gaps in the drivers of nutrient exchange and macroalgal blooms, this thesis has the overarching aim of investigating the connection between submarine groundwater discharge (SGD) and surface water circulation. This will be accomplished by addressing the following research questions:

1. What are the likely fluxes of nutrients from pore-water/groundwater exchange?
2. Where are the likely hot spots of non-point (non-river input) nutrient fluxes in the harbour?

3. How do climatic variations such as El Niño southern oscillation (ENSO) influence harbour flushing times?
4. What effect do spring-neap tidal ranges have on the exchange and transport of nutrients?

This thesis will add to the literature by applying a unique combination of techniques such as natural geochemical tracers (^{223}Ra,^{224}Ra,^{226}Ra) and hydrodynamic modelling (Delft 3D) to better understand the complex interactions between groundwater and surface water exchange in estuaries. Artificial neural networks (ANN) have also been applied to help bridge the gap in scales between coastal processes and climate signals. I hypothesise that large amounts of nutrients are delivered and/or recycled through submarine groundwater discharge (fresh and re-circulated pore-water), which when combined with climatic driven changes to surface water hydrology and hydrodynamics can lead to the development of algal bloom events. To investigate the above aims and questions, field surveys ('snapshot' and time series) were conducted within Tauranga Harbour, New Zealand, alongside laboratory analysis and computer based numerical modelling.

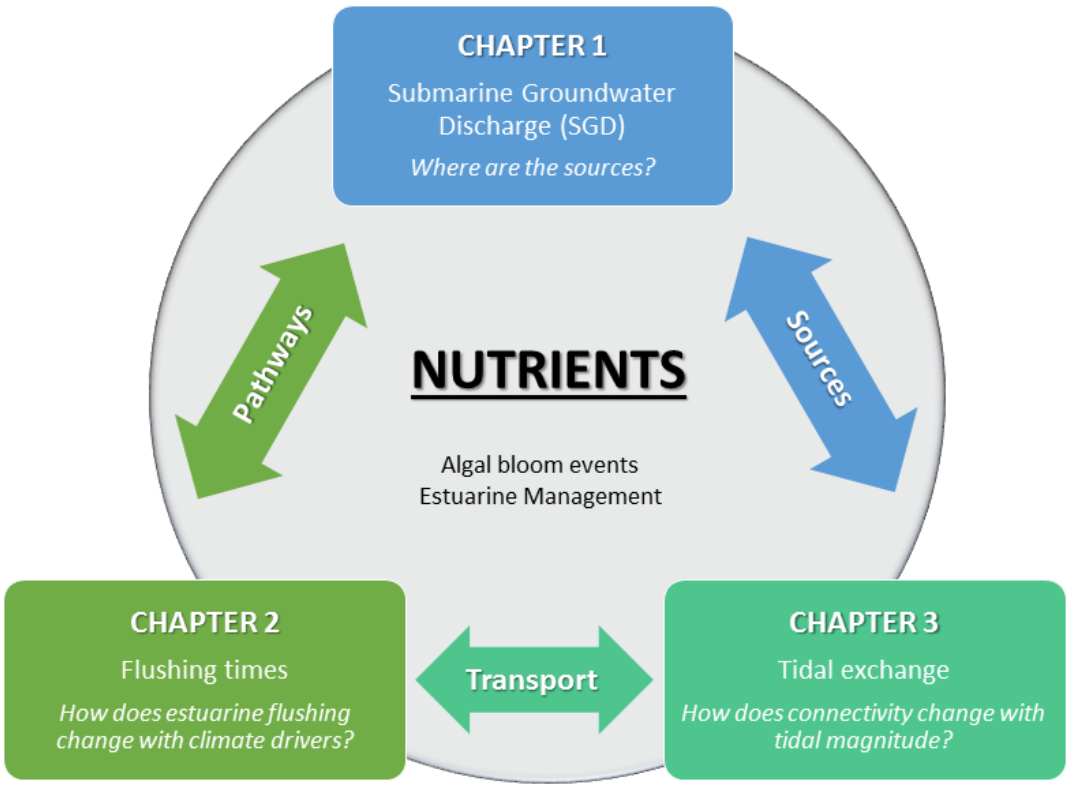

Figure 1.3 Conceptual diagram demonstrating the connection between chapters.

1.3 Thesis Structure

The main research questions of this thesis are broken down into three scientific journal articles which are presented in Chapters 2, 3 and 4 respectively. These chapters can be read separately, each with their own abstract, introduction, methods, results, discussion, and conclusions. However, the common theme of nutrient exchange and algal blooms relate each of the chapters together. Chapter 5 presents a summary of findings and general conclusions, including future recommendations. Finally, the Appendix briefly presents a summary and preliminary results of additional work conducted during my PhD in the Firth of Thames and Hauraki Gulf.

The first research article of this thesis **(Chapter 2)** is entitled *'Submarine groundwater discharge estimates using radium isotopes and related nutrient inputs into Tauranga Harbour, New Zealand'* (Stewart et al., 2018), and has been published in the journal 'Estuaries and Coasts' July 2017. This chapter aimed to address the following questions**: "where are the sources of groundwater and nutrients in Tauranga Harbour"** and **'Is groundwater significant compared to riverine sources?"**. The objectives of this paper were to 1) determine possible SGD hot spot areas and the apparent water age using radium isotopes as a natural geochemical tracer, 2) quantify the relative SGD fluxes and associated dissolved inorganic and organic nitrogen and phosphorus inputs and 3) to assess the significance of SGD inputs in comparison to surface water inputs. This was achieved through a comprehensive spatial survey of the harbour, including groundwater and river sampling across the catchment.

The second research article **(Chapter 3)** is entitled '*ENSO-driven variations in estuarine flushing revealed by Delft3D-Flow modelling and trained artificial neural networks'* (Stewart et al., (2021) in prep). This chapter addresses the questions **"how do estuarine flushing times change under different climate conditions?" and "do climate signals such as ENSO have a direct relationship to flushing times?"** The objectives of this paper were to (1) determine the variation of dilution rates and salinity over seasonal and event time scales, (2) predict inter annual dilution rates using a trained Artificial Neural Network (3) assess the inter annual relationships between dilution rates, climate signals and hydro-meteorological conditions. To achieve these objectives, I developed a 'domain decomposition' hydrodynamic model of Tauranga harbour and immediate offshore region using Delft 3D. Part of the model development was done during research visits at MARUM, University of Bremen, Germany

under the supervision of Prof. Dr. Christian Winter (as part of the INTERCOAST collaboration). Survey data used to validate the model was provided by former PhD student Dr. Alex Port, who was also part of the INTERCOAST group.

The third and final research article **(Chapter 4)** is entitled *'Spring-neap tide variations in estuary water ages and flushing times revealed by radium isotopes and Delft3D-Flow modelling'* (Stewart et al., (2021) in prep). This chapter aims to address the question of **"how does the connectivity and exchange between harbour regions change with tidal magnitude?"** The objectives were to 1) assess daily radium (^{223}Ra, ^{224}Ra and ^{226}Ra), salinity, nutrient, and carbon concentrations over a spring-neap period, 2) determine water mass ages using radium isotopes, and 3) quantify flushing times and the relative contributions of different water masses within the harbour using numerical modelling. This was achieved by conducting a time series field experiment over a two-week period (covering a spring-neap period), where daily water surface water samples were obtained over two different spatial scales within Tauranga Harbour, at the single constriction point of Waikareao sub-estuary and the harbour mouth. Groundwater and river water samples were also collected. Artificial tracer experiments were carried out using the Delf3D hydrodynamic model developed in the previous chapter.

In Chapter 5, I present a summary of the main findings and conclusions of this thesis and recommendations for future work.

For clarification, Table 1.1 defines the main used throughout this thesis.

Table 1.1 Terms and definitions.

Term	Definition
Flushing time	The time required to replace an initial mass of water contained in an estuary with both freshwater and oceanic inflows.
Dilution rate	The rate at which an initial concentration is diluted within an estuary.
Residence time	The average time a water parcel or introduced substance remains within a system or area of interest.
Radium ages	The time that radium of a given water sample was last in contact with its source (usually from groundwater or desorption from suspended river sediments).

CHAPTER 2

Submarine groundwater discharge estimates using radium isotopes and related nutrient inputs into Tauranga Harbour (New Zealand)

Benjamin T. Stewart [a], Karin R. Bryan [a], Conrad A. Pilditch [a], Isaac R. Santos [b] (published in *Estuaries and Coasts* (2018) 41:384–403. DOI 10.1007/s12237-017-0290-6)

[a] School of Science, University of Waikato, Private Bag 3105, Hamilton, New Zealand

[b] National Marine Science Centre, School of Environment, Science and Engineering, Southern Cross University, PO Box 4321, Coffs Harbour, 2450 NSW, Australia

Contribution of Authors:

Field work was planned, organised, and undertaken by BTS with the help of university technicians. Volunteers assisted with harbour and groundwater sampling. I carried out all laboratory preparation and analysis with assistance from university laboratory technicians. I analysed all data and wrote initial and subsequent drafts. My co-authors provided guidance and direction during the process and edited drafts, including editorial advice on the response to reviewers' comments.

2.1 Abstract

Land-based pollutants such as fertilizers and wastewater can infiltrate into aquifers and discharge into surrounding coastal water bodies as submarine groundwater discharge (SGD). Oceanic islands, with a large coastal length to land area ratio, may be hotspots of SGD into the global ocean. Although SGD may be a major pathway of dissolved nutrients, carbon and metals to coastal waters, studies have been limited due to the difficulties in measuring this often diffuse process. This study used radium isotopes (^{223}Ra, ^{224}Ra, ^{226}Ra) to investigate SGD and the associated fluxes of nutrients into Tauranga Harbour, New Zealand. We calculated the apparent water mass ages of the harbour to be between ~4.1 – 7.8 d, which was similar to a previous numerical model of ~2 – 8 d. A ^{226}Ra mass balance was constructed to quantify SGD fluxes at the harbour scale. A minimum SGD flux rate of 0.53 cm d^{-1} was calculated by using the maximum groundwater endmember value from 22 sample sites. However, using the geometric mean from these samples as a representative endmember, a final value of 2.83 cm d^{-1} or a flux of 3.09 x10^6 m^3 d^{-1} was calculated. These values were between ~1 and 2.8 times greater than all the major river and creeks discharging into the harbour during the sampling period. Due to the higher observed nutrient concentrations in groundwater, the SGD derived dissolved inorganic nitrogen (DIN), dissolved organic nitrogen (DON) and total dissolved phosphorus (TDP) fluxes were calculated to be 1.07 mmol m^2 d^{-1}, 0.87 mmol m^2 d^{-1} and 0.05 mmol m^2 d^{-1} respectively. These SGD inputs were ~5 times (for nitrogen) and ~8 times (for phosphorus) greater than the input from surrounding rivers and streams. The average N:P ratio in groundwater samples was 36:1 (which was greatly in excess of the Redfield ratio of 16). The harbour water had a N:P ratio of ~17:1. A positive relationship between radium isotopes and N:P ratios in the harbour further supported the hypothesis that SGD can have major implications for primary production, including recurrent algal bloom events which occur in the harbour. We suggest SGD as a major driver of nutrient dynamics in Tauranga Harbour and potentially other similar coastal lagoon systems and estuaries on oceanic islands.

2.2 Introduction

Submarine groundwater discharge (SGD) is the flow of both fresh terrestrial groundwater from coastal aquifers and seawater recirculation through permeable sediments (Moore, 2010). Tidal pumping, hydraulic water table gradients, wave energy, bio-irrigation and temperature density gradients can drive these advective flows (Santos et al., 2012). SGD is becoming increasingly important in the context of both aquatic and coastal/marine systems because it is one of the key pathways that connect the land and sea (Knee and Paytan, 2011). SGD delivers freshwater, nutrients, carbon, metals, and other chemical constituents to coastal waters. Similar to river estuaries, the composition of SGD is modified in subterranean estuaries that occur along most shorelines with permeable sands (Moore 1999; Santos et al., 2008; Knee and Paytan, 2011).

While many studies have focused on rivers, streams and oceanic drivers to assess nutrient budgets in coastal environments, SGD can deliver disproportionally large amounts of dissolved inorganic and organic nutrients (Slomp and Cappellen, 2004, Moore et al., 2011; Waska and Kim 2011, Su et al., 2013). The overall higher concentrations of nutrients in groundwater compared to surface water can potentially have a profound impact on the biogeochemistry and functioning of coastal systems (Burnett et al., 2006; Moore, 2007; Liu et al., 2012). Recent studies also suggest that SGD flows may rival or even exceed river inputs on islands (Moosdorf et al., 2015) as well as continental margins (Kwon et al., 2014; Moore et al., 2010; Peterson et al., 2008). Therefore, SGD is now considered a major component of coastal hydrological and biogeochemical cycles. Population increases have placed stresses on these cycles and subsequent land use changes, particularly in agriculture, have resulted in excess nutrient loading and nitrogen pollution in coastal waters worldwide (Smith et al., 2012). The delivery of these nutrients through SGD can be significant enough to modulate the dynamics and structure of microbial communities, trigger algal blooms, promote eutrophication, and facilitate hypoxia events in poorly renewed water bodies (Hwang et al., 2005; Hu et al., 2006; Rodellas et al., 2016). However, the patchy spatial distribution and temporal variability mean that it is difficult to quantify SGD pathways (Burnett et al., 2006). As a result, the contributions of SGD to many coastal chemical budgets, including nutrient loadings on islands, are often unknown.

Coastal aquifers on islands, with high pressure gradients and fast flow rates through the reactive subterranean zone, may have less time for biological utilization and therefore deliver more 'new' nutrients to adjacent water bodies (Slomp and Cappellen, 2004). Large volcanic islands, such as New Zealand, have the potential for large SGD fluxes into the ocean due to high soil permeability, steep relief, and strong orographic precipitation (Moosdorf et al., 2015; Santos et al., 2014; Knee et al., 2016). However, there are limited studies, especially in the South Pacific regions, of regional scale SGD fluxes and associated solutes into the ocean. Studies on oceanic islands such as Hawaii (Peterson et al., 2009; Knee et al., 2010), Jeju Island, Korea (Kim et al., 2003; Hwang et al., 2005), Mauritius (Provinec et al., 2012), Heron Island (Santos et al., 2010) and the Cook Islands (Tait et al., 2013; Cyronak et al., 2013) have all observed high SGD rates. Because of the associated high nutrient concentrations, all these studies speculated or demonstrated that SGD can be a major contributor to the productivity of the oceanic waters surrounding these islands.

Multiple methods are used to quantify the spectrum of SGD processes (Burnett et al., 2003; Swarsenski, 2007, Moore, 2010). Radium (Ra) isotopes have proved to be a powerful tool in qualitative and quantitative SGD studies (Charette et al., 2001; Moore 1996; Moore et al., 2010). Radium is a decay product of either a thorium or uranium parent isotope, which is bound to source rocks including sediments (Swarsenski, 2007). Water–sediment ion exchange processes in brackish to saline waters release radium into solution by desorption. As a result, coastal groundwater is often highly enriched in radium compared to surface sources, allowing for radium to be used as a geochemical fingerprint of SGD. Contributions from other radium sources, such as desorption from suspended sediments and diffusion are relatively small in comparison to SGD and can be quantified (Beck et al., 2007). Once mixed in coastal seawater, radium often behaves conservatively with mixing and decay becoming the only significant loss terms. The application of different isotopic ratios can integrate processes occurring at different spatial and temporal scales (Charette et al., 2006). The two isotopes with the shortest half-lives (^{224}Ra half-life = 3.66 d, ^{223}Ra half-life = 11.4 d) are useful on the short timescale of mixing and dynamic coastal processes. The longer-lived isotopes (^{228}Ra half-life = 5.75 years, and ^{226}Ra half-life = 1600 years) are useful for longer timescale processes, such as capturing older aquifer derived groundwater (Moore and Wilson, 2005).

Here we use radium isotopes to quantify SGD and related nutrient fluxes into Tauranga Harbour, a coastal lagoon system on the largely volcanic North Island of New Zealand. Coastal lagoon systems, which act as a dynamic interface between terrestrial headwaters and oceanic forces, have been suggested as groundwater discharge 'hotspots' (Rapaglia et al., 2010, Sadat Noori et al., 2016). While northern hemisphere coastlines such as Europe, Asia and America have been the focus for SGD and associated nutrient investigations, regions in the southern hemisphere, including oceanic islands such as New Zealand, remain poorly quantified and understood. We hypothesised that SGD plays an important role in the delivery of nutrients into the system. Our objectives were to 1) to determine possible SGD hotspot areas and the apparent water age using radium isotopes as a natural geochemical tracer, 2) quantify the relative SGD fluxes and associated dissolved inorganic and organic nitrogen and phosphorus inputs, and 3) assess the significance of SGD inputs in comparison to surface water inputs. We discuss the results in the context of oceanic islands as hotspots of SGD.

2.3 Methods

2.3.1 Study site

Tauranga Harbour is an estuarine lagoon, on the Bay of Plenty coast of the North Island of New Zealand. The Harbour is enclosed by Matakana Island, a large sand barrier island 25 km long (Figure 2.1). Two barrier tombolos, Bowentown Heads (northern basin) and Mount Maunganui (southern basin) define the main exchange passages with the Pacific Ocean. While the two basins are connected, large intertidal flats and poor tidal connectivity mean that water exchange is limited, making them nearly two independent systems (Spiers et al., 2009, Tay et al., 2013). This investigation focused on the southern basin of the harbour surrounded by the cities of Tauranga and Mount Maunganui. At a catchment scale, the current dominant anthropogenic pressures are from extensive horticultural and agricultural land use. The harbour has suffered reduced water quality over the past decades and is also vulnerable to inter-annual macro algal blooms of *Ulva* spp. (sea lettuce) (Park, 2011). We hypothesize that SGD may play a role in providing the nutrients that sustain these blooms in Tauranga Harbour.

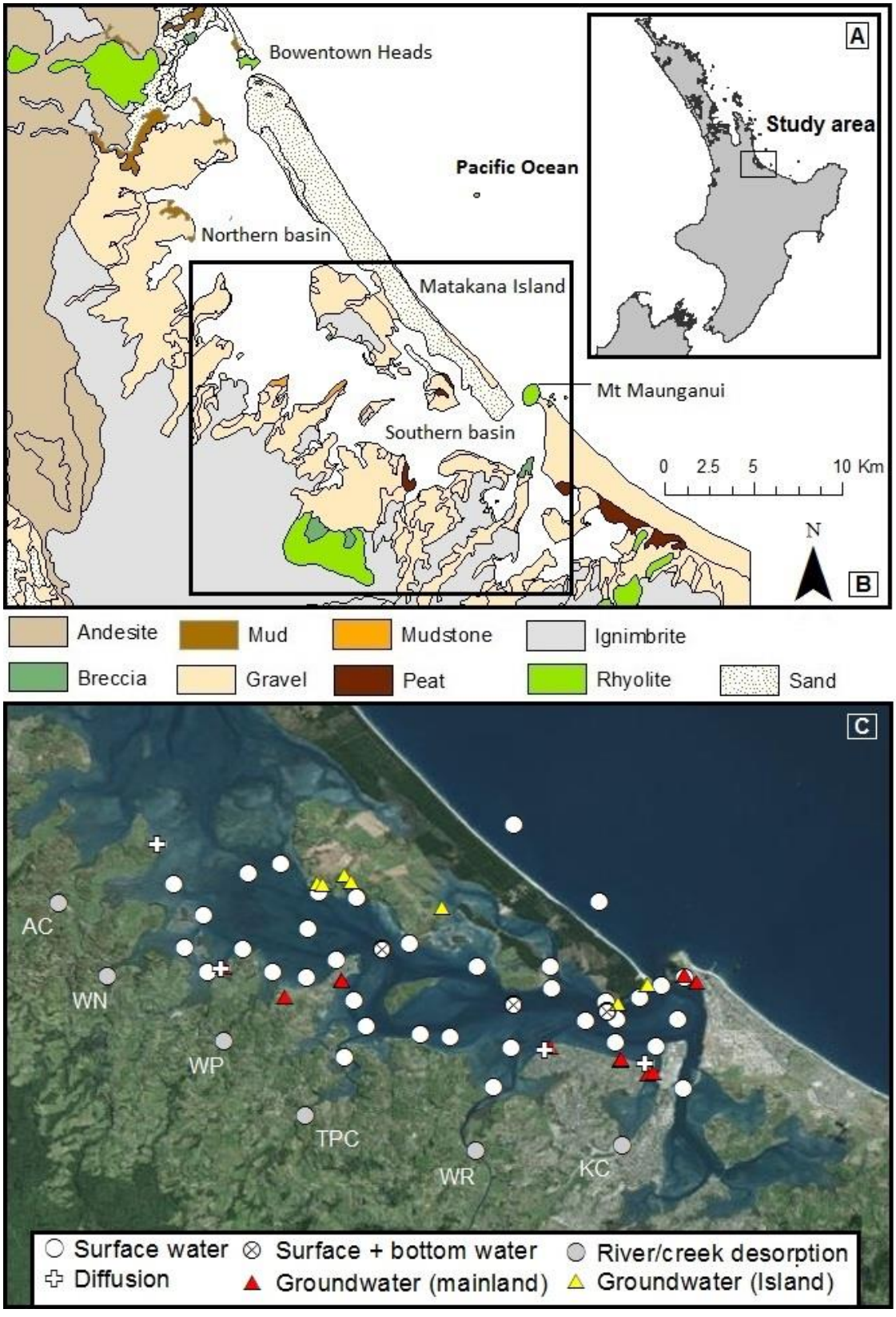

Figure 2.1 (A) Location of the study site (Tauranga Harbour) on the North Island of New Zealand, (B) regional geological setting, (C) aerial image and sampling sites (AC = Aongatete creek, WN = Wainui creek, WP = Waipapa creek, TPC = Te Puna creek, WR = Wairoa River, KC = Kopurererua creek).

The catchment geology is relatively young and of volcanic origin. Much of the harbour is comprised of terrestrial and estuarine volcanoclastic sediments, and non-welded or partially welded distal ignimbrites and airfall tephras known as the Tauranga group sediments (Briggs et al., 1996; Pearson, 2013). Sediments over primary volcanic features have been dated at 6500 years old whereas tidal sediments are much younger at 700 to approximately 3400 years old (Davis and Healy, 1993). River and streams have formed from Holocene and late Pleistocene alluvium and peat deposits composed of fine to coarse silts, sands, clays, and carbonaceous material (Briggs et al., 1996). Increased silts, clays and mud in the mid to upper reaches of the harbour can create local confining layers or 'sediment caps' (White et al, 2008). The primary volcanic rocks found in the region are rhylolite, dacite, ignimbrites and tephras (Briggs et al., 1996). Fractures are commonly found in these rock types, creating a highly permeable matrix that facilitates fresh groundwater flows. An extensive low-temperature geo-thermal network also lies underneath the Tauranga region. This provides a heat source to the array of large aquifers found in the area and can produce spring water temperatures between 22 – 39° C (White et al., 2008). Local Māori, who have had a cultural connection to the land and water over many centuries, describe a multitude of freshwater springs and seeps that discharge directly into coastal waters (Rosen and White, 2001). To date, SGD rates have not been quantified at the harbour scale. However, a previous investigation quantified porewater exchange in two small sub-estuaries using a radon mass balance (Santos et al., 2014).

The harbour is well flushed and tidally dominated with semi-diurnal tides ranging from ~1.9m (spring) to ~1.2m (neap). While having a mostly shallow and a vertically well mixed water column, deeper channels are also present (Heath, 1985). Tidal scouring has developed highly channelized currents with the strongest flows and shortest residence times occurring around the harbour mouth (Tay et al., 2013). The large surface area of intertidal flats consists of sandy mud islands, tidal channels, and the colonization of young mangrove forests along the upper fringes of the harbour (Stokes et al., 2010). A higher frequency of rainfall events occurs during late autumn and the winter months from April through to September (Cliflo – NIWA). The Southern Basin catchment has a total area of 1,300km² and is provided with freshwater inputs from the Wairoa River and a number of smaller streams and creeks (Figure

2.1). The total mean freshwater input is 30.5 $m^3 s^{-1}$ where the Wairoa River delivers the bulk supply of this at a flow rate of 17.6 $m^3 s^{-1}$ (Park, 2004).

2.3.2 Water column sampling

Sampling of surface waters around the harbour was conducted between 12th of October and 16th of October 2015 (Figure 2.1) at the end of the high rainfall months between May and September. Samples were obtained from 37 surface water sites and 3 bottom waters sites in the deeper channels of the harbour to assess if there was any stratification. Two samples were also collected outside the harbour to obtain an oceanic end member. All samples in the middle to lower regions of the harbour were obtained during the ebb stage of the tide, whereas samples from the much shallower (<1m depth) upper reaches of the harbour were collected at slack high tide. At low tide, this area becomes largely exposed intertidal flats and is not accessible by boat (the implications on sampling are discussed later).

To measure radium isotopes (^{223}Ra, ^{224}Ra and ^{226}Ra), 100 L of water (~1 - 2 m from the surface or ~1 - 2 m from the bottom) were pumped into plastic containers. The 100 L sample was then gravity-drained through cartridges containing 15 g of manganese impregnated fibres at a flow rate of <1 L/min (following Moore and Reid, 1973). A calibrated seabird electronics CTD was cast at each site to measure water column temperature, conductivity, and salinity. Samples for total nitrogen, phosphorus and nutrients were collected using a sample-rinsed syringe and filtered through 0.45 µm cellulose acetate syringe filters (Sartorius Minisart). These were stored in sterile 50 ml polyethylene centrifuge tubes, kept on ice in the dark for a few hours, and then frozen at -20 ˚C until analysis.

2.3.3 Groundwater sampling

A total of 26 groundwater samples were collected from Matakana Island and along the coastal fringes of the harbour to establish groundwater endmember values (Figure 2.1). Samples were collected between the 19th of November 2015 and 22nd January 2016, with an additional deeper coastal aquifer sample collected on the 16th of February 2016. Shallow bores were dug between 1 -1.5 m deep from above the high tide mark and across the intertidal zone at low (ebbing) tides. Bores were dug using a posthole digger and a hand auger.

A PVC piezometer was inserted with a 50 cm fine slotted end section fitted to allow groundwater to infiltrate the pipe. Water was purged from the pipe using a peristaltic (low flow) pump and sampled after at least 3 purge/recharge cycles. Samples were collected for total nitrogen, phosphorus and nutrients as described above. For radium samples a known volume between 15 – 30 L was filtered through Mn fibres. A calibrated YSI probe was used to measure temperature, conductivity, and salinity. Groundwater discharge from surface seeps was taken at two separate locations, including Matakana Island and a geothermal outlet at the base of Mt Maunganui (Figure 2.1). Three deeper aquifer samples (~40 m depth) were collected from bore pumps at Matakana Island and the mainland with the permission of local landowners.

2.3.4 River and creek desorption experiments

In order to establish a mass balance, radium desorption experiments at four of the six major creek and river systems draining into Tauranga Harbour were conducted between the 2nd and 12th of November 2015. This involved collecting two 30 L containers of fresh river water (salinity ~0.5) from each site. One container was filtered immediately through a cartridge containing Mn impregnated acrylic fibers. Sea salt was added to the second container and monitored with a YSI water parameter Sonde until the salinity reached 35 (similar to the salinity of the harbour). Adding salt enables Ra bounded to suspended sediments in the sample water to desorb due to ion exchange processes. The salted container was mixed, left for ~12 h, and run through another cartridge containing Mn fiber. Desorption was assumed to be the difference between salted and unsalted river water. Radium contamination by the salt addition was ruled out by adding salt to radium free fresh water and measuring dissolved radium in that water. Access to freshwater on the Te Puna stream and Wainui creek was not possible. However, samples were still taken at higher salinities (~4.8 - 6.13 ppt). These two desorption experiments were omitted from further analysis due to probable initial radium release from the brackish water. To compensate, an average value of the remaining three creek systems was applied to these two systems (combined contribution of ~5% of total river water input). Suspended particulate matter (SPM) concentrations in the Waiora River were low, between 4.73 and 5.97 mgl^{-1} during the study period, and even lower in the smaller creek systems. SPM concentrations were extracted from the Port of Tauranga

continuous monitoring system and converted from NTU to mgl^{-1} using a laboratory-based calibration with native sediment (pers. comm. M. Cussioli).

2.3.5 Diffusion experiments

A total of four sediment cores, two coarse grained (sandy) and two fine grained (muddy) were collected at four separate intertidal locations within the harbour to estimate the molecular diffusive fluxes of ^{223}Ra and ^{224}Ra. Sediment from the cores were spread evenly over the bottom of a plastic container (width = 32.5, length = 51.5 cm). Between 15 – 22 L of Ra-free water from Tauranga Harbour (salinity ~32) was carefully delivered into the containers to avoid any sediment disturbance (following Luek and Beck, 2014). The overlying water was then added with an air stone to gently oxygenate the water and prevent changes in redox characteristics (Beck et al., 2007). A plastic lid was added to minimise loss of water through evaporation. The sediment was left to incubate for at least 2 months. The water overlying the sediment was then extracted and passed through Mn fiber as described above. Diffusive fluxes were made under the assumption that after 2 months (> 5 half-lives for ^{224}Ra and ^{223}Ra), an equilibrium between sources (diffusion) and sinks (decay) within each container had been reached (Santos and Eyre, 2011). This method could not be applied for ^{226}Ra due to its very long half-life (1600 years).

2.3.6 Analytical methods and uncertainties

Radium samples were analysed using a radium delayed coincidence counter (RaDeCC) (Moore and Arnold, 1996). Each sample was thoroughly rinsed with fresh Ra free water at least 3 times to remove any particles and salts impregnated on the fibre. The fibres were then partially dried and placed into a cartridge for measuring the alpha decays of the radon daughters of ^{223}Ra and ^{224}Ra. All the ^{224}Ra results reported here represent excess ^{224}Ra after correction for ^{228}Th decay (Garcia-Solsona et al., 2008a). The calculated analytical uncertainties in coastal water samples averaged 15 % for ^{223}Ra and 4 % for ^{224}Ra. These uncertainties were lower in radium enriched groundwater samples and averaged 12 % for ^{223}Ra and 3 % for ^{224}Ra, which was consistent with previous error propagation studies in the literature (eg. Garcia-Solsona et al, 2008a). For ^{226}Ra analysis, samples were placed into gas

tight cartridges, flushed with compressed air for one minute then sealed for at least one week prior to being run through the RaDeCC. Activities of ^{226}Ra were determined based on the ^{222}Rn ingrowth within these gas tight cartridges (Peterson et al., 2009; Waska et al., 2008). The calculated analytical uncertainty in all samples averaged 7 % for ^{226}Ra. Nutrient samples were analysed by the University of Washington's Marine Chemistry Laboratory (Seattle, Washington, USA) using a Technicon AAII gas segmented /continuous flow system (SFA). All filtered samples were analysed for ammonium (NH_4^+) (EPA method 349), nitrate (NO_3^-) (EPA method 353.4, 2.0, 1997), nitrite (NO_2^-) (EPA method 353.4, 2.0, 1997), Phosphorus (PO_4^{-3}) (EPA method 365.5, 1.4, 1997), total dissolved nitrogen (TDN) (SM 4500-P J) and total dissolved phosphorus (TDP) (SM 4500-P J). The calculated method detection limits (MDL) for NH_4^+, NO_3^-, NO_2^-, PO_4^{-3}, TDN and TDP were 0.11µM, 0.46 µM, 0.02 µM, 0.02 µM, 0.336 µM and 0.017 µM respectively. Dissolved organic nitrogen (DON) and dissolved organic phosphorus (DOP) were estimated by difference between the total dissolved concentrations and the respective inorganic nutrient concentrations.

2.3.7 Calculations

To derive the apparent radium age (*t*) of the water mass in Tauranga Harbour, we used the ratio of short-lived radium isotopes to a longer lived one (Moore, 2000; Dulaiova & Burnett 2008; Eller et al., 2014). The large-scale input of radium isotopes along the coastline and the boundaries of estuaries are similar to an artificial tracer release, with the short-lived radium isotopes providing the rate of dispersion based on their exponential decay as they mix away from the source (Charette et al., 2013). The assumptions in using this approach include: (1) a single major source of radium exists with a constant isotopic ratio, (2) offshore waters contain negligible amounts of short-lived isotopes and (3) the losses of radium after leaving its source are only through mixing and radioactive decay. With these assumptions in mind, we estimated water mass ages using a combination of activity ratios (ARs).

$$t = ln\frac{\left[\frac{X_{Ra}}{Y_{Ra}}\right]_i}{\left[\frac{X_{Ra}}{Y_{Ra}}\right]_{obs}} \times \frac{1}{\lambda X_{Ra} - \lambda Y_{Ra}} \quad (d)$$

Equation 2.1

where $(^{X}Ra/^{Y}Ra)_{obs}$ represents the observed AR of a short lived (X) to a longer lived (Y) isotope measured at the harbour sampling locations; $(^{X}Ra/^{Y}Ra)_i$ is the initial activity ratio of the same isotope pair in the groundwater source; λ defines the decay constant for the individual isotopes (0.189 d^{-1} for ^{224}Ra, 0.0608 d^{-1} for ^{223}Ra and 1.1869×10^{-6} d^{-1} for ^{226}Ra). We investigated a large tidally dominated lagoon system, and therefore chose to apply both the $^{224}Ra/^{223}Ra$ and $^{223}Ra/^{226}Ra$ ARs using Equation (1) to provide a reasonable range of ages (discussed later).

We calculated the excess inventory of ^{226}Ra to estimate submarine groundwater discharge in Tauranga Harbour. This includes all sources and sinks of radium other than groundwater such as rivers, diffusion from the sediments and tidal exchange. This can be expressed as follows:

$$J^{226}Ra = \left[\frac{(^{226}Ra_{obs} - ^{226}Ra_{sea}) \times V}{t}\right] - \left[\left(^{226}Ra_r + ^{226}Ra_{des}\right) \times Q_r\right] - \left[^{226}Ra_{diff}\right]$$

Equation 2.2

where $J^{226}Ra$ represents the missing ^{226}Ra flux into the harbour in dpm d^{-1} (assumed to be related to SGD), $^{226}Ra_{obs}$ represents the average concentration observed in individual samples, $^{226}Ra_{sea}$ represents the lowest concentration observed during the survey assumed to represent oceanic background conditions, *V* is the volume of the harbour area at mid tide (approximately equal to MSL) in m^3, *t* is the residence time calculated from Equation (1) in d, $^{226}Ra_r$ is the concentration in fresh river water (in dpm m^{-3}), Q_r is the freshwater river discharge (m^3 d^{-1}), $^{226}Ra_{des}$ is the desorption from suspended river sediments (dpm m^{-3}), $^{226}Ra_{diff}$ is the diffusion rate from bottom sediments (dpm d^{-1}) (evaluated over the whole surface area of the harbour at MSL). To calculate the Tauranga Harbour ^{226}Ra inventory, we

averaged the excess radium activities within the harbour and multiplied this value by the average calculated volume (the first term in equation 2). Negligible salinity and temperature differences observed from surface and bottom waters indicate the system was well mixed and not stratified. To convert this unaccounted ^{226}Ra flux in equation (2) (assumed to be from groundwater) into a SGD we used measurements from 26 spatially variable wells around the harbour coastline in the equation

$$SGD = \frac{J^{226}Ra}{226_{Ra_{GW}}}$$

Equation 2.3

where $^{226}Ra_{GW}$ is the representative activity of ^{226}Ra in the observed wells. The sensitivity of the outcome to the end member concentration is discussed later. Nutrient concentrations in groundwater were multiplied by the ^{226}Ra-derived SGD rate to obtain fluxes of N and P via SGD. River and creek discharge rates were calculated from gauged average daily discharge data provided from the Bay of Plenty Regional Council.

2.4 Results

2.4.1 Ancillary surface water data

A total of ~329 mm of rainfall was recorded in the 3 months prior to surface water sampling (CLiFLO - NIWA). The average total discharge rate from the Waiora River and smaller creek systems over the survey period was 11.4 $m^3 s^{-1}$. Salinity during the survey ranged from 35.1 – 29.2 (Figure 2.2). Low salinities were observed along the coastal fringes within the harbour around the mouths of the smaller sub estuaries where fresh river and creek inputs occur. Lower salinity was also observed off Matakana Island where no fresh surface waterways exist. There were no significant temperature and salinity differences (<0.1° C and <0.06°C respectively) observed from the three deeper bottom samples when compared to surface waters, indicating a well-mixed system.

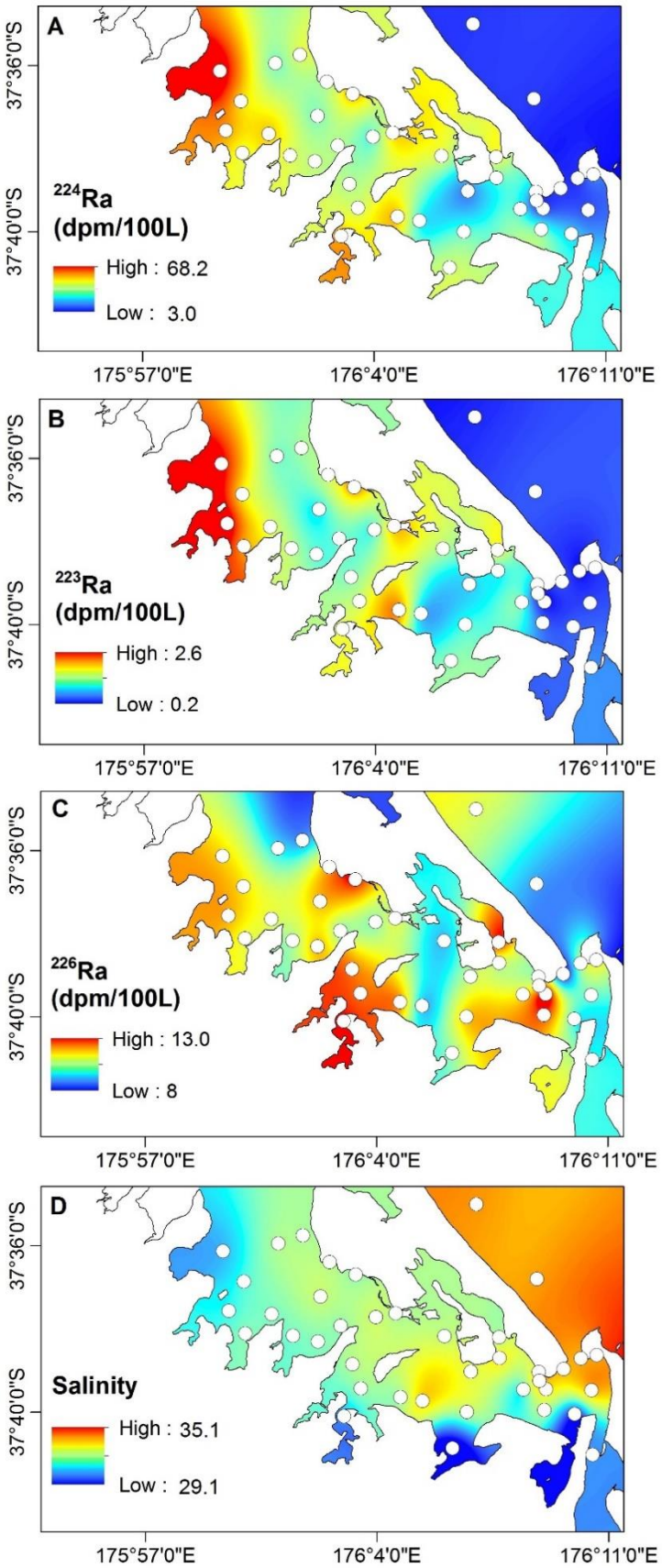

Figure 2.2 Spatial distribution of (A) ^{224}Ra, (B) ^{223}Ra, (C) ^{226}Ra and (D) salinity in Tauranga Harbour.

2.4.2 Surface water ^{223}Ra, ^{224}Ra and ^{226}Ra activities within Tauranga Harbour

The highest concentrations of the shorter lived radium isotopes ^{224}Ra and ^{223}Ra were observed in the shallower upper regions of the harbour (Figure 2.2). High concentrations for both isotopes were also recorded off the upper western coast of Matakana Island and across the mid region of the harbour. The shortest lived isotope ^{224}Ra had a peak value of 68.2 ± 1.8 dpm/100L in the upper embayment and decreased to 3.0 ± 0.2 dpm /100L around the harbour mouth as it decayed and mixed with oceanic waters. A similar pattern was seen with ^{223}Ra with a high concentration over a slightly larger area in the upper harbour waters potentially from a more integrated signal with its longer half-life. Both ^{224}Ra and ^{223}Ra decay on timescales that are comparable to tidal estuarine processes, including pore water exchange. As these isotopes move away from their sources, the measured levels of unsupported isotopes quickly drop below the threshold for detection.

The longest lived isotope ^{226}Ra revealed areas of higher concentrations not observed with the shorter lived isotopes (Figure 2.2C). The sources that sustain this isotope, including fresh groundwater delivery, occur on timescales much greater than dynamic estuarine processes. The very long regeneration rate in shallow sediments and slow decay rate (half-life 1600 years) allows groundwater affected by much older processes to become detectable in the harbour. The highest ^{226}Ra concentration was 12.9 ± 0.6 dpm/100L, which was observed in near shore waters around the mid region of the harbour. Even though the harbour is well mixed and not stratified, ^{226}Ra was 1.8 ± 0.55 dpm/100L higher in the bottom sample from the main deep channel than in the surface sample, reflecting a possible submarine seep. Conversely, both ^{223}Ra and ^{224}Ra were lower in bottom waters (with an average of 0.6 dpm /100L and 11.8 dpm /100L respectively) when compared to surface waters (average of 0.8 dpm / 100L and 14.4 dpm / 100L respectively). The short lived isotopes ^{223}Ra and ^{224}Ra showed a negative relationship with salinity, however, no clear relationship was observed between ^{226}Ra and salinity in harbour waters (Figure 2.3).

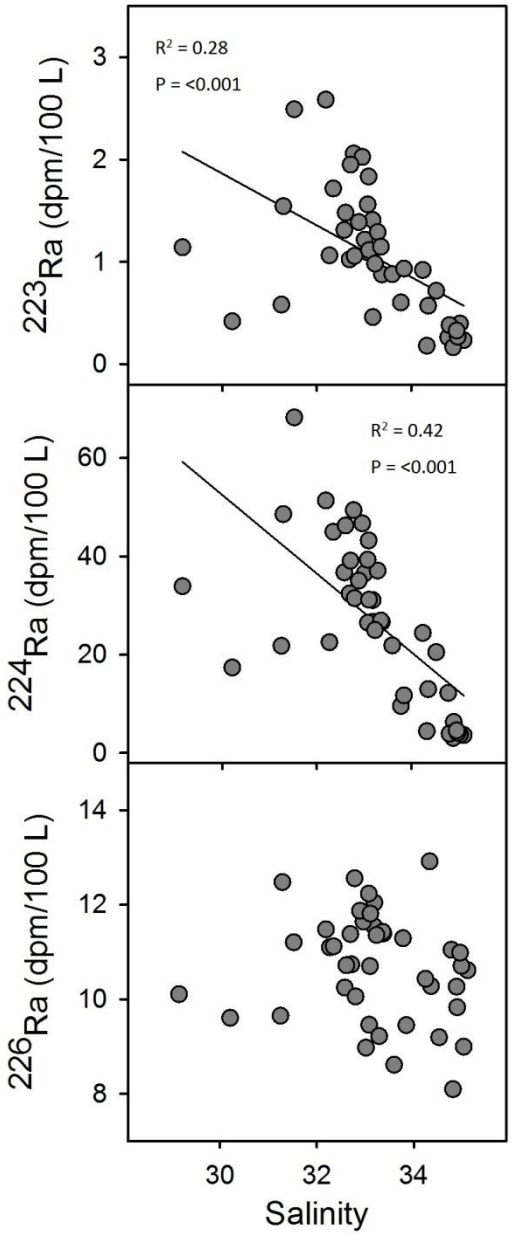

Figure 2.3 Relationship between (A) ^{224}Ra, (B) ^{223}Ra, (C) ^{226}Ra (dpm/100L) and salinity in harbour water.

2.4.3 Surface water nutrient concentrations within Tauranga Harbour

Dissolved organic nitrogen (DON) was found to be in highest concentration towards the upper reaches of the harbour, peaking at 10.8 µM off the eastern coastline (Figure 2.4A). The concentration decreased towards the lower region and mouth of the harbour to 4.2 µM. A small spike was observed at the harbour mouth (7.7 µM), which was sampled on an ebb tide. Dissolved organic phosphorus (DOP) also followed a similar pattern with higher concentrations (up to ~0.5 µM) in the upper reaches of the harbour (Figure 2.4C). Dissolved inorganic nitrogen (DIN) was low within the mid to upper regions of the harbour reaching a

low of 0.2 µM. High concentrations of DIN in surface waters were seen in the lower region of the harbour and around the harbour mouth (Figure 2.4B). Dissolved inorganic phosphorus (PO_4) also had higher concentrations (up to ~0.5 µM) in the lower harbour regions and harbour mouth (Figure 2.4D). The average TDN:TDP ratio in the harbour was ~17:1, slightly higher than the Redfield ratio of 16:1.

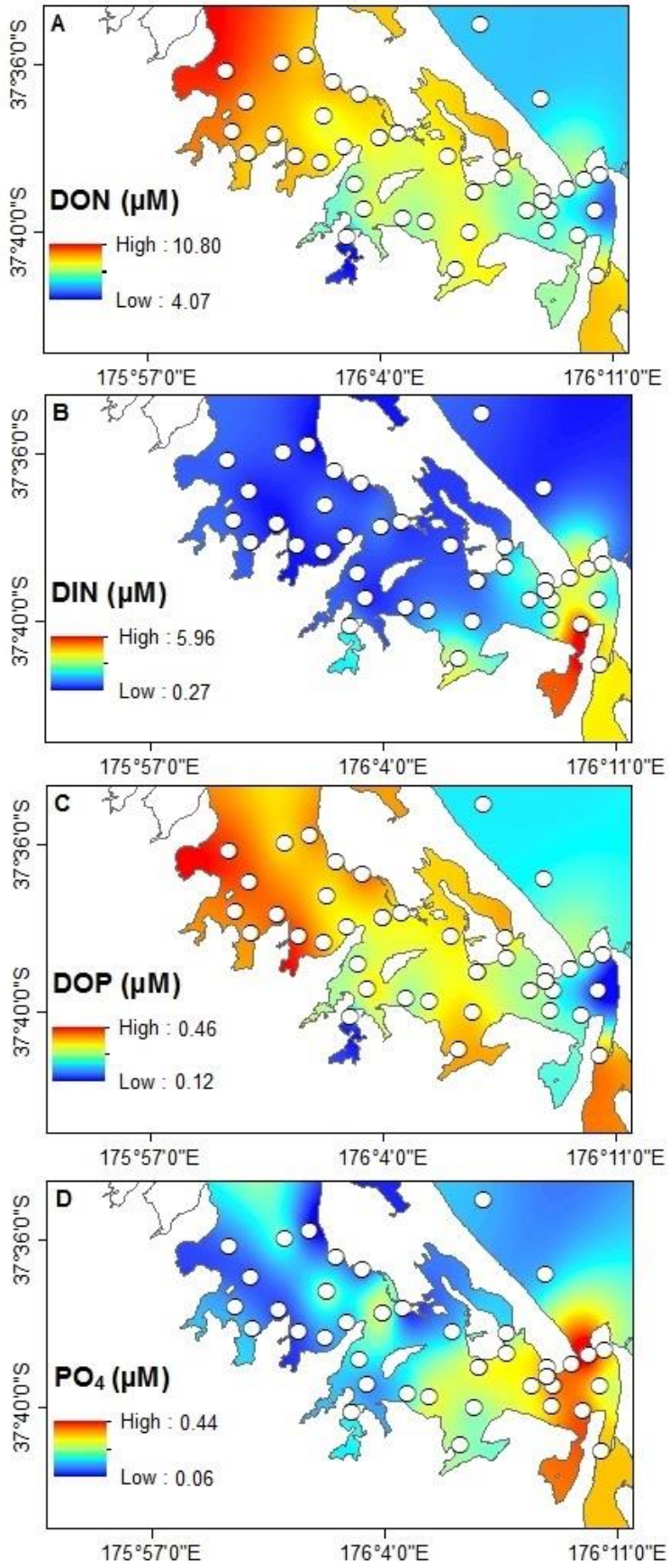

Figure 2.4 Spatial distribution of DIN (A), DON (B), DOP (C) and PO_4 (D) in Tauranga Harbour.

2.4.4 River and creek observations and Ra desorption

Nutrient concentrations were higher in rivers and creeks than in harbour waters (Figure 2.5) with average DIN, DON, DOP, PO_4 concentrations of 33.2 µM, 17.2 µM, 0.5 µM and 0.6 µM respectively in the Wairoa River. A combined average of 22.3 µM for DIN, 20.7 µM for DON, 0.4 µM for DOP and 0.3 µM for PO_4 was observed from the smaller creek systems. Overall, river and creek waters had an average concentration of 24.1 µM for DIN and 20.1 µM for DON, which was ~1.5 times lower than the average groundwater concentrations (Figure 2.5). DOP concentrations were also ~1.5 times lower, however PO_4 was up to ~ 4 times lower than the average groundwater concentrations.

Desorption experiments revealed little to no desorption of radium isotopes from the surrounding river and creek systems (Table 2.1). A small increase in ^{226}Ra concentration was observed after the addition of salt (7.6 ± 1.2 dpm/100L to 9.8 ± 1.4 dpm/100L) in the Wairoa River sample. However, overall, the changes in concentrations following salt addition were undetectable, implying desorption is a minor source of radium isotopes to Tauranga Harbour.

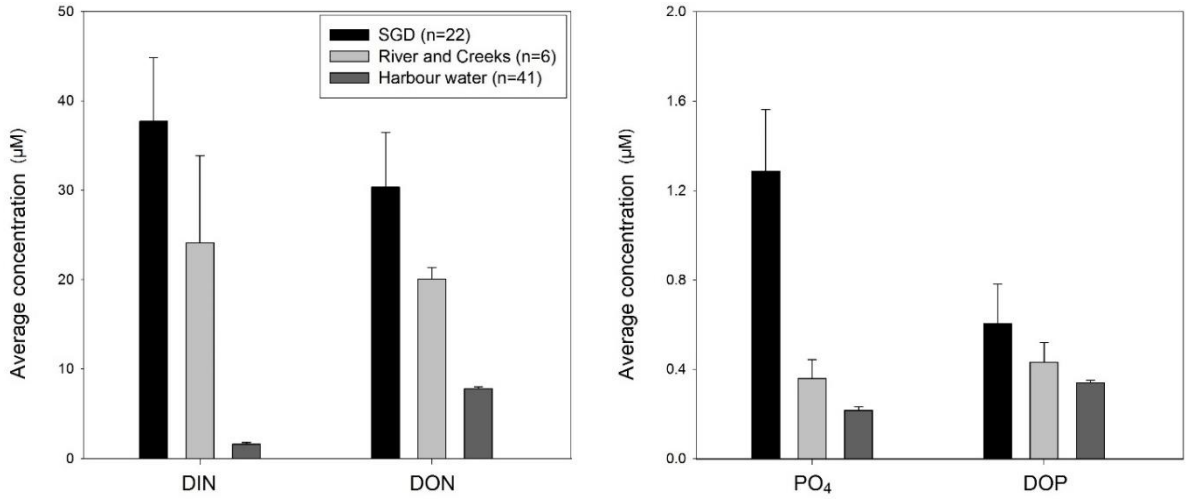

Figure 2.5 The average concentration of DIN, DON (left), PO_4 and DOP (right) found in SGD, river and creeks and Harbour water. Error bars represent propagated standard error.

2.4.5 Radium diffusion

Diffusion rates were greater in muddy than sandy sediments for both ^{223}Ra (0.33 dpm m^2 d^{-1} vs 0.15 dpm m^2 d^{-1}) and ^{224}Ra (24.67 dpm m^2 d^{-1} vs 10.47 dpm m^2 d^{-1}). Approximately 84% of harbour bed sediments are made of sandy sediments and 16% fine muddy sediments (Hancock et al., 2009). Extrapolating these estimates to the harbour area revealed an overall diffusion rate of 1.91 x 10^7 dpm d $^{-1}$ for ^{223}Ra and 1.39 x 10^9 dpm d^{-1} for ^{224}Ra. This is comparable to rates from other studies done globally, including Beck et al., (2007) and Luek et al., (2014).

2.4.6 Groundwater samples

Groundwater samples collected from the mainland and Matakana Island had highly variable ^{223}Ra, ^{224}Ra and ^{226}Ra concentrations with no clear relationship to salinity (Figure 2.6). Highest concentrations were observed in brackish waters with salinities of 10 – 20. The average concentrations of ^{223}Ra, ^{224}Ra and ^{226}Ra on Matakana Island were higher than those observed on mainland (Table 2.2).

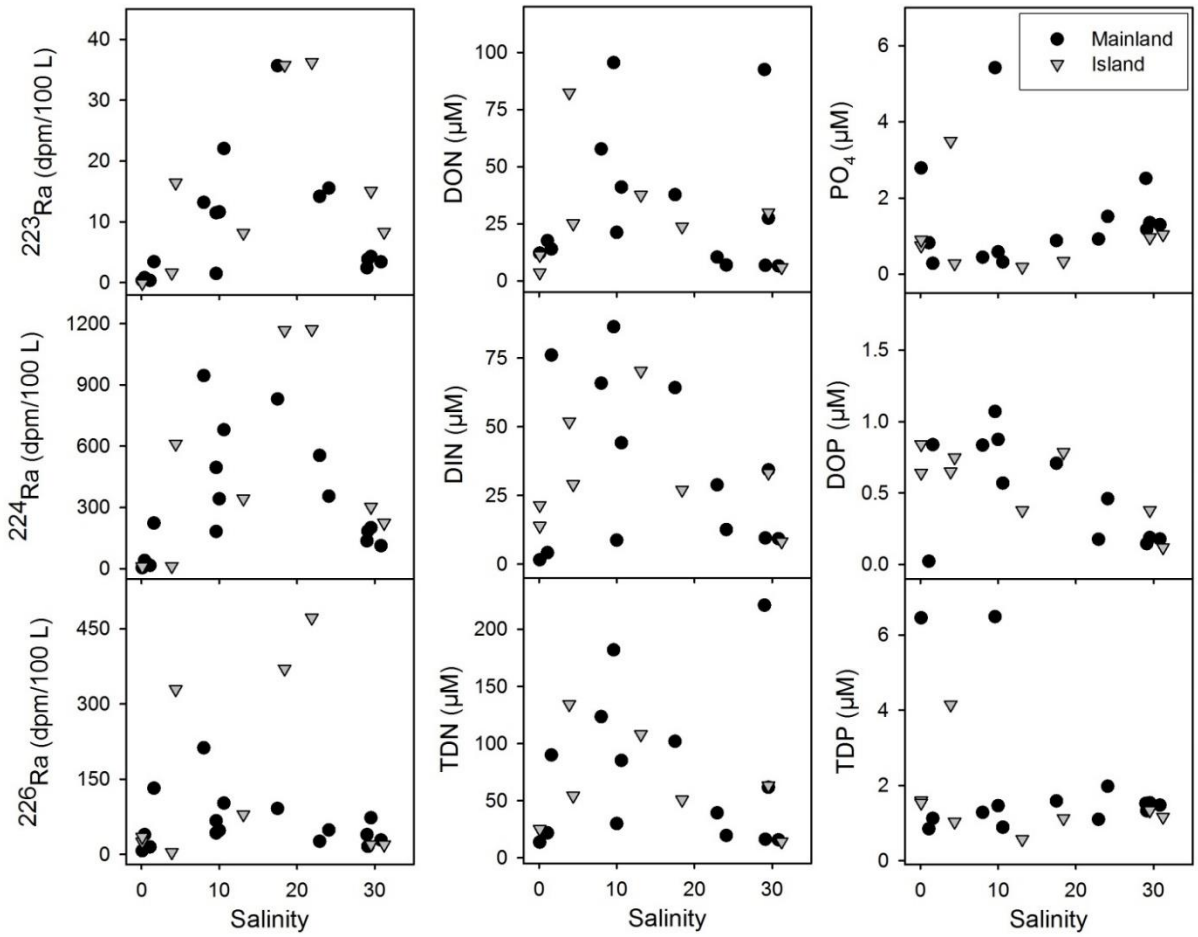

Figure 2.6 Relationships between ^{224}Ra, ^{223}Ra, ^{226}Ra (dpm/100L) and salinity (left); and with DIN, DON, TDN (µM) and salinity (centre) and PO_4, DOP, TDP and salinity (right) from different groundwater sources.

Table 2.1 Dissolved and desorbed radium fluxes of the major rivers and creeks draining into Tauranga Harbour during the study period.

River name and gauge ID #	Daily Discharge (m^3/day)	Freshwater flux (dpm/day)			Desorption river flux (dpm/day)		
		^{223}Ra	^{224}Ra	^{226}Ra	^{223}Ra	^{224}Ra	^{226}Ra
Kopurereoa DO406909	4.0×10^4	3.3×10^2	1.6×10^6	2.1×10^6	1.3×10^5	1.6×10^5	2.6×10^6
Aongatete SH 2	5.6×10^4	0	0	6.0×10^5	2.1×10^4	1.5×10^3	2.8×10^6
Waipapa CP353091	1.2×10^4	0	1.5×10^5	5.2×10^5	2.5×10^4	n/d	1.1×10^6
Waiora River CO923457	8.0×10^5	6.9×10^4	5.1×10^7	6.0×10^7	1.4×10^6	n/d	1.7×10^7
Te Puna ungauged	6.0×10^4	1.6×10^2	2.3×10^6	2.7×10^6	1.1×10^5	n/d	3.4×10^6
Wainui ungauged	8.1×10^4	1.9×10^3	2.8×10^6	3.6×10^6	1.5×10^5	n/d	4.8×10^6
Total	1.0×10^6	7.2×10^4	5.8×10^7	7.0×10^7	1.8×10^6	1.6×10^5	3.2×10^7

Note: Discharge rates were acquired from the Bay of Plenty Regional Council (BOPRC) gauge data. The average discharge rate per watershed area was assigned to Te Puna and Wainui creeks as they were ungauged. n/d represents the slightly negative desorption values due to low values and analytical uncertainties. These were assumed to be zero

Table 2.2 Summary of groundwater radium and nutrient concentrations from mainland and Matakana Island sample sites.

Site	Salinity	Temp (˚C)	^{223}Ra (dpm/100L)*	^{224}Ra (dpm/100L)*	^{226}Ra (dpm/100L)*	DIN (µM)	DON (µM)	PO_4 (µM)	DOP (µM)	TDN (µM)	TDP (µM)
Mainland											
Mean	15.3	20.5	5.8	208.8	48.5	41.0	32.0	1.5	0.6	73.0	2.1
(± S.E)	(± 2.8)	(± 1.2)	(± 24.6)	(± 145.0)	(± 14)	(± 10.2)	(± 8.1)	(± 0.4)	(± 0.3)	(± 17.6)	(± 0.5)
Range	0.1 - 30.8	16.2 - 38.5	0.3 - 425.8	4.2 - 2503.4	7.2 - 212.6	1.6 - 128.6	6.6 - 95.5	0.3 - 5.4	-1.0 - 3.7	13.7 - 221.0	0.8 - 6.5
n	17	17	17	17	17	14	14	14	14	14	14
Matakana Island											
Mean	13.6	22.8	2.6	78.3	20.1	31.9	27.5	1.0	0.6	59.4	1.6
(± S.E)	(± 4.1)	(± 0.4)	(± 2.7)	(± 70.9)	(± 13.0)	(± 7.2)	(± 8.9)	(± 0.4)	(± 0.1)	(± 14.9)	(± 0.4)
Range	0.1 - 31.2	19.9 - 24.5	0.1 - 15.1	10.8 - 343.1	4.2 - 79.7	8.2 - 70.3	3.7 - 82.4	0.2 - 3.5	0.1 - 0.8	14.2 - 134.3	0.6 - 4.1
n	9	9	5	5	5	8	8	8	8	8	8
Total											
Mean	14.8	21.3	4.8	167.1	39.7	37.7	30.4	1.3	0.6	68.0	1.9
(± S.E)	(± 6.1)	(± 7.6)	(± 90.8)	(± 533.7)	(± 45.3)	(± 7.0)	(± 6.0)	(± 0.3)	(± 0.2)	(± 12.3)	(± 0.3)
Range	0.1 - 31.2	16.2 - 38.5	0.1 - 425.8	4.2 - 2503.4	4.2 - 212.6	1.6 - 128.6	3.7 - 95.5	0.2 - 5.4	-1.0 - 3.7	13.7 - 221.0	0.6 - 6.5
n	26	26	22	22	22	22	22	22	22	22	22

** Samples > 3 standard deviations above the mean were removed from analysis. The geometric mean was applied to all radium samples.*

DIN and DON concentrations were highly variable with no clear relationship observed with salinity (Figure 2.6). Similar to the isotope observations high nutrient concentrations were also observed in brackish waters. Mainland samples had an overall higher average concentration of DIN and DON compared to Island samples (Table 2.2). There was no clear trend with salinity among PO_4; however, DOP was observed to decrease in concentration with higher salinity (Figure 2.6). The concentration of DIN, DON and TDP in groundwater samples were 23, 3.8 and 3.4 times greater, respectively, than concentrations observed in harbour water with an average TDN:TDP ratio of 36:1.

The TDN pool in groundwater consisted of 44.6 % DON and 55.4% DIN (43.56 % Nitrate + Nitrite and 11.84% ammonium) (Figure 2.7). This was in contrast to harbour water, whereby DON dominated DIN concentrations in the total nitrogen pool of the surface waters at 82.8% of TDN. Nitrate made up 10.5 % of the TDN pool with 1.8 % and 4.7 % for nitrite and ammonium respectively. Overall, the TDN in groundwater was ~7 times greater than harbour water and ~1.5 times greater than surrounding river and creeks (Figure 2.7).

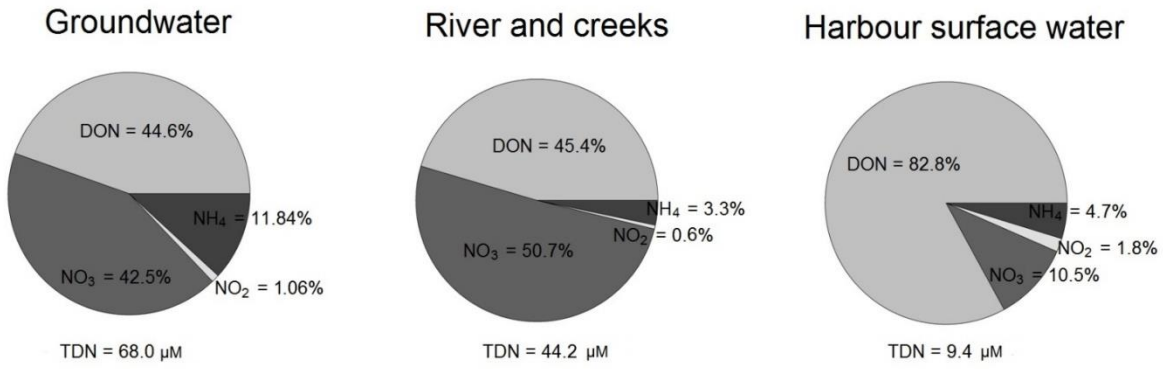

Figure 2.7 The relative contribution of the different nitrogen species to the TDN pool in groundwater, river and creeks and harbour surface water.

2.4.7 Radium ages

In order to estimate SGD rates using radium isotopes, it is essential to understand residence times and the transport of water masses in Tauranga Harbour. Here, we used ratios between radium isotopes to estimate the apparent water age. A combination of two isotope activity ratios (AR) were used (^{224}Ra /^{223}Ra AR and ^{223}Ra / ^{226}Ra AR) to compare water ages. Using the ^{224}Ra/^{223}Ra AR equation, ages were calculated between 0.47 and 11.7 days with a mean of 4.1 ± 1.3 d (Figure 2.8 A). Using the ^{223}Ra / ^{226}Ra AR equation, ages were calculated between 1.6 – 22.8 d with a mean of 7.8 ± 2.7 d (Figure 2.8 B). The ^{223}Ra / ^{226}Ra AR ages increased to a mean of ~7 d in middle region of the harbour and a mean of ~16 d around the mouth of the harbour. This was a similar pattern to the ^{224}Ra/^{223}Ra AR, however on a differing timescale, whereby only a slight increase in age from the upper region (mean 3.8 d) to the harbour mouth (mean 4.2 d) occurred. Both methods show distinct areas of younger ages towards the upper reaches of the harbour.

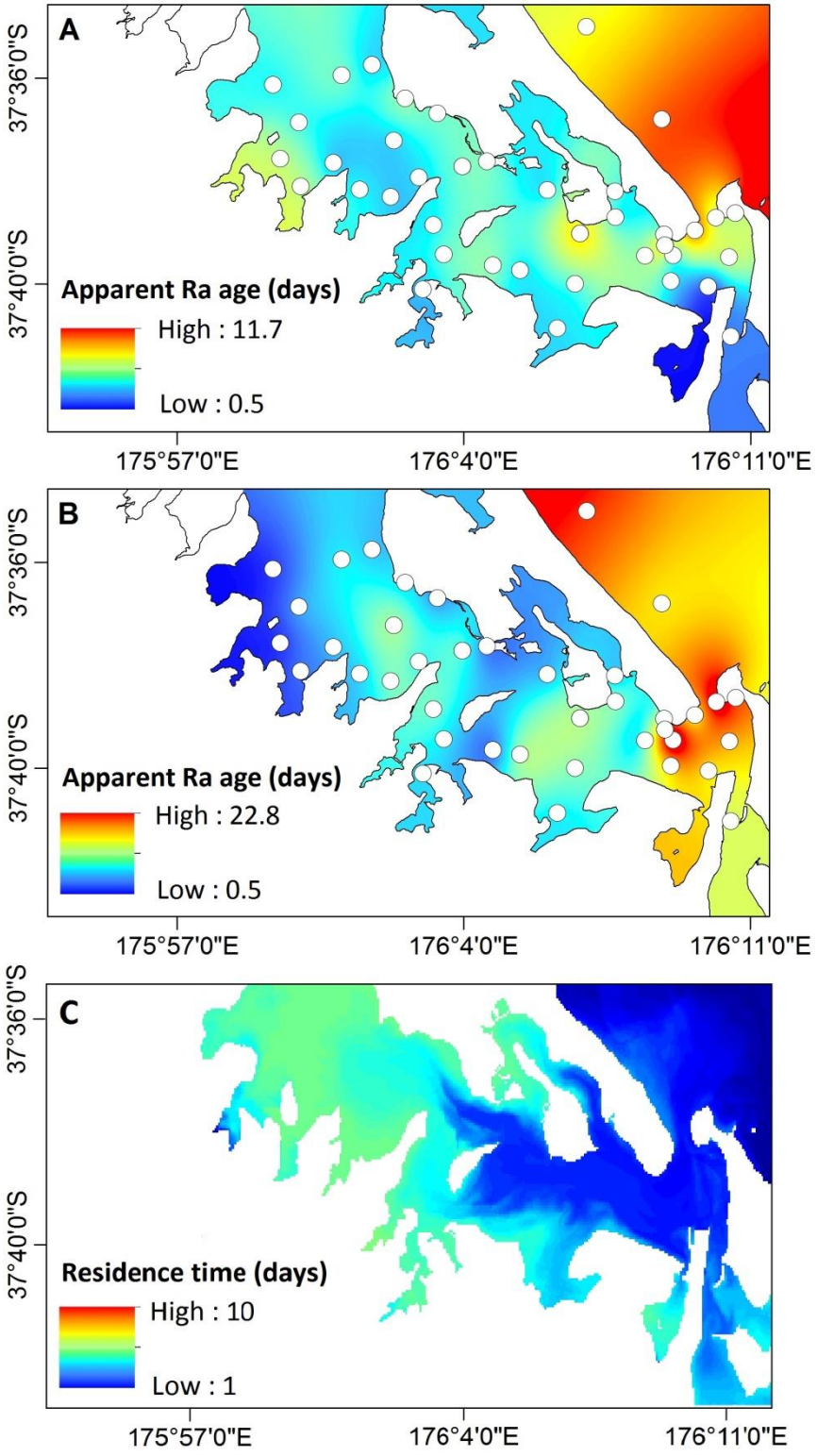

Figure 2.8 The apparent Ra age of surface water in Tauranga Harbour using (A) the $^{224}Ra/^{223}Ra$ AR and (B) the $^{223}Ra/^{226}Ra$ AR compared with (C) a previous physical residence time model using numerical modelling (provided by Tay et al., 2013).

2.5 Discussion

2.5.1 Determining water mass ages and transport rates using Ra isotopes

Ages, residence time and flushing time are all suitable descriptions for describing how long water remains in an estuary. These can be calculated using physical methods, numerical models, or isotopic tracers such as radium (Moore, 1999; Charette et al., 2001; Moore, 2006; Swarsenski et al., 2007; Rapaglia et al., 2010). Each method may give different estimates depending on the assumptions used to make the calculations and inherent limitations of the method. We compared the estimated apparent Ra ages to an existing hydrodynamic model of Tauranga Harbour (Figure 2.8 C). This model calculated residence times of between 2 to 4 d near the harbour mouth which increased to between 4 – 8 d towards the north end of the basin (Tay et al., 2013). The average residence time among all simulated conditions (different wind and current scenarios) and regions for the numerical model was 4.8 d. The region around the harbour mouth had the shortest residence time in spite of deeper waters due to strong currents and proximity to the source of new water provided by oceanic exchange (Tay et al., 2013). There is a general agreement in the time scales between both approaches in the upper and mid regions of the harbour, and a large disagreement around the southern exchange passage, where the hydrodynamic model estimates young ages and the radium isotope model implies older ages (i.e., long time since groundwater seepage). In broad terms the two measures of Ra age (Figure 2.8 A & B) are inversely related to the hydrodynamic model (Figure 2.8 C). The older Ra ages, which were also correlated with higher salinity in the harbour mouth region (Figure 2.9), suggest the water mass had moved away from its potential source in the fresher regions of the upper and mid harbour. The $^{223}Ra/^{226}Ra$ AR (mean of 7.8 days) may have captured a larger portion of older water exiting the harbour, due to the longer life of the isotopes used. However, if we exclude the harbour mouth region which contained much older water ages and a large oceanic component, the mean of the $^{223}Ra/^{226}Ra$ AR age would drop to ~5 days, which is within the error range of both the $^{224}Ra/^{223}Ra$ AR and the hydrodynamic model.

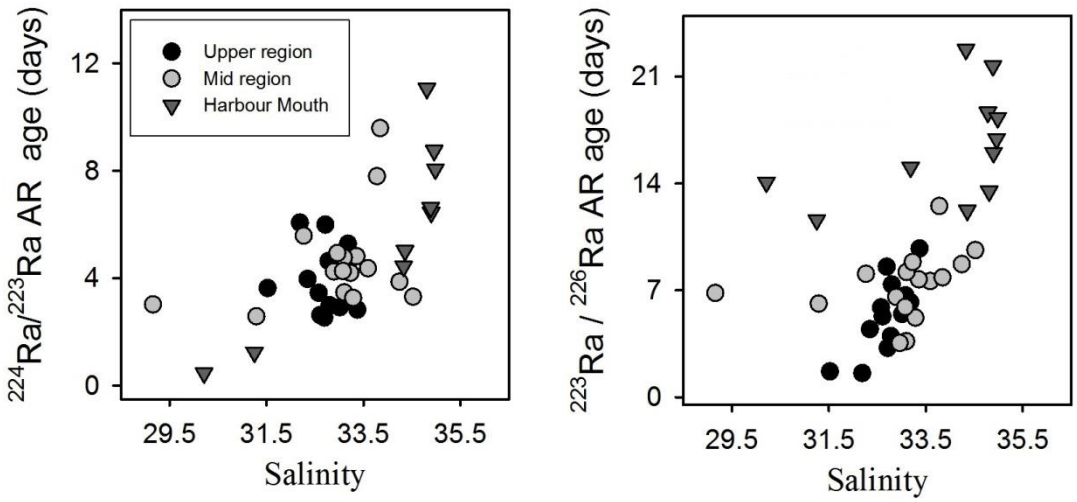

Figure 2.9 Comparison of $^{224}Ra/^{223}Ra$ AR age (days) and salinity (left); and $^{223}Ra/^{226}Ra$ AR age (days) and salinity (right) in the different harbour regions.

The residence time calculated using the hydrodynamic model is defined as the average time a parcel of water spends within a specified region before moving, driven by physical processes such as winds, freshwater inflow, tidal exchange with the open ocean, and residual currents (Tay et al., 2013). The time scale starts when water enters the model (new water) at the oceanic and riverine boundaries. Therefore, water near the open boundaries and near the freshwater sources will be defined as young. Conversely, radium ages reflect the time elapsed since the sampled harbour water became enriched in radium isotopes and isolated from its main source (Dulaiova and Burnett, 2008; Moore, 2000). Therefore, areas with younger apparent Ra ages may be major sources of SGD into the system since other sources such as desorption from the streams and rivers were negligible (Table 2.1). The decay and mixing with oceanic waters through physical processes are the major cause of reduced radium concentration in estuarine environments (Moore, 2000, Kim et al., 2008). However, as radium enriched water is transported out of the harbour away from its source, a large amount of older aged water is likely to be recirculated in currents and flushed back in with tidal movements through the single narrow exchange passage.

Being a tidally dominated system, the return flow of the water mass out of the harbour has the potential to extend radium ages as water flushed out is pushed backed in with the high tide (Sanford et al., 1992; Moore et al., 2006; Waska and Kim, 2011). The hydrodynamic model tracks this water as new water, whereas the radium isotope model tracks this as much

older water. Figure 2.9 illustrates that the apparent age of both isotopic ARs increase with salinity, especially in the harbour mouth region where there is regular fresh oceanic exchange. Tomasky-Holmes et al., (2013) also observed Ra ages increasing with salinity using the ^{223}Ra / ^{228}Ra AR in Waquoit Bay, USA and concluded that using radium to measure water mass age provided estimates that were longer than those obtained with other methods such as the tidal prism approach and numerical models. This reaffirms that applying a combination of methods, such as radium isotope ratios and physical models, can provide more insight into mixing under differing timescales driven by different processes (Monsen et al., 2002; Moore et al., 2006).

2.5.2 Quantifying SGD flux rates

A steady state radium mass balance model was applied to quantify SGD fluxes into Tauranga Harbour at MSL high water (Table 2.3). We used the long lived ^{226}Ra isotope for its larger integrative capacity and the ability to neglect decay rates on the timescales investigated (Moore, 2010). Due to its long half-life (1600 years) oceanic waters have a relatively constant background ^{226}Ra concentration of ~8 dpm/100L (Moore, 2010a). Long-lived Ra isotopes do not decay significantly in coastal waters; however, their inventories are continually diluted by mixing with the ocean (Moore, 2010). The waters within the harbour were enriched in ^{226}Ra relative to oceanic water (Figure 2.2 C). To derive excess ^{226}Ra values, the lowest observed sample concentration of 8.1 ± 0.5 dpm/100L was subtracted from each sample collected within the harbour to correct for background levels. To maintain a steady state, the observed enrichments of ^{226}Ra in harbour waters must be supplied from the following possible sources: (1) diffusion from bottom sediments, (2) dissolved ^{226}Ra from river and surrounding streams, (3) desorption from riverine suspended sediments, and (4) SGD. The only loss of Ra from the system is mixing with oceanic waters. Radioactive decay is negligible on the timescale of Tauranga Harbour mixing and can be ignored.

To calculate the amount of dissolved ^{226}Ra inputs from the local rivers and streams, we multiplied the discharge rates during the study period by the measured ^{226}Ra freshwater end members. This yielded only ~0.05% of the excess ^{226}Ra mixing losses. Runoff from rainfall in the weeks before sampling would have been negligible as no significant rainfall events occurred (total rainfall was 12.4 mm in the two weeks prior to sampling) and the residence

times of the harbour (4 – 8 d) is relatively short. River discharge rates were also observed as steady in the weeks before and during sampling. Further freshwater inputs of ^{226}Ra through desorption of suspended sediments accounted for only ~0.02 to ~0.04 % of the mixing losses. This is consistent with estimates from other systems globally (Beck et al., 2008, Garcia-Solsona et al., 2008a; Garcia-Orellana et al., 2010; Luek and Beck 2014; Stewart et al., 2015). However, some systems in New Zealand suffer from heavy total suspended sediment loads from a combination of intensive land use changes, fine volcanic soils, and steep topography (Thrush et al., 2004). To estimate molecular diffusion from sediments, we used the global average diffusion rate of 0.42 dpmm^{-2} d^{-1} (Beck et al., 2007), which accounts for only ~3.5% of the excess ^{226}Ra mixing losses. To give more confidence in using this value, we also assessed our shallow groundwater ^{226}Ra concentrations as diffusion occurs at the sediment-water interface (Corbett et al., 1998). The comparison of our shallow groundwater concentrations to other shallow concentrations globally can provide a cross check of ^{226}Ra activity in surficial sediments. Our observations were slightly under ^{226}Ra global averages assembled by Kim et al., (2005), implying diffusion rates should also be slightly lower than global diffusion averages. While variations may occur, diffusive fluxes of ^{226}Ra have been shown as a minor input to mass balance models in other studies (Beck et al., 2008, Kim et al., 2005, Liu et al., 2014, Peterson et al., 2008; Stewart et al., 2015).

With all the possible radium sources accounted for, the ^{226}Ra mass balance was missing a source equivalent to ~89% or 1.1× 10^{9} dpm d^{-1} of the total mixing losses (Table 2.3). We assume this to be SGD. Dividing this missing flux by a representative groundwater ^{226}Ra concentration (39.7 dpm m^{3}) a total SGD flux of 3.09x 10^{6} m^{3} d^{-1} was estimated. When up scaled to the whole southern basin area of Tauranga harbour a rate of 2.83 cm.d^{-1} was calculated. Similar to several previous regional radium investigations in other embayments (Stewart et al., 2015; Swarsenski et al., 2007), the major uncertainties are in (1) the harbour water mass ages / transport rates and (2) the groundwater end member values.

The differences in water mass ages observed in Figure 2.8 between the two ARs may be attributed to a combination of (1) the sensitivity to the natural variability of the end member used (2) the specific isotope characteristics including the associated errors and (3) multiple sources of radium affecting the relative ARs. AR-based water ages that are shorter than 3-5 d have been demonstrated to often have relative uncertainties greater than 100%, limiting their

utility (Knee et al., 2011). However, due to the calculated ages of the system and the close similarity in the timescales between the different methods, including a numerical model, it is likely we have selected an appropriate overall age for the system. To calculate the mass balance needed to estimate SGD, we used an average of the $^{223}Ra/^{226}Ra$ AR (excluding the harbour mouth region) and $^{224}Ra/^{223}Ra$ AR, which was ~5 days. When applying (Equation 2.1) to calculate apparent ages, the greatest source of uncertainty lies with the natural variability in the endmember isotopic ratio (Charette et al., 2008; Tomasky-Holmes et al., 2014; Liu et al., 2014). There was approximately 20% variation in endmember values. Propagating this variation through our calculations would result in changes of ±1 d to the estimated age, which would lead to overall changes of 19 % to the total SGD rate. Studies by Rapaglia et al., 2010; Liu et al., 2014 and Stewart et al., 2015 have also observed similar errors.

Constraining an accurate and representative groundwater endmember is critical in determining the overall SGD rate (Michael et al., 2011; Moore 2010a, Beck et al., 2008). Complex chemical modifications in the subterranean mixing zone such as redox reactions, pore water residence times and salinity gradients are generally the most important factors controlling variations in radium activity within the subterranean estuary (Gonneea et al., 2008; Beck et al., 2016; Cho and Kim, 2016). Moreover, low-salinity groundwater can bypass the subterranean estuary reaction zone and may be very different in chemical composition from groundwater that is more thoroughly mixed and modified before discharge (Charette and Sholkovitz 2002; Gonneea et al., 2008; Beck et al., 2016). We attempted to capture a large range of spatially variable samples (n=26) with mixed salinities across the seepage face and coastal fringes (Table 2.2). These were taken on both the mainland and Matakana Island which featured a mix of local geological features and environments surrounding the harbour.

Cho and Kim (2016) suggest that using an endmember value with salinity >10 may avoid overestimating the final SGD flux rates. However, we hypothesise that the young volcanic environment surrounding Tauranga Harbour is likely to have freshwater seeps directly into the water column through fractures in underlying ignimbrite and rhyolite aquifer systems (White et al, 2008). Higher concentrations of ^{226}Ra in surface waters, not seen in the short-lived isotopes (Figure 2.2), may reflect these deep radium rich seeps and geothermal discharges. To explore this further we provide a range of possible SGD rates based on differing end member scenarios. For the purpose of this analysis, we first excluded three outlier values

(MI-3, MI-4, MI-5) from our 26 groundwater samples which were > 3 times the standard deviation (Table 2.2). Firstly, if we applied the maximum concentration from our endmembers (212.0 dpm/100L) and kept the remaining parameters of the mass balance constant, the final SGD flux rate would be 5.77 x 10^5 m^3 d^{-1} or 0.53 cm d^{-1}, which was approximately 60% of the combined river and creek input during the study period. If we were to exclude 10 of our endmember values which had a salinity <10 (as suggested by Cho and Kim, 2016) and apply the geometric mean to the remaining samples our endmember value would become 46 dpm/100L. This would translate into an overall flux rate of 2.67 x10^6 m^3 d^{-1} or 2.44 cm d^{-1}, which was ~2.8 times greater than the combined river and creek inputs during the study period. Finally, if we were to apply the geometric mean of 39.7 dpm/100L from our sample set and keep all other parameters constant a similar total SGD flux rate of 3.09 x10^6 m^3 d^{-1} or 2.83 cm d^{-1} would be calculated, which is ~3 times the combined river and creek input into Tauranga Harbour during the sampling period.

Due to our relatively large and spatially variable sample size, the geometric mean of 39.7 dpm/100L was chosen as our representative endmember to calculate our final SGD flux rate (3.09 x10^6 m^3 d^{-1} or 2.83 cm d^{-1}, equivalent to ~3 times the river input). This demonstrates that the SGD rates to Tauranga Harbour are significant and comparable to the local river and stream inputs regardless of uncertainties in the endmember and residence time estimates. However, comparing our results to other island environments proved difficult due to the different scales, techniques and normalizations used for each environmental setting. Here we provide a comparison to other studies from embayments and harbours from much larger continental land masses. Our results are comparable to the approximate calculated SGD flux rate from Tampa Bay, USA at 0.22 – 1.45 cm d^{-1} (Swarsenski et al., 2007), Moreton Bay, Australia at 0.7 – 4.4 cm d^{-1} (Stewart et al., 2015) and Tolo Harbour, Hong Kong at 2.66 - 5.42 cm d^{-1} (Luo and Jiao, 2016). This demonstrates that New Zealand has the potential to contribute SGD into the coastal ocean at rates comparable or larger than continental land masses.

Table 2.3 Summary of the ^{226}Ra mass balance model used to estimate SGD into Tauranga Harbour. The calculated value was based on using the geometric mean of groundwater samples as the representative endmember. See Table 4 (below) for an endmember sensitivity analysis. Further details are described in the text.

Parameter	Units	Description	Calculated value
Flushing time	d	Average ± standard error derived from both Ra activity ratios	5 ± 1
Excess ^{226}Ra inventory	dpm	Individual sample minus background (8.1 dpm/100L) upscaled to the harbour MSL volume representative of each sample; 20% uncertainty assumed	6.88×10^{9}
Mixing losses	dpm d^{-1}	Excess ^{226}Ra inventory divided by the apparent Ra water age	1.25×10^{9}
Dissolved ^{226}Ra inputs	dpm d^{-1}	Dissolved 226Ra in fresh river water multiplied by the combined river and creek flux	7.00×10^{7}
Diffusion from sediments	dpm d^{-1}	Global diffusion average multiplied by the bottom surface area of harbour; 100% uncertainty assumed	4.58×10^{7}
Desorption of ^{226}Ra from freshwater sediments	dpm d^{-1}	^{226}Ra desorbed from fresh river water multiplied by the combined river and creek flux	3.20×10^{7}
Total ^{226}Ra inputs (excluding SGD)	dpm d^{-1}	Sum of previous 3 terms	1.48×10^{8}
Missing ^{226}Ra inputs (assumed to be SGD)	dpm d^{-1}	Mixing losses minus the other 3 identified sources	1.23×10^{9}
^{226}Ra groundwater endmember	dpm m^3	Geometric mean ± standard error all groundwater samples	396.80 ± 11.6
Total SGD	m^3 d^{-1}	Missing ^{226}Ra divided by the groundwater endmember	3.09×10^{6}
Specific SGD	cm d^{-1}	Total SGD divided by the harbour area	2.83

Table 2.4 Comparison of the estimated nutrient loads (DIN, DON and TDP) to Tauranga Harbour from SGD and river and creek discharge (in mol d^{-1}).

	Average groundwater concentration (n=22) (µM)	**SGD nutrient flux (mol d^{-1})[a]**	**SGD nutrient flux (mol d^{-1})[b]**	**Average river and creek concentration (n=6) (µM)**	**River and creek nutrient flux (mol d^{-1})**	**SGD nutrient flux[a]: River and creek nutrient flux**	**SGD nutrient flux[b]: River and creek nutrient flux**
DIN	37.7	1.17×10^5	2.19×10^4	24.1	2.35×10^4	5	0.9
DON	30.4	9.4×10^4	1.76×10^4	20.1	1.96×10^4	4.8	0.9
TDP	1.9	5.88×10^3	1.10×10^3	0.8	7.71×10^2	7.6	1.4
DIN	37.7	1.17×10^5	2.19×10^4	24.1	2.35×10^4	5	0.9

The river and creek discharge rate is the combined total calculated from Table 2.

[a] SGD calculated using the geometric mean as the endmember value

[b] SGD calculated using the maximum endmember value

2.5.3 Groundwater derived nutrient loading

Nutrient concentrations in groundwater were observed to be higher than surrounding river and streams and adjacent harbour waters (Figure 2.7). We estimated the SGD derived nutrient fluxes by multiplying the calculated SGD flux rate by the average end member concentration of DIN, DON and TDP (DOP + PO_4) (Table 2.4). The sensitivity to radium end member uncertainty was tested while holding the nutrient concentrations constant at the average values. If the radium end member concentration increases, then the SGD flux rates decrease, which means the nutrient fluxes will also decrease. We provide a range of estimates by using both the maximum and average endmember assumptions. Using the maximum radium endmember assumption to calculate the SGD flux rate the DIN, DON and TDP flux rates were 0.19 mmol m^2 d^{-1}, 0.16 mol m^2 d^{-1} and 0.01 mmol m^2 d^{-1} respectively. Considering the Harbour area at low tide (5.2 x 10^7 m^2), those fluxes would translate into 9.8 x 10^6 mmol d^{-1}, 8.3 x 10^6 mmol d^{-1}, and 5.2 x 10^5 mmol d^{-1} respectively. Using the more appropriate geometric mean as our representative radium endmember value for the SGD flux rate would result in DIN, DON and TDP flux rates of 1.07 mmol m^2 d^{-1}, 0.87 mmol m^2 d^{-1} and 0.05 mmol m^2 d^{-1} respectively. This would upscale to 5.5 x 10^7 mmol d^{-1}, 4.5 x 10^7 mmol d^{-1} and 2.6 x 10^6 mmol d^{-1} respectively to the low tide Tauranga Harbour area. To compare this contribution to river and stream inputs into the harbour we multiplied the total average fresh river end member of DIN (24.1 µM), DON (20.0 µM) and TDP (0.8 µM) concentrations by the total average discharge rate of all river and creeks (from Table 2.1). The calculated rates were 2.35 x 10^4 mol d^{-1}, 1.96 x 10^4 mol d^{-1} and 7.71 x 10^2 mol d^{-1} respectively. This demonstrates that SGD was a major source of N and P loading into Tauranga Harbour with 1 to 5 (N inputs) and 1 to 8 (P inputs) times greater than the amount delivered by the combined surface riverine inputs during the survey period (Table 2.4). Large fluxes of SGD-derived nutrients have been observed from other oceanic islands including a volcanic island in Korea (Hwang et al., 2005; Kim et al., 2011; Kim et al., 2013), the Hawai'ian Islands Maui, Moloka'i, and Hawai'I (Big Island) (Street et al., 2008), and Raratonga in the Cook Islands (Tait et al., 2014). Such large inputs may not only be significant in the context of local coastal environments but be an important source to the global ocean, continually fuelling oceanic production.

Global estimates of N inputs through SGD to coastal waters imply it may have increased from about 1.0 to 1.4 Tg of nitrate (NO_3-N) per year over the second half of the 20th century.

These SGD fluxes of N are linked to areas with high runoff and intensive anthropogenic activity on land (Beusen et al., 2013). The transport of SGD derived nitrate is an important factor for the development of harmful algal blooms in coastal waters. However, the geochemical framework of the groundwater system, land use practices and residence times must also be considered (Smith and Swarsesnki 2012; Buesen et al., 2013). The Tauranga Harbour catchment is surrounded by mostly agricultural (pastoral) and horticultural (kiwi fruit orchards) practices (White, 2005). While SGD-derived DIN has been the focus of N delivery from terrestrial systems (Rodellas, et al., 2015; Charette et al., 2001), agricultural soils, which are common on the North Island of New Zealand, have the potential to store high concentrations of DON. Little information is available on the magnitude of these DON fluxes relative to the inorganic fluxes of ammonium and nitrate (Lorite-Herrera et al., 2009). Recent studies highlight that DON may be enriched in groundwater relative to surface waters (Kim et al., 2013; Santos et al., 2013; Sadat-Noori et al., 2016). This can have implications on surrounding waters as enriched DON groundwater can be transformed to more readily bio-available nutrient forms such as ammonium through the process of ammonification in sediments. The observed TDN of groundwater consisted of almost equal proportions of DON and NO_3 with considerably more NH_4 than surrounding rivers and creeks (Figure 2.7). Due to the surrounding land use, anthropogenic loading (i.e. sewage, wastewaters, fertilizer, and agricultural manure and urine) may be the most likely source of this relatively high DON and NO_3 in groundwater. Remineralisation and recycling of estuarine organic matter in sediments may account for the higher concentrations of NH_4 in groundwater samples (Kroeger et al., 2007; Smith and Swarsenski, 2012).

The harbour was highly elevated in DON and DOP in the upper reaches of the catchment (Figure 2.3 B) surrounded by intensive agricultural and horticultural land use. DIN and PO_4 concentrations on the other hand were much lower in most of the harbour regions with a small spike observed towards the urbanised southern area. A positive relationship between the short-lived isotope tracers ^{223}Ra and ^{224}Ra with organic nutrients DON and DOP was accompanied by a negative relationship with inorganic nutrients DIN and PO_4 in the water column (Figure 2.10). DIN can be readily used by marine species in near shore waters under N-limited conditions whereas DON can remain in the system much longer and be transported to surrounding coastal waters (Kim et al., 2013). As the distance away from the harbour

mouth increases so does the surface water residence time (Figure 2.8 A & B). Increased residence times as well as nitrogen enrichments in estuarine systems have been linked to algal bloom and eutrophication events (Tomasky-Holmes et al., 2014). Our apparent radium ages were short around the upper reaches of the harbour and were associated with high radium concentrations or 'hotpsots' (89% of radium budget). This combination of low chemical residence times (assumed SGD inputs) with long surface water residence times may be a major driver of nutrient dynamics at the harbour scale and requires further investigation.

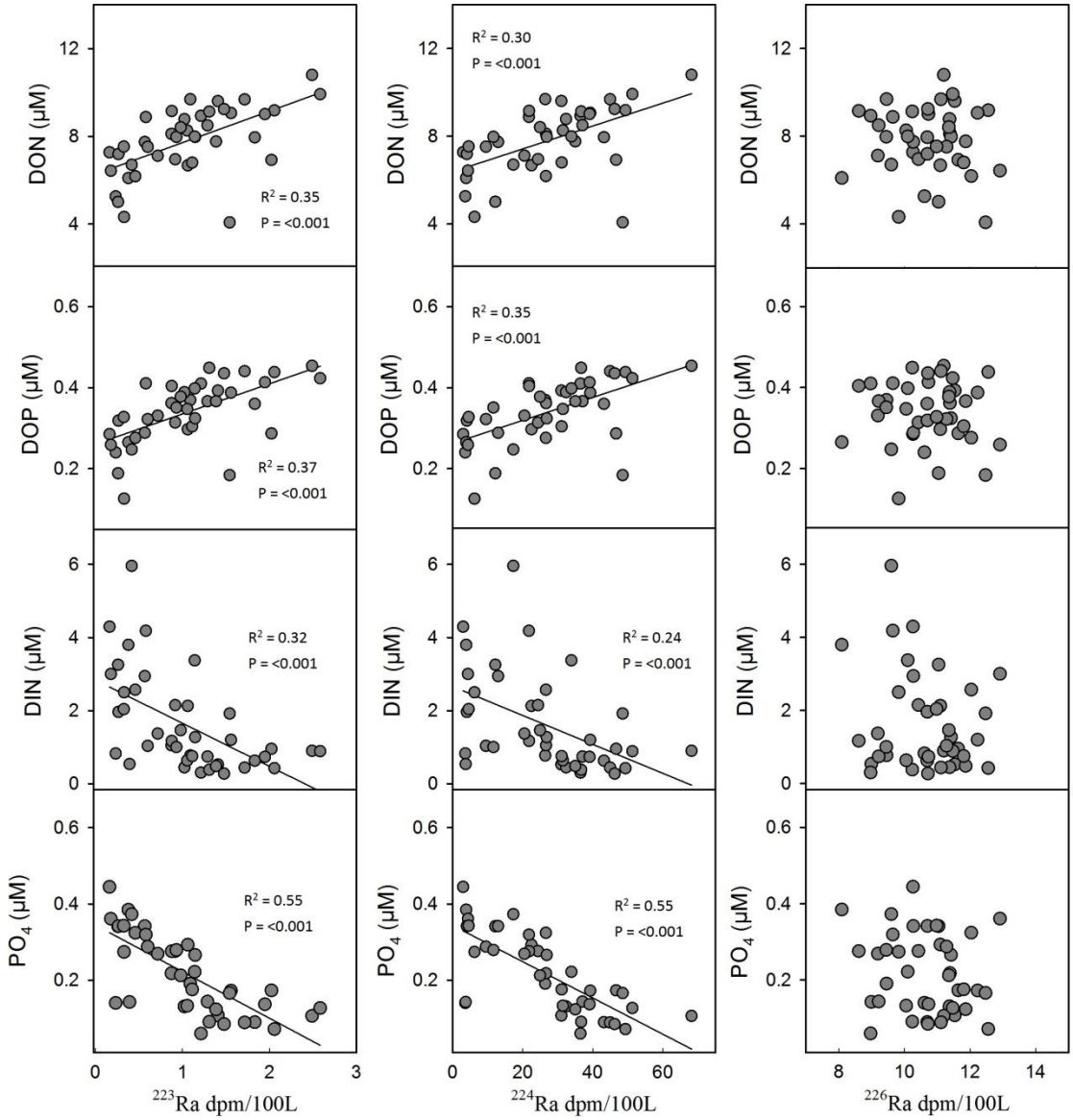

Figure 2.10 Relationship between radium isotope and nutrient concentrations in harbour water.

To better understand the influence of SGD on estuarine nutrient dynamics, bottom up (porewater/ SGD flux estimates) and top down (nutrient responses and transformations in the water column) evidence was required (Santos et al., 2014). We used N:P ratios to assess the nutrient responses in surface waters subject to SGD. The harbour had a TDN:TDP ratio of ~17:1. Algae in coastal waters typically require a N:P ratio of 16 (Redfield ratio) for their growth. Many coastal waters are characterized by an N:P ratio that is below Redfield and are thought to be N-limited (Howarth and Marino, 2006). Under these conditions biological uptake may remove a large amount of terrestrial derived NO_3 and NH_4 in harbour waters (Figure 2.3 A). The N:P ratio in observed groundwater was much higher at 36 (Table 2.2). These high N:P ratios are greatly in excess of the Redfield ratio of 16. Similarly, high N:P ratios have been observed in groundwater elsewhere, especially in agricultural areas (Buesen et al., 2013; Slomp and Cappallen, 2004; Santos et al., 2013). Since phosphorus (P) is most efficiently retained in soils and groundwater systems, SGD tends to deliver relatively higher N fluxes that increase surface water N:P ratios (Spiteri et al., 2008). We observed high N fluxes that were not accompanied by relatively high P fluxes (Figure 2.5). The large fluxes of nitrogen derived from SGD (Table 2.4) may therefore have the potential to impact nutrient ratios towards P limitation in surrounding waters. A significant finding of this study was the positive correlation observed between radium isotopes and TDN:TDP ratios in the harbour (Figure 2.11). Interestingly, no significant relationship between ^{226}Ra and TDN:TDP ratios was observed, perhaps due to the long timescales this isotope reflects. Both ^{224}Ra and ^{223}Ra reflect short timescale processes, such as tidal pumping, which occur in intertidal flats and dynamic estuarine waters. Similar comparisons and positive relationships between groundwater tracers and N:P ratios have been made from an enclosed lagoon system, USA (Su et al., 2014) and an Australian tidal creek and coastal wetland system (Gleeson et al., 2013; Santos et al., 2013). This relationship further supports the hypothesis that reactions in the subterranean estuary (facilitated by both porewater re-circulation and fresh groundwater exchange) can drive nutrient dynamics and have implications on surrounding biological communities.

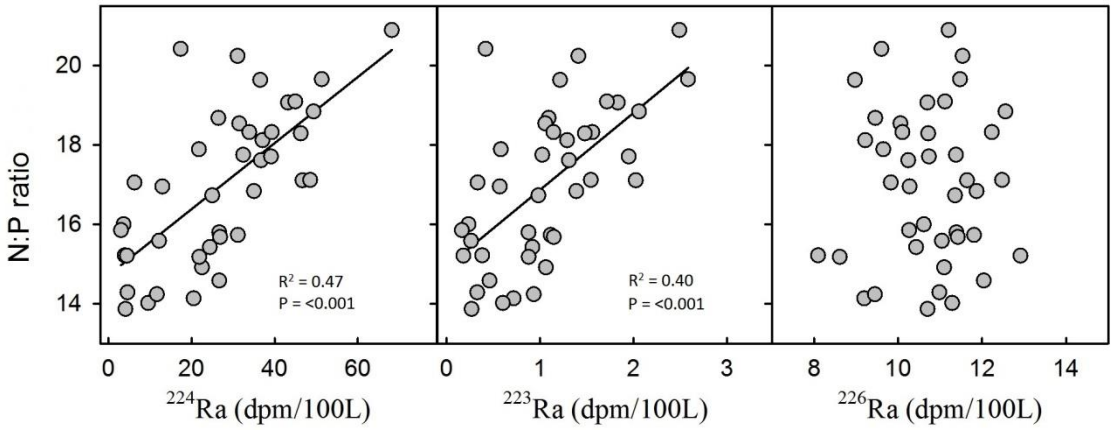

Figure 2.11 Relationship between radium isotope concentrations and N:P ratios in harbour water.

Tauranga Harbour is predominately intertidal with 66% of the harbour area with exposed tidal flats. Our tracers prevent us from separating the fresh aquifer-derived nutrients compared to those derived from sediment-surface water processes. However, studies conducted along tidal flats elsewhere have demonstrated the high productivity rates and SGD's ability to re-supply dissolved nutrients, which enhances and accelerates the array of complex biogeochemical processes (Moore et al., 2011, Beck and Brumsack, 2012; Waska and Kim et al., 2011; Santos et al., 2014). The subterranean areas of tidal flats can therefore be considered biogeochemical reactors (Beck and Brumsack, 2012). Here, we used ^{226}Ra to calculate flux rates, which would most likely capture older groundwater (Michael et al., 2011) mixed with recirculated brackish and saline waters (Kim et al., 2011). This brackish component must also be considered an important part of SGD since it can deliver regenerated DIN and DON from microbial processes in the sediment to surface waters (Kroeger et al., 2007). Previous SGD investigations in New Zealand used radon (^{222}Rn) as a natural groundwater tracer in two sub estuarine tidal flats of Tauranga Harbour to estimate porewater exchange rates and associated nutrient fluxes (Santos et al., 2014). The TDN and TDP released from porewater were found to be 1.9 and 1.6-fold higher than freshwater creek inputs. Although the spatial scale of the previous study was smaller, the relative importance of nutrient fluxes remained significant. Due to its large spatial scale, a limitation of our study was that we were not able to measure all areas at exactly the same stage of the tide. The upper region of the harbour was sampled at slack high tide compared to an ebbing tide for all other regions. Therefore, the spatial pattern would likely be more pronounced than what is represented in Figure 2.2 and Figure 2.4, because the radium and nutrient concentrations decrease toward high tide. This temporal trend has also been demonstrated in two studies in harbour sub-

estuaries Tay et al. (2012) who quantified tidal variations in nutrient concentrations and Santos et al., (2014) who quantified variations in both nutrient and radon (also a groundwater tracer). However, our results at the harbour scale show that larger scale processes can deliver large amounts of nutrients, which may be processed under a range of driving forces, such as sediment water interactions and residence times of the system.

2.6 Conclusions

This study describes submarine groundwater discharge and associated fluxes of nutrients into Tauranga Harbour, New Zealand. Naturally occurring radioisotopes including, ^{223}Ra, ^{224}Ra and ^{226}Ra revealed SGD 'hotspots' along the coastline of the mainland, particularly in the upper regions of the harbour as well as the surrounding sand barrier island. Using the ^{224}Ra / ^{223}Ra AR and ^{223} Ra /^{226}Ra AR, we calculated water mass ages of ~4.1 and ~7.8 days (average of 5 days) respectively which was within the residence time ages calculated using a numerical model (up to ~8 days, Tay et al., 2013). The Ra age models revealed younger ages in the upper harbour and older ages towards the harbour mouth. ^{226}Ra was applied to construct a mass balance and calculate SGD flux rates for the entire harbour region. SGD was estimated to be 3.09 x10^6 m^3 d^{-1}or 2.83 cm d^{-1} whereby the minimum estimate using the maximum endmember was 5.77 x 10^5 cm d^{-1} or 0.53 cm d^{-1}. These SGD rates were between ~1 and ~2.8 times the combined freshwater inputs from the surrounding rivers and streams. This demonstrated that the SGD rates to Tauranga Harbour are significant and comparable to the local river and stream inputs regardless of uncertainties in the endmember and residence time estimates. SGD derived DIN, DON and TDP fluxes were calculated to be 1.07 mmol m^2 d^{-1}, 0.87 mmol m^2 d^{-1} and 0.05 mmol m^2 d^{-1} respectively when using the most appropriate endmember (geometric mean). When upscaled to the Tauranga Harbour area, these SGD fluxes were ~ 5 times (for N inputs) and ~ 8 times (for P inputs) greater than the input from surrounding rivers and streams. A positive relationship between ^{224}Ra and ^{223}Ra concentrations and N:P ratios further support that these fluxes can have implications on the stoichiometry of Tauranga Harbour, which suffers from frequent macro-algal bloom events. These findings suggest that regional inputs of SGD from large oceanic islands should be considered as a major source of nutrients to surrounding coastal waters and global nutrient budgets.

CHAPTER 3

ENSO-driven variations in estuarine flushing revealed by Delft3D-FLOW modelling and trained artificial neural networks

Benjamin T. Stewart [a], Karin R. Bryan [a], Conrad A. Pilditch [a], Christian Winter[b] (to be submitted to *Water Research*)

[a] School of Science, University of Waikato, Private Bag 3105, Hamilton, New Zealand

[b] Institute of Geoscience, Christian-Albrechts-Universität zu Kiel, 24118, Germany

Contribution of Authors:

Numerical model development was undertaken by BTS with guidance and direction from KRB and CW. Field data used for model calibration was collected from previous studies by UW students and the POT. The BoPRC also kindly provided historical datasets. KRB provided helpful guidance with MATLAB codes and the development of a neural network. BTS wrote the initial and subsequent drafts with and my co-authors providing valuable direction and comments.

3.1 Abstract

Future changes in climate over the coming century will impact coastal systems and associated water resources. These impacts, driven by short (seconds) and long (inter-annual) time scale processes, are often studied separately. Here, we quantified estuarine flushing times between January 1995 and December 2016 in various regions of a large barrier enclosed lagoon (Tauranga Harbour, New Zealand). A numerical model was developed and was combined with machine learning techniques to 'emulate' dilution rates based on time series of historical hydro-metrological data. This approach considerably reduced computational times and matched timescales between estuarine processes and larger scale climatic drivers. Our results from a 22-year hind cast revealed the spatial variability of flushing times over short term 'event' and long range inter annual timescales. A significant relationship (r^2 = 0.43 p = <0.001) between flushing rates and the southern oscillation index supported our hypothesis that variations in climate such as the El Nino Southern oscillation (ENSO) alter estuarine functioning. ENSO events thus have direct and indirect implications for water quality by altering nutrient availability, storage, and transport across different regions. Higher loads of inorganic and organic nitrogen from surrounding water catchments combined with changes to estuarine flushing times can trigger algal blooms. Applying such data driven predictive tools to monitor and forecast water movement will be important for managing sensitive estuaries into the future.

3.2 Introduction

Estuaries form a vital connection between the land and the sea. Tidal forces, hydrological inputs (freshwater delivery) and meteorological processes (wind regimes), dominate the hydrodynamics in these systems, influencing water residence times and flushing characteristics over multiple spatiotemporal scales (Defne and Ganju, 2014). Freshwater delivery, including the effect of river flows, streams, and groundwater discharge, can substantially alter salinity gradients and supply large amounts of dissolved contaminants, including nutrients (Slomp and Campellan 2004; Sheldon 2014). Excessive anthropogenic nutrient loading into estuaries combined with poor flushing rates and longer residence times may increase primary production, resulting in eutrophication (Gonzalez et al., 2008; Savage et al., 2004). This can have cascading effects across entire ecosystems driving the development of algal blooms (Anderson et al., 2002), reducing growth or die-offs among aquatic plants (Lehtiniemi et al., 2005), degrading overall water quality (Smith & Schindler 2009), and creating hypoxic or anoxic 'dead zones' lacking sufficient oxygen to support multi cellular organisms (Chislock et al., 2013).

Changes in global climate patterns are expected to modify coastal system functioning over the next century, impacting water quality (Schindler 2006). The major inter-annual global-scale climate oscillation is the El Niño -Southern Oscillation (ENSO), with primary features of alternating warm (El Niño), intermediate, and cold (La Niña) conditions in the eastern tropical Pacific Ocean (Glantz 2001; McPhaden et al. 2006). The development of ENSO events displays a close relationship with the seasonal cycle, beginning in the austral autumn, growing during winter and spring, and reaching maximum intensity in the summer, and finally decaying rapidly during the following autumn (Timmermann et al., 2018). Teleconnections manifest in areas across the world, resulting in changes to temperature, wind and rainfall patterns (Deser et al., 2010). Studies across Australia (Chiew et al., 1998; Power et al., 2006), the South Pacific (Salinger, 2005), North America (Childers et al., 2006; Wilson et al., 2014), South America (Cai et al., 2020) and East Asia (Wang et al., 2000) demonstrate the widespread influence of ENSO, including its disturbance to regional hydrology and occurrence of extreme drought and flood events.

Climate drivers, such as ENSO, may have a unique control on the interannual flushing times within estuarine systems. While previous studies have found connections between regional rainfall and river flow patterns (Sheldon et al., 2014), direct relationships between climate signals and daily flushing rates within estuaries are challenging to determine. Coastal lagoons are generally shallow estuarine systems with flushing times and associated water quality influenced by a combination of short and long-term processes. These locations host fragile ecosystems, which are highly specialised on the local conditions. Understanding drivers of coastal lagoon flushing times under different climatic conditions, temporal scales, hydrological forcing, and wind patterns will allow management plans to target the cause of water quality issues. For example, a given catchment nutrient load can be problematic in a poorly flushed system but play a minor role in a well-flushed system (Plew et al., 2018; Heggie & Savage 2010). Establishing cause-effect relationships is essential for future water quality protocols, especially with respect to predicted changes associated with future climate scenarios.

One of the difficulties in establishing causative links is that natural processes vary on timescales from seconds to decades, making it computationally challenging to use standard numerical models to capture all the scales critically needed to test linkages between effects and climate drivers. Promising new methods involve using process-based modelling in combination with machine learning (ML) to bridge the gap in scales (Reichstein et al., 2019). Process based numerical models are used to train the ML models (creating an 'emulator'), ultimately allowing long space and time scales to be hind and forecasted (in similar way that machine learning models are currently used for long predictions, for example in shoreline modelling (Montaño et al., 2020), and water quality limits (Garcia-Alba et al., 2019).

Here, we coupled a hydrodynamic model with a dynamic emulator to determine the dominate drivers of flushing times and how these vary spatially and temporally in Tauranga Harbour, a large coastal lagoon system in New Zealand. Using a novel machine learning approach, we address the question if climate signals such as ENSO have a direct relationship to flushing times in the estuary. We hypothesise that flushing times will change in different regions of the harbour depending on the phase of the ENSO cycle. Our objectives were to (1) determine the variation of dilution rates and salinity over seasonal and event time scales, (2) predict inter annual dilution rates using a trained Artificial Neural Network (3) assess the inter

annual relationships between dilution rates, climate signals and hydro-meteorological conditions. We discuss our findings in the context of long-term climate changes, with implications to water quality and the development of algae blooms.

3.3 Methods

3.3.1 Study area

Tauranga Harbour is a barrier enclosed estuarine lagoon located on the North Island of New Zealand (Figure 3.1). The harbour is enclosed by Matakana Island, which is a large sand barrier island (25km long), resulting in two main inlets to the Pacific Ocean (north and south). This study focused on the southern basin and exchange passage, which can be considered hydrodynamically independent from the northern basin due to poor tidal connectivity and large surface area of intertidal flats (Tay et al., 2013, Spiers et al., 2009). The system has a large volume of tidal exchange and is generally shallow and vertically well mixed (Heath, 1985). The surface area and volume of the southern basin at mean high water are 115.8 km^2 and 2.7 x 10^8 m^3 respectively.

Semi-diurnal tides, ranging from 1.9m (spring) to 1.2m (neap), as well as wind speed and direction influence harbour circulation patterns. Tidal scouring has developed highly channelized currents, resulting in strong flow rates at the constriction points of the sub-estuaries and the harbour entrance (Tay et al., 2013). During the ebb tide, strong currents create a large plume of water that extends ~3.5 km out from the inlet (Spiers et al., 2009). This plume increases in width and decreases in current speed as it moves away and mixes offshore with the ocean.

The southern basin of the harbour has a total catchment area of 1300km^2, which is surrounded by predominately agricultural and horticultural land use, covering 33.7% and 5% respectively of the total catchment area (Hall, 2013). Population has been steadily increasing in the region, with Tauranga city projected to reach 164,100 in 2033 (Tauranga statistical information report, 2018). Water quality has been declining over the past few decades with increasing macro algal blooms of *Ulva* spp (sea lettuce). Higher abundance of algae biomass has been correlated with phases of El Niño, while lower abundances occur during La Niña (Park, 2011). This interannual variability was attributed to shelf upwelling nutrient inputs.

Climate conditions in New Zealand are often complex and nonlinear due to the influence of multiple air masses from three dominant directions combined with steep, variable topography (Mullan, 1996). During El Niño periods, westerly wind flows lead to less rainfall and river flow over the east coast of the North Island, while increased rainfall and flooding occur on the west coast of the South Island due to increased moisture and steep topography (Salinger & Mullan, 1999). Although the ENSO only accounts for approximately 25% of yearly variance in weather conditions across New Zealand, the impacts from an El Niño or La Niña phase can be significant, and vary depending on geographic region (Mosley, 2000).

The region of Tauranga has a temperate climate with a mean annual rainfall of ~1200 mm (Stokes et al., 2010). The wettest months are expected in winter from June to August. 'Dry spells', which are periods of fifteen days or longer with less than 1 mm of rain are common during the summer and early autumn from December to March (NIWA, 2013). The typical prevailing wind is from the west to southwest direction with an average speed of 3.3 $m.s^{-1}$ (Tay et al., 2013). However, variations and trends in the regional climate respond significantly to circulation changes in the southwest Pacific (Salinger & Mullan, 1999) including fluctuations in the values of the southern oscillation index (SOI), which is the pressure difference between Darwin, Australia, and Tahiti, and is used as a metric for measuring and predicting El Niño and La Niña events. Negative values of this index below -0.5 correspond to El Niño conditions, while positive SOI values above 0.5 coincide with La Niña episodes. These can alter the air flows to be more from the west and shelter rain-bearing winds during El Niño periods. North easterly winds bringing moist, rain bearing air from the sub-tropics, are often associated with tropical cyclones during La Niña periods (Mosley., 2000; Gordon., 1986). This can cause greater extremes and high inter-annual variability of wind, rainfall, and river flows. The Wairoa River is the largest freshwater source flowing into the harbour (~60% of surface water discharge) with nine other smaller rivers and streams making up the remaining freshwater input.

3.3.2 Numerical Modelling Approach

The hydrodynamic module Delft3D – FLOW is a multi-dimensional (2D or 3D) hydrodynamic model which calculates non-steady flows and transport processes. Delft3D – FLOW solves the Navier-Stokes equations on a staggered model grid for an incompressible fluid under the shallow water and Boussinesq assumptions. The system solves the horizontal equations of motion, the continuity equation, the transport equations for conservative constituents, and a turbulence closure scheme. Equations and modules are described in Deltares (2018a). Delft3D has been specifically developed to simulate the dynamics of complex coastal regions controlled by a wide range of physical processes. A calibrated 2D numerical domain-decomposed model was developed using Delft3D-FLOW for this study. The model determined the role of discharge, wind, and rain on flushing rates within the harbour, and later used to explain observed patterns of nutrients, salinity, and groundwater. A dynamic emulator approach, trained on Delft3D model output, was then used to hind cast conditions over inter annual time scales, needed to explore relationships to climate patterns.

The modelling domain was divided into three nested depth-integrated model domains of decreasing resolution: inside the southern basin of Tauranga harbour; outside the harbour; and thirty kilometres offshore into the Pacific Ocean (Figure 3.1). The largest domain was needed to reach open ocean conditions because of the poor availability of information on shelf salinity variations needed to force the inner models. Sensitivity tests (discussed later) were used to justify a depth-integrated approach. The large domain had a low grid cell resolution of 500 $\times$ 500m, covered the coastal ocean off Tauranga harbour and consisted of three open ocean boundaries. Five harmonic tidal constituents (K1, O1, M2, N2, S2), derived from the NIWA national computer tide model (Walters et al., (2001), were applied to generate the astronomic tidal forcing at these boundaries. A water level boundary was used, which was determined by the amplitude and phase of the major tidal constituents, obtained from the NIWA tidal model. A reflection parameter (alpha) value of 50 was applied to the north and south boundaries to dampen instabilities at the start of the simulation. To ensure numerical stability and continuity at the domain boundaries a smaller offshore domain with a grid cell resolution of 100$\times$100m was chosen as an intermediary to connect the coarser grid sized offshore domain, with the refined inner harbour domain. This domain, which covers the southern basin of Tauranga Harbour, was chosen to have the highest grid cell resolution of

20×20m. This allowed more detailed hydrodynamics to be resolved by the model, including complex channel networks and shallower intertidal areas at the harbour scale. This domain was forced by the water level conditions generated from the offshore grids as well as 10 individual discharge points, which represented the main river and creek flow inputs into the southern basin of the harbour (Figure 3.2).

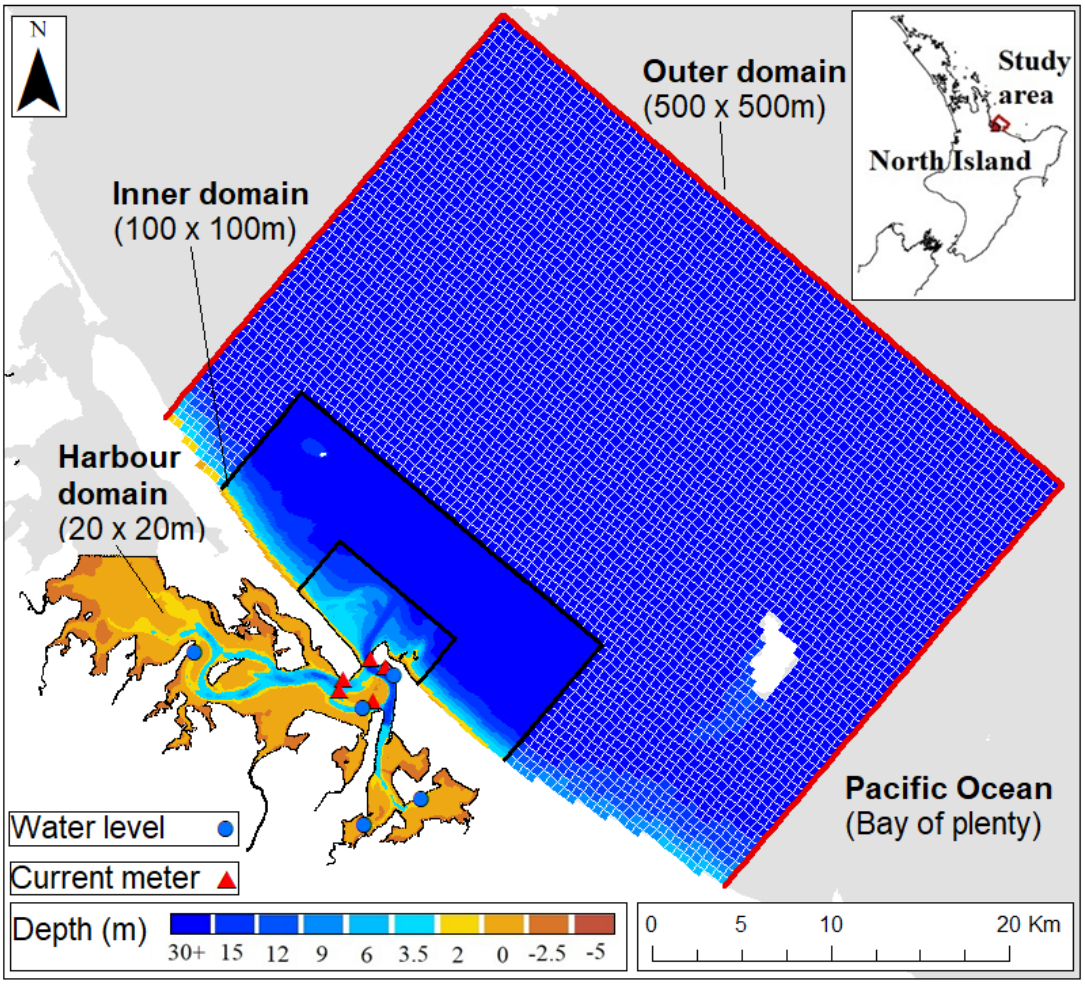

Figure 3.1 Hydrodynamic model gird and locations of water level recorders and current meters used for calibration/validation.

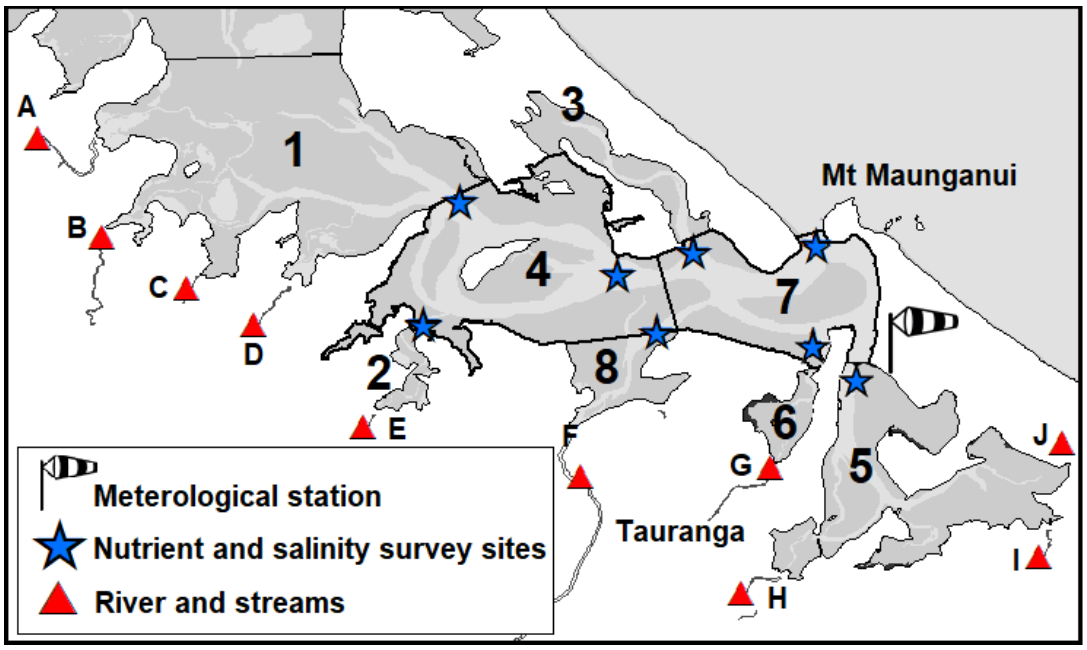

Figure 3.2 Study area including harbour regions, water quality sites, river locations and meteorological station used to derive wind data.

The model bathymetries for each domain were assembled by interpolating measured data of seabed elevations onto regular orthogonal grids. Offshore grids were interpolated using LINZ hydrological charts, NZ 541, and NZ 5411, 2016. The harbour domain was assembled with bathymetry prepared using a combination of data from multiple sources: including, Multibeam, LiDAR (Light Detection and Ranging) and LINZ hydrological charts NZ 5411, 2016. These were converted from chart datum (lowest astronomical tide) to mean sea level after interpolation by adding a uniform value of 1.05 m to the data.

Continuous flow data provided by the Bay of Plenty Regional Council (BoPRC) were used to create a timeseries of discharge for four of the major rivers (Wairoa, Waimapu, Kopurererua, Waipapa). These were input as a daily average rate in m^3/s. Flow at the remaining six river and creek systems was only sparsely measured (Waitao, Aongatete, Rocky stream), or the streams were ungauged (Te Puna, Apata, Wainui). Due to the similarity in the land usage, soil types and rainfall across the catchments, a regression model was created to predict the discharge rates for these freshwater inputs, using data from the continuous and sparse sites as input and output. Daily time series for the sparsely measured sites were reconstructed by applying a regression-based correction to discharge measurements at the gauged sites (Appendix C). For the sites with no measurements, a relationship between

discharge and catchment size (developed using all available data) was used to determine which of the gauged catchments to use as a proxy.

Meteorological conditions of wind, rainfall and evaporation were input uniformly over the harbour domain as a timeseries. Data were obtained from the Tauranga aero weather station (AWS) (Figure 3.2) extracted from the NIWA Cliflo database. Wind data were input hourly as speed (m^3/s) and direction (°) while rainfall and evaporation (assuming open water conditions) were input as an additional parameter with a constant hourly rate in millimetres (mm) based on the daily average recording.

3.3.3 Model calibration and validation

Time series data from available water level and current gauges in the study area were compared with model simulations over the same time periods. Water level data were provided by the BOPRC, and the Port of Tauranga, while current speeds and direction were provided by a harbour survey conducted in March 2017, by the Port of Tauranga and University of Waikato. The model was calibrated by adjusting the eddy viscosity value and Chézy friction coefficient value ($m^{1/2}/s$), which represents the total bed roughness, where spatially varying bottom roughness was used. Calibration resulted in a Chézy of 75 $m^{1/2}/s$ assigned for deep channels and 35 $m^{1/2}/s$ for shallow intertidal areas. The model was run for a calibration period of 15 days to cover a complete spring – neap cycle between the 8th – 23st of March 2017 to match with collected field data. This was then validated over another 15 days to cover a neap-spring cycle between 24th of March – 8th April 2017. Being a tidally dominated system, capturing and calibrating to these tidal variations was important to adequately cover the fundamental driver of hydrodynamics in the estuary (demonstrated later). All river and creek discharge points were assigned the average annual flow rates during the calibration and validation periods (salinity was not calibrated but verified with the seasonal runs discussed in the next section). Multiple statistical analyses were carried out to assess the bias, accuracy and skill between the datasets and the performance of the model. This included the $Bias_a$ (m), Mean absolute error (MAE), Root mean square error (RMSE), and Brier Skill Score (BSS) (Sutherland et al. 2004) which are summarised in Table 3.1. A BSS score of 1 is considered a perfect match between the model and measured data whereby zero and negative values indicate that the model has little to no predictive skill. An excellent score is

above 0.65, very good for 0.65 - 0.5, good for 0.5 – 0.2 and poor for less than 0.2 (Allen et al. 2007; Ralston et al. 2010; Sutherland et al. 2004). Our model had skill scores in the excellent range for all parameters over both the calibration and validation period. More information on the model setup parameters and model calibration can be found in Appendix C and Appendix D.

Table 3.1 Calibration and validation statistics for model. Values are based on the average of five separate water level and current meter locations to give an overall skill score. A full summary of model calibration can be provided with attached supplementary material.

Period	Parameter	Statistics			
		Bias	MAE	RMSE	BSS
Calibration (08.03.2017 - 23.03.2017)	Water levels	0.04	0.12	0.15	0.91
	Current velocity	0.03	0.09	0.11	0.72
Validation (24.03.2017 - 08.04.2017)	Water levels	0.09	0.13	0.16	0.92
	Current velocity	0.03	0.09	0.13	0.74

3.3.4 Salinity and transport model scenarios

Multiple scenarios were defined to investigate the seasonal and climatic controls on the hydrodynamics, flushing times, and salinity of the harbour (summarised in Table 3.2). Seasonal runs were run to simulate a period where salinity surveys were available, and climate runs were based on various stages of the ENSO cycle. These runs were used to train an emulator, which was used to reconstruct a 22-year hind cast of dilution rates (as a measure of flushing time).

Seasonal:

The seasonal scenarios were simulated from July 2012 – June 2013 to match the availability of the existing seasonal surveys of salinity and nutrient data in the harbour between 18/7/2012 and 6/6/2013 (Port., 2016) (Figure 3.2). Water samples for nutrient analysis of Dissolved Inorganic nitrogen (DIN), Dissolved Organic Nitrogen (DON), Dissolved Inorganic Phosphorus (DIP), Dissolved Organic Phosphorus (DOP) were taken at depths up to 1 m from the surface, while salinity profiles were taken with a calibrated conductivity, temperature and depth sensor (CTD), the resolution depending on depth and site location. Nutrient and salinity samples were taken at ebb and flood stages of the tide at the main harbour entrance and from locations capturing the distinct upstream subregions, sub

estuaries, deep central channels (Figure 3.2). A salinity gradient between the upper and lower regions of the harbour can also occur and is affected by discharge events from the major rivers (Tay et al., 2013).

The initial conditions were established by creating spatially varying salinity map files based on measured data for the earliest survey. Offshore salinity conditions for forcing the seaward boundary of the model were based on data collected from three separate observational profiles (up to 2000 m depth) from a nearby ARGO drifter sensor (D5904537), which visited the offshore boundary waters between 19/8/2014 – 17/4/2015. Historical offshore transects (~100 survey sites between -36.503049°, 176.242501° and -37.450446°, 177.996782°) up to 200km offshore and time series of CTD measurements between 1982 – 2016 were also provided by NIWA (Bell & Chiswell, 2017 pers. comm.). These measurements were combined to provide an estimate of average seasonal variations of salinity of open ocean water in the Bay of Plenty, which ranged from ~34.5 – 35.6. River discharge, rainfall and evaporation were input into the model as a timeseries file to replicate the conditions of the modelled time period. Wind forcing (spatially uniform speed and direction across the domain) was also applied to the model.

Climate extremes:

Further simulations were run to investigate the effect of anomalous climate conditions on wind, river discharge and rainfall, typical of El Niño and La Niña events. To avoid the difficulty of recreating typical synthetic discharge and wind events (e.g., creating realistic sequencing, Daly et al., 2014), we instead used real timeseries to recreate the conditions. Using constant discharge and winds can result in quite unnatural outcomes and problematic consequences (for example, the wind setting up a constant recirculating flow). We assessed monthly averaged southern oscillation index values from the years 1995 – 2016 to determine when significant El Niño and La Niña phases occurred. Indices for summer (December, January, and February) and winter seasons (June, July, August) were ranked to determine years that were associated with moderate to strong El Niño and La Niña phases. Moderate values were < -1 and >+1. Strong to extreme phases occurred when values were < -2 and >+2. Simulations were then conducted for years displaying a strong SOI for both El Niño and La Niña summer and winters. Simulations were hydro-meteorologically forced with historical time series of

wind speed, wind direction, rainfall, evaporation, and discharge corresponding to 90 days of 4 strong ENSO phases (total of 360 days).

Table 3.2 Summary of modelled scenarios.

Scenario	Time Period	Description
Seasonal		
1	07/2012 – 09/2012	Winter /spring
2	09/2012 – 12/2012	Spring/summer
3	12/2012 – 02/2013	Summer
4	02/2013 – 04/2013	Summer/Autumn
5	04/2013 – 06/2013	Autumn/Winter
Climate extremes		
1	12/1997 – 02/1998	El Niño (summer)
2	12/2010 – 02/2011	La Niña (summer)
3	06/1997 – 08/1997	El Niño (winter)
4	06/2010 – 08/2010	La Niña (winter)

3.3.5 Calculation of harbour flushing times

To calculate the flushing times of the harbour, we conducted simulations using passive neutrally buoyant conservative tracers. Quantifying flushing time from tracers allowed the mixing of multiple water masses and tidal oscillation patterns to be accounted for at the system scale. All simulations were done using the water quality module Delft3D-WAQ, which coupled together the hydrodynamic outputs from Delft3D-FLOW. D-WAQ is a multi-dimensional water quality model framework. It solves the advection-diffusion reaction equation on a predefined computational grid for a wide range of model substances (Deltares, 2017). D-WAQ makes use of the hydrodynamic conditions (velocities, water elevations, density, salinity, vertical eddy diffusivity) calculated in the Delft3D–FLOW module. Clusters of the finer hydrodynamic grid cells from the Delft 3d-FLOW model were merged using DIDO, a grid aggregation program, to create larger aggregated volumes for Delft3D-WAQ simulations. After a suitable spin up time of approximately 3 days, tracers were released into the harbour domain. All cells within the harbour were uniformly set to an initial concentration value of 1 gm^{-3} and released at high water on a neap tide. This ensured all areas within the harbour were covered with water at the release time but not overestimated. Areas outside the harbour,

freshwater sources, and oceanic boundaries ('new' water) were all set with a tracer concentration of 0 $g.m^{-3}$. The e-folding flushing time was then calculated by fitting an exponential curve to the tracer concentration over the time period until the concentration reached 1/e (37%) of the initial tracer. This means that only 63% of tracer was removed from the cell/area and was not completely flushed. Therefore, the flushing time reflects the average amount of time the tracer spends in the cell, often referred to as the average residence time (Monsen et al., 2002; Sheldon and Alber, 2002). We calculated flushing times within 8 harbour sub regions (Fig.1B). The sub-regions were defined based on circulation patterns and constriction points around sub-estuaries to be consistent with earlier work (Tay et al., 2013, NIWA 2009). Estimated flushing times were also verified with earlier models of the harbour (Tay et al., 2013, A. Port., 2016). Tracer concentration in each cell was averaged over the area of the defined sub regions for each time step. The flushing times were then derived as the time for tracer concentration in that sub region to fall below 1/e (37%). The total flushing time for the entire harbour was taken as the average of these 8 individually calculated sub regions. The dilution rate then was calculated by rearranging:

$$C = C_O \times e^{-kt}$$

Equation 3.1

where C is concentration at time (t), C_0 is the initial concentration and k is the dilution coefficient. To clarify the terms of flushing times and dilution rates, a definition of key terms is presented in Table 1.1.

3.3.6 Neural network model for predicting harbour dilution rates

To predict daily harbour dilution rates over the interannual timescales needed to assess the role of climate drivers, we developed a supervised artificial neural network (ANN) which we trained on the 'climate' and the 'seasonal' suite of model runs. These models, which are inspired by the functioning of a human brain, have been increasingly used across multiple fields as a powerful predictive tool in complex, nonlinear systems (Hsieh & Tang., 1998; Thrush et al., 2008; Goldstein et al., 2019). Here, we have structured our ANN to consist of an

input layer with six variables, a single hidden layer, containing between three to twelve nodes (or 'neurons') and a single output layer resulting in a final prediction (Figure 3.3). Input variables selected for the ANN included, high tide and low tide water level values, wind speed and direction, river discharge and rainfall. Outputs of daily dilution rates from 23 modelled Delft 3D scenarios, which covered a period of approximately 22 months in total (~29 days per scenario) were used as training data. This allowed the network to learn how the variables effect the system behaviour, resulting in biases and weights used for its calculations (Olden & Jackson., 2002). To generate sufficient data to train the model, tracer dilution rates were calculated between two consecutives low (or high tides), resulting in 13668 data points over the 22-month training dataset. This dataset was then divided into training and validation, the latter which was used to assess the performance of the ANN's predictions, with the goal of minimising the difference in performance between the training and validation set. A feed-forward network using one hidden layer and the Levenberg-Marquardt backpropagation algorithm was used (van Maanen., et al. 2010). Adding neurons into the hidden layer improve the ability of the network to solve for more complicated problems, but over-training can decline the performance and predictive power (van Maanen., et al. 2010). An automated early training stop technique was used when performance did not improve to avoid any overtraining. Adding a time lag to input variables can also lead to better predictions in dynamic systems which may be auto correlated. For example, the effect of a major discharge event on dilution can build over several tidal cycles. Incorporating the previous two days input values for our system, provided the best predictive outcome. In the models with the highest r-value and lowest bias across training, validation and test data were used for the final predictions.

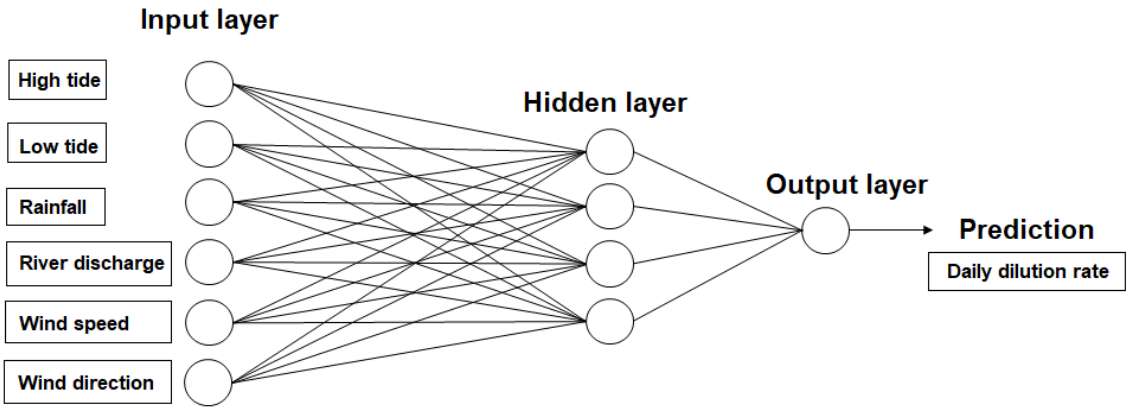

Figure 3.3 Neural network setup and architecture.

3.4 Results

We present our results as 1) process-based model validation against salinity, calculated flushing times over seasonal scenarios and calculated tidal dilution rates. 2) Seasonal nutrient variations from a historic dataset 3). Neural network validation to process based model, including hindcast results and finally 4). The correlation between interannual dilution rates and the Southern Oscillation Index (SOI).

3.4.1 Process based model validation

The measured salinity values in Tauranga Harbour had a greater spatial range during winter (21.9 – 34.2) compared to summer (31.8 -34.8), with the lowest mean (27.5) at ebb tide in winter 2012 (Figure 3.4). Salinity maximums were measured during autumn 2013 (35.1) and minimums in winter 2012 (21.9). The influence of seasonal freshwater inputs from land are reflected in the lowest salinities being measured at ebb tides, with large variations (range = 21.9 - 33.1) across harbour regions in the winter and spring periods (Figure 3.4).

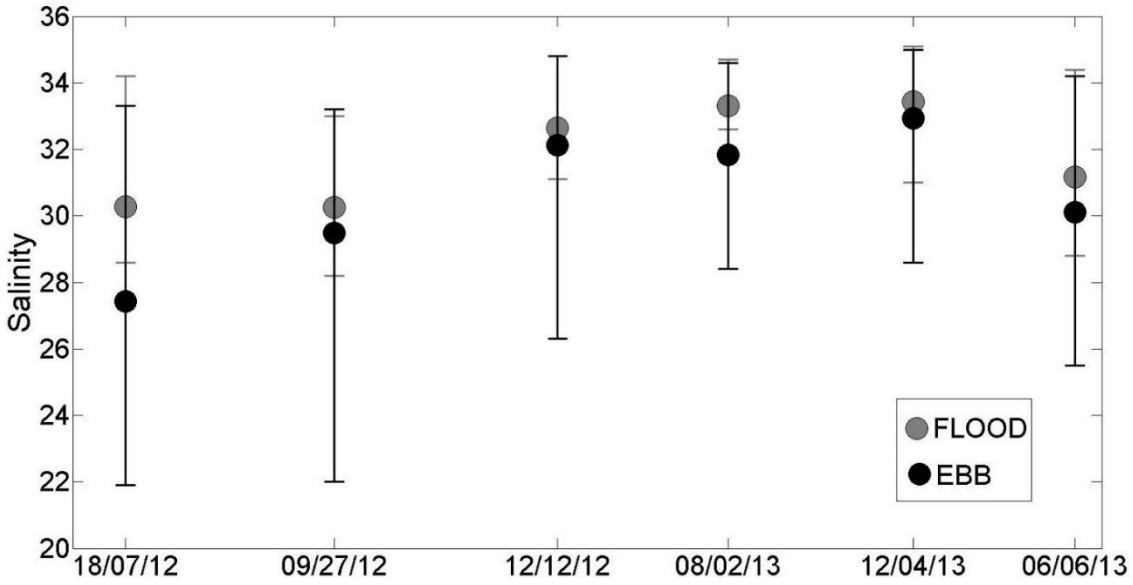

Figure 3.4 Measured salinity averaged across all regions in Tauranga harbour between 18/07/2012 - 6/6/2013. Error bars represent the maximum and minimum salinity range between the 8 regions on the sampling date.

The model was able to reproduce observed salinities across the seasonal scenarios (Figure 3.5). The model generally reproduced observed salinities within a smaller cluster range of 32-35 during the summer and autumn scenarios. This was compared to the spring and winter scenarios, where salinity had a higher variability (29-34) across the different sites (Figure 3.5). The region with the largest error in tidal fluctuations and variability in the model was region 8 (Wairoa River region), where the model under predicted the salinity by ~5 in winter and ~10 in autumn. During the summer and autumn scenarios, salinity was mostly over predicted in the model by 1–~3. Areal comparisons of the annually averaged observed and predicted salinity levels are also illustrated (Figure 3.6).

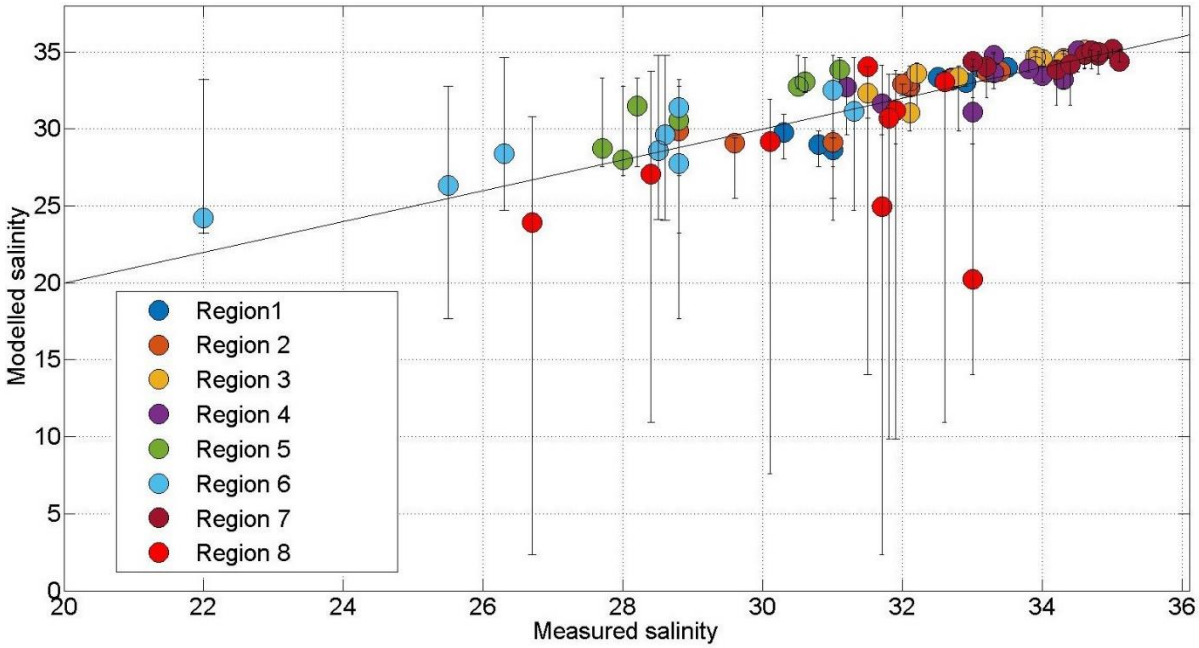

Figure 3.5 Comparison between the measured and modelled salinity in Tauranga harbour. Error bars represent low tide and high tide variability in modelled salinity before/after measurement was taken. The black line represents a 1:1 match.

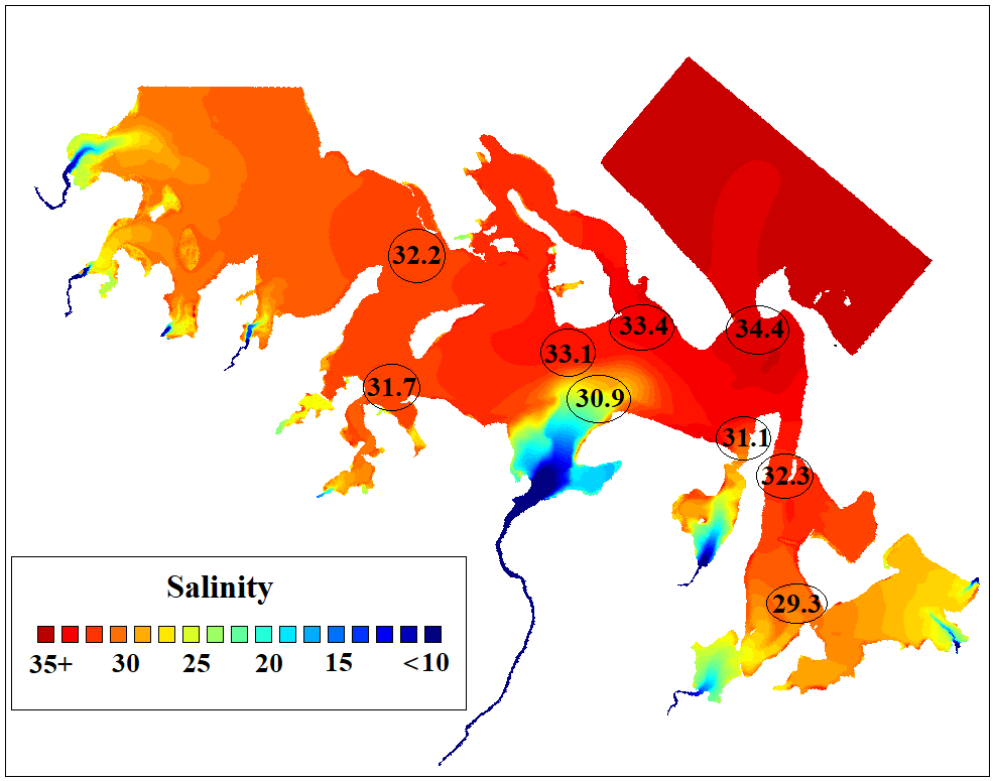

Figure 3.6 Annual average of modelled salinity (shading) and measured salinity (values inside black circles).

The longest flushing times across all seasonal scenarios were observed in region 1 (mean of ~15 days) and 5 (mean of ~ 9.6 days). These regions are the furthest away from oceanic and/or significant river influences. The harbour mouth (region 7) and Wairoa River (region 8) had the shortest flushing times, ranging from 3.0 to 4.4 days respectively (Figure 3.7). The average flushing time amongst all regions and scenarios was 8.3 days, which was ~3.5 days longer than a previous numerical model of the harbour based on idealised scenarios (Tay et al., 2013). Tracer concentrations over time for all harbour regions are shown over a summer scenario (Figure 3.8). The flushing time of tracer concentration varied spatially across the different harbour regions. Regions 6, 7 and 8 reached the 0.37 e-folding threshold most quickly within <4 days (Figure 3.8). Regions 1, 2 and 5 flushed more slowly with tracer concentration taking >18 days to reach the threshold. These patterns in tracer dilution were typical over all simulated scenarios.

The dilution rates showed little variability between high tide and low tide in region 1 and 3 (Figure 3.9). Regions close to the Wairoa River (region 8) and Harbour mouth (region 7) showed large variabilities in the dilution rate between tidal cycles over time due to the proximity of freshwater inputs and faster tidal currents.

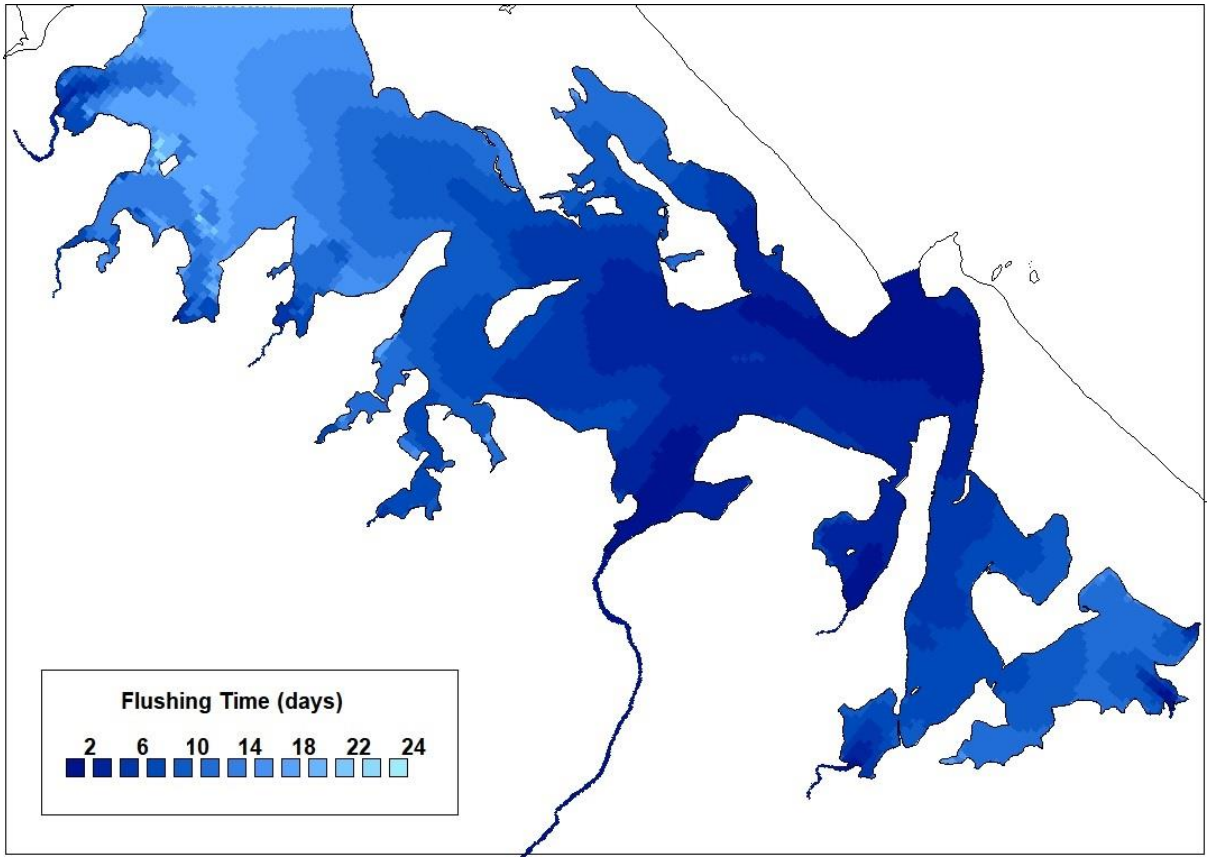

Figure 3.7 Average flushing times of Tauranga Harbour (Average derived over 5 seasonal scenarios).

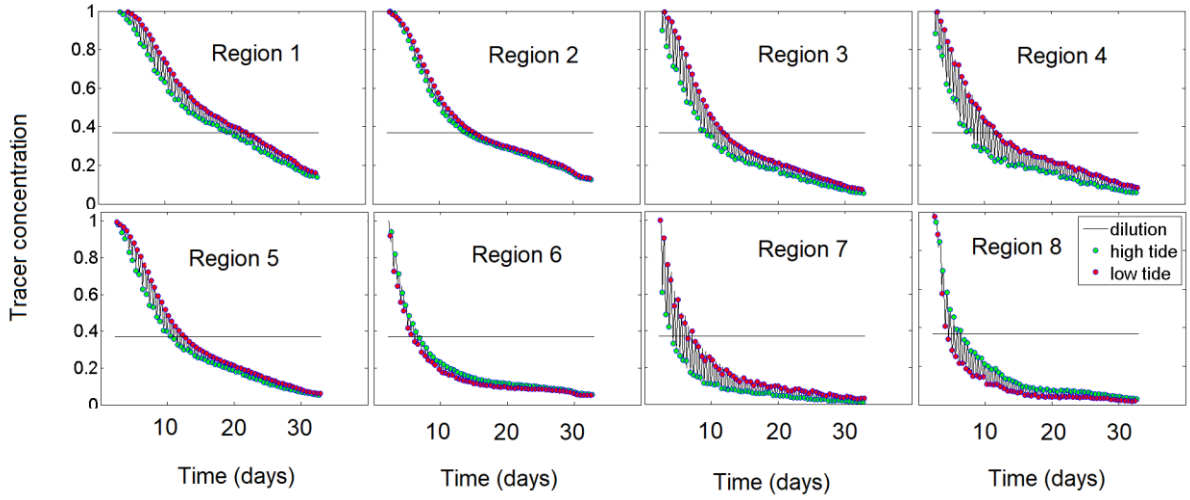

Figure 3.8 Dilution of tracer concentration over time for harbour sub-regions. Red circles represent concentration at high tide and green circles represent concentration at low tide. Black line represents the e-folding threshold (37% of initial tracer concentration). Region is considered flushed once falling below this line.

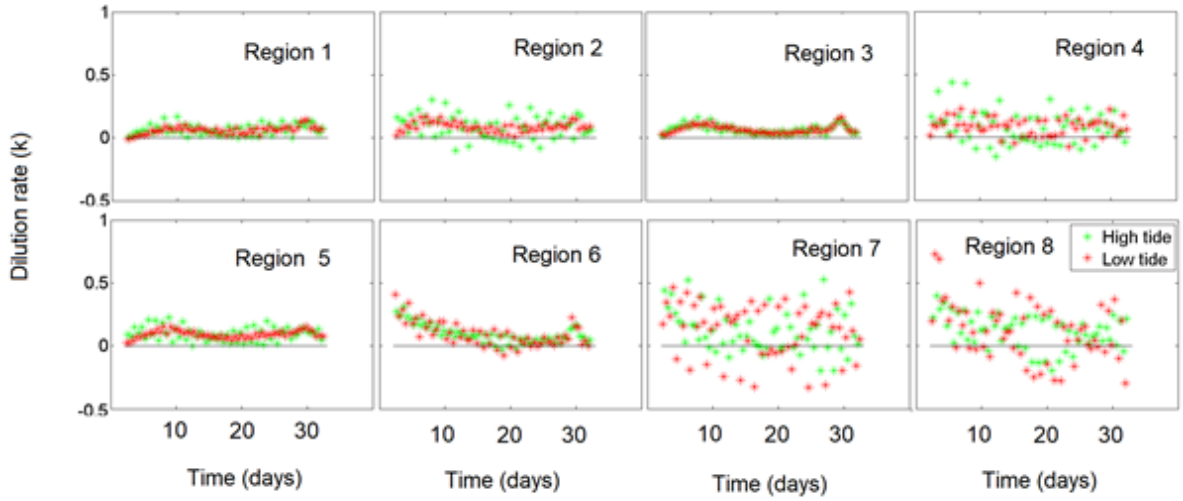

Figure 3.9 Calculated dilution rates over time for high and low tide. Red markers indicate the dilution rate at high tide and green markers indicate the dilution rate at low tide.

3.4.2 Nutrient variations in historic dataset

Dissolved inorganic nitrogen (DIN) had the highest mean (8 µM) and greatest range of concentrations across harbour regions (max of 19.8 µM and a min of 2.8 µM) when sampled in winter 2012 (Figure 3.10 A; Port., 2016). The lowest mean concentration of DIN (1.5 µM) was recorded in summer 2013 and also had a lower range of ~4 µM across all regions. Dissolved organic nitrogen (DON) has the highest means across the summer months of 2012 and 2013 (Figure 3.10 A) and broadest spatial variability (~10 µM). Concentrations of dissolved inorganic phosphate (DIP) and dissolved organic phosphate (DOP) varied the most across all harbour regions during summer 2013 with a range of 0.4 µM and 0.65 µM respectively (Figure 3.10 B). The mean DIP was highest in the winter of 2012 (0.25 µM), while the mean DOP was highest in summer of 2013 (0.33µM).

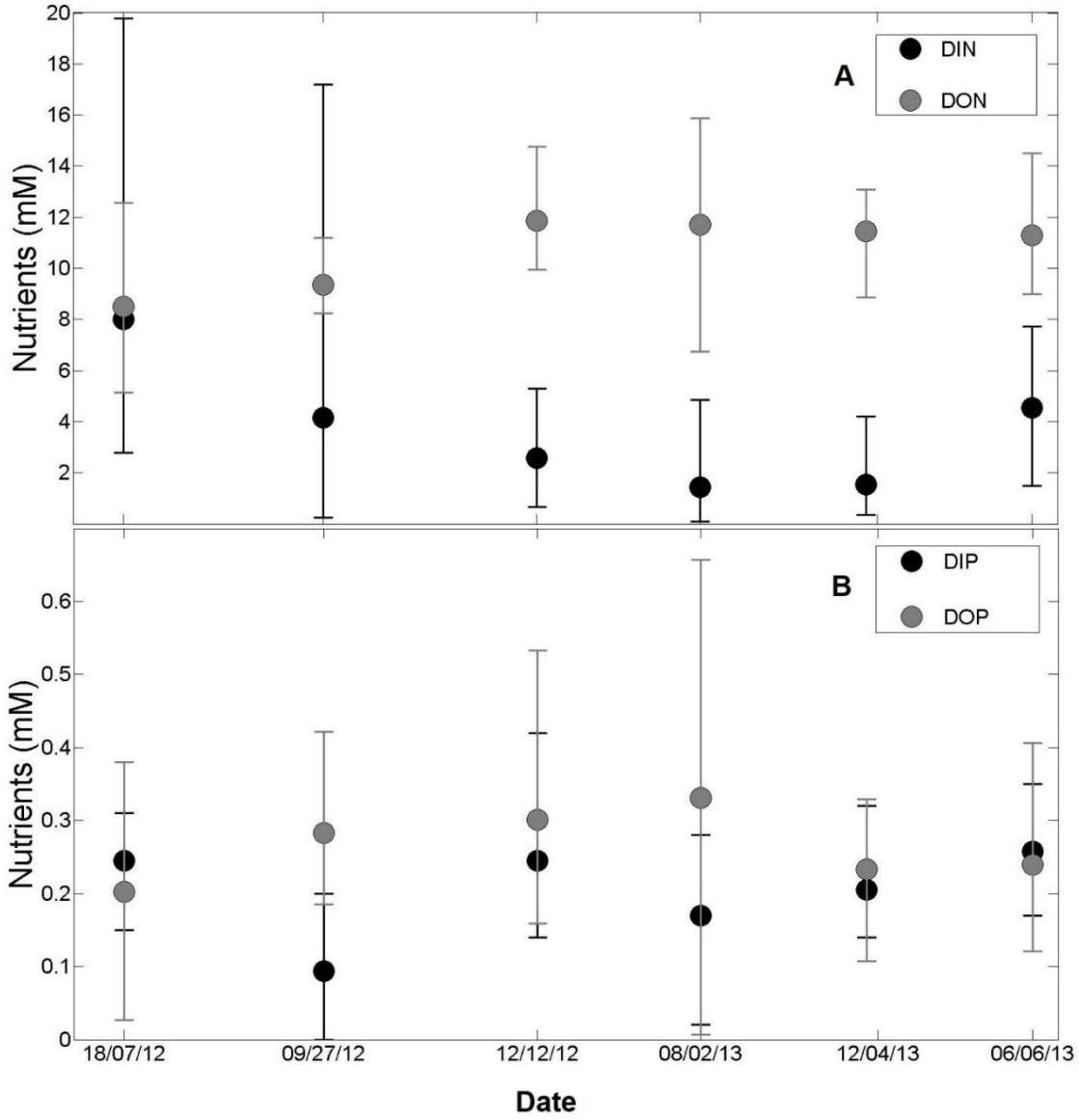

Figure 3.10 (A). Measured dissolved nutrient concentrations averaged across all regions in Tauranga harbour between 18/07/2012 - 6/6/2013 as sampled by A. Port., 2016. A) Dissolved inorganic nitrogen (DIN) and dissolved organic nitrogen (DON). B). Dissolved inorganic Phosphorus (DIP) and dissolved organic phosphorus (DOP). Error bars represent the maximum and minimum concentration between the 8 regions on a sampling date.

3.4.3 Neural network model validation

The daily dilution rates predicted using the ML emulator between January 1995 and December 2016 confirmed large spatial variability (Figure 3.11). As with our training datasets, regions 7 (harbour mouth) and 8 (Wairoa River) showed the most variability in the probability of dilution rates. Regions 1,3,4,5 had more leptokurtic distributions around a dilution rate of 0.1 d^{-1}. Regions 2 and 6 (Te Puna and Waikareao sub estuaries) showed more variability than

the other sub estuarine regions in the harbour. Region 8 often had negative rates, which meant that tracer concentration increased locally between subsequent tidal cycles. This occurred when higher concentration water masses were advected into the river region (for example from the poorly flushed upper reaches of the estuary). Region 7 had markedly higher dilution rates compared to other sub estuarine regions, which is accounted for by the very large volume exchange across the entrance at each tidal cycle. Tidal range was the most important contributor across all regions, particularly in central parts of the harbour, including regions 7, 4, and 3. Removing tide in these regions resulted in a loss of up to 63% of the predictive power. Rainfall and discharge were observed as important contributors to the calculated dilution rates, particularly in regions close to freshwater inputs such as region 1, 5, and 8. Wind had the lowest influence on dilution and did not result in significant changes in predictive power if excluded.

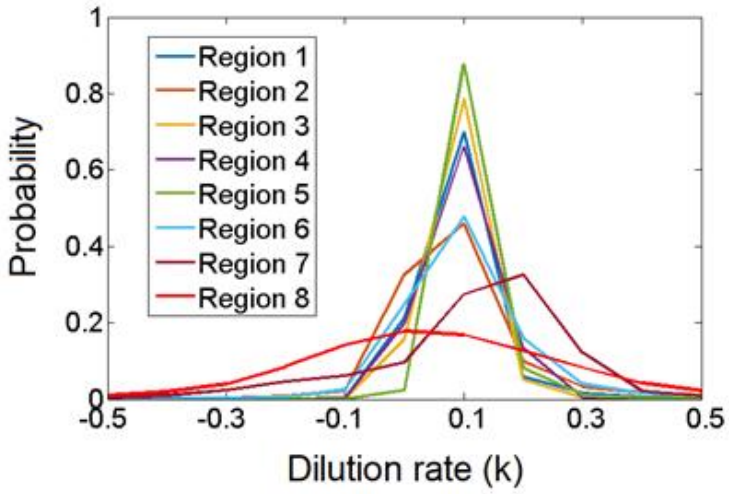

Figure 3.11 Probability density function (PDF) of predicted inter annual dilution rates (k / d^{-1}) for all harbour regions.

3.4.4 Inter annual dilution rates and southern oscillation index

The mean annual dilution rate for the whole harbour was compared with the Southern Oscillation Index (SOI) between 1995/96 to 2015/16, showing a significant relationship (r^2 = 0.37 p =0.003) (Table 3.4). However, due to the anomalous nature of El Niño and La Niña events resulting in extreme values in drivers, averaging may not always provide the best

indictor. We observed a stronger relationship ($r^2$0.43 p =0.001) between dilution rates and the SOI using the monthly maximum values (instead of averages), and so maxima were used for further analysis. Years which were in La Niña phases were observed to have the highest annual dilution rates, with the 1998/99 and 2010/11 years having annual dilution rates of 0.6 d^{-1} and 0.55 d^{-1} respectively. Years of El Niño had lower annual dilution rates which did not exceed an annual dilution rate of 0.4 d^{-1} over the 22 years (Figure 3.12). During neutral SOI phases, dilution rates varied with the highest and lowest annual rate occurring over the 2001/02 and 1996/97 periods, respectively. The relationship between the annual dilution rates and SOI also varied spatially within the harbour sub regions. The regions with the strongest relationship to the SOI using the maximum dilution values were region 1 (r^2 = 0.43 p =0.001), region 6 (r^2 = 0.45 p =<0.001), region 7 (r^2 = 0.50 p =<0.001) and region 8 (r^2 = 0.39 p =0.002) (Table 3.3). These sub regions highlight important areas of the estuary with proximity to major river sources (regions 8 and 6) and covering large surface areas of the harbour (regions, 1 and 7). A weaker seasonal relationship (r^2 = 0.30 p =0.01) was also observed between the summer maximum dilution rate for the entire harbour and the preceding winter SOI (i.e., mean SOI from two seasons before).

Table 3.3 Correlation between dilution rates and (1) the interannual SOI, (2) discharge events. Also presented in (1) is the correlation between annual SOI and river discharge and rainfall.

(1) Annual SOI					
	R^2	**P value**	**Slope coeff**	**SE**	**tstat**
Dilution rates (annually averaged monthly maximums)					
Entire harbour	0.4264	0.0013	0.0703	0.0187	3.7585
Region 1 (Upper)	0.4349	0.0011	0.0301	0.0079	3.8243
Region 2 (Te Puna)	0.1628	0.0698	0.0435	0.0226	1.9219
Region 3 (Inside Matakana)	0.2414	0.0237	0.0112	0.0046	2.4586
Region 4 (Mid region)	0.1045	0.1528	0.0051	0.0034	1.4894
Region 5 (Welcome bay)	0.2219	0.0311	0.0263	0.0113	2.3281
Region 6 (Waikareao estuary)	0.4457	0.0009	0.0456	0.0117	3.9087
Region 7 (Harbour mouth	0.5041	0.0003	0.0505	0.0115	4.3952
Region 8 (Wairoa river)	0.3941	0.0023	0.3811	0.1084	3.5158
Dilution rates (annually averaged monthly means)					
Entire harbour	0.3705	0.0034	0.0059	0.0018	3.3441
Region 1 (Upper)	0.3259	0.0069	0.0035	0.0012	3.0309
Region 2 (Te Puna)	0.0964	0.1707	0.0064	0.0045	1.4238
Region 3 (Inside Matakana)	0.0048	0.7653	-0.0003	0.0010	-0.3029
Region 4 (Mid region)	0.0097	0.6714	0.0004	0.0009	0.4309
Region 5 (Welcome bay)	0.0712	0.2423	0.0017	0.0014	1.2069
Region 6 (Waikareao estuary)	0.2868	0.0124	0.0051	0.0018	2.7638
Region 7 (Harbour mouth)	0.3599	0.004	0.0068	0.0021	3.2686
Region 8 (Wairoa river)	0.4088	0.0018	0.0388	0.0107	3.6243
River discharge (annual monthly mean)	0.4784	0.0005	2.7322	0.6544	4.1749
High discharge events (mean annual frequency)	0.3588	0.0041	6.0480	1.8549	3.2606
Rainfall (mean annual totals)	0.2990	0.0100	154.5040	54.2750	2.8467

(2) Discharge events (annual frequency)					
	R^2	**P value**			
Dilution rates (annually averaged monthly maximums)					
Entire harbour	0.4298	0.0013	0.0070	0.0018	3.7846

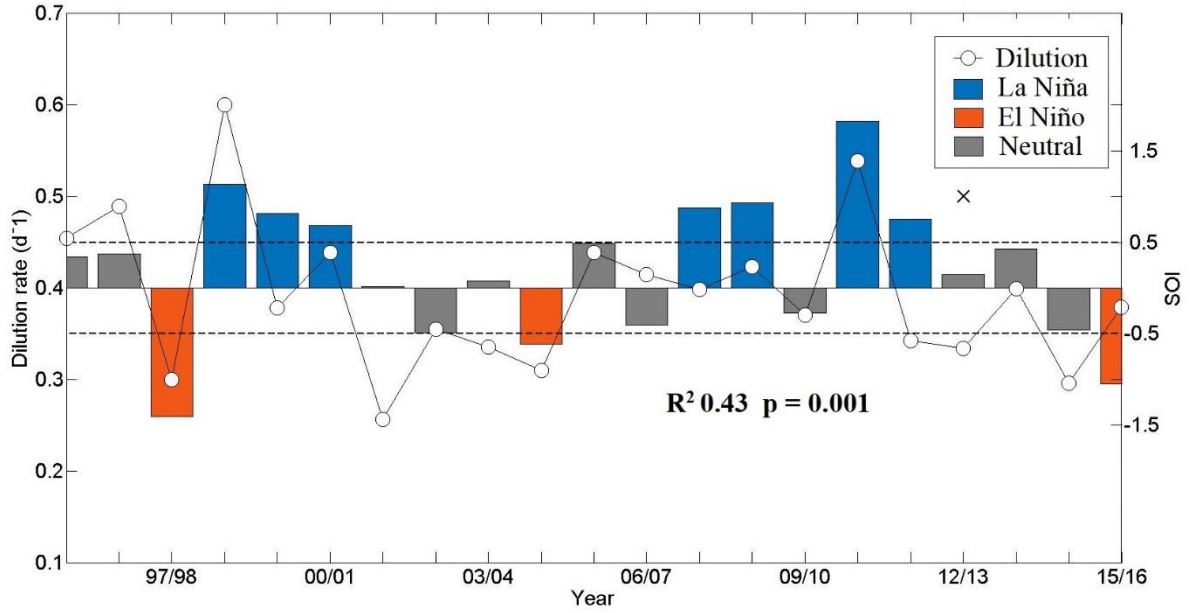

Figure 3.12 Relationship between the Inter annual dilution rates (annual maxima) and southern oscillation index (SOI) between 1995 and 2017. SOI values below the dashed line (<-0.5) correspond to El Niño conditions whereas SOI values above the dashed line (>0.5) correspond to La Niña conditions. SOI values in between the dashed lines (-0.5 and 0.5) are considered neutral. The X symbol marks the year when salinity and nutrient observations were taken.

The link between dilution rate and the SOI can be explained by the combined influences of the SOI on wind, rain, and discharge, which were earlier shown to be important drivers, with the degree of importance depending on the region within the harbour. A multiple linear regression analysis revealed that rainfall was most significantly correlated with dilution rates in region 1 (r^2 = 0.63 p = <0.001), which would increase to (r^2 = 0.71 p = <0.001) in combination with a northward wind (V) component (longer dilution rates with wind from the north and faster dilution rates with wind from the south). This combination of rainfall and northward wind (V) component also explained 63% of the variance observed in region 5 (r^2 = 0.63 p = <0.001). For regions 2, 4, 6 and 8 a combination of river discharge and rainfall, (both variables cross correlated) accounted for between 25%–46% of the observed variance, with rainfall being more important in regions 2 and 6. Region 7, which covered the harbour entrance was dominated by tidal forces, however a combination of river discharge and both wind components contributed to the remaining variance (6%).

The wind speeds and direction between 1995 and 2017 varied between El Niño, La Niña phases (Figure 3.13). During El Niño years, the frequency of wind coming from the west increases compared to La Niña. During La Niña years, the wind direction is less frequently

from the west but increases from the North and easterly direction (Figure 3.13 B). Neutral SOI phases (data not shown) resembled wind speeds and direction similar to El Niño with a high frequency of moderate to strong wind from the west. Neutral years of ENSO have been associated with significant anomalies across other global oceans and land masses (Lin and Qian, 2019), which can also influence wind patterns across New Zealand.

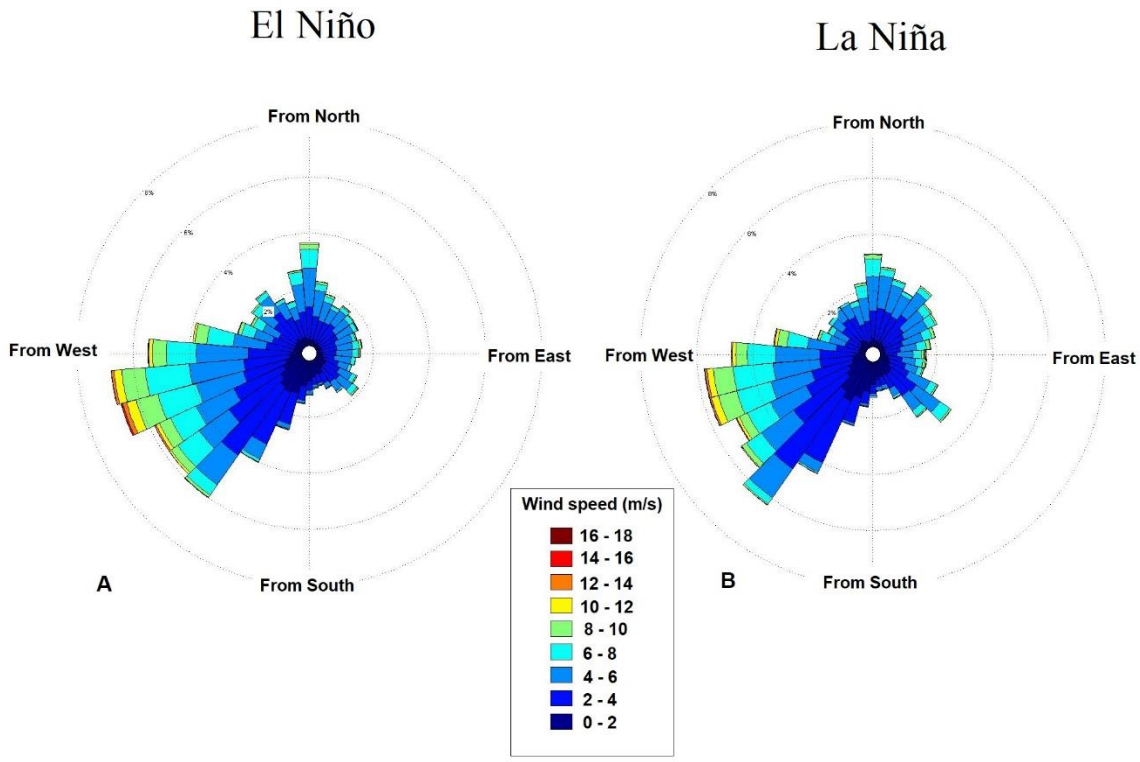

Figure 3.13 Frequency of wind speed and direction over Tauranga harbour during years between 1995 – 2017 during (A) El Niño and (B) La Niña years. Wind data provided by MetService, New Zealand (2018) from Tauranga Airport weather station.

The mean annual river discharge correlated with the annual SOI (r^2=0.48 p<0.001) as well as the frequency of inter annual high discharge events (Table 3.3). High discharge defined as 3 × median of river flow (approx. 2 × the mean) had a positive correlation with the annual SOI (r^2=0.36 p<0.001). The year with the highest discharge events were observed to occur during La Niña phase, with a maximum of 34 events occurring in the 2000/01 year (Table 3.4). During El Niño phases, annual high discharge events did not exceed 16 per year. The year with the lowest high discharge events occurred in 2001/02 and was in a neutral SOI phase with only 3 high discharge events. Rainfall also had a positive correlation with the annual SOI

(r^2=0.3 p=0.01). Rainfall was highest during La Niña phases with the 2010/11 year having the highest annual rainfall (Table 3.4). The 1997/98 and 2015/16 El Niño years recorded below average annual rainfall totals compared to the 2004/05 year, which reached a total of 1500 mm + (~ 300 mm above average, Stokes et al., 2010).

Table 3.4 Summary of annual rainfall, river flow and SOI between 1995 and 2016. Bold text indicates years that were in a El Niño or La Niña phase.

Year	Total cumulative Rainfall (mm)	Average river flow rate (m^3/s)	Number of high discharge events*	SOI (yearly averaged)	ENSO phase
1995/1996	1386	17.61	18	0.34	Neutral
1996/1997	1331.2	16.94	21	0.38	Neutral
1997/1998	**995.2**	**14.59**	**13**	**-1.41**	**El Niño**
1998/1999	**1215.8**	**19.28**	**25**	**1.13**	**La Niña**
1999/2000	**1177.4**	**14.71**	**11**	**0.82**	**La Niña**
2000/2001	**1518.5**	**22.66**	**34**	**0.68**	**La Niña**
2001/2002	972.6	13.04	3	0.02	Neutral
2002/2003	967.6	13.60	11	-0.49	Neutral
2003/2004	1224.6	16.39	16	0.08	Neutral
2004/2005	**1535.2**	**14.43**	**13**	**-0.62**	**El Niño**
2005/2006	1421.2	19.43	28	0.49	Neutral
2006/2007	1004.1	15.41	10	-0.40	Neutral
2007/2008	**1110.4**	**15.37**	**16**	**0.88**	**La Niña**
2008/2009	**1249.9**	**17.11**	**23**	**0.93**	**La Niña**
2009/2010	1198.8	14.87	14	-0.28	Neutral
2010/2011	**1769.6**	**25.35**	**31**	**1.83**	**La Niña**
2011/2012	**1245.3**	**18.60**	**23**	**0.75**	**La Niña**
2012/2013	1201.8	17.08	23	0.15	Neutral
2013/2014	1004	14.70	12	0.43	Neutral
2014/2015	936.6	14.04	10	-0.46	Neutral
2015/2016	**1078.2**	**14.98**	**16**	**-1.05**	**El Niño**

** High discharge events were calculated as >3x the median flow rate.*

3.5 Discussion

3.5.1 Variations in the El Niño-southern oscillation (ENSO) and harbour dilution rates:

The sensitivity to minor changes in discharge, wind and rain revealed how dilution responds to some of the subtle climate shifts associated with El Niño and La Niña. During the 1997/98 and 2015/16 El Niño years, rainfall was below average, however above average rainfall was recorded in the 2004/05 El Niño year. This was driven by a high monthly total in the final month of that year which otherwise had low rainfall. Large rain events may still occur during El Niño phases but the probability and frequency of them occurring are much lower than when in La Niña phase, especially along the north and eastern parts of New Zealand (Mullan 1998).

The frequency and intensity of rain events over the harbour area has implications to increasing dilution rates by increasing river discharge and freshwater input. The dilution rates in regions of the harbour close to river and streams may therefore be driven mostly by rainfall and discharge events. The frequency of high discharge events was positively correlated to the SOI with more events occurring during La Niña periods than El Niño. While the freshwater discharge into Tauranga harbour is relatively small compared to other systems within New Zealand and globally, changes in rainfall and discharge can drive significant changes in harbour dilution rates, salinity variations and circulation patterns. Previous studies have demonstrated that seasonality and interannual climatic differences (i.e., wet vs. dry years) strongly affects hydrologic conditions and the variability in water residence times of large estuarine systems (Paerl et al., 2006). High discharge events were observed to change the circulation and dilution of harbour sub regions differently, temporally increasing water levels in adjacent shallower sub regions and a creating a bulge effect before and after the event. Faster river water during events would cause the main channel flow to by-pass the large shallow embayment's to get to the sea, effectively trapping water temporarily in some areas. This allowed some areas to be diluted quickly while other areas took much longer to dilute (a lagged dilution effect). During periods of prolonged "dry spells" river discharge from Wairoa river (largest freshwater input) can be as low as <5 m^3/s. Persistent wind patterns may

therefore have an enhanced effect in harbour circulation and dilution with slight changes in the predominant wind directions across El Niño and La Niña years.

The type of El Niño or La Niña can change these wind directions on different regions. Not all El Niño deliver the persistent westerly winds expected (Sallinger and Mullan 1999; Timmerman et al., 2018). The persistent westerly winds associated with 'typical' El Niño periods increase circulation around the harbour mouth region but retain water around the central sub regions due to back currents and eddies (Tay et al., 2013). Persistent wind direction may also restrict dilution in other regions of the harbour due to the orientation of constriction points. During high discharge and wind events as observed during the 2010/11 La Niña period, north to easterly wind patterns across the harbour are likely to retain outgoing water masses around the harbour mouth region, however the effects of flushing from the harbour due to the magnitude and frequency of discharge events may override this effect. The use of variable historic time series data in our simulations demonstrated this complex interaction between tides, wind speed, direction, rainfall, and discharge on the dilution rates of the harbour. The small estuary volume allows flushing to respond relatively quickly to events. While dilution rates increased with rainfall and discharge, many local patterns were observed, such as temporarily dropping below zero as poorly flushed water was advected from surrounding regions.

3.5.2 Relationship between dilution rates, salinity, and water quality

Changes in climate may affect the transformation, transport, and storage of nutrients through changes in the system state of estuaries. Biogeochemical cycling and nutrient dynamics are strongly influenced by freshwater and terrestrial nutrient inputs (Eyre and Balls 1999; Childers et al., 2006) as well as changes in water movement and flushing characteristics (Sheldon et al., 2014). We observed lower dilution rates (increased residence times) with a decrease in DIN concentrations in the upper regions of the harbour (r^2 = 0.4 p =0.02), suggesting that a higher residence time assists in drawing down bioavailable DIN in the adjacent water column. Higher DON concentrations were observed to have a positive relationship with lower dilution rates (increased residence times) (r^2 = 0.19 p = <0.05) in the upper sub regions of the harbour. We suspect the remineralisation and recycling of organic nutrients in sediments are enhanced by lower dilution rates and consequent longer residence

times, allowing the transformation and uptake of nutrients by primary producers in the water column. Studies elsewhere have demonstrated the importance of these transformations, with changes from DON to DIN counteracting the removal of nitrate through denitrification (Ran et al., 2017).

Higher seasonal freshwater flows delivering nutrients can take time to transform into available nutrients and often have seasonal lags, and so can be used elsewhere in the system (Scavia et al., 2002; Savage et al., 2012). Hence, regions in the harbour with low dilution rates and poor circulation, such as region 1, 2, 3 and 5 can be important areas for nutrient storage throughout the year. The annual variations in salinity in Tauranga harbour coincided with changes in freshwater input. During winter, when freshwater inputs and run off from land were highest, salinity was low and negatively correlated with high concentrations of DIN (r^2 0.39 p = 0.01). However, during summer, when freshwater inputs were low, a positive correlation was observed between salinity and concentrations of DON (r^2 0.34 p = 0.01). Inputs of DON can remain in the system much longer and be transported to surrounding coastal waters (Kim et al. 2013). The areas of elevated DON concentrations were found in the upper and sub estuarine regions, which are surrounded by intensive agricultural and horticultural land uses. Other studies have demonstrated the importance of biogeochemical transformations within coastal zones, finding that despite lower river discharge and lower nutrient fluxes that dry years had the greatest risk of eutrophication and bloom events (Romero et al., 2019).

Diffuse inputs of submarine groundwater discharge (SGD) have also been recognised as a large source of DIN and DON, with hotspots in the upper regions and sub estuaries of Tauranga harbour and an overall SGD flux estimate of between 5.77×10^5 m^3 day and 3.09×10^6 m^3 day (Stewart et al., 2018). However, it was unclear how much of that estimate comprised of fresh aquifer derived water or saline pore waters. Our model was able to match the observed seasonal salinity variations without the addition of another large freshwater source (and slightly over-predicted salinity in regions). This indicates that the freshwater component of the calculated groundwater fluxes must be closer to the lower bound estimates, with a large portion ~81% of the total SGD flux being made up of saline pore waters. Nevertheless, the addition of nutrients through both fresh and saline SGD are significant and can supply a continual source when surface flows from rivers cease (Santos et al., 2014).

Furthermore, the saline/brackish component can also deliver regenerated DIN and DON from microbial processes in the sediment to surface waters (Kroeger et al. 2007). The legacy of nutrients stored in the sediments can then be released slowly over time, contributing to a build-up of nutrient-laden waters in sensitive regions with lower dilution rates. Inputs of SGD can also have long lag times, meaning pulses of nutrients may not reach coastal waters immediately after hydro-climatic events but seasons later (Michael et al., 2005).

Understanding the natural variability of estuarine systems in response to changes in hydro-climatic forcing will help in devising more robust and strategic water quality sampling protocols, especially under predicted large-scale changes in climate patterns (IPCC, 2014). Nutrient dynamics within estuarine environments are sensitive to climate forcing and can often change between longer constant inputs, delivered at a lower magnitude and longer duration) or pulses (low frequency, large magnitude, and short duration), such as storm events (Fong and Fong, 2018; Yang et al., 2008). For example, rainfall events across California are predicted to become increasingly rare, making the run-off derived nutrient subsidies more pulsed in nature (Fong and Fong, 2018). Estuarine flushing, nutrient loading and the development of harmful algae blooms have also been reported to be enhanced by storm events driven by El Niño phases in Florida, USA (Philips et al., 2020).

Our results over a 22-year hind cast include a long enough period to cover background variations and pulse events and demonstrate the connection between ENSO and inter annual dilution rates. Anomalous events during ENSO periods may help shift the balance of estuarine functioning. For example, during El Niño years longer dry periods may slow down flushing times in most regions of harbour, altering nutrient dynamics and creating conditions that assist in the development of algal bloom events. Other studies have demonstrated that changes in state can also lead to imbalances and shift to dominance by macro algae under higher anthropogenic nutrient loads (Fong and Kennison, 2010).

3.5.3 Model limitations, and uncertainties

The hydrodynamic model used for this study has proven a powerful tool for assessing water transport patterns and dilution rates; however, it is important to make clear the limitations and assumptions used. For numerical models such as Delft3D, the equations that govern the physical processes and hydrodynamics are well established and tested (Deltares 2017). Measurements in key sub regions, including the upper regions of the harbour would help to improve the model further, although as in most cases, a compromise in sufficient field data and the application purposes of the model must be achieved. All hydrodynamic models intimately rely on the accurate representation of bathymetry (Ralston et al. 2010, Ganju et al. 2011), and high-quality bathymetric data is therefore fundamental to reducing uncertainty in hydrodynamic models (Plant et al. 2009). The model developed for this study used multiple bathymetry sources, with smoothing processes to eliminate artefacts and ensure accurate continuity across all cells. However, in doing this a loss of accuracy in depths may have resulted for some regions. This did not have a major influence on the overall hydrodynamics of the model, although caution must be taken when assessing depths at higher resolutions. The 20m spatial scale was high resolution for our application but may not be enough for some complex sub estuarine regions (where causeways and bridges add further complexity). However, Reckhow note that "small-scale temporal and spatial resolution gives the illusion of substantial knowledge" (Reckhow 1999), when we simulate spatial patterns that we cannot confirm, cannot validate, and may not fully understand (Ganju et al., 2016).

Defining the boundary conditions (tidal water levels) and forcing (discharge, wind, rainfall, salinity) is relatively straight forward technically, but can be restricted by data availability. We used available discharge rates from 4 gauged river and streams entering the harbour domain. A regression analysis was applied to the remaining 6 rivers under the assumption that they were similar in characteristics to the gauged rivers. Rainfall and evaporation were added as uniform value based on available data over the harbour domain; however, rainfall may vary over the catchment and contribute to localised surface land runoff from urban areas or farmland. This was not considered in this model. Due to New Zealand having large rainfall and surface runoff as well as groundwater seeps into coastal waters, salinity may change depending on season and currents. More frequent, high resolution salinity measurements in coastal waters off New Zealand would benefit future modelling

studies immensely. Even salinity from regional oceanographic models (e.g., Hycom) are only as good as the terrestrial discharge used to force them, which is often input as a mean discharge rather than incorporating events. In estuaries where wind may have an effect on mixing, the selection of weather stations is important in adequately representing wind magnitude and distribution over water (Scully, 2016). Wind was forced uniformly over our harbour domain, with measurements taken in close proximity to the lower harbour regions. This likely reflects the dominant wind patterns across the harbour, especially at the scale of our investigations, however more localised patterns, particularly towards the upper reaches are more challenging to capture at higher resolutions.

Using hydrodynamic model outputs with predictive neural networks, as used in this study, demonstrates the applicability for future coastal water monitoring. A typical criticism of an ANN predictor (or any other data driven predictor) is that its validity is limited and intrinsically linked to the distribution of the input variables in the training dataset (Van Maanen et al., 2010). ANNs can create highly nonlinear functions which relate independent and dependent variables although due to the complex structure it is it is difficult to disentangle the interactions between the input variables (Van Maanen et al., 2010). We applied numerous model runs and combinations of variables with evaluating the effect of adding or removing specific predictors (for example no discharge). This demonstrated that tidal currents were the major driver of dilution rates with rainfall and discharge contributing more to the predictive power than wind speed and direction. We selected low tide values to ensure outgoing water was being used and generally gave the best predictions. Noisy data in the sub regions (Te Puna) may have led to variable results. Overall, the best predictors were from the river region and the harbour mouth region. A limitation to our predictive power could be from the number of training samples used. We covered data from an entire year as well as multiple seasons with extreme conditions in discharge, rainfall, and wind. This was under the assumption that it would cover the range of conditions experienced in the harbour. In the long time series predictions data may have been either under of overrepresented from the training data and therefore increase some of the noise and variability in the data. Our PDF plots of the training data and the 22-year hind cast were well matched.

3.6 Conclusions

A combination of modelling techniques was used to produce a 22-year hind cast of dilution rates, including the development of a hydrodynamic model coupled with machine learning to create a dynamic emulator. The calculated dilution rates demonstrated significant spatial variations within Tauranga harbour, with lower dilution (longer flushing times) observed in the upper regions and sub estuaries and higher dilution rates (faster flushing times) close to the harbour entrance riverine region. These times varied in response to pulse events associated with high discharge, such as storm events. A significant relationship (r^2 0.43 p = 0.001) between dilution rates and the southern oscillation index (SOI) was established, highlighting the importance of global scale climate patterns on estuarine functioning. The changes in hydro-meteorological forcing associated with climate shifts between El Niño and La Niña periods was demonstrated to influence dilution rates within different regions of the harbour. These climate induced changes in system functioning can have significant implications for water quality, including nutrient availability, storage, and transport within the harbour and to the coastal shelf. For example, the supply of organic nutrients can be converted to more readily available forms for biological uptake at the sediment/water interface, especially in regions of the harbour and during periods with slow flushing times. This may help facilitate in the development of algal blooms, which have become problematic over the past decades. The dynamic emulator approach provides an adaptive way of feeding changes in hydro-climatic forcing data for robust predictions of flushing times, as well as the probability of events and their likely impact. Applying such data driven predictive tools to monitor and forecast water movement within estuaries will be very important for monitoring and managing these environments into the future with climate change.

Appendix

Model Sensitivity tests

To test whether our depth-integrated approach was appropriate, sensitivity experiments were conducted comparing the depth averaged 2D model to a two layered 3D model. A combination of conservative tracer simulations with and without wind were executed using both the 2D and 3D models. The time of the conservative tracer was released into the model was also tested for its sensitivity to the stage of tide, with both a peak spring and neap tide. A constant river flow (annual daily average) was selected for all river inputs with no wind forcing. All scenarios began at high water to ensure there was enough tracer released across the cells of the harbour domain (66% of harbour is exposed tidal flats at low tide).

There was a ~5% difference in flushing times between 2D and 3D models with no wind when averaged over all regions (Figure 3.14). When wind was added (annual average direction and speed) across the domain there was only a ~2% decrease of the flushing times in the 3D model compared to 2D. The difference between wind and no wind in the 3D model alone was also only a small difference of ~1.5%. When wind and no wind scenarios were compared in the 2D simulation alone, a ~4% difference in average flushing times over all regions were observed. These tests demonstrated that the addition of layers into the model had a negligible effect on the overall calculated flushing times and that the input of wind reduced the flushing times in the 2D model more than the 3D model. A large proportion of Tauranga harbour is shallow, well mixed, and exposed intertidal flats at low tide. Although stratification and vertical process representation can be important, in these geometries similar model predictions can be obtained using 2D models (Sandbach et al., 2018). Therefore, to minimise computational cost, all scenarios were conducted using a depth-averaged 2D model setup.

Tests were also conducted to assess an appropriate release time. Tracer released on a spring tide had the longest flushing times (when averaged over all regions) of 9.6 days. A neap tide release resulted in average flushing times of 8.5 days, which was approximately a 1-day (13%) decrease compared to a spring tide release. Due to flushing times on timescale of weeks, a release at neap tide meant a smaller harbour volume was inundated initially and tidal forces increased during the first week of simulation. A release on spring tide would in turn have the

opposite effect, with more of the harbour volume inundated initially and a decrease in tidal magnitude throughout the first week of simulation. Tracer released at the middle stage of the tide resulted in flushing times to be 9% longer on a mid-neap release than a mid-spring release due to the stronger spring tidal forces in the following days after release. The greatest differences were detected in regions 7, 5 and 1, whereas regions 3 and 4 were less sensitive. (Figure 3.15). To maintain consistency, we derived the shortest possible flushing times with respect to the tide by releasing tracer into the model at high water on a neap tide for all scenarios.

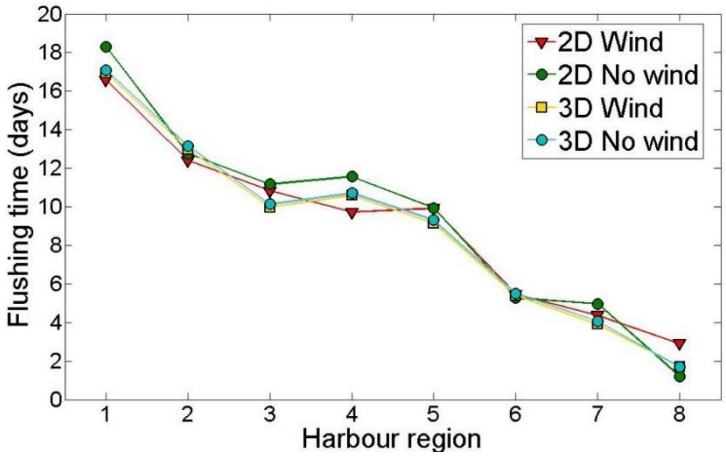

Figure 3.14 Comparison of harbour flushing times between a 2D (wind and no wind) and 3D (wind and no wind) model setup. The probability of hydro-meteorological conditions experienced during a summer El Niño and La Niña phase.

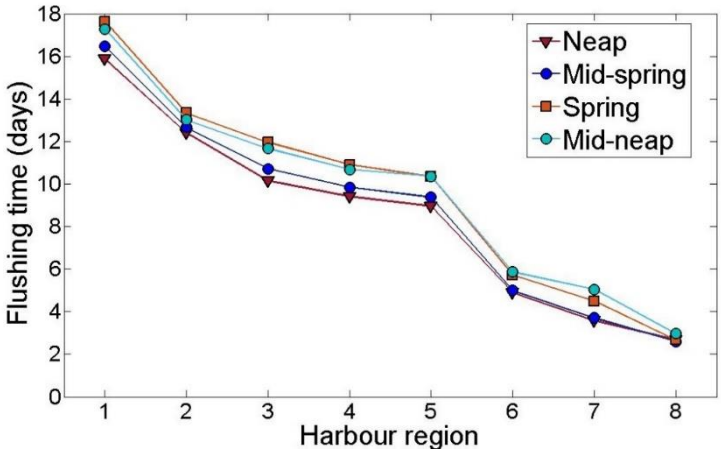

Figure 3.15 Comparison of harbour flushing times with tracer released at different stages of the tide

CHAPTER 4

Spring-neap tidal variations of estuarine flushing times revealed by radium isotopes and Delft3D modelling

Benjamin T. Stewart [a], Karin R. Bryan [a], Conrad A. Pilditch [a], Christian Winter[b], Isaac R. Santos [c] (to be submitted to *Continental Shelf Research*)

[a] School of Science, University of Waikato, Private Bag 3105, Hamilton, New Zealand

[b] Institute of Geoscience, Christian-Albrechts-Universität zu Kiel, 24118, Germany

[c] National Marine Science Centre, School of Environment, Science and Engineering, Southern Cross University, PO Box 4321, Coffs Harbour, 2450 NSW, Australia

Contribution of Authors:

Field investigations, including preparation, design and implementation were done by BTS with guidance from IS and KRB. Volunteers assisted in field sampling. Laboratory analysis was carried out by BTS with assistance from UW and SCU laboratory technicians. BTS wrote the initial and subsequent drafts with co-authors IS and KRB providing valuable feedback and comments.

4.1 Abstract

Tides drive estuarine connectivity in most coastal regions. Quantifying estuarine flushing and water ages is challenging but essential to resolve biogeochemical cycles in estuaries. This study quantified flushing times combining hydrodynamic modelling with radium isotope measurements over a spring-neap period at the sub-estuary (1 km) and harbour (10 km) scales within a shallow coastal lagoon (Tauranga Harbour, New Zealand). At the harbour scale, younger apparent radium ages (2 – 6 days) were observed on the spring tide than the neap tide (mean ~13 days). The opposite effect was observed at the sub-estuary scale, with older apparent radium ages at the main harbour at spring tide (mean ~7.3 – 9.7 days). Radium and nutrients at the sub-estuary scale were up to 4× higher than observed at the harbour scale, suggesting a significant source of chemical constituents. Flushing times estimated from Delft 3D-FLOW hydrodynamic modelling also varied between sub-estuarine regions. The modelled flushing times across all harbour regions (~4-20 days) were able to compliment the calculated apparent radium ages. A negative relationship (r^2=0.50 p =<0.05) between water ages and tidal range for $^{224}Ra/^{223}Ra$ apparent ages was observed at the harbour scale, with older apparent water ages occurring toward the neap phase of the tide. Longer residence times as estimated both from radium isotopes and modelling were observed with shifts in tidal magnitudes. Overall, combining methods builds confidence in flushing time estimates at varying scales and provides a range of timescales important for estuarine processes.

4.2 Introduction:

Water circulation and the exchange of solutes are important variables within estuarine systems. Overlapping drivers, such as tides and hydro-climatic forces, can result in highly variable water circulation patterns (Paerl et al., 2006), with large imprints on biogeochemical cycles (Statham, 2012; Bauer et al., 2013) and estuarine ecology (Tomasky-Holmes et al., 2013). Estuarine water circulation can be investigated based on multiple concepts such as residence time (the time it takes for a water parcel to leave a system through an outlet), flushing time (a bulk or integrative parameter that describes the general exchange characteristics) and water ages (the time a water parcel has spent since entering an estuary through one of its boundaries) (Monsen et al., 2002; Sheldon and Alber, 2002). In a system under steady state, all three measures should agree, although estuarine systems are rarely in steady state (Lemagie & Lerczake, 2015). Disagreements between these terms are common and can be attributed to the specific processes being measured, the methods used, and their relevance to different spatial and temporal scales.

Radium (Ra) isotopes ^{223}Ra, ^{224}Ra, ^{226}Ra, and ^{228}Ra with half-lives of 11.4 d, 3.7 d, 1600 y, and 5.7 y, respectively, have been increasingly used as natural geochemical tracers to determine the age of water masses in coastal systems (Moore, 2000; Charette et al., 2001; Moore et al., 2006; Dulaiova and Burnett, 2008; Tomasky-Holmes et al., 2013). Radium isotopes are continually produced in rocks and sediments by uranium and thorium decay. Radium remains largely particle-bound in freshwater, but desorbs from particles in contact with brackish to saline waters of coastal aquifers, resulting in high radium activities in coastal groundwater relative to seawater (Moore 1999). Radium ages are calculated using the ratio of short to long-lived isotopes and are interpretable as a tracer release from the source (usually groundwater or desorption from suspended river sediments). Hence, the radium isotopes act like an internal clock measuring the time since a given water sample was last in contact with its source. Radium is mostly conservative in seawater, so decay and mixing away from their source become the key loss terms (Charette et al., 2001).

Tidal processes and variations are one of the primary influences on the delivery of radium and solutes into coastal systems (Moore et al., 2011, Sadat Noori 2017, Taniguichi et al., 2019). However, due to the labour-intensive collection and processing of samples, many

studies have been limited to 'snapshot' spatial surveys or timeseries over tidal cycles at single locations. This has limited our understanding on the temporal and spatial behaviour of radium delivery and associated water ages over bi-monthly spring-neap tidal patterns. Hydrodynamic models, such as Delft3D, provide a suite of processes which allow the release of tracers to determine transport time scales at much higher resolution to geochemical tracer methods. Such models can assist in assessing the connectivity and tidal sensitivity of coastal systems (Cucco et al., 2009). Using hydrodynamic models together with field-based radium tracer studies allows an important cross validation between independent approaches (Rapaglia et al., 2010). However, radium investigations and numerical modelling are commonly done by researchers as separate studies. Combining these methods ultimately allows a better assessment of residence times in estuaries which are rapidly being altered directly and indirectly through increased human activity, such as land use changes across catchments and coastal development (Cloern et al., 2016).

In this study, we combine radium isotopes and numerical modelling to understand how changes in tides can drive flushing times of an estuarine lagoon. Combining methods allows insight into different process occurring over different temporal and spatial scales within the estuary. We address the question of how connectivity and exchange between different sub regions change with tidal magnitudes. It is hypothesized that greater tidal magnitudes will influence radium-derived water ages and increase the exchange of new and legacy nutrients between sub regions of the estuary. Our objectives were to 1) assess radium (^{223}Ra, ^{224}Ra and ^{226}Ra) and salinity and nutrient dynamics over a spring-neap period, 2) determine water mass ages using radium isotopes, and 3) assess flushing times and the relative contributions of different water masses within the harbour using numerical modelling.

4.3 Methods

4.3.1 Study site

The study was conducted within Tauranga Harbour on the Bay of Plenty coast, New Zealand (Figure 4.1). The harbour is a tidally dominated estuarine lagoon driven by semi-diurnal tides, ranging from 1.2 m (neap) to 1.9 m (spring). The harbour is enclosed by

Matakana Island, a large (25 km long) sand barrier island resulting in two main exchange passages with the Pacific Ocean (north and south). This study focused on the southern basin and exchange passage (Figure 4.1), which can be considered hydro-dynamically independent from the northern basin due to poor tidal connectivity and large intertidal flats (Spiers et al., 2009, Tay et al., 2013). The large surface area of intertidal flats within the harbour (66%) consists of sandy mud islands, tidal channels and young mangrove forests along the upper regions (Stokes et al., 2010). Overall, the system is shallow and vertically well mixed (Heath, 1985). Tidal scouring has developed-highly channelized currents with strong flow rates at the constriction points of the sub-estuaries and harbour mouth (Tay et al., 2013). The sub estuary of Waikereao, located 4.5 km south of the harbour mouth is defined by large intertidal areas, mangroves and a single constricted mouth (Figure 4.1 B).

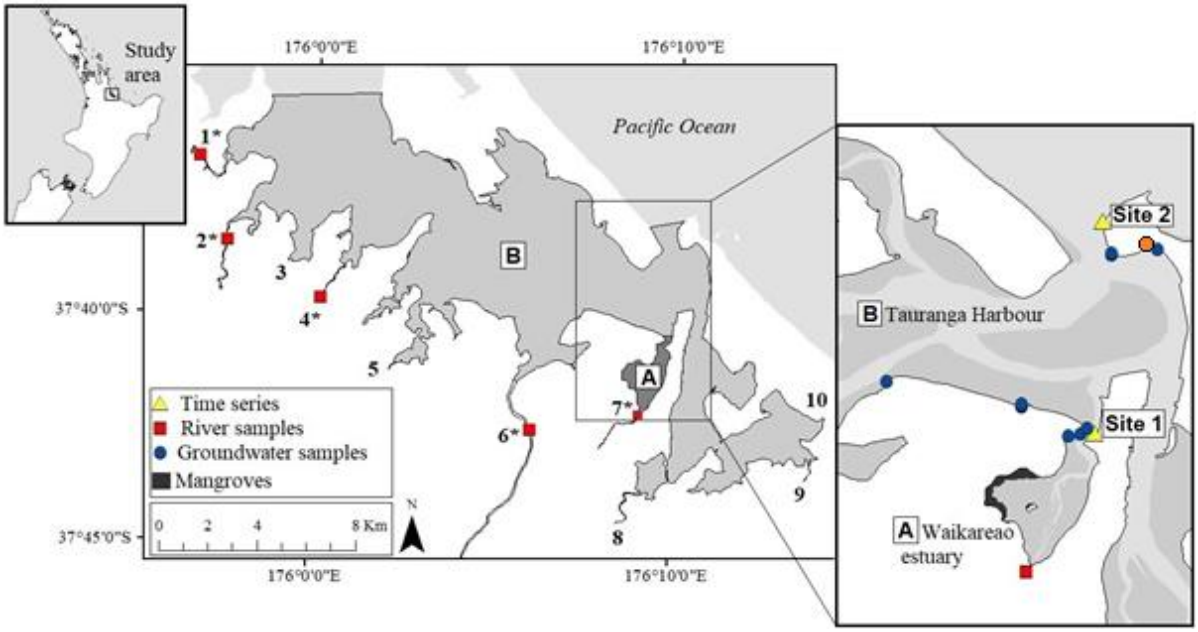

*Figure 4.1 Waikereao estuary (A), and Tauranga Harbour (B), New Zealand. Yellow triangles indicate time series stations for Site 1 (Waikereao constriction) and Site 2 (main harbour entrance). Red squares and blue circles are where river and groundwater samples were collected, and the black shading in Panel B shows where mangroves are located (mangroves also occur throughout the harbour in Panel A but are not shown). The numbers refer to rivers and streams, and * is location of sampled rivers. Orange circle indicates geothermal spring at the base of Mauao.*

The system is well flushed with an average residence time varying between 4 – 8 days, measured using both chemical based tracers (Stewart et al., 2017) and numerical modelling

(Tay et al., 2013). The southern basin has a number of smaller sub-estuaries which connect with the main harbour. There is a time lag in the tide (± 1 hour for upper harbour) and resulting water movement in these regions. This results in a circulation pattern with longer residence times (flushing time of >10 days) in the upper harbour regions compared to the harbour mouth (flushing time of 1–3 days). The southern basin of the harbour has a total catchment area of 1300 km^2 and is surrounded by predominately agricultural and horticultural land use covering 33.7% and 5% respectively of the total catchment area (Hall, 2013). The growing population in Tauranga and Mt Maunganui (predicted to be up to 164,100 in 2033 (Tauranga statistical information report, 2018)) also surrounds the southern Harbour. The area has a temperate climate with a mean annual rainfall of 1200 mm (Stokes et al., 2010). The wettest months are expected in winter from June to August. 'Dry spells' (periods of fifteen days or longer with less than 1mm of rain) are common during the summer and early autumn from December to March (NIWA, 2013). The region is influenced by La Niña and El Niño weather patterns, which can create high variability and greater extremes in rainfall.

4.3.2 Surface water time series measurements

A field campaign was undertaken from the 20th of September 2017 to the 1st of October 2017. Sampling was conducted in a typically wet time of year. The area received ~93 mm of rainfall in the two weeks before the study took place and ~42 mm during the sampling period (data sourced from CliFlo, 2018). The rainfall was accompanied by higher than average river discharges. The Wairoa river, the largest freshwater source flowing into the harbour (~60% of surface water discharge), contributed an average flow rate of ~20 m^3/s over the two weeks before and during sampling (data sourced from BoPRC, 2018).

To construct a two-week time series, water samples were obtained over two different spatial scales within Tauranga Harbour, at the single constriction points of Waikereao sub-estuary (Site 1) and the harbour mouth (Site 2). Sampling was undertaken over 12 consecutive days and consisted of radium (^{223}Ra, ^{224}Ra & ^{226}Ra), salinity, nutrients (organic nitrogen/phosphorus and inorganic nitrogen/phosphorus), dissolved inorganic carbon (DIC) and dissolved organic carbon (DOC) sampling. All measurements were taken twice daily over one tidal cycle, approximately ± 1 hour of both high and low tide. Samples were also collected weekly from the rivers and creeks entering the harbour and sub-estuary.

To measure radium isotopes (^{223}Ra, ^{224}Ra and ^{226}Ra), 100 L of estuarine water at each sampling point were hand-pumped into plastic barrels. The sample was then gravity drained through cartridges containing 15 g of manganese-impregnated fibres at a flow rate of <1 l/min (following Moore and Reid (1973)). The slow flow rate allowed dissolved radium in the water to be adsorbed onto the fibres effectively. At each site, a calibrated YSI probe was used to measure water column temperature (˚C) and salinity (ppt). Samples for total nitrogen, phosphorus, and nutrients were collected using a triple sample-rinsed syringe and filtered through 0.45 µm cellulose acetate syringe filters. These were stored in sterile 50 mL polyethylene centrifuge tubes, kept on ice in the dark and then frozen at -20˚C until analysis. Samples for dissolved organic carbon (DOC) were filtered through 0.7 µm Whatman GF/F filters. These were stored in acid rinsed and pre-combusted (450˚C for 4 h) 40 mL volatile organic carbon (VOC) borosilicate vials.

4.3.3 Groundwater sampling:

A total of 12 groundwater samples were collected near each time series site at low, mid and high tide marks (Figure 4.1). Sampling was done between the 10th and 12th of October 2017. Shallow bores were dug to a depth ranging between 0.5 and 1.5m across the intertidal zone on outgoing tides. The bores were dug using a posthole digger and hand auger. A PVC piezometer with a 50-cm fine slotted screen at the end allowed groundwater to infiltrate into the pipe once installed. A peristaltic (low flow) pump was used to purge water from the bore for least three recharge cycles before samples were collected. Total nitrogen, phosphorus and DOC were collected as described above. For radium measurements, a known volume of between 20 –30 L was collected in drums and filtered through Mn fibres. A calibrated YSI probe was used to measure temperature and salinity. Direct groundwater discharge from a natural geothermal spring was also collected from the base of Mauao (Mt. Maunganui) (Figure 4.1).

4.3.4 Radium desorption and diffusion from sediments:

Radium desorption from suspended particles occurs due to ion exchange processes in brackish to saline waters. In order to account for this process, we conducted weekly radium

desorption experiments in the Wairoa River (largest freshwater source to the harbour) and Kopurererua Stream during the time series sampling period (20th September – 1st October). One 100 L plastic barrel was filled at each site with fresh river/stream water (salinity ~ 0.1) and filtered immediately through a cartridge containing 15g of manganese impregnated fibre. Another plastic barrel was filled with fresh river water at each site and taken back to the laboratory, where natural sea salt was added. Salt additions were monitored with a calibrated YSI probe until the salinity reached similar levels to those observed in the harbour (33). The salted barrels were well mixed and left for at least 12 hours to allow particles bound with radium to desorb. These were then run through another cartridge containing 15 g of Manganese fibre. The difference between fresh / unsalted and salted river water was assumed to be caused by desorption. Radium contamination by the salt addition itself was ruled out by adding salt to radium free freshwater and measuring the dissolved radium in that water.

To measure the molecular diffusive fluxes of ^{223}Ra and ^{224}Ra, four sediment cores, two coarse grained (sandy) and two fine grained (muddy) were collected from four separate intertidal locations within Tauranga Harbour in 2015 (refer to Stewart et al., 2018). The sediment from the cores were spread over the bottom of a plastic container and filled with between 15 – 22L of radium free water from Tauranga Harbour (salinity ~22). The samples were incubated for at least 2 months, (>5 half-lives of both ^{223}Ra and ^{224}Ra) which was the assumed equilibrium between sources (diffusion) and sinks (decay) within the containers. The overlaying water was then extracted and filtered through 15g of manganese impregnated fibre for ^{223}Ra and ^{224}Ra analysis. This method could not be applied for ^{226}Ra due to its very long half-life (1600 years).

4.3.5 Radium age calculations

The apparent age of the water was calculated using a radioactive decay equation comparing the activity ratio (AR) of short-lived radium isotopes to a longer-lived one (Moore 2000a; Dulaiova and Burnett 2008; Eller et al. 2014).

$$t = \ln\left(\frac{\left[\frac{\mathrm{X}_{Ra}}{\mathrm{Y}_{Ra}}\right]_i}{\left[\frac{\mathrm{X}_{Ra}}{\mathrm{Y}_{Ra}}\right]_{obs}}\right) \times \frac{1}{\lambda \mathrm{X}_{\mathrm{Ra}} - \lambda \mathrm{Y}_{Ra}} \quad \text{(d)}$$

Equation 4.1

where $(^{X}Ra/^{Y}Ra)_{obs}$ represents the observed AR of a short lived (X) to a longer lived (Y) isotope measured at the harbour sampling locations; $(^{X}Ra/^{Y}Ra)_{i}$ is the initial activity ratio of the same isotope pair in the groundwater source; λ defines the decay constant for the individual isotopes (0.189 d^{-1} for ^{224}Ra, 0.0608 d^{-1} for ^{223}Ra and 1.1869×10^{-6} d^{-1} for ^{226}Ra).

The input of radium isotopes into coastal systems are similar to an artificial tracer release, with the short-lived radium isotopes providing the rate of dispersion based on their exponential decay as they mix away from their source (Charette et al., 2013). The assumptions in using this approach include (1) a single major source of radium exists with a constant isotopic ratio, (2) offshore waters contain negligible amounts of short-lived isotopes and (3) the losses of radium after leaving its source are only through mixing and radioactive decay. We investigated a tidally dominated lagoon system, with an average residence time of around 5 - 9 days and therefore chose to apply the $^{224}Ra/^{223}Ra$ and $^{224}Ra/^{226}Ra$ using Equation 4.1.

4.3.6 Hydrodynamic model, flushing time calculations and tracer experiments

A calibrated 2D numerical domain-decomposed model was used for this study, developed using Delft3D-FLOW (Deltares, 2017). The model was divided into three nested depth-integrated model domains of decreasing resolution: inside the southern basin of Tauranga harbour (20 × 20m); outside the harbour (100 × 100m); and thirty kilometres offshore into the Pacific Ocean (500 × 500m). Five harmonic tidal constituents (K1, O1, M2, N2, S2), derived from the NIWA national computer tide model (Walters et al., (2001), were applied to generate the astronomic tidal forcing at the boundaries (refer to Stewart et al. (2020) in prep for further information).

Conservative tracers were used to simulate transport and calculate flushing times within the harbour. Quantifying flushing time from tracer allowed the mixing of multiple water masses and tidal oscillation patterns to be accounted for at the system scale. All cells

within the harbour were uniformly set to an initial concentration value of 1 gm^{-3} and released at high water. This ensured all areas within the harbour were covered with water at the release time. Areas outside the harbour, freshwater sources, and oceanic boundaries ('new' water) were all set with a tracer concentration of 0 g m^{-3}. The e-folding flushing time was then calculated by fitting an exponential curve to the tracer concentration over the time period until the concentration reached 1/e (37%) of the initial tracer. This means that only 63% of tracer was removed from the cell/area and was not completely flushed. Therefore, the flushing time reflects the average amount of time the tracer spends in the cell, often referred to as the average residence time (Monsen et al., 2002). Tracer concentration in each cell was spatially integrated over the area of each defined region and at each time step. The flushing times were then derived as the average time for tracer in all cells within that sub region to fall below 1/e (37%).

$$C = C_O \times e^{-kt}$$

Equation 4.2

where C is concentration at time (t), C_0 is the initial concentration and k is the dilution coefficient. This can be re-arranged to solve for k (the dilution rate). Tracer release experiments were conducted across different harbour sub-regions defined in Stewart et al., 2020 (in prep). A uniform concentration of 1 gm^{-3} was released across all cells. To control for the different areas and volumes of the defined sub-regions, tracer was normalised to the initial tracer mass at the time of release by multiplying region area, volume, and tracer concentration. Tracer loss for each region was calculated as the tracer mass at each time step divided by the initial tracer mass. We used the tracers to assess the sources of water passing the locations where our time series were collected (sites 1 and 2) by calculating the ratio of tracer mass (%) from each region. Ratios were calculated as the tracer mass from the origin region (normalised to the water mass of site 1 and 2) divided by the sum total of tracer mass from all regions. Ratios were calculated over each model time step and subsequently averaged for each ebb and flood tide. Tracer mass that was transported outside the harbour on outgoing tides was partially returned with incoming tides and also partially lost at the open ocean boundaries of the model domain. We assumed that no mass returns to the system from the ocean boundary (constant input of 0 $g.m^{-3}$); however, this assumption may underestimate the flushing times.

4.4 Results

4.4.1 Surface water timeseries

A large difference in salinity ranges between low tide (19-22) and high tide (29- 30) samples was observed at Site 1 (Figure 4.2 C). Salinity ranges were slightly greater at the spring tide phase of the survey but dropped considerably during the neap tide following a rainfall and discharge event. Two distinct rainfall events (>10 mm/d) and associated increases in river discharge occurred on day 3 and days 8–10 of the survey period (Figure 4.2 B). The variations in salinity at Site 2 showed only slight differences between low tide and high tide ranging from 29.8 and 31.1 respectively (Figure 4.2 I). The salinity values at both high and low tide increased towards the neap end of the survey. Significant relationships between salinity and tidal range for both low tide (r^2=0.39 p =0.01) and high tide (r^2=0.43 p=<0.01) were observed over the spring neap period at Site 2.

At Site 1, concentrations of ^{224}Ra were two-fold greater at low tide than high tide, with values having a greater range at the spring phase (Figure 4.2 E). Values of ^{223}Ra showed a similar trend with greater ranges at the spring phase than the neap phase. The values of ^{226}Ra showed less variability between tidal cycles but did have high low tide concentrations (14 dpm/100L) during the spring phase of the survey (Figure 4.2 F).

At Site 2, concentrations of ^{223}Ra and ^{224}Ra showed no strong differences between high tide and low tide over the duration of the spring-neap cycle, with the exception of ^{224}Ra increasing slightly at the beginning of the survey (Fig. 2K). Concentrations of ^{226}Ra had a larger difference between high tide (8 dpm/100L) and low tide (13 dpm/100L) during the first 6 days (spring phase) of the survey, which decreased toward the neap phase (Figure 4.2 L).

Dissolved inorganic nitrogen (DIN) at Site 1 had a greater range (0.5 – 30 µM) and higher mean concentration (15 µM) at low tide than high tide over the duration of the survey (Figure 4.3 A). A spike in values at low tide occurred between days 6 – 8 of the survey, coinciding with increased river discharge and reaching a maximum of 30 µM, which was also observed in dissolved inorganic phosphorus (DIP) values (Figure 4.3 C). Dissolved organic nitrogen (DON) at Site 1 had less variability between high and low tide, whereas values of dissolved organic phosphorus (DOP) were higher at low tides compared to high tide.

At Site 2, the maximum value of DIN at low tide (7µM) was orders of magnitude lower than the maximum value at Site 1 (30 µM) and showed little variation between high and low tide, which as similar in values of DIP (Figure 4.3 F). Both DIN and DIP showed the lowest concentration values during the neap phase of the survey. Multiple spikes in concentration were observed following rainfall/discharge events, temporarily increasing concentrations of DIN and DIP. Dissolved organic nitrogen (DON) values had higher variability than Site 1 (Figure 4.3 G), although dissolved organic phosphorus (DOP) had a smaller range in values (0.01 – 0.29 µM).

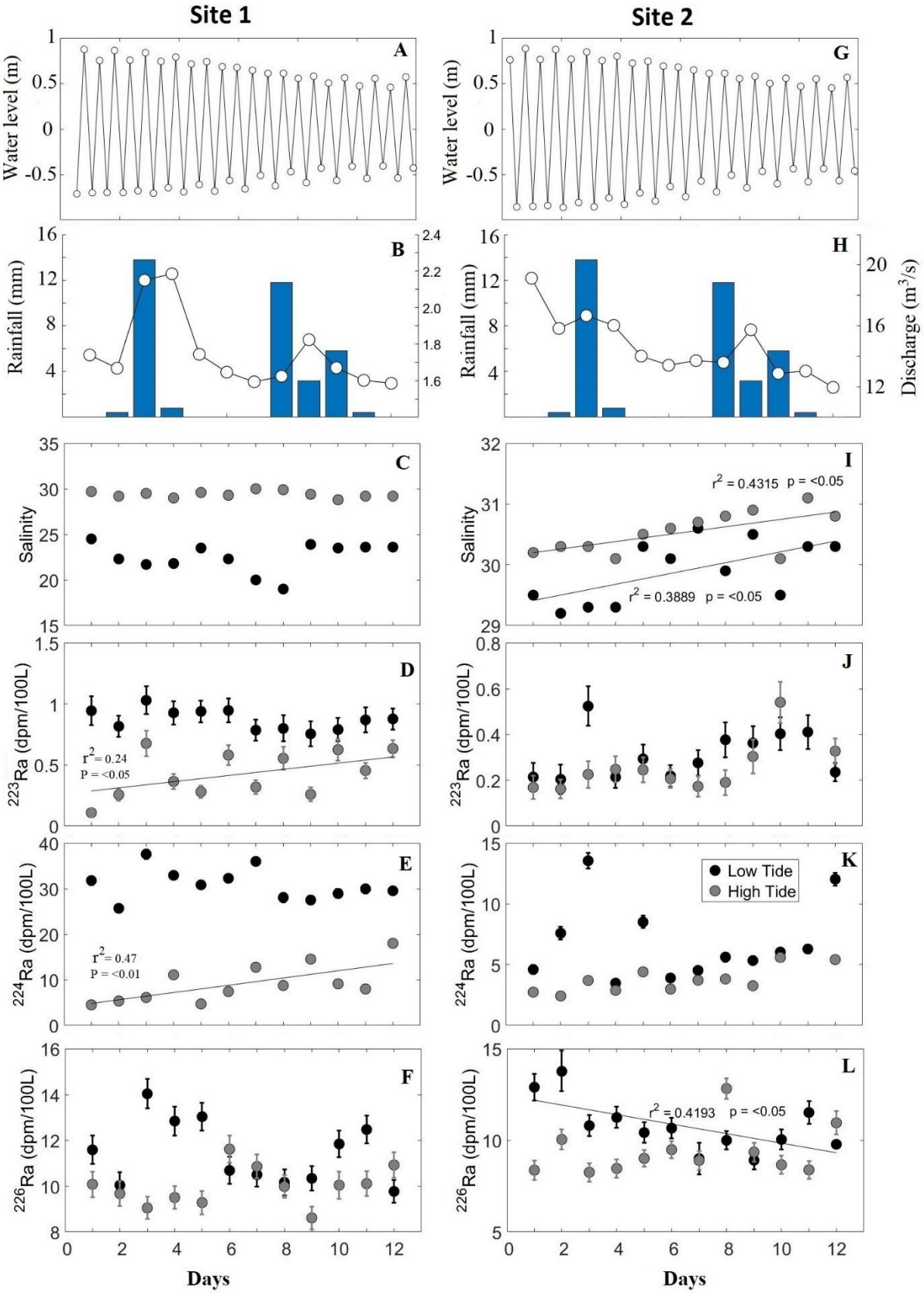

Figure 4.2 Time series measurements of surface water radium and ancillary data at Site1 and Site 2.

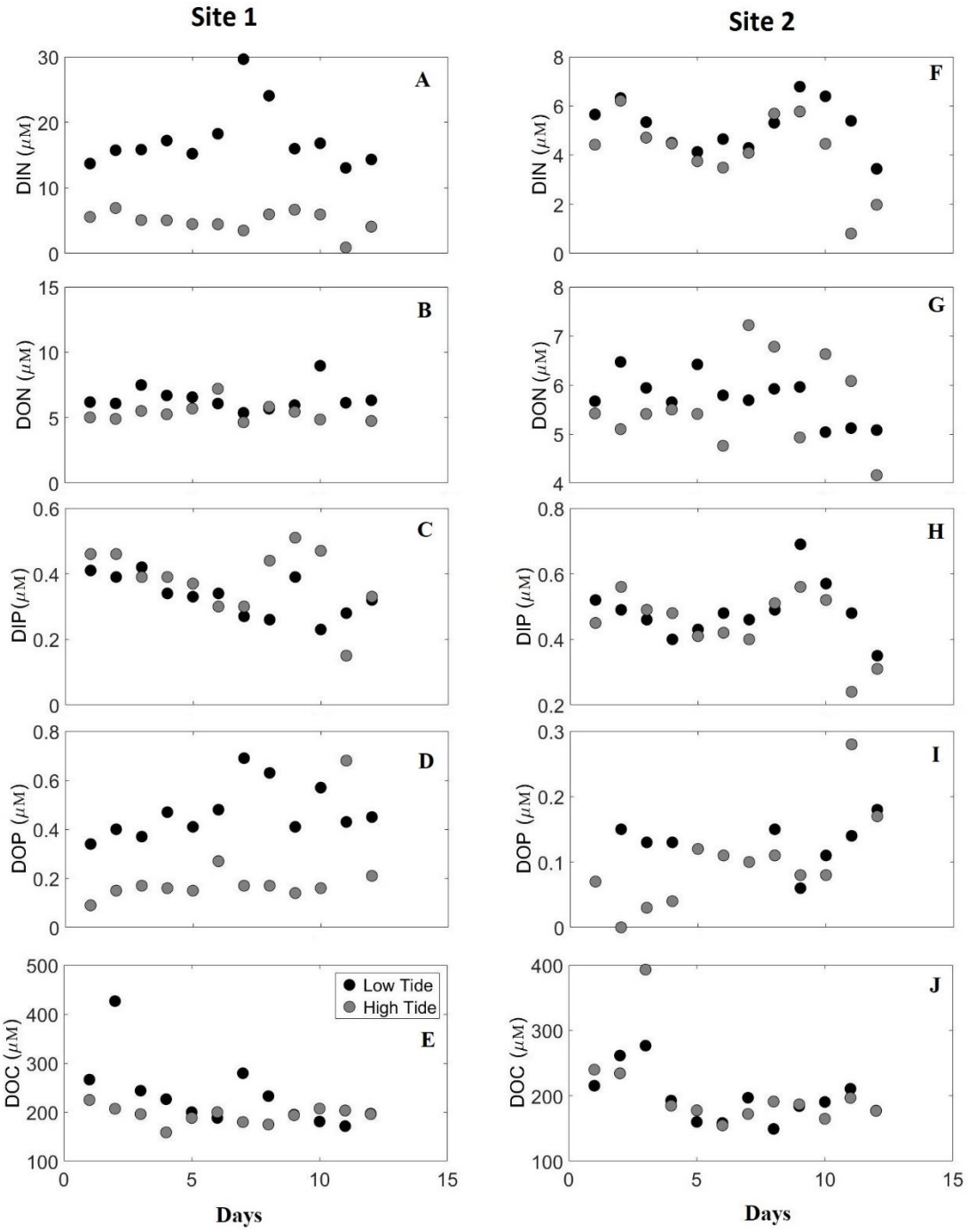

Figure 4.3 Time series measurements of surface water nutrients and carbon (DOC) data at Site1 and Site 2.

4.4.2 Groundwater samples and desorption from freshwater sources

Shallow groundwater samples were collected across a range of salinities from fresh (1.0) to saline (28.1). The average concentrations of ^{224}Ra (127.5±18.4 dpm/100L), ^{223}Ra (4.3±0.71 dpm/100L) and ^{226}Ra (26.1±5.4 dpm/100L) observed in groundwater were orders of magnitudes higher than surface waters (Table 4.1). The average ^{224}Ra/^{223}Ra AR for all groundwater samples was 32, which was comparable to a previous spatial survey (~35), consisting of 22 groundwater endmembers (Stewart et al., 2018). DIN and DON had an average of 14.3 µM and 17.8 µM respectively across all wells. DIP and DOP had averages of 2.43 µM and 1.09 µM respectively. Both inorganic and organic nutrients observed in ground waters had greater ranges and averages then adjacent surface waters (Table 4.1).

Desorption experiments revealed a calculated average ^{224}Ra/^{223}Ra AR of 25.2 and ^{224}Ra/^{226}Ra AR of 0.48. This was slightly lower than estuarine waters and groundwater endmember ARs, implying that desorption cannot be the main source of radium to surface waters (Figure 4.4 A & B). The source of initial ARs to calculate apparent radium ages are therefore unlikely to be significantly affected by desorption inputs over the survey period (discussed later).

Table 4.1 Groundwater radium and nutrient concentrations, including physiochemical parameters in Tauranga Harbour. AR = Activity Ratio.

	Salinity (ppt)	Temperature (˚C)	Depth (m)	^{223}Ra (dpm/100L)	^{224}Ra (dpm/100L)	^{226}Ra (dpm/100L)	^{224}Ra/^{223}Ra AR	^{224}Ra/^{226}Ra AR	DIN (µM)	DON (µM)	PO_4 (µM)	DOP (µM)
GW1	3.1	14.8	1.8	2.8	141.7	57.7	51.6	2.5	5.6	18.2	1.6	1.0
GW2	24.9	14.5	0.0	3.3	162.6	21.6	48.9	7.5	6.4	21.8	0.8	0.4
GW3	1.0	15.5	1.0	1.0	13.7	9.8	13.4	1.4	19.5	17.1	0.3	0.9
GW3.2	14.5	15.9	1.0	3.1	128.2	20.6	41.7	6.2	13.1	17.1	2.2	1.4
GW3.3	28.1	15.9	1.0	8.2	196.5	17.3	24.0	11.4	15.2	12.0	1.9	0.3
GW4	17.3	16.2	1.0	6.7	225.9	61.8	33.7	3.7	46.7	30.0	2.6	1.2
GW5	23.6	15.7	0.5	5.2	133.0	13.6	25.8	9.8	5.6	10.5	3.7	1.4
GW6	12.0	16.1	0.5	5.6	84.6	9.6	15.1	8.8	7.7	9.7	8.0	2.0
GW 7	27.5	16.5	0.7	3.03	114.5	33.0	37.8	3.5	13.2	4.9	1.0	0.2
GW 8	25.1	15.8	0.8	1.32	51.9	17.2	39.4	3.0	14.6	3.1	1.1	0.1
GW 9	23.4	15.0	0.5	6.75	149.7	25.5	22.2	5.9	9.5	51.5	3.4	3.1
Mean	18.2	15.6	0.8	4.27	127.5	26.1	32.1	5.8	14.3	17.8	2.4	1.1
Range	27.1	2.0	1.8	7.16	212.2	52.2	38.2	10	41.1	48.5	7.7	3.1
SE	2.9	0.2	0.1	0.71	18.4	5.4	3.9	1.0	3.5	4.1	0.6	0.3

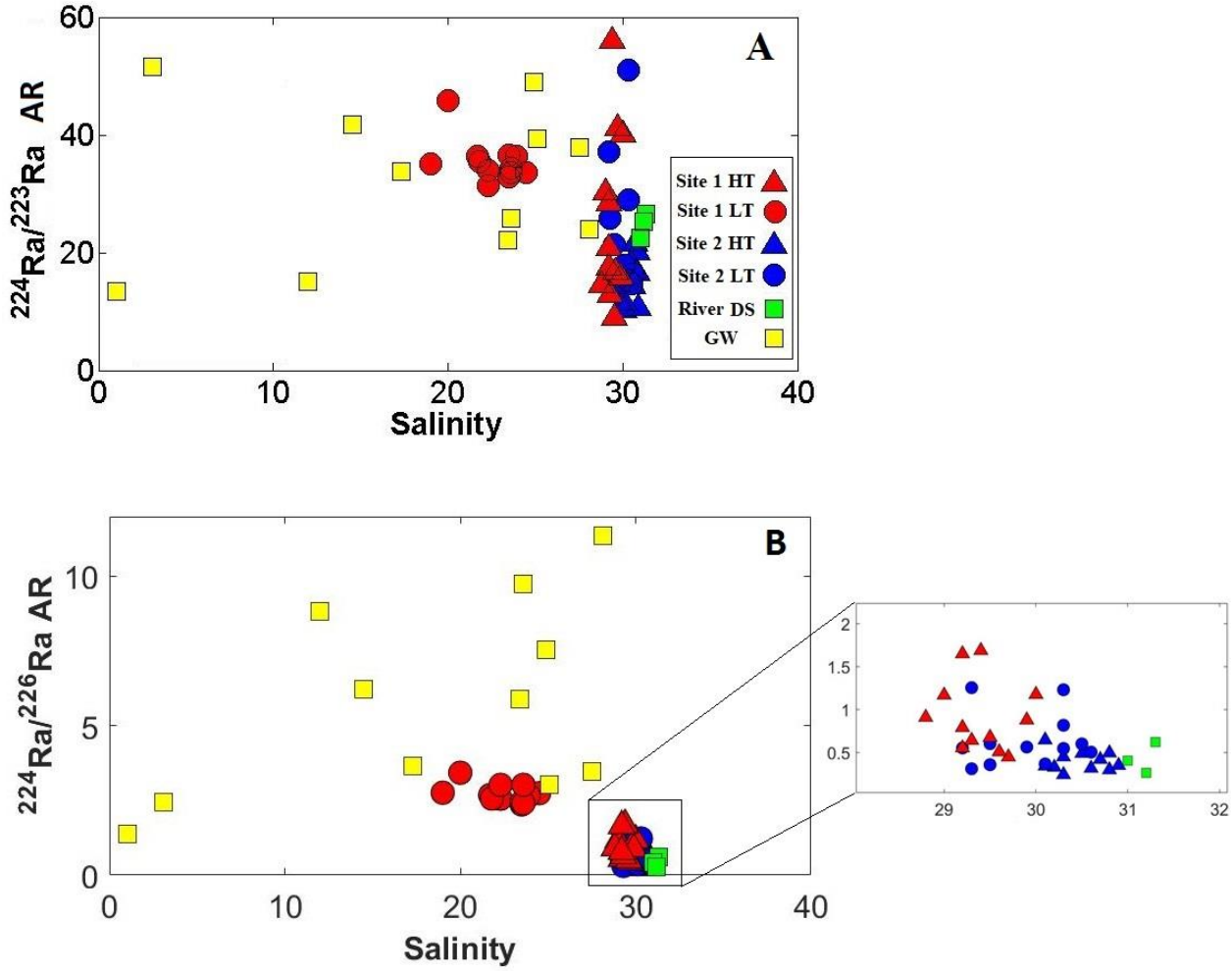

Figure 4.4 A). ^{224}Ra / ^{223}Ra Activity ratios (AR) of surface water samples, river desorption and groundwater samples during the survey period. B). ^{224}Ra / ^{226}Ra Activity ratios (AR) of surface water samples, river desorption and groundwater samples during the survey period

4.4.3 Apparent Ra water ages and tidal range

The maximum $^{224}Ra/^{223}Ra$ AR from groundwater at Site 1 was used as the initial AR to derive the apparent Ra water ages (Figure 4.4 A). Samples taken at high tide and low tide were calculated to have a mean age of 7.3 days and 2.9 days respectively, with an overall mean of 5.0 days (Table 4.2).The mean of groundwater from Site 1 was used as the initial AR for $^{224}Ra/^{226}Ra$ age estimates which had a mean of 9.7 days at high tide, 3.5 days at low tide and a total of 6.6 days over the survey period. A positive relationship (r^2=0.51 p=<0.01) was observed between tidal range and high tide ages, with older aged water entering the estuary

at spring high tides. The age of low tide samples for both age calculations was relatively consistent over the spring-neap period (Figure 4.5 A & C).

At Site 2, we elected to use the mean groundwater $^{224}Ra/^{223}Ra$ and $^{224}Ra/^{226}Ra$ as our initial AR to derive the apparent Ra water ages. Groundwater $^{224}Ra/^{226}Ra$ AR were markedly higher than sub-estuarine and harbour water ARs (Figure 4.4 B). Samples taken at high tide and low tide had a mean $^{224}Ra/^{223}Ra$ apparent water age of 5.9 and 4.5 days, respectively, with an overall mean of 5.2 days (Table 4.2). A negative relationship (r^2=0.50 p =<0.05) between low tide water ages and tidal range for $^{224}Ra/^{223}Ra$ apparent ages was also observed at Site 2 (Figure 4.5 B), with older apparent water ages occurring toward the neap phase of the tide. $^{224}Ra/^{226}Ra$ apparent ages were significantly older, with a mean at high tide of 14.4, low tide 12.1 and an overall mean of 13.2.

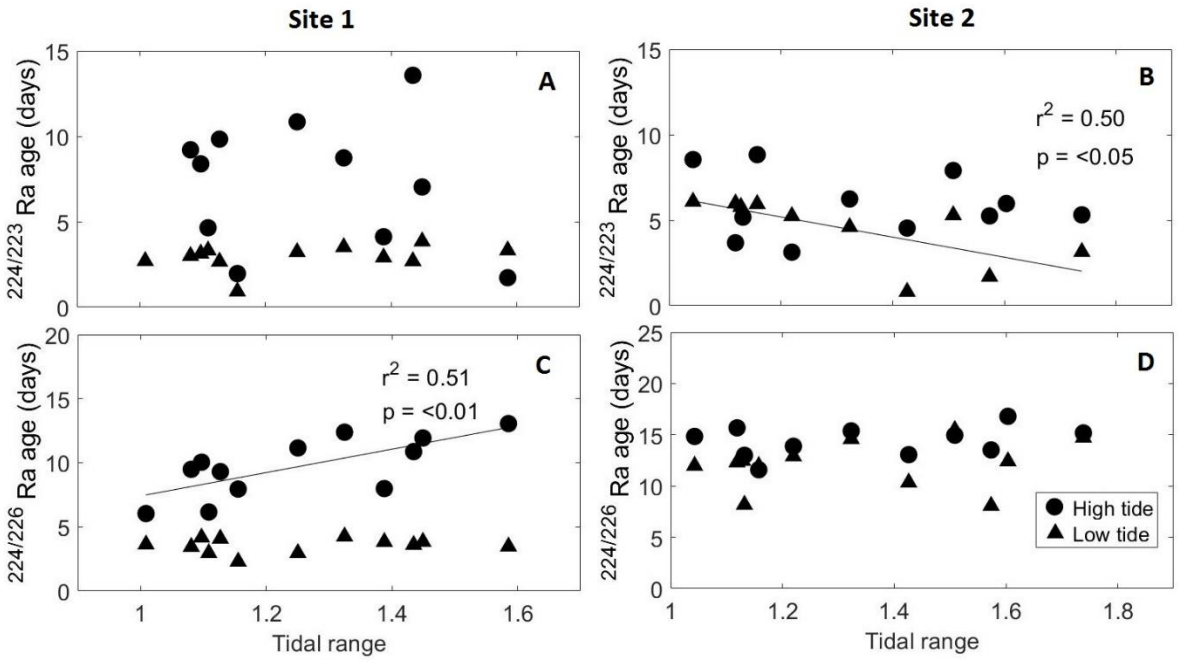

Figure 4.5 Apparent radium ages at Site 1 and Site 2 calculated using $^{224}Ra/^{223}Ra$ AR (A & B) and $^{224}Ra/^{226}Ra$ compared to tidal range.

Table 4.2 The mean calculated ^{224}Ra /^{223}Ra AR and ^{224}Ra /^{226}Ra AR water ages (+/- Standard deviation) from high tide and low tide samples and model derived flushing times over the survey period and neap and spring tide.

Location	Tidal stage	Mean Time (days)	Method
Site 1	High	7.3 +/- 3.8	Water mass age ($^{224}Ra/^{223}Ra$ AR)
	Low	2.9 +/- 0.7	
	Total	**5.0 +/- 3.4**	
	High	9.7 +/- 2.3	Water mass age ($^{224}Ra/^{226}Ra$ AR)
	Low	3.5 +/- 0.6	
	Total	**6.6 +/- 3.5**	
	Spring tide (survey period)	**4.5**	Flushing time (numerical model)
	Neap tide**	4.9	
	Spring tide**	5.7	
Site 2	High	5.9+/- 1.9	Water mass age ($^{224}Ra/^{223}Ra$ AR)
	Low	4.5 +/- 3.2	
	Total	**5.2 +/- 2.9**	
	High	14.4 +/- 1.5	Water mass age ($^{224}Ra/^{226}Ra$ AR)
	Low	12.1+/- 2.3	
	Total	**13.2 +/- 6.1**	
	Spring tide (survey period)	**4 – 20***	Flushing time (numerical model)
	Neap tide**	3.6 - 15.9*	
	Spring tide**	4.5 - 17.6*	

** = Flushing time calculated in the lower harbour mouth region and upper region (providing a range of times).*
***= Simulations where tracer was released at neap tide and spring tide under constant boundary conditions (i.e., average discharges assigned for all river inputs and no wind).*

4.4.4 Hydrodynamic model flushing times

Flushing times were calculated over multiple simulations using artificial conservative tracers (summarised in Table 4.2). For Site 1, the mean flushing time was 4.5 days, with tracer released at the start of the spring tide of the survey. Under steady boundary conditions (constant discharge, no wind), the mean flushing time for a neap tide and spring tide release was 4.9 and 5.7 days respectively. Site 2 had a mean flushing time of 4 days during the survey period. A neap tide and spring tide release under constant discharge conditions would result in a flushing time of 3.6 ad 4.5 days, respectively. The distribution of flushing times across the entire harbour was mainly dependent on the distance from the main entrance and deeper channels as well as proximity to freshwater sources from rivers and streams.

The model was adjusted to match measured salinity during the field survey, which required a 20% reduction of river flows at the boundaries (due to too much freshwater). High

tide salinity values at Site 1 and Site 2 were well matched but low tide values were more variable (Figure 4.6).

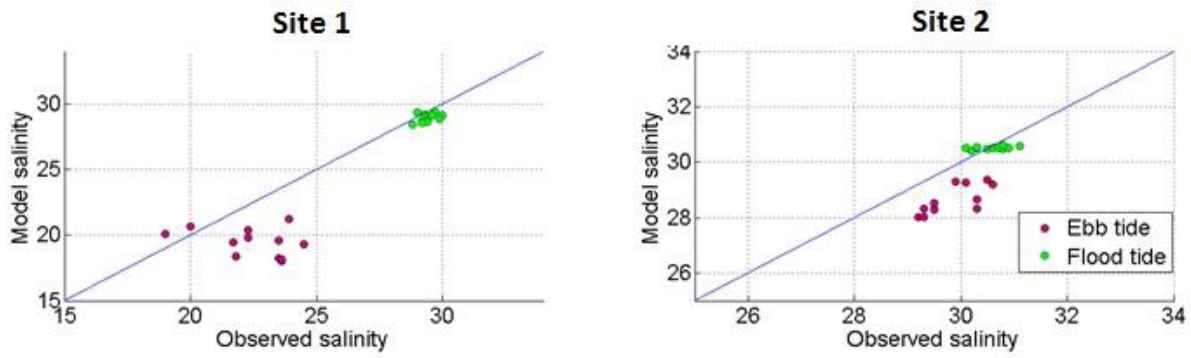

Figure 4.6 Comparison between modelled and observed salinity over the survey period. The blue line represents a 1:1 match.

4.4.5 Artificial tracer experiments:

To determine the likely origins of our water samples, we modelled the release of conservative tracers simultaneously across nine harbour sub regions (Figure 4.7 B). This approach allowed us to establish the relative contribution, expressed as a percentage, of different water masses at each of the two time series sites during the survey period.

At Site 1, samples taken on ebb tide were predominately sourced from the Waikareao estuary (region 6), which made up a mean contribution of 45% of the tracer mass at ebb tide over the survey period (Figure 4.7 A). At flood tide this changed dramatically, with only 3% of the tracer mass originating from region 6 making up the total relative tracer contribution (mainly due to the small relative volume). A large proportion of tracer from Site 1 was lost at the first ebb tide (~80%), with up to 33% returning on the following incoming tide (Figure 4.8 b). The upper reaches (region 1), middle of the harbour (region 4) and outside the harbour (region 9) made up the majority of the tracer mass entering back at flood tide (18%, 21% and 21% respectively) (Figure 4.8 b). This demonstrated the intimate connectivity between sub-regions and that a large proportion of water at Site 1 on high tide was sourced from different origins across the harbour.

At Site 2, the contribution from different regions was clearly well mixed on both ebb and flood tides (Figure 4.7 A). Samples taken on ebb tide were composed of 23% tracer mass sourced from region 1 and 4, with 20% of the total tracer mass sourced from outside the harbour (region 9). At flood tide, this changed to 28% of the tracer mass being sourced from region 9, 20% from region 4 and 16% from both region 1 and region 7 (Figure 4.7 A). Up to ~90% of initial tracer was lost on the first ebb tide, with~30% returning on the following flood tide (Figure 4.8 c). The sub estuaries with smaller relative volumes, such as, regions 2, 3, 6 and 8 made up < 10% of the total tracer mass at Site 2 over the survey period.

To account for upstream river inputs into sub-regions, a constant input of tracer was assigned to river inputs over the survey period. This resulted in an increase of tracer mass across some regions over time, particularly region 6 and region 8, which are close to a major supply of freshwater input. By the end of the survey period and at the neap phase of the tidal cycle, the sub-regions 8, 1, 5 and 6 had the highest amount of tracer mass in the system (Figure 4.8 a).

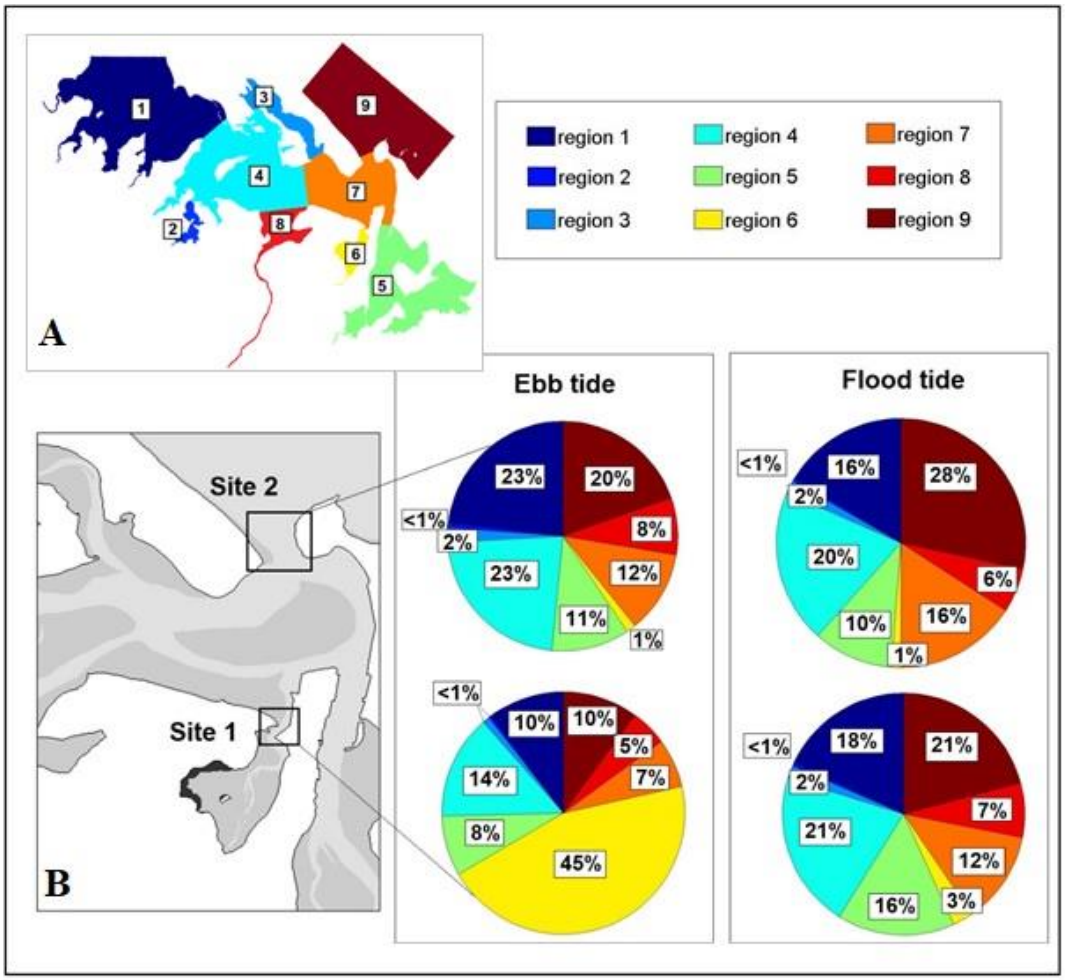

Figure 4.7 A). Map illustrating the nine different regions across the harbour where artificial tracer was uniformly released into the model. B). Pie charts illustrating the average tracer mass values (%) from ebb tide and flood tide samples at Site 1 and Site 2 over the survey period. This indicates the source and relative composition of waters collected during sampling.

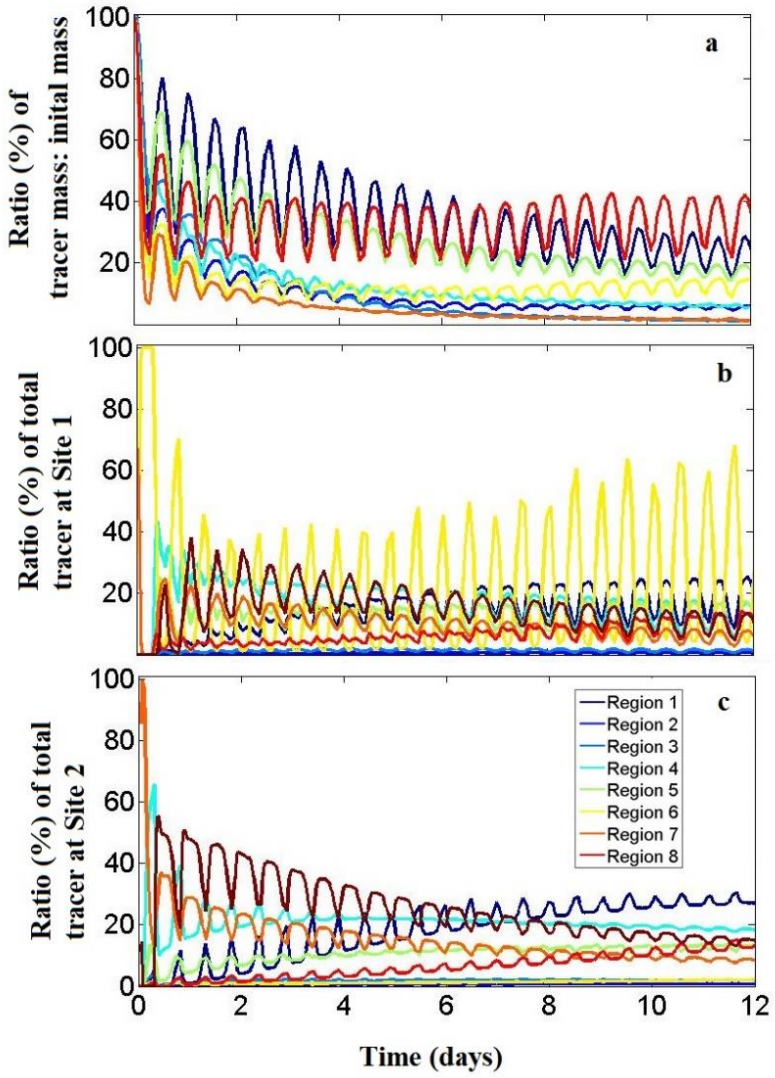

Figure 4.8 a) Ratio (%) of tracer mass lost over time to the initial tracer mass at each region of release. The ratio (%) of tracer mass from different regions contributing to the water mass at Site 1 (b) and Site 2 (c) over survey period.

4.5 Discussion

Daily measurements of radium over a spring-neap cycle demonstrated that the temporal variability in surface water radium ages was related to changes in tidal range, the effect of which depended on the scale of the water body. The approach of having time series stations chosen to target water bodies of different size revealed processes occurring over different scales such as tidal pumping (Santos et al., 2009a) and river discharge related 'pulse' events (Yang et al., 2008). Since our study covered 12- days of sampling, we observed temporary changes in biogeochemical concentrations at both sites following rainfall and

increased discharge. The proximity of Site 1 to upstream stream inputs may have made these 'pulse' events skew the relative tidal relationships between water ages by increasing mixing rates (faster flushing times). A large volume of the tidal prism at Site 1 (mean of 58%) is also exported each ebb tide.

The difference between high tide and low tide ^{224}Ra and ^{223}Ra concentrations was well pronounced at Site 1, with mean concentrations up to ~4 times higher compared to Site 2. This suggests the largely intertidal sub-estuary acts as a source of radium to the harbour, which is predominately through pore-water exchange (Santos et al., 2014) and submarine groundwater discharge (Stewart et al., 2018). Large fluxes of radium through tidally driven pore-water exchange have been demonstrated across other intertidal areas, including a tidal creek system in Australia (Sadat Noori et al 2016), and in the large tidal flats of the Wadden Sea, Germany (Moore et al., 2011).

Due to larger scale dilution processes and the mixing of multiple water masses from different harbour regions, the shorter-lived ^{224}Ra and ^{223}Ra isotopes would be decaying away from its sources as it moves towards the ocean, hence the relatively lower concentrations observed at Site 2. However, we hypothesise that a relationship between salinity, increased tidal range and concentrations of the longer lived ^{226}Ra (low tide samples only) at Site 2 may reflect larger regional scale tidal forces 'pumping' larger amounts of radium associated with fresher, older aquifer derived groundwater and/or river water into the harbour and coastal shelf.

While the role of tidal pumping in radium delivery has been investigated (Santos et al 2009b; Burnett et al., 2003; Moore 2010), the variations in radium over spring-neap cycles and multiple spatial scales have been less studied (Sadat-Noori et al., 2017). Radon (^{222}Rn), a natural gas tracer alternative to radium, has been used more frequently for extended time series studies due to the availability of 'in-situ' automated measurements, with applications in freshwater (de Weys et al., 2011), mangrove creeks (Call et al., 2019), estuaries (Sadat Noori et al., 2016) and coastal embayment's (Oliveira et al., 2003). However, due to its short half-life (3.8 days) and single isotopic decay product, radon alone cannot provide information on the spatially integrated age of water masses.

Using radium isotopes for assessing water ages highlighted important processes occurring in an estuarine lagoon over a spring-neap period. The delivery of ^{224}Ra, ^{223}Ra and

^{226}Ra into the water column is sensitive to the subtle changes in magnitude of the tidal phase at different scales. At the sub-estuarine scale a positive relationship (r^2 = 0.51 p=<0.01) between ^{224}Ra/^{226}Ra apparent Ra ages and tidal range demonstrated that older water from the harbour and shelf can be drawn in under stronger tidal forces. At Site 2, a negative relationship (r^2 = 0.5 p=<0.05) between tidal range and apparent ^{224}Ra/^{223}Ra water ages supported the hypothesis that tidal pumping associated with higher amplitude spring tides can yield younger apparent radium aged water, most likely from sub-estuarine regions and pore-water / groundwater exchange sources. Variations in flushing with respect to tide can also have important biogeochemical implications, as it has been suggested that a portion of tidal water that infiltrates sediments during spring tides is retained within the sediments before progressively seeping back into surface waters as tidal amplitude decreases (Call et al., 2019).

We assumed that the major input of radium isotopes in Tauranga harbour occurs through SGD rather than from sediment resuspension or diffusion from sediments (Stewart et al., 2018). Minor river and desorption ARs (Figure 4.4 A & B) were observed, along with relatively small freshwater inputs (2 - 17 m^3/s) and a SPM average of 5 $mg.l^{-1}$ (Cussioli et al 2019). Desorption from suspended sediments was a small contributor of radium in other systems, such as tidal ponds (Hougham and Moran 2007) and estuarine canals (Macklin et al., 2017). This is likely to be more significant for large rivers with high sediment loads, such as the Yellow River, China (Peterson et al., 2008) and other river dominated systems that contribute a single dominant source of radium (Dulaiova and Burnett, 2008).

The largest source of uncertainty in radium age calculations lies in the variability of the endmember initial activity ratio (AR) (Charette et al., 2008; Tomasky-Holmes et al., 2013; Cho and Kim, 2016). The initial activity ratio in this study is assumed to be supplied by brackish/saline pore-water from sediments, where the radium is produced by decay of the parent isotopes in the sediment or aquifer material (Hougham and Moran 2007). The geochemical behaviour of radium can be highly variable both spatially and temporally within subterranean estuaries (Gonnea et al., 2008; Beck et al., 2016). Applying an average of groundwater endmembers has been utilized in other tidally dominated estuaries to derive Ra ages (Tomasky-Holmes et al., 2013). We attempted to collect a range of spatially diverse groundwater endmember samples (n=11) covering variable salinities across intertidal areas.

However, this wide variability may not have been applicable to the smaller, largely intertidal sub-estuary of Site 1. Other studies which have faced challenges in defining a variable groundwater initial AR compensated by applying the highest value from surface water samples (Su et al., 2014).

We chose to use the maximum endmember as our initial $^{224}Ra/^{223}Ra$ AR for Site 1, although this may underestimate ages as the AR may be higher across the intertidal flats within the estuary. Due to the shallow sub-estuary environment, water is likely to have high radium activity from recent contact with nearby tidal flats outside the sub-estuary, resulting in surface waters with a high relative AR. However, the resulting apparent Ra ages (5 days) were in good agreement with the flushing times derived by the hydrodynamic model (4.5 - 5.7 days), which further validated this choice. For $^{224}Ra/^{226}Ra$ ages the mean groundwater endmember was chosen due to the higher ARs in the source groundwater (Figure 4.5 B). Using the maximum groundwater endmember for the initial AR would not affect the data trend but would result in substantial changes to the overall mean age by ~ 4 days, which demonstrates the sensitivity of Equation 4.1 to the initial AR.

When different water masses mix, the activity ratio of the younger water mass will dominate the mixture, particularly if there is a significant difference between the ages of the initial waters (Delhez et al., 2003, Rasmussen, 2003, Hougham and Moran 2007). For Site 2, the mean of all groundwater samples (mean AR = 32.1) was used to derive $^{224}Ra/^{223}Ra$ apparent ages. This was comparable to a previous survey of 22 mixed groundwater wells (mean AR = ~35) surrounding the harbour (Stewart et al., 2018). Changing this initial ratio to the maximum groundwater AR (~51) would result in an increase in the mean apparent Ra ages by ~3 days but would not affect the overall trend in results. Previous studies have also noted these sensitivities in apparent Ra ages to the initial endmember (Knee et al., 2011; Peterson et al., 2008).

Both the mean and maximum initial ARs used to derive $^{224}Ra/^{226}Ra$ apparent ages at Site 2 resulted in timescales that were ~ 4 – 5 times the half-life of ^{224}Ra (3.66 days), suggesting the water has travelled a distance away from its source (mean of 13 days, means ~90% of ^{224}Ra would have decayed). Although this is the upper limit to which these isotopes are applicable, they may still be underestimating older water masses from upper regions of the harbour. The spatially diverse flushing times of Tauranga harbour make the application of

either ^{224}Ra or ^{223}Ra isotopes valid to derive radium ages, although both techniques have drawbacks (^{224}Ra decays quickly and may not give the true upper age limits and ^{223}Ra is generally associated with higher errors due to lower activity (Peterson et al., 2008a). In systems that have expected flushing times greater than 10 days ^{223}Ra is generally applied together with a longer-lived isotope to derive ages (Charette et al., 2008). However, in either case, these underlying methods are based on apparent ages from the separation of its source.

Artificial tracer experiments using numerical modelling revealed the close connectivity between harbour sub-regions. For example, tracer that was injected in the upper regions of the harbour took multiple days to move towards the harbour entrance (Site 2) but then subsequently become a dominant source (23%) of the total tracer mass as the simulation continued over the spring-neap period (Figure 4.8 C). Water in the sub-regions of the harbour can take weeks to be flushed out and can be particularly sensitive to tidal changes (Tay et al., 2013). Water that reaches the harbour mouth can therefore have a large portion of 'older' waters as also noted through apparent Ra ages. Modelled flushing times revealed that water in the upper region of the harbour took between 16 – 20 days to be flushed, which was based on using a threshold of 37% (1/e) of tracer remaining across all cells in the region. However, if this assumption was changed and a 5% threshold was defined as the flushing time this would increase the timescales in the upper region by more than double (> 50 days).

The network of mangroves (Stokes et al., 2010) and intertidal flats across the harbour and within sub-estuarine regions would also likely retain water masses with changes to tidal amplitude and would not be flushed toward the ocean until another spring tide. This can have further biogeochemical implications for the transformation and uptake of nutrients and chemical constituents in the system. The influence of tidal pumping with changes to spring-neap tidal variations on carbon cycling has also been less studied (Taillardat et al., 2018). However, the variations in flushing with respect to tide can have important biogeochemical implications as it has been suggested that a portion of tidal water that infiltrates sediments during spring tides is retained within the sediments before progressively seeping back into surface waters as tidal amplitude decreases (Call et al., 2015).

We observed older aged water entering a sub-estuary region (Site 1) on a spring tide using apparent Ra ages which coincided with lower concentrations of dissolved inorganic nitrogen (DIN). Due to the distances within the harbour, older waters which circulate may

have lost nutrients to primary production and uptake in the water column (Kim et al., 2013). However, dissolved organic nitrogen (DON) remained at steady concentrations over both high and low tides (Figure 4.3) and can be transported over longer timescales. While the agricultural soils surrounding New Zealand catchments potentially hold large concentrations of DON, the significance of their presence in coastal systems relative to DIN is less understood (Lorite-Herrera et al., 2009). Remineralisation and recycling of DON within sediments, particularly in areas with longer flushing times can lead to increased higher concentrations of more bioavailable nutrients over time. The temporal variations in water circulation patterns over different scales can therefore have an important control on biogeochemical behaviour (Rueda et al., 2006). Longer flushing times in sub-regions combined with younger apparent Ra ages (assumed to be from pore-water/groundwater exchange) may also facilitate the build-up and transformation of nutrients in the water over time, possibly resulting in the occurrence of algal bloom events (Romereo et al., 2019). By assessing different processes of water transport, such as apparent Ra ages and hydrodynamics, the fate of chemical solutes, including nutrients and carbon within estuaries can be better understood and managed.

4.6 Conclusions

This study combined radium time series observations with hydrodynamic modelling to establish water ages and flushing times within an estuarine environment over a spring-neap period. Greater tidal magnitude resulted in younger radium water ages at different scales. At the harbour scale younger radium ages (2-6 days) were observed on spring tide using $^{224}Ra/^{223}Ra$, with older waters revealed using $^{224}Ra/^{226}Ra$ (mean ~13 days). The sub-estuary demonstrated large intertidal fluctuations in radium and had concentrations up to 4× higher than what was observed at the harbour entrance, with younger ages (mean ~3 days) at low tide and older waters entering from the main harbour at high tide (mean ~7.3 – 9.7 days). Hydrodynamic modelling provided flushing time estimates that were comparable to the timescales of apparent radium age estimates. Tracer experiments also established the relative contribution of different water sources, demonstrating the connectivity and mixing between regions within the harbour over a spring-neap period. The different timescales of water movement within different regions of estuaries must therefore be considered by managers.

GENERAL DISCUSSION

4.7 Summary of findings

This thesis aimed at increasing the knowledge in hydro-climatic drivers of nutrient exchange and macroalgal bloom events by investigating the role of submarine groundwater discharge and surface water interactions. The main findings are summarised below:

1. A comprehensive spatial survey using radium as natural groundwater tracers revealed 'hot spots' or likely areas of groundwater discharge occurring throughout a large estuary.
2. Significant groundwater and associated nutrient fluxes can occur through both re-circulated and fresh groundwater processes and be comparable to fluxes from major rivers and creeks.
3. Nutrient fluxes derived from groundwater can alter water column chemistry and provide the conditions needed to sustain macroalgal growth.
4. Large scale climate variations, such as El Niño southern oscillation can alter flushing times and estuarine functioning over seasonal and inter-annual timescales.
5. Changes in tidal magnitude and 'pulse' events play an important role in the transport and exchange of nutrients and radium between estuarine sub regions and the coastal shelf.

The main questions posed in the introduction of this thesis are revisited and discussed below:

1. What are the likely fluxes of nutrients from pore-water/groundwater exchange?

Chapter 2 provided a 'snapshot' spatial survey of the harbour and the surrounding catchment. Using radium isotopes, a mass balance was constructed to calculate the submarine groundwater discharge (SGD) flux rates for the entire harbour region. This was estimated to be 3.09 $\times 10^6$ m^3 day^{-1} or 2.83 cm day^{-1}, whereby the minimum estimate was 5.77×10^5 or 0.53 cm day^{-1}. These SGD rates were between ~1 and ~2.8 times the combined freshwater inputs from the surrounding rivers and streams during the survey period. This

demonstrated that groundwater discharge is a significant part of the hydrological cycle in the region. Groundwater nutrient concentrations (from shallow and deep bores) were observed to be orders of magnitude higher than river and harbour waters. The groundwater derived nutrient fluxes associated with SGD were ~5 times (Nitrogen) and ~8 times (Phosphorus) greater than the inputs from surrounding river sources. This suggests that regional inputs of SGD should be considered as a major source of nutrients into coastal waters.

2. ***Where are the likely hot spots of non-point (non-river input) nutrient fluxes in the harbour?***

The mass balance done in Chapter 2 attributed a large amount of the measured radium concentrations (~89%) to be attributed to SGD. The spatial survey was able to provide insight into likely areas where SGD could be occurring. The highest concentrations of the shorter-lived radium isotopes ^{224}Ra and ^{223}Ra were observed in the shallower upper regions of the harbour and sub estuarine regions. Both ^{224}Ra and ^{223}Ra decay on timescales that are comparable to tidal estuarine processes, including pore water exchange and likely give a picture of where recirculated saline waters are pumping through the sediments. The longest-lived isotope ^{226}Ra revealed areas of higher concentrations not observed with the shorter-lived isotopes in sub estuary regions of the harbour and across the harbour basin. Due to the very long regeneration rate in shallow sediments and slow decay rate (half-life 1600 years), this likely reflected fresher groundwater which is driven by older/slower processes.

The highest concentrations of dissolved inorganic nitrogen (DIN) were found to be in the lower regions of the harbour and around the harbour mouth. Dissolved inorganic phosphorus (DIP) was also highest in these regions. Due to the largely agricultural activity across the catchment high levels of dissolved organic nitrogen (DON) were observed in groundwaters and surface water. The upper regions of the harbour had the highest concentrations of DON, which decreased toward the harbour mouth. The large exposed tidal flats in the upper regions suggest the recycling of nutrients and transformation of organic/inorganic forms of nitrogen may be occurring in the sediments.

3. How do climatic variations such as El Niño southern oscillation (ENSO) influence harbour flushing times?

Chapter 3 determined water circulation patterns and flushing times with a hydrodynamic model developed with Delft 3D. Using conservative tracers, the calculated flushing times demonstrated significant spatial variations, with the longest flushing times observed in the upper regions. Seasonal simulations were run to match previous spatial surveys to validate the model. In addition to harmonic tidal forcing, the simulations and were forced with a historic timeseries of hydro-meteorological data. Although the system is tidally dominated, the flushing times revealed significant changes in response to river discharge, rainfall, and wind.

A challenge faced during this chapter was how to match the timescales of inter-annual climate signals (southern oscillation index) with the high resolution but computationally prohibitive model simulations. To overcome this, I used the outputs from 23 model simulations, covering a range of different forcing conditions (including extreme events) to train an artificial neural network (ANN). This approach provided an adaptive way of feeding changes in hydro-climatic forcing data for robust predictions of flushing times.

A 22-year hindcast (1995-2016) of daily dilution rates (a measure of flushing times) was predicted using the ANN. The changes in hydro-meteorological forcing associated with climate shifts between El Niño and La Niña periods was then demonstrated to influence dilution rates within different regions of the harbour. A significant relationship (r^2 0.43 p =0.001) between dilution rates and the southern oscillation index (SOI) was established, highlighting the importance of global scale climate patterns on estuarine functioning.

It was demonstrated that these climate induced changes in system functioning can have significant implications for water quality, including nutrient availability, storage, and transport within the harbour and to the coastal shelf. For example, the supply of organic nutrients can be converted to more readily available forms for biological uptake at the sediment/water interface, especially in regions of the harbour and during periods with slower flushing times.

4. ***What effect do spring-neap tidal ranges have on the exchange and transport of nutrients?***

In Chapter 4, I combined multiple radium time series stations and hydrodynamic modelling to establish water ages, flushing times, and dissolved chemical fluxes over a spring-neap period. This demonstrated the usefulness of applying different techniques to assess water movement in an estuary. This chapter established the relative contribution of different water sources and demonstrated the connectivity between regions within the harbour. Flushing time estimates using tracers in the model matched the timescales of calculated $^{224}Ra/^{223}Ra$ age estimates. The sub-estuary revealed large intertidal fluctuations in radium and had concentrations up to 4X higher than what was observed at the harbour entrance. The different timescales of water movement and processes occurring within different regions of estuaries in respect to tide must therefore be an important consideration in further studies, including monitoring due to the important implications for biogeochemical behaviour.

4.8 Conclusions

In summary, this research highlights the complex interactions between diffuse groundwater processes, climate variations and water circulation on nutrient exchange. A conceptual diagram illustrating these interactions is presented below (Figure G.1). Understanding these interactions is of importance because increased human population and changes in climate are impacting water quality across the world. This thesis found that regional scale groundwater-derived nutrient fluxes can be greater than that from rivers and creeks into a coastal lagoon system. These findings have contributed much needed estimates for the South Pacific region. Large scale climate variations, such as El Niño southern oscillation, were also demonstrated to influence estuarine functioning by altering regional hydrology, water circulation patterns and flushing times. This body of work has contributed to new applications in the field by using novel machine learning tools that are able to link across scales to get a highly variable and important flushing time. This has made it possible to match timescales of flushing times with long term climate drivers and has opened new questions for how climate might influence estuaries into the future. Tidal variations, apparent water ages and nutrient exchange were also assessed using numerical modelling and natural geo-chemical tracers. This has added insights into the application of multiple methods being used

to measure flushing times and water ages at different scales within an estuary. Overall, the results were able to shed light on natural processes that have historically been difficult to constrain (groundwater discharge) or limited by large differences in scales (climate signals and flushing times). These should be considered as important drivers of nutrient exchange and the development of algal blooms into the future and demonstrates the need for further multi-disciplinary approaches to estuarine management.

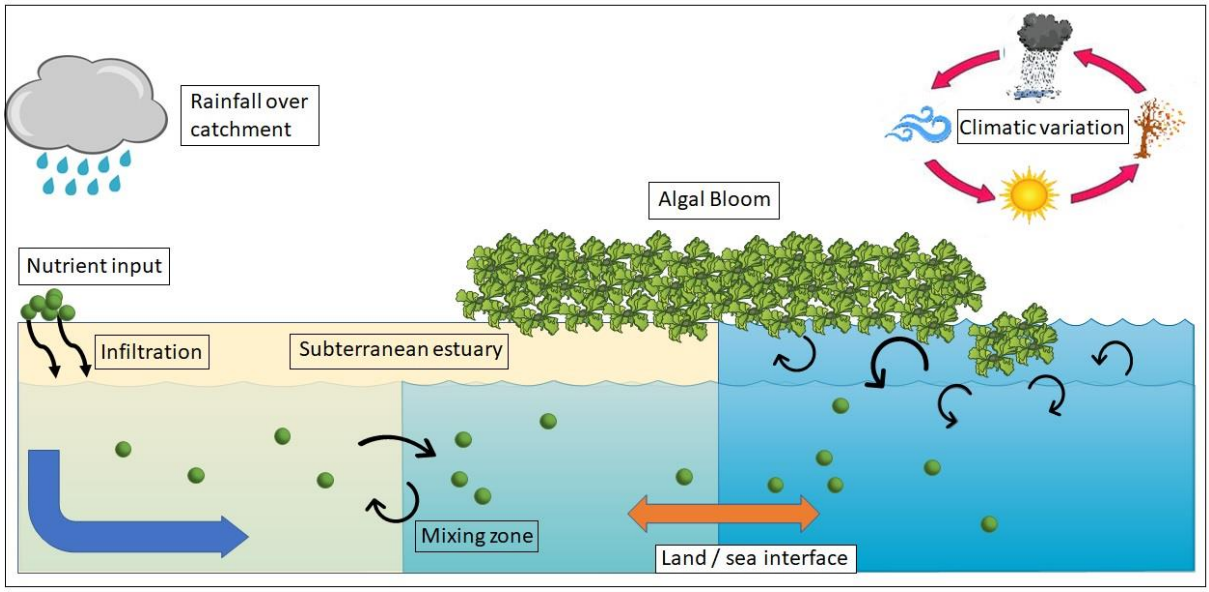

Figure G.1 A simplified conceptual diagram of the drivers of nutrient exchange and algal blooms.

4.9 Suggestions for future research

While this thesis was able to address some important questions regarding the drivers of nutrient exchange and estuarine water quality it has also helped to generate many more interesting research questions. The following suggestions would further build on the work presented.

Firstly, future studies investigating submarine groundwater discharge should also attempt to quantify the ages and residence times of the fresh groundwater flows between the land and ocean. Since groundwater generally moves slower than surface water, establishing the likely lag times would help better understand the timescales of contaminant inputs into surrounding aquifers and its release in a coastal area. For example, does wastewater infiltrated into groundwater in winter enter the coastal water column in summer? Investigating how flows change over different timescales such as seasons and different hydro-

climatic ‘pulse’ events (flood and drought) would be an interesting and important question for future research.

Separating and quantifying fresh groundwater flows to re-circulated pore-water processes in coastal environments is a challenge that is an active area of research. Due to the complex mixing processes that occur in subterranean estuaries it can be difficult to define where or when mixing of fresh and saline water starts and ends. Predicted changes in sea level and the dynamic shifting of coastlines can further complicate this matter. The aerial reconnaissance of coastal environments with drones fitted with high-resolution thermal infrared cameras or specialised satellites could help to better separate these processes by differences in water temperatures. Preliminary mapping of freshwater seeps is especially of interest for oceanic and volcanic islands. Although currently unexplored, the offshore shallow and volcanic environment across the Bay of Plenty region may provide large amounts of freshwater and dissolved chemical constituents through diffuse SGD, hydrothermal vents, and volcanic plumes to the surrounding ocean. What role does this play in water and biogeochemical cycles?

In regard to nutrients and algal blooms, I have three suggestions: 1). Land based human activities, such as land clearing, development and excessive agriculture have undoubtedly contributed to higher nutrient loads into our oceans. Sediment coring and dating of regions surrounding coastal catchments would provide a chronology of enrichments and help establish timescales and sources. 2). To mitigate nutrient uptake across catchments, re-establishing native forests and trees could create employment opportunities along with numerous environmental benefits for human health, biodiversity, and water quality. Excessive algal bloom biomass currently in our estuaries could perhaps even be used as nutrient rich fertiliser to start this process! 3). The use of numerical models is useful for management decisions and monitoring but must be complemented with targeted field investigations and baseline data. Coupled groundwater and coastal process models with the inclusion of biogeochemical additions, such as nutrients, will aid in threshold limits to be set for the future and allow better predictions for estuarine water quality to be made.

APPENDIX A

The role of mangroves in filtering groundwater-derived nutrients in the Firth of Thames (New Zealand)

Strategic investment fund project 2016 – present:

Problem / Research question:

Nutrient loading to coastal systems is a global problem that is likely to increase as population pressure increases demand to food production. Establishing pathways and predicting the timescales over which these pathways change is an essential component to understanding how our coastal ocean will change. Moreover, understanding subtle and long-term changes to the chemical composition of the ocean is a critical step in assessing how systems may cope with climate change. We explore the question: 'to what degree do mangroves influence the nutrient loading of groundwater entering the Firth of Thames?' Is this comparable to similar-sized fringing non-mangrove wetlands and similar sized non-vegetated intertidal regions?

Overall Aim / Description of research initiative:

Nutrients are used intensively in farming to enhance production. A consequence of this is that nutrient run-off from pasture land can exceed native forest by several orders of magnitude, and cause stress on coastal ecosystems, including excess vegetation growth, low oxygen and invasive species. Rivers and streams are relatively easy pathways to monitor for nutrients. Conversely, groundwater pathways are currently an insurmountable challenge, mainly because of the long timescales involved and the complex structure of New Zealand's coastal aquifers that are heavily influenced by volcanic and tectonic processes. Moreover, this thesis has suggested that large volcanic islands may contribute a disproportionate amount to fresh and recirculated groundwater into the global coastal ocean. We have demonstrated the usefulness of radium isotopes ^{224}Ra (half-life=3.7 days), ^{223}Ra (half-life=11.4 days), ^{228}Ra (half-life = 5.75 years), ^{226}Ra (half-life = 1600 years) as groundwater

tracers within Tauranga harbour, an estuary with a steep catchment, sandy sediments and limited fringing vegetation. Radium isotopes, which are effective within coastal and marine environments and decay from naturally occurring Uranium and Thorium, are activated when the parent rock material comes into contact with saltwater. Our results in Tauranga harbour confirmed that groundwater is an unusually important source of chemical constituents to the coast. To extend this work we have undertaken further surveys of an extremely contrasting estuary (Firth of Thames) to provide a more nationally relevant platform for New Zealand on the processing of catchment derived nutrients by coastal fringing ecosystems. Due to the large river inputs with high suspended sediment loads and extensive fringing vegetation (mangroves in particular) the groundwater signature may be substantially diminished in the coastal nutrient budget. Comparing and identifying areas which may be river dominated and/or groundwater dominated systems will be important in the appropriate management of coastlines into the future.

The research team involved in this project are Karin Bryan (University of Waikato), Isaac Santos (Southern Cross University / Gothenburg University), Conrad Pilditch (University of Waikato) and Luitgard Schwendenmann (Auckland University). Isaac Santos has conducted numerous groundwater investigations and results from previous work show groundwater contributions are comparable, and in some instances, higher in New Zealand than similar systems in Australia. We extended our investigations to a very different type of impacted site (fine sediment dominated, extensive mangroves, very intensive dairying), with the Firth of Thames an ideal complement. Luitgard has successfully published work in this region and has a background in forest/wetland ecology that further strengthens this multidisciplinary team. This will allow a broader understanding of forest pathways and the process of excess nutrient up-take and mediation. We expect that the influence of mangroves in the Firth of Thames will play a far more dominant role than in Tauranga Harbour.

This project consisted of multiple field surveys conducted during 2016. Offshore transects were conducted parallel to the shoreline, which were sampled at 1 km intervals into the Hauraki Gulf. A survey of the Waihou river was also carried out which captured the transitioning salinity gradient from the river mouth to upstream regions. Groundwater collection was undertaken across the fringing mangrove forests and surrounding catchment area. Samples from 2~metre long wells dug into sediments and deeper aquifer derived water

from surrounding wells were collected. River samples from the Piako and Waihou rivers as well as other minor streams and freshwater inputs were also collected to have a clear understanding of landward inputs. Samples were processed in the laboratory using a radium delayed coincidence counter (RaDeCC), which was on loan from Southern Cross University. Hydrodynamic models were also implemented and are critical in calculating the bulk fluxes of nutrients in and out of the system. Existing hydrodynamic data on the tidal currents through the mangroves will be used from Masters student Rebekah Haughey, who was supported by the Waikato Regional Council.

Preliminary results

Surface water surveys of salinity using CTD cast measurements provided data on the salinity gradient from the Waihou River and offshore (Figure A.1). These measurements are useful validation data for calibrating hydrodynamic models that will later be used. Salinity increased further offshore into the Hauraki Gulf.

The effect of desorption of ^{223}Ra from suspended sediments in the Waihou river is demonstrated in Figure A.2. Once river waters become brackish ^{223}Ra concentrations increase and become variable before steadily increasing up to higher salinities. Considering desorption as a source of radium into the Firth of Thames will be an important consideration in further analysis and mass balances due to the high volume of suspended sediments from land. Radium can also be used as a geochemical tracer method to track the transport and mixing of river derived water into the Haruki Gulf. This will further compliment any hydrodynamic modelling done.

Concentrations of ^{223}Ra were observed to be in high concentrations adjacent to the mangrove fringes on the western coast (Figure A.3). While a mass balance of radium is yet to be carried out, these results indicate initial 'hotspots' of relatively higher concentrations. Mid to high concentrations (1.15 -2 dpm/100L) were also observed to be in close proximity to river sources as well as the western coastline. These concentrations reduced offshore into the Hauraki Gulf.

Concentrations of the longest-lived isotope (^{226}Ra) with a half-life of 1600 years revealed different patterns to the short-lived isotope (^{223}Ra). The highest concentrations (~13

dpm/100L) were observed along the western offshore transect closet to shore (Figure A.4). Peaks were also observed in the middle regions of the offshore transect. This is an interesting finding as older isotopes such as ^{226}Ra are not affect by decay or short scaled processes but rather much older process such as contact with deep aquifers. Coupling our results with regional groundwater models will be useful to better understand sources in coastal areas and invite further collaboration.

Analysis and write-up of results is underway and will build to the knowledge of groundwater / surface water interactions across New Zealand into the future.

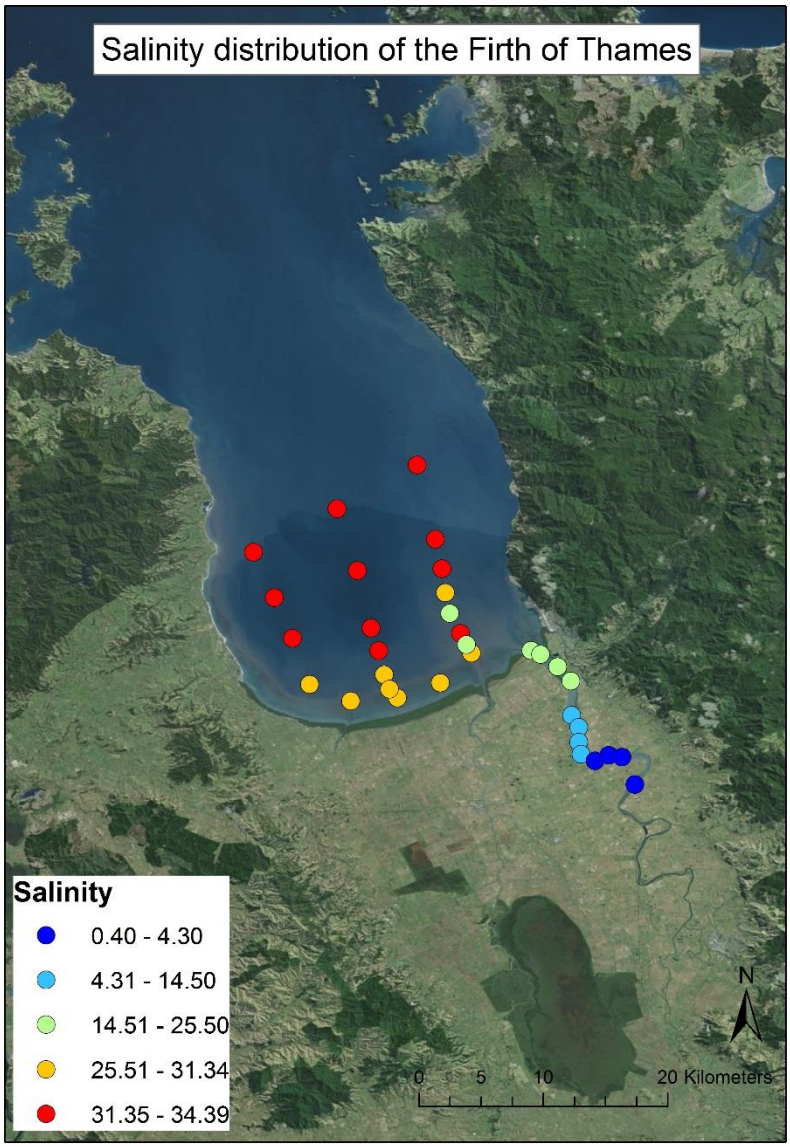

Figure A.1 Spatial distribution of salinity in the Firth of Thames, including upstream Waihou River.

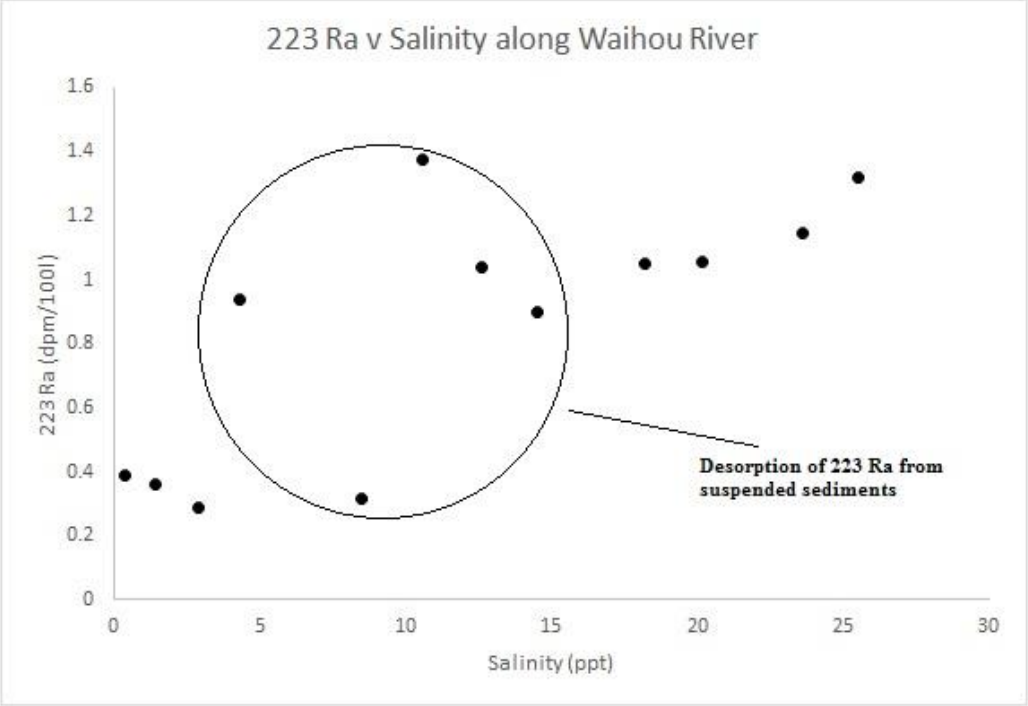

Figure A.2 The relationship between ^{223}Ra and salinity within the Waihou River. Increases in ^{223}Ra activities after a salinity of ~5 suggest desorption from suspended sediments.

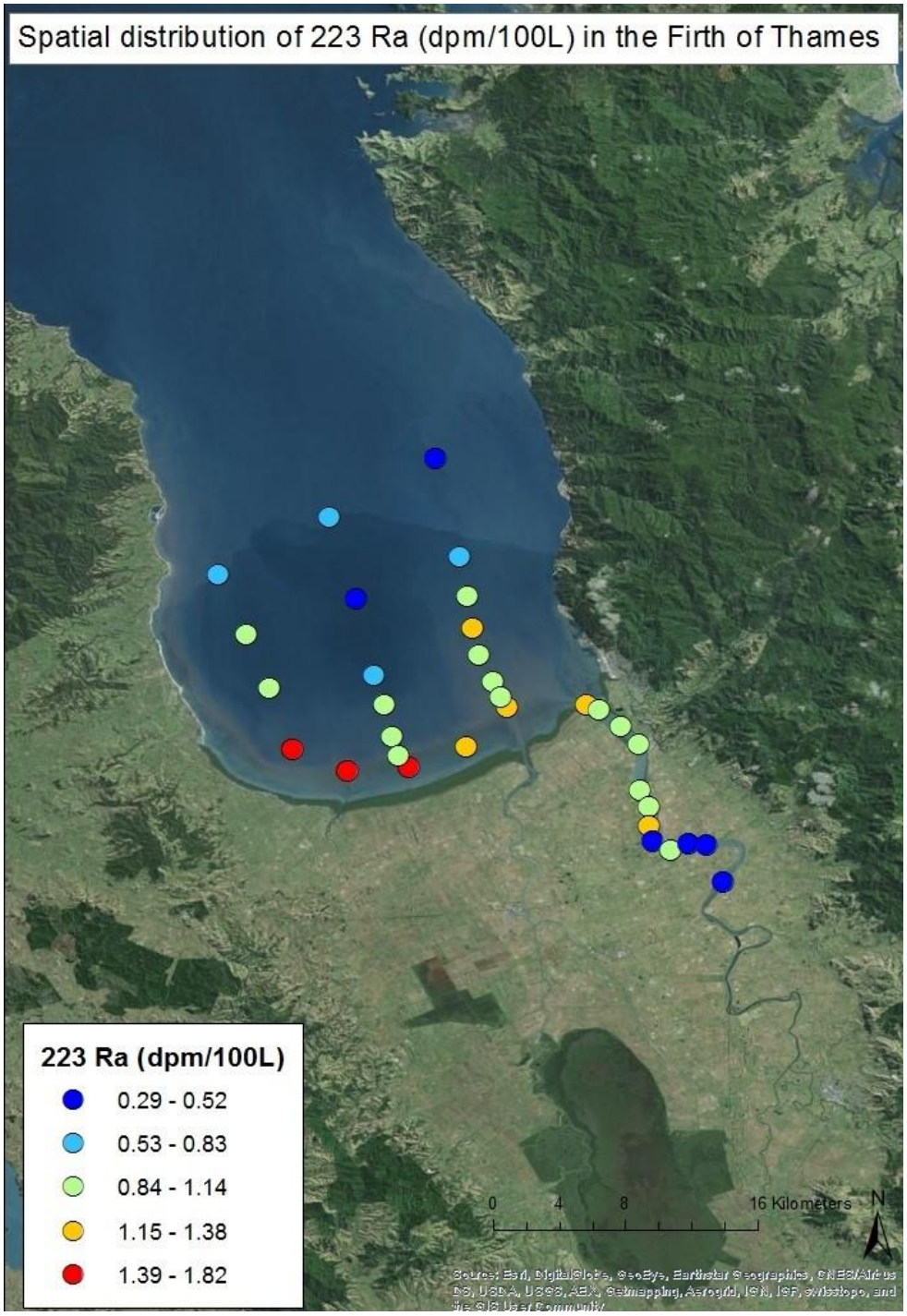

Figure A.3 Spatial distribution of ^{223}Ra within the Frith of Thames and Waihou River.

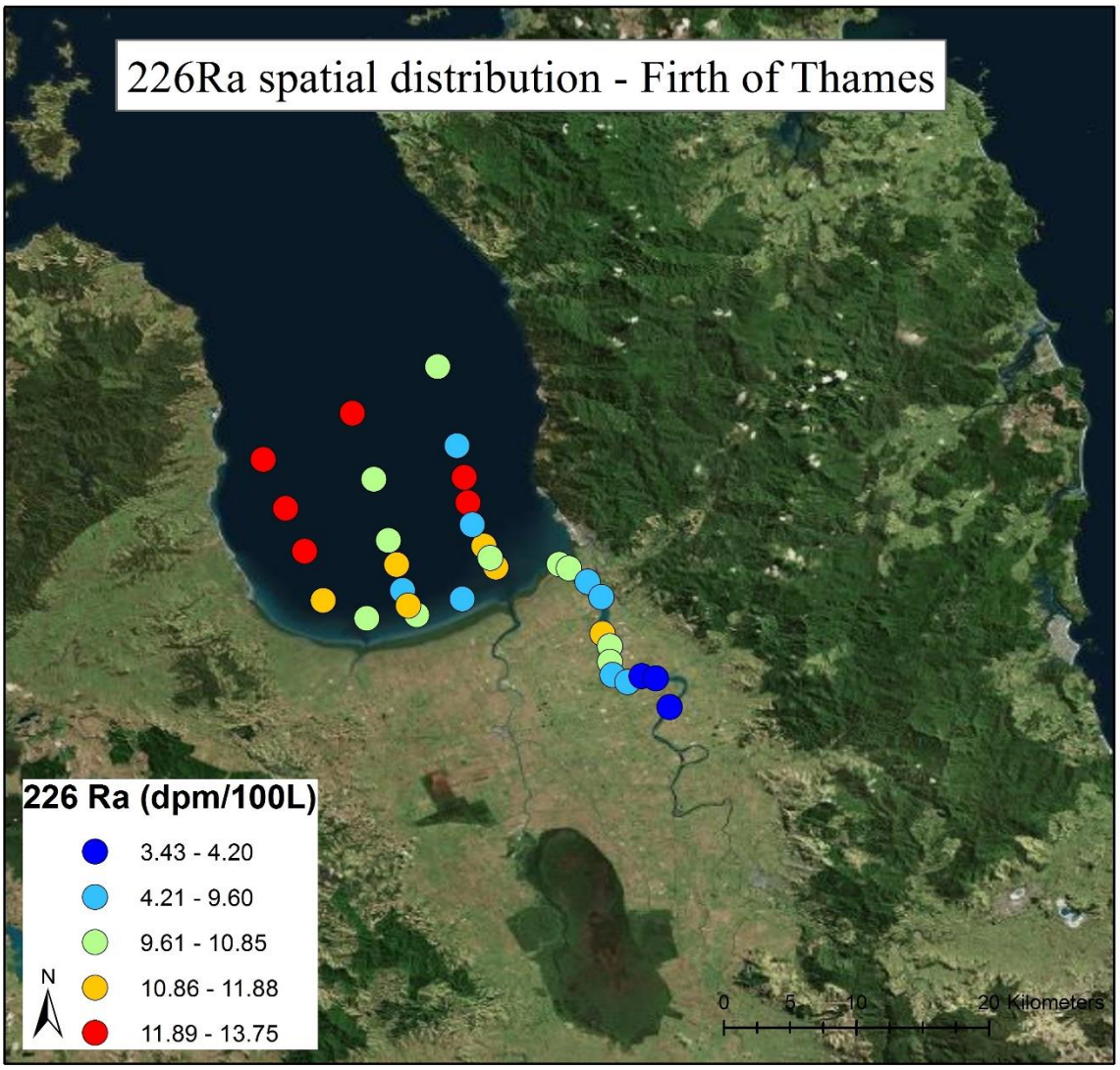

Figure A.4 Spatial distribution of ^{226}Ra within the Frith of Thames and Waihou River.

APPENDIX B

Determining coastal water mass ages and tracer mixing using radium isotopes and hydrodynamic modelling (Delft-3D)

One of the challenges of using radium (Ra) isotopes to derive apparent Ra water ages is a good understanding of the sources and activity of initial groundwater endmembers. During this thesis we have applied radium isotopes alongside hydrodynamic modelling. It is common in the literature for field-based investigations and numerical simulations to be carried out independently of each other. However, new developments in modelling techniques allows both methods to complement each other and provide further insights into radium ages and mixing in coastal waters as well as groundwater/surface water exchange.

As an addition to using conservative tracers I have been able to simulate the input radium (^{223}Ra,^{224}Ra,^{226}Ra), a natural radionuclide tracer of groundwater, as a decayable tracer using the DELWAQ module (Delft3D). This involves in knowing the potential sources, flux rate estimates and relative decay constants of radium into a coastal system (which we established in the first paper of this thesis). I conducted tracer tests to simulate the release of radium into Tauranga Harbour and allowed simulations to run for 1 month to allow for mixing. Tracer was released from cells within the model of suspected groundwater sources as a continuous input. Flux rates were estimated based on our previous study (Stewart et al., 2018). This demonstrated interesting results for the relative ages of ^{224}Ra (Figure B.1), ^{223}Ra (Figure B.2) and ^{226}Ra (Figure B.3). The ages from our initial test simulations were well matched with the age timescales derived from the empirical Ra age calculations.

This shows promise as a useful method to further assess the timescales of water movement in the harbour and includes potential groundwater sources in harbour hydrodynamics. It may also help minimise errors associated with common assumptions of 'snapshot' studies and help provide a dynamic framework for future studies. A technical paper on this method will be further developed for publication.

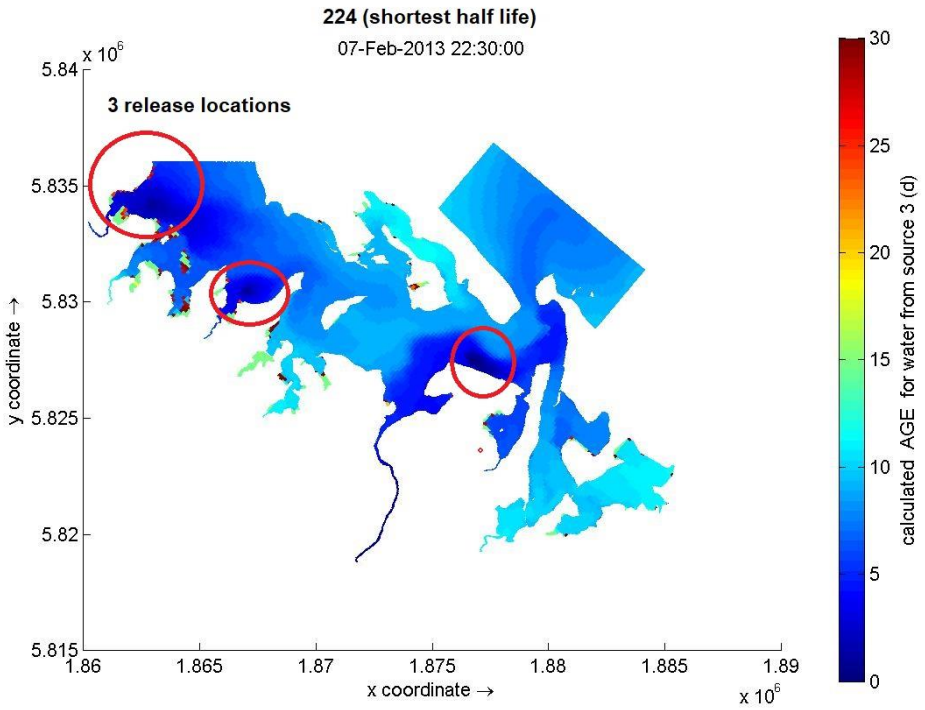

Figure B.1 Spatial distribution of ^{224}Ra ages within Tauranga harbour. Circles indicate the 3 release locations that were assumed to be areas of submarine groundwater discharge (SGD). Ages appear younger close to the source due to the continual input throughout the simulation.

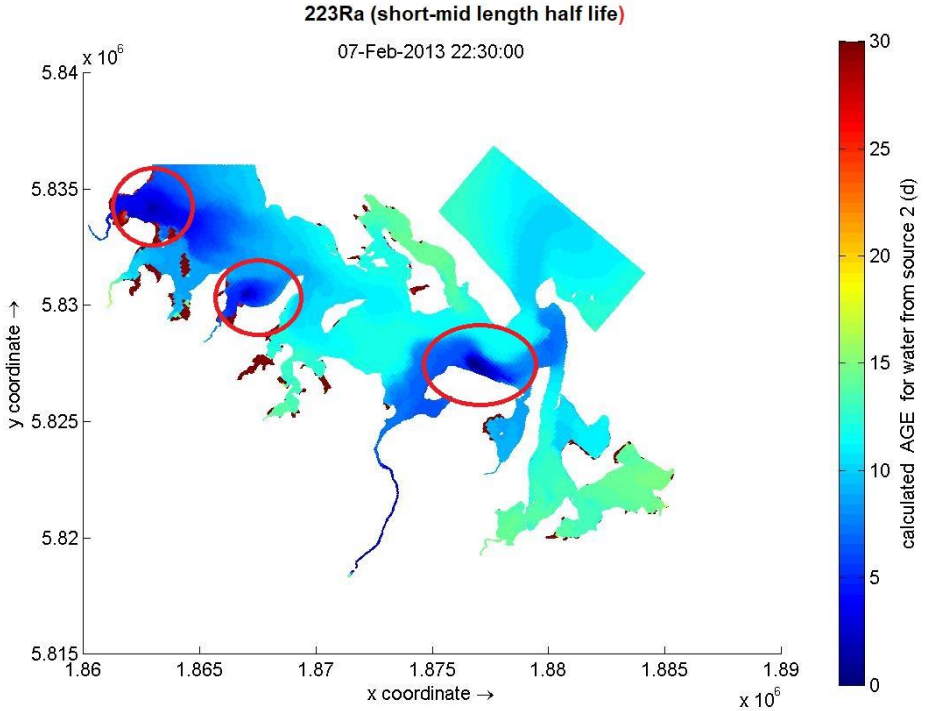

Figure B.2 Spatial distribution of ^{223}Ra ages within Tauranga harbour. Circles indicate the 3 release locations that were assumed to be areas of submarine groundwater discharge (SGD). Ages appear younger close to the source due to the continual input throughout the simulation.

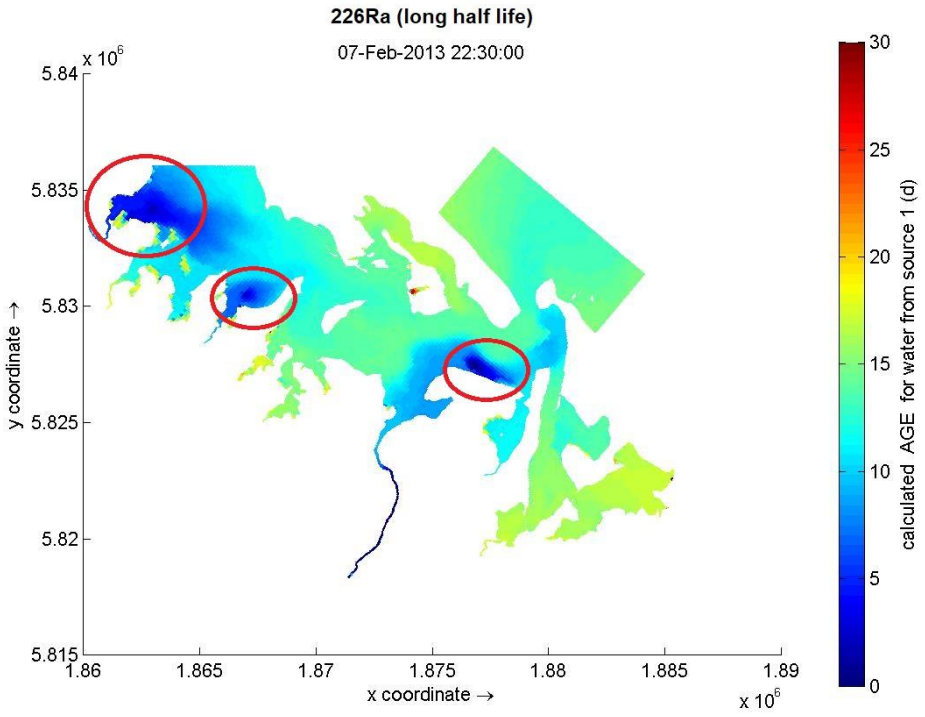

Figure B.3 Spatial distribution of ^{226}Ra ages within Tauranga harbour. Circles indicate the 3 release locations that were assumed to be areas of submarine groundwater discharge (SGD). Ages appear younger close to the source due to the continual input throughout the simulation.

APPENDIX C

Hydrodynamic Simulation Setup and Parameters

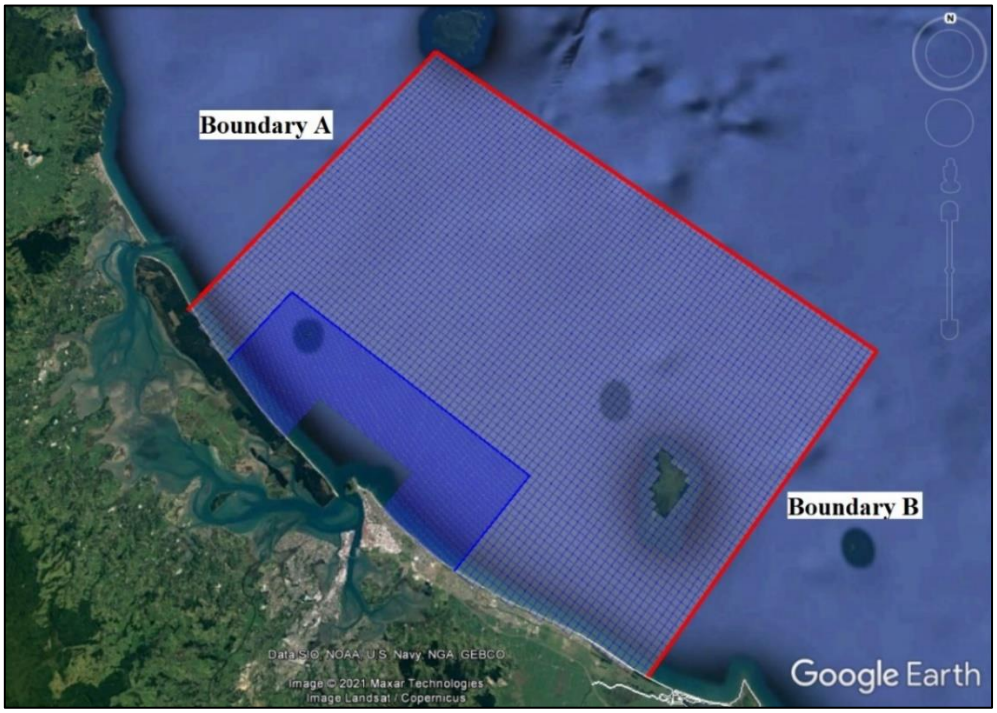

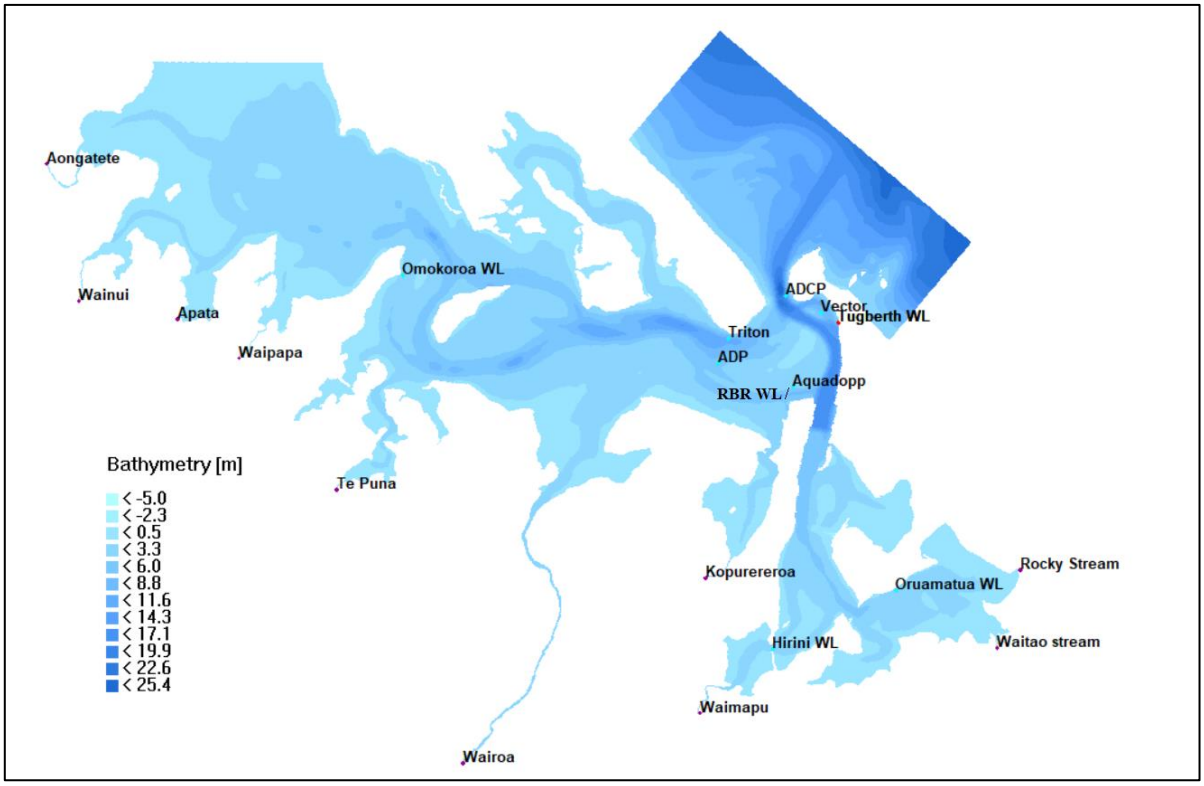

Figure C.1 Model domain, bathymetry, open boundaries (red lines), and instruments locations (blue circles and red triangles).

Table C.1 Model parameters used in the calibration of the hydrodynamic module

Time step	0.5	minutes
Gravity	9.81	m/s^2
Water density	1000	kg/m^3
Roughness	75 - 35	Spatial varying map used
Horizontal eddy viscosity	10	m^2/s
Threshold depth	0.1	m
Advection scheme for momentum	cyclic	
Depth at grid cell faces	mean	
Drying and flooding check at	grid cell centres and faces	
Open boundary type	water level	
Reflection parameter alpha	50	
forcing type	astronomic	

Table C.2 Amplitude and phase of tidal constituents used as astronomic forcing for water level at the open boundaries. Note offshore open boundary used interpolated values between A and B boundaries (Source: NIWA tide forecaster).

Tidal Constituent	Amplitude (m)	Phase (deg.)
Boundary A		
K1	0.0766	171.55
O1	0.0177	133.47
M2	0.6984	180.59
N2	0.1569	147.06
S2	0.0731	260.38
Boundary B		
K1	0.0769	172.5
O1	0.0212	124.31
M2	0.7066	179.72
N2	0.1557	144.11
S2	0.0735	262.97

Table C.3 River discharge used during the calibration and validation runs (Source: Watson, 2016).

River name	Discharge (m3/s)
Aongatete	2.30
Wainui	0.94
Apata	0.21
Waipapa	1.01
Te Puna	0.69
Wairoa	17.60
Kopurererua	2.28
Waimapu	3.34
Waitao stream	1.03
Rocky Stream	1.09

River discharge predictions

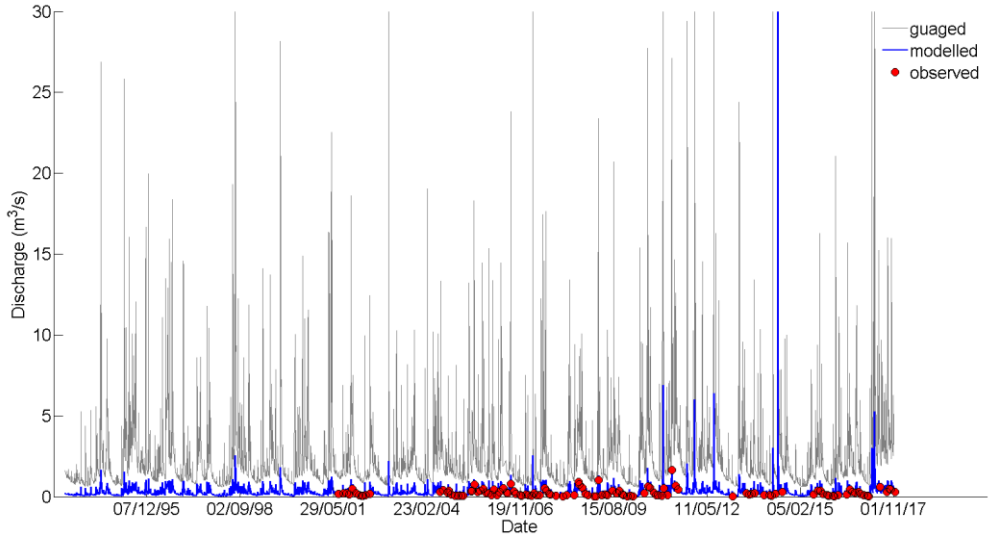

Figure C.2 Reconstructed river discharge of Rocky Stream using Waimapu river discharge data as a predictor.

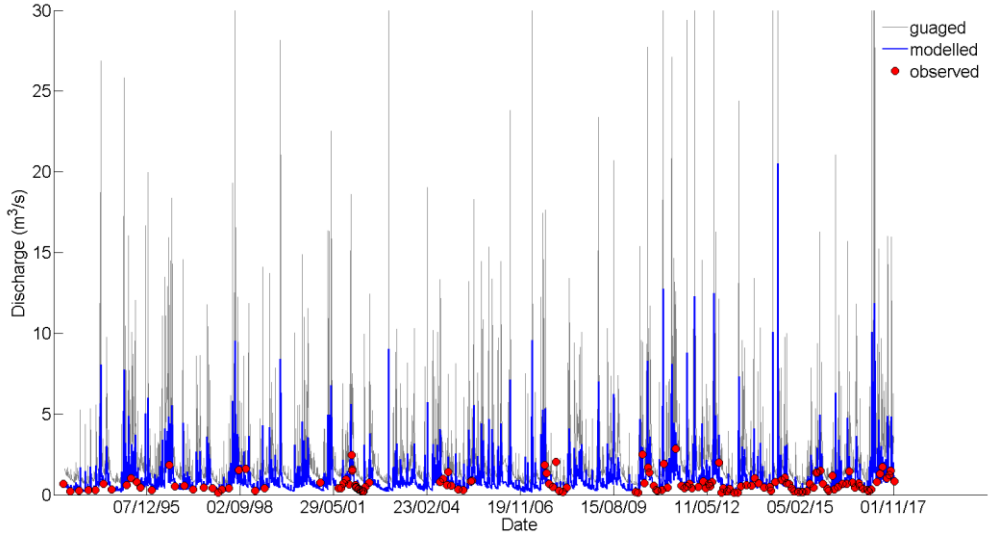

Figure C.3 Reconstructed river discharge of Waitao Stream using Waimapu river discharge data as a predictor.

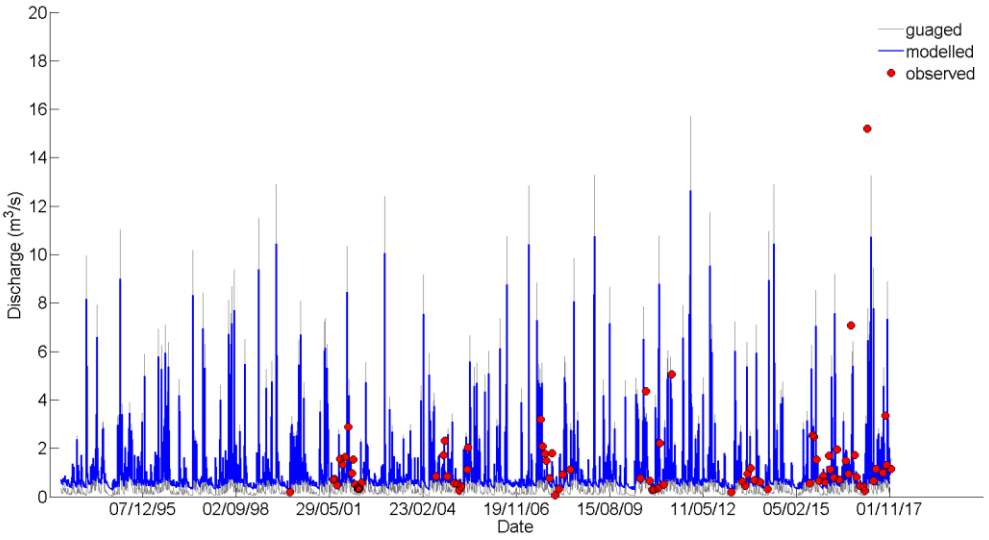

Figure C.4 Reconstructed river discharge of Aongatete River using Waipapa river discharge data as a predictor.

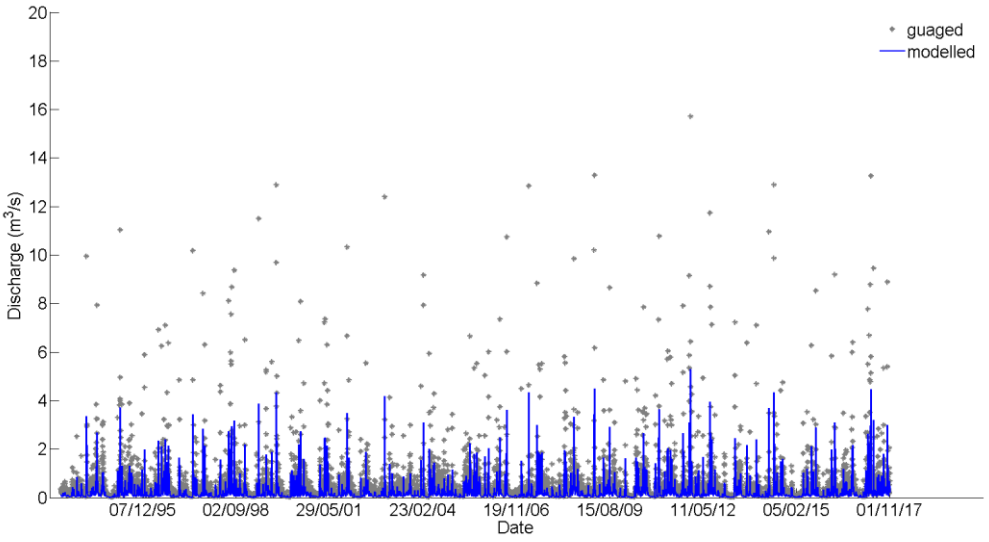

Figure C.5 Reconstructed river discharge of Apata River using relationship between catchment size and Waipapa discharge data as a predictor.

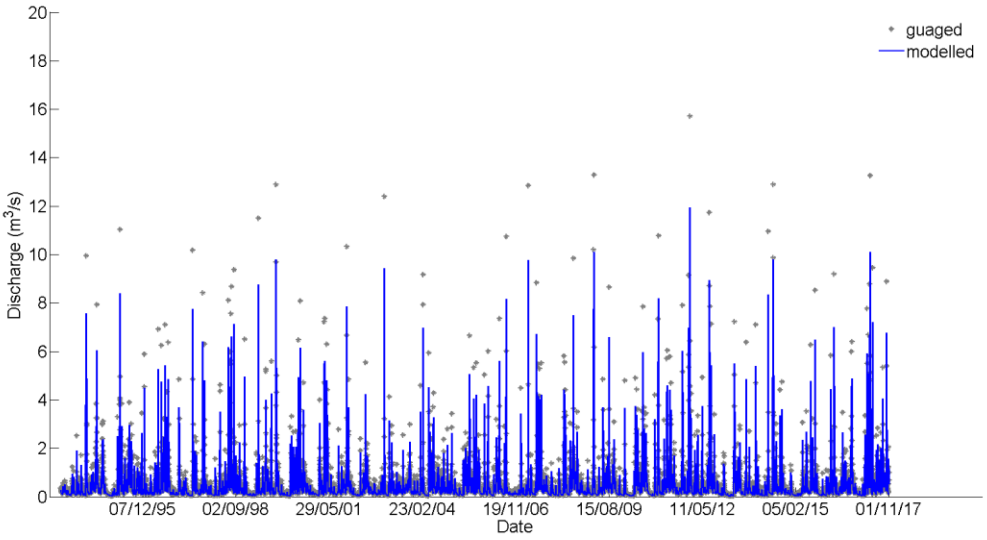

Figure C.6 Reconstructed river discharge of Te Puna Stream using relationship between catchment size and Waipapa discharge data as a predictor.

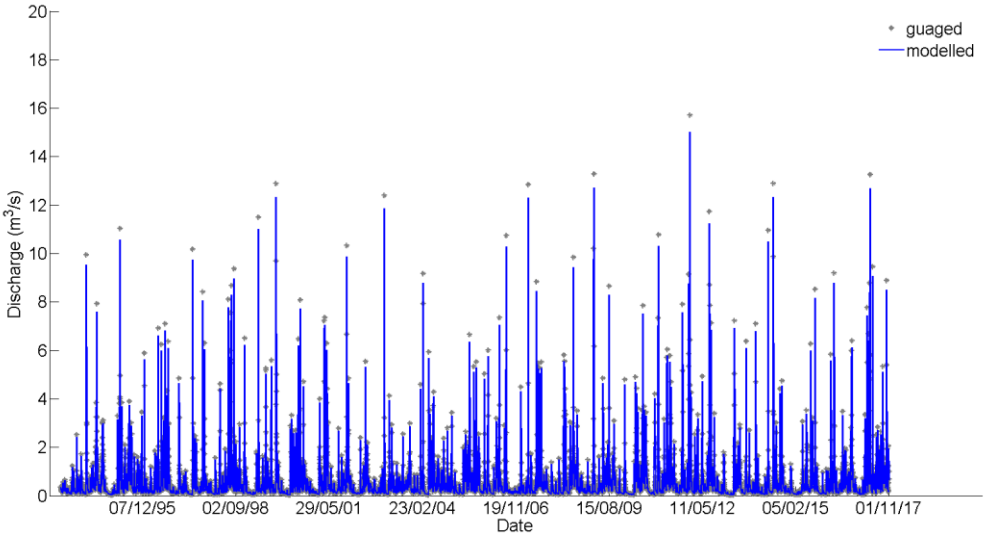

Figure C.7 Reconstructed river discharge of Wainui River using relationship between catchment size and Waipapa discharge data as a predictor.

APPENDIX D

Hydrodynamic Calibration and Validation

Statistical analyses (bias, accuracy, and skill) were based on Sutherland et al. (2004). Bias was determined following the equation:

$$Bias = \frac{1}{J}\sum_{j=1}^{J}(y_j - x_j) = \langle Y \rangle - \langle X \rangle$$

where Y is the model results, X is the measured data, J is the number of predictions and observations occurring at the same time and location. Angular brackets represent the mean.

Accuracy was determined by the Mean Absolute Error (MAE) and by the root mean square error (RMSE):

$$MAE = \frac{1}{J}\sum_{j=1}^{J}(y_j - x_j) = \langle |Y - X| \rangle$$

$$RMSE = \sqrt{\frac{1}{J}\sum_{j=1}^{J}(y_j - x_j)^2} = \sqrt{\langle (Y-X)^2 \rangle}$$

where straight brackets represent the absolute value of the errors.

Bias was calculated using the following equation:

$$BSS = 1 - \frac{MSE(Y,X)}{MSE(B,X)} = 1 - \frac{\langle (Y-X)^2 \rangle}{\langle (B-X)^2 \rangle}$$

where B is the average of measured data.

The classification based on BSS score ranges from bad to excellent according to Sutherland et al. (2004):

BSS score	Classification
BSS <0.0	bad
0.0> BSS <0.1	poor
0.1> BSS <0.2	reasonable/fair
0.2> BSS <0.5	good
0.5> BSS <1.0	excellent

Results of Calibration and Validation

*Table D.1 Statistical parameters calculated to evaluate the calibration of the hydrodynamic model at location of current meters and water level sensors deployed during field campaign in March 2017. *Current direction measured by the Vectrino was excluded from the calibration.*

	Bias	MAE	RMSE	BSS
Speed	**(m/s)**	**(m/s)**	**(m/s)**	
Triton	0.02	0.08	0.11	0.78
ADP	-0.03	0.07	0.08	0.56
AQUA	0.01	0.06	0.08	0.80
ADCP	-0.17	0.19	0.22	0.72
VEC	0.00	0.06	0.07	0.72
Direction	**(deg.)**	**(deg.)**	**(deg.)**	
Triton	-2.54	17.28	38.24	0.85
ADP	-14.77	49.09	80.98	0.33
AQUA	-2.76	13.91	40.44	0.79
ADCP	4.09	38.80	55.82	0.29
VEC*	11.95	70.92	115.01	-0.01
Water Level	**(m)**	**(m)**	**(m)**	
Omokoroa	-0.14	0.14	0.17	0.90
Hirini	0.02	0.08	0.10	0.97
Oruamatua	-0.04	0.16	0.18	0.90
Tug berth	-0.14	0.15	0.19	0.87
RbR	0.01	0.08	0.10	0.96

Table D.2 Statistical parameters calculated to evaluate the validation of the hydrodynamic model at the locations of current meters and water level sensors.

	Bias	MAE	RMSE	BSS
Speed	**(m/s)**	**(m/s)**	**(m/s)**	
Triton	0.06	0.09	0.12	0.80
ADP	-0.04	0.07	0.10	0.56
AQUA	0.01	0.06	0.08	0.82
ADCP	-0.17	0.20	0.25	0.80
VEC	0.01	0.07	0.08	0.72
Direction	**(deg.)**	**(deg.)**	**(deg.)**	
Triton	-4.31	18.15	0.12	0.84
ADP	-20.99	39.89	64.98	0.50
AQUA	-2.89	13.36	39.12	0.80
ADCP	2.49	36.81	56.36	0.33
VEC	-1.83	67.45	111.15	0.13
Water Level	**(m)**	**(m)**	**(m)**	
Omokoroa	-0.15	0.15	0.18	0.90
Hirini	0.01	0.08	0.10	0.97
Oruamatua	-0.15	0.16	0.18	0.90
Tug berth	-0.17	0.19	0.23	0.84
RbR	0.01	0.09	0.10	0.97

Calibration plots - Currents

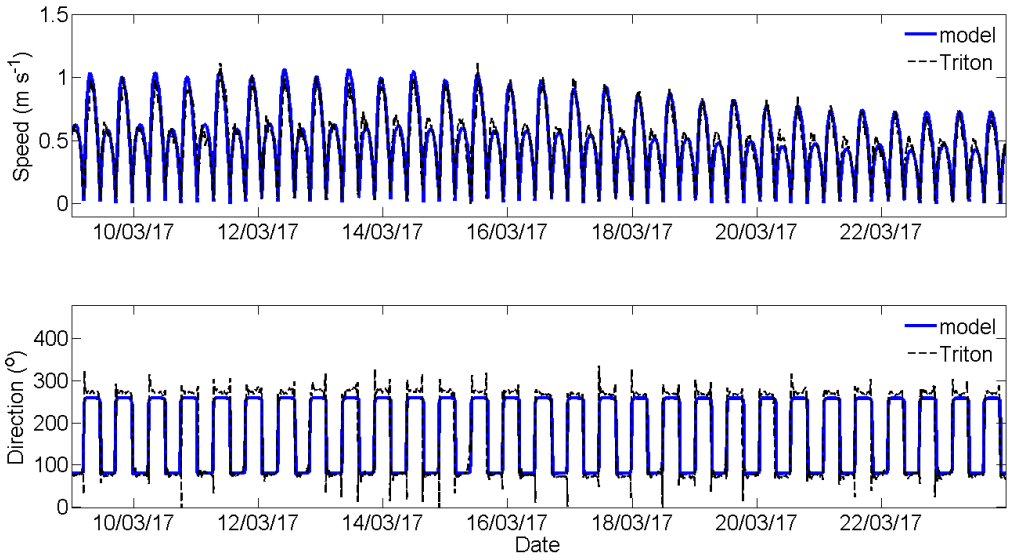

Figure D.1 Calibration plots of measured (black dashed line) and modelled (blue solid line) current speed (m/s) and direction (dir.) at the location of the Triton current meter.

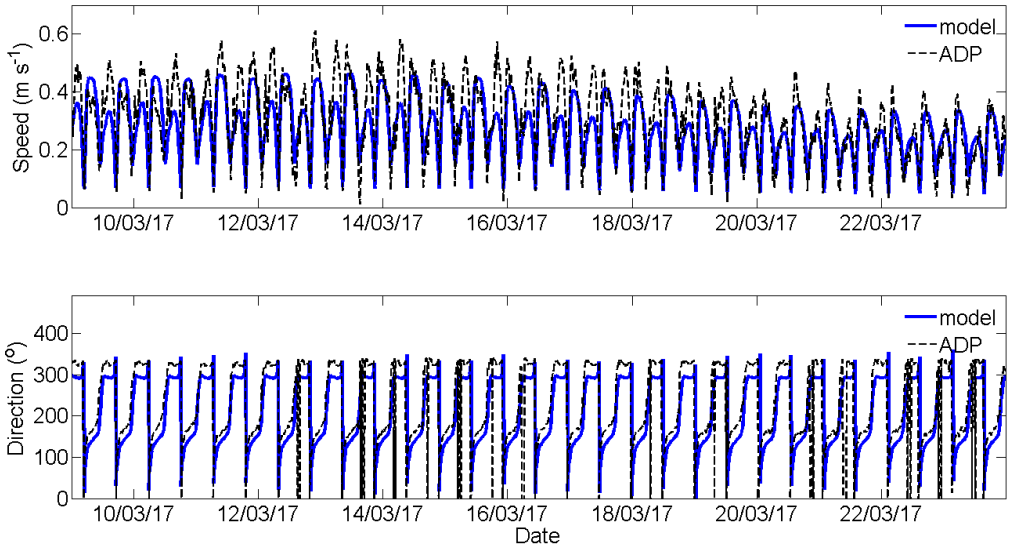

Figure D.2 Calibration plots of measured (black dashed line) and modelled (blue solid line) current speed (m/s) and direction (dir.) at the location of the ADP current meter.

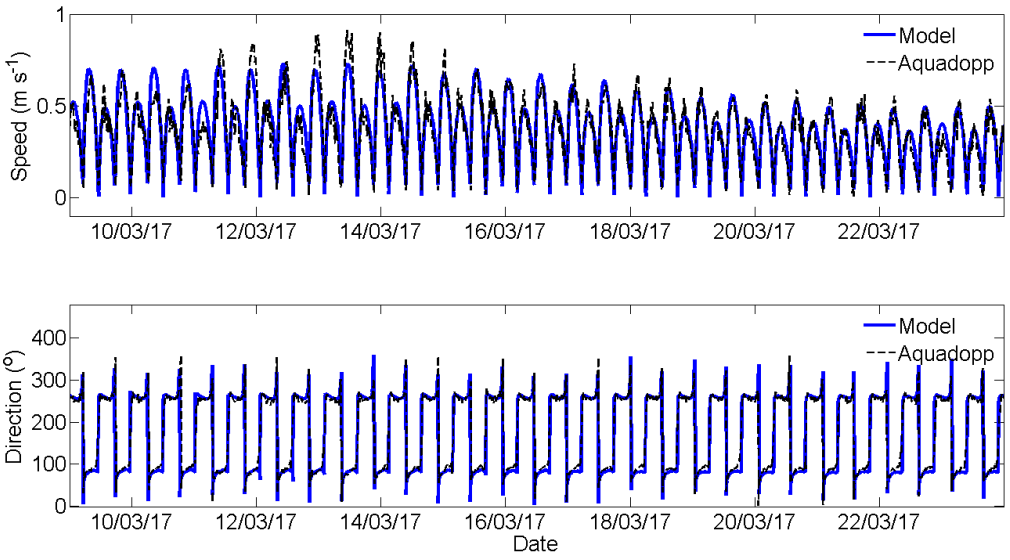

Figure D.3 Calibration plots of measured (black dashed line) and modelled (blue solid line) current speed (m/s) and direction (dir.) at the location of the Aquadopp current meter.

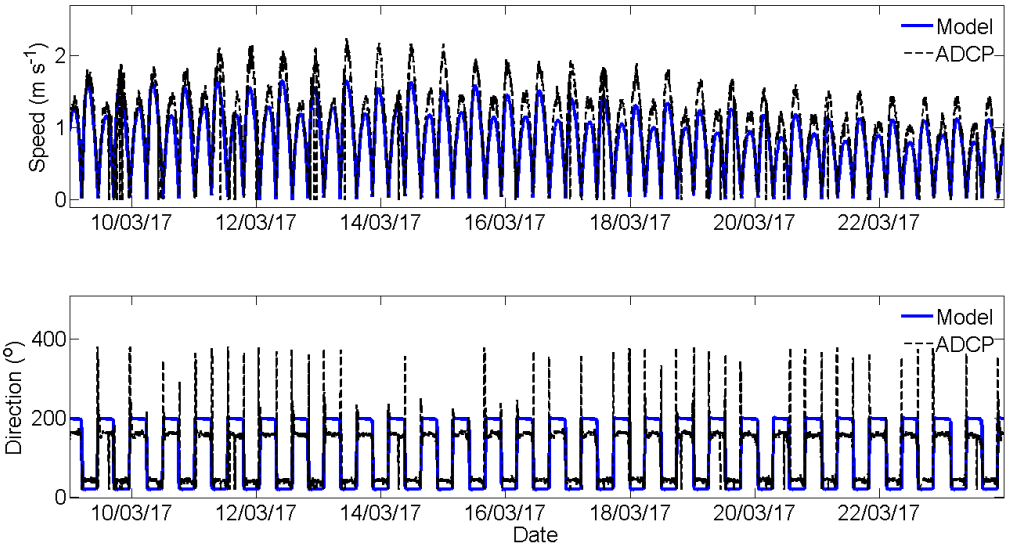

Figure D.4 Calibration plots of measured (black dashed line) and modelled (blue solid line) current speed (m/s) and direction (dir.) at the location of the ADCP current meter.

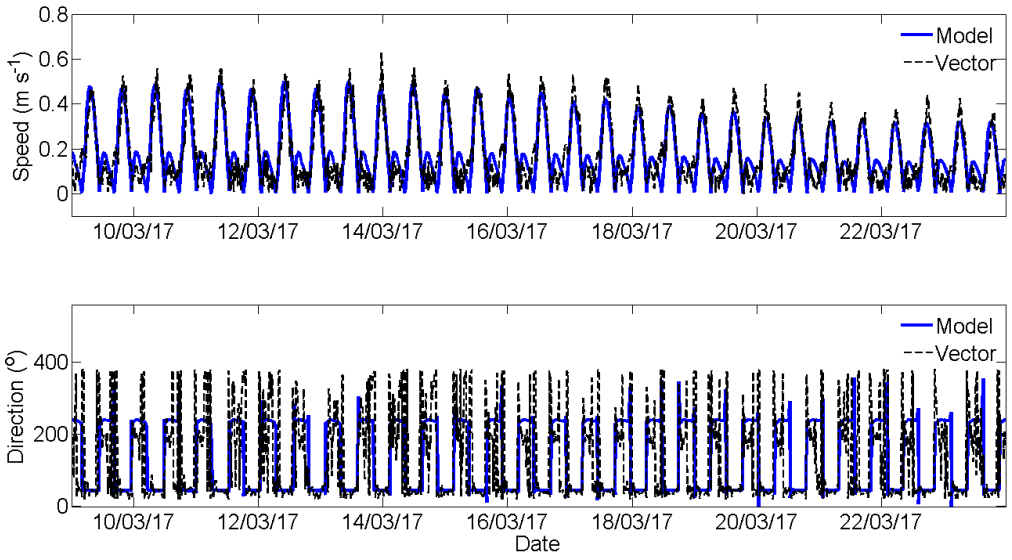

Figure D.5 Calibration plots of measured (black dashed line) and modelled (blue solid line) current speed (m/s) and direction (dir.) at the location of the Vectrino current meter.

Calibration plots – Water Level

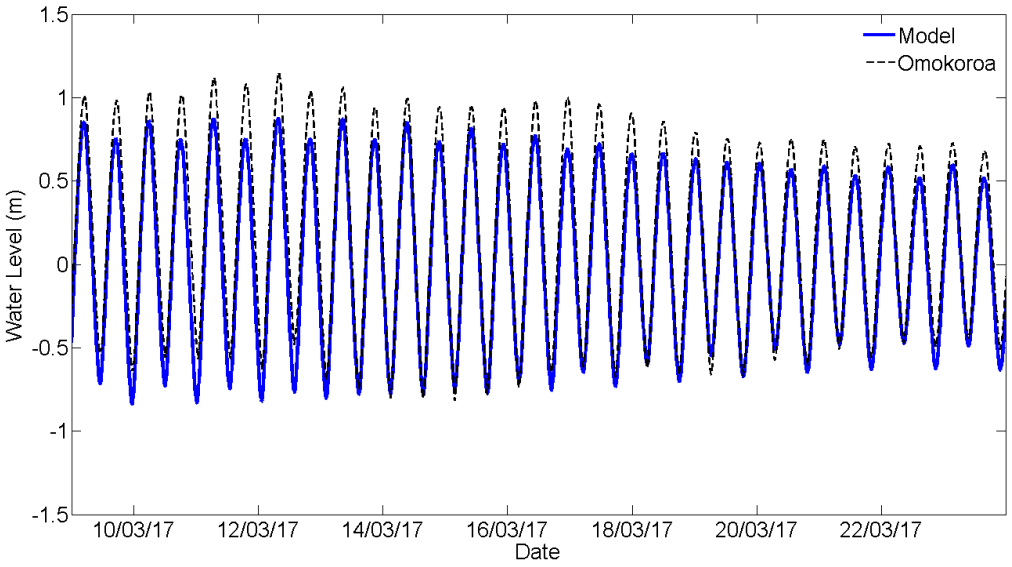

Figure D.6 Calibration plot of measured (black dashed line) and modelled (blue solid line) water level (m) at Omokoroa tide gauge.

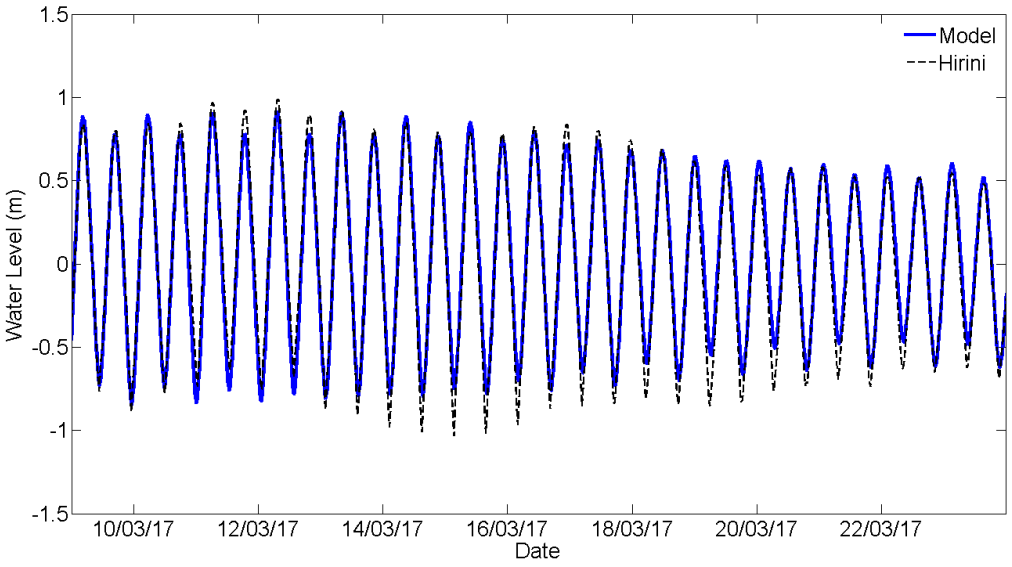

Figure D.7 Calibration plot of measured (black dashed line) and modelled (blue solid line) water level (m) at Hirini tide gauge.

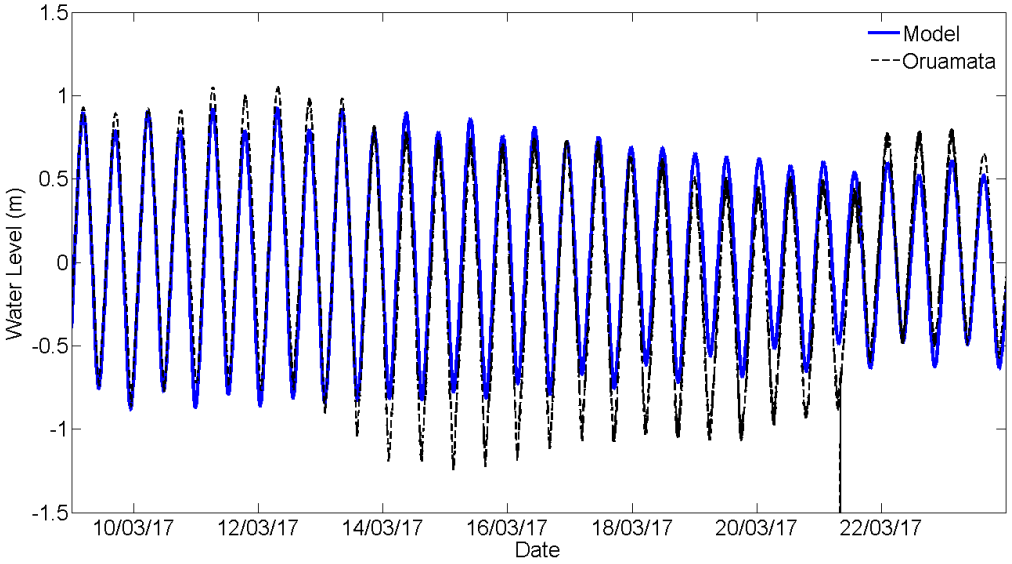

Figure D.8 Calibration plot of measured (black dashed line) and modelled (blue solid line) water level (m) at Oruamata tide gauge.

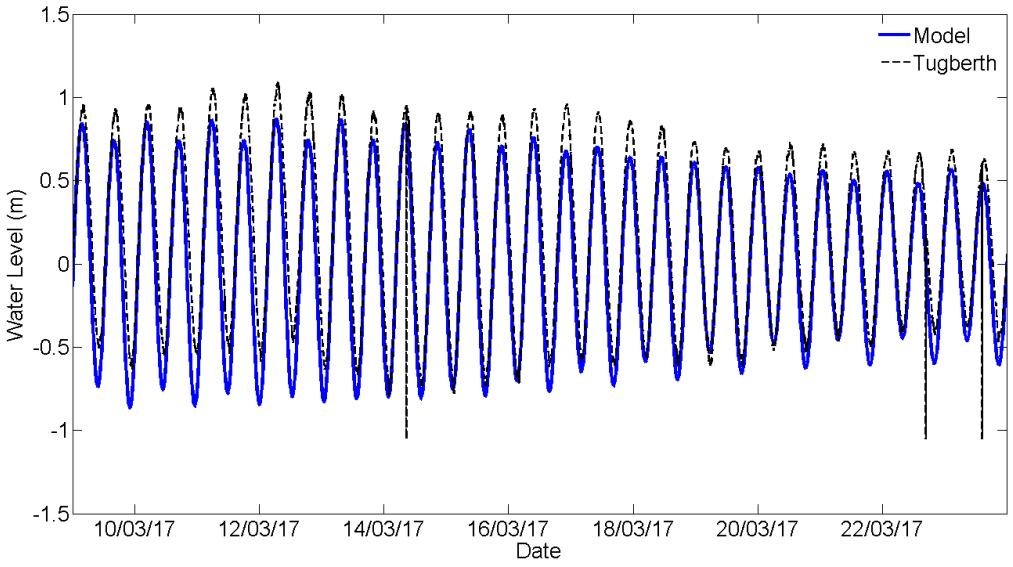

Figure D.9 Calibration plot of measured (black dashed line) and modelled (blue solid line) water level (m) at Tugberth tide gauge.

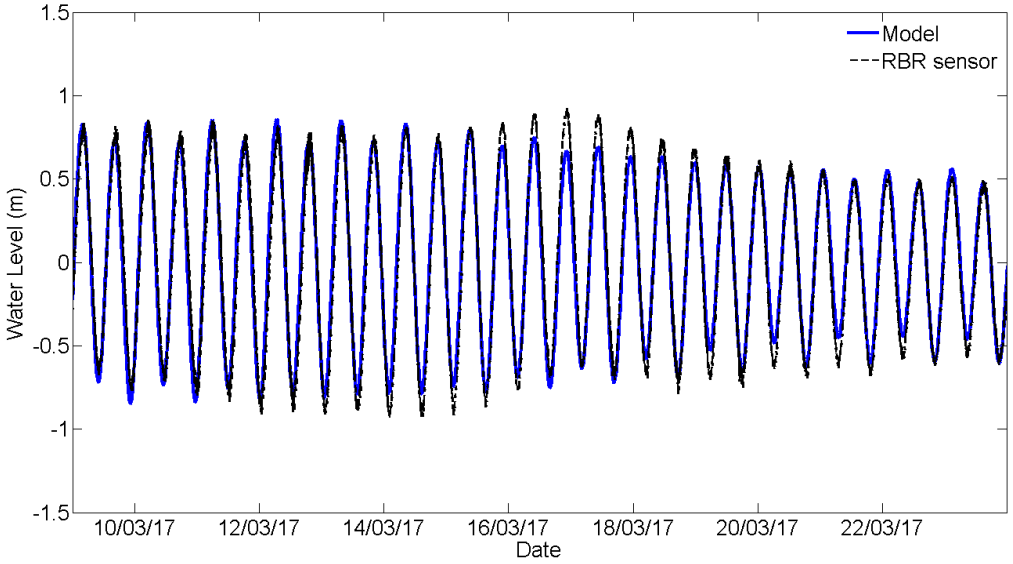

Figure D.10 Calibration plot of measured (black dashed line) and modelled (blue solid line) water level (m) at the location of the RBR deployment.

Validation plots - Currents

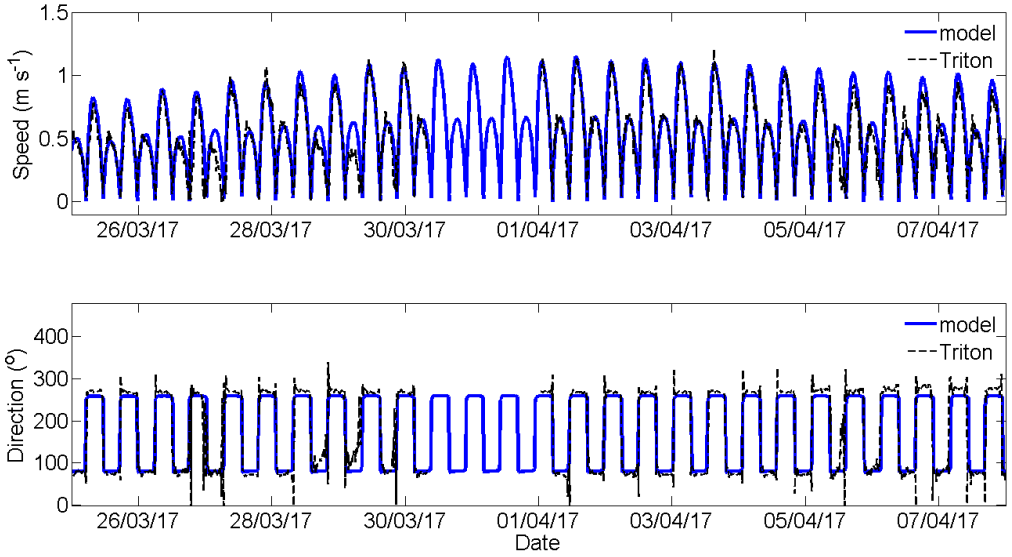

Figure D.11 Validation plots of measured (black dashed line) and modelled (blue solid line) current speed (m/s) and direction (dir.) at the location of the Triton current meter.

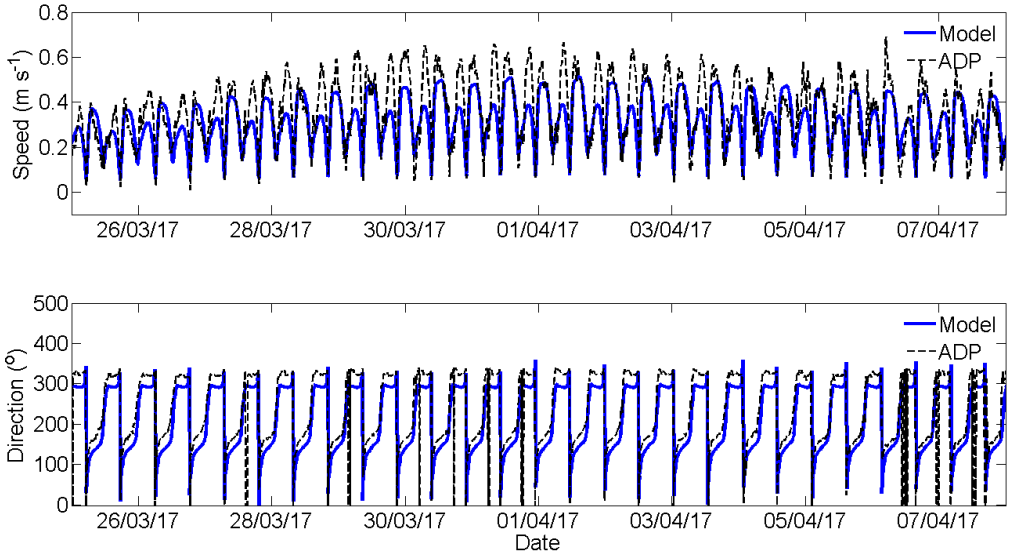

Figure D.12 Validation plots of measured (black dashed line) and modelled (blue solid line) current speed (m/s) and direction (dir.) at the location of the ADP current meter.

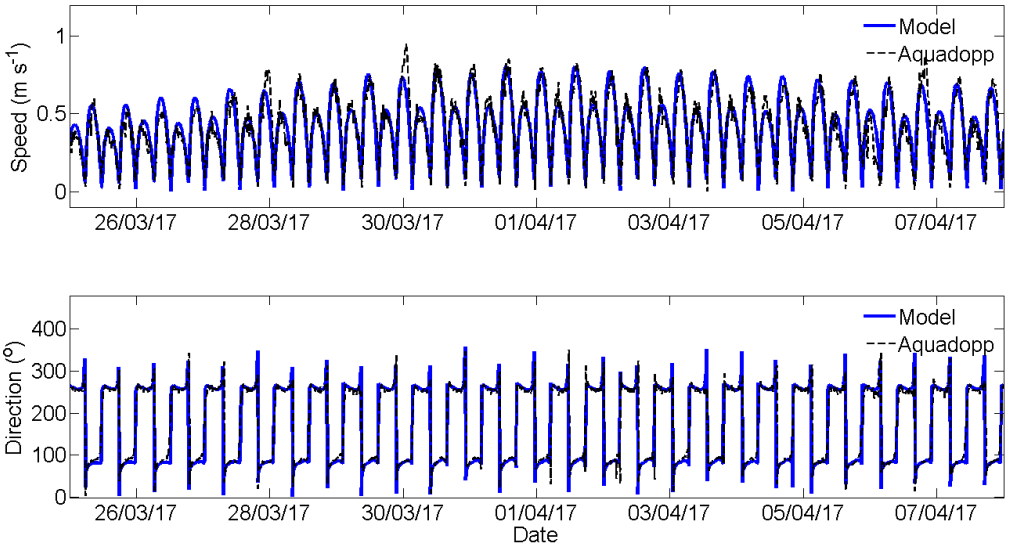

Figure D.13 Validation plots of measured (black dashed line) and modelled (blue solid line) current speed (m/s) and direction (dir.) at the location of the Aquadopp current meter.

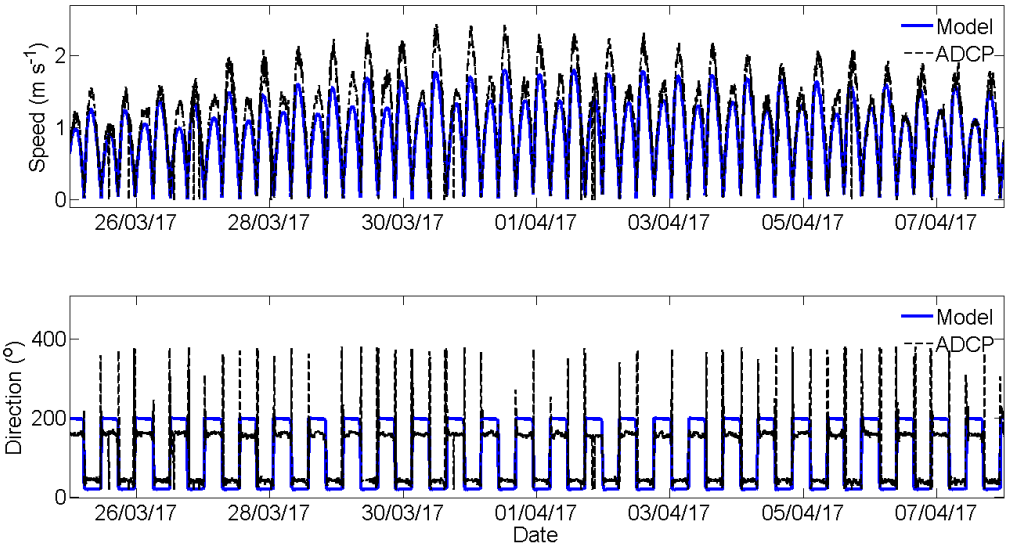

Figure D.14 Calibration plots of measured (black dashed line) and modelled (blue solid line) current speed (m/s) and direction (dir.) at the location of the ADCP current meter.

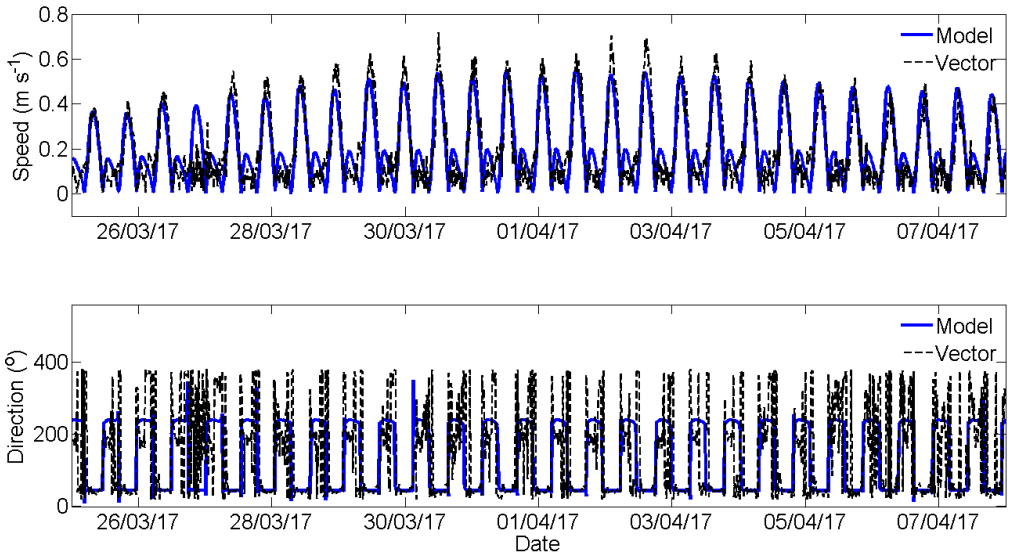

Figure D.15 Validation plots of measured (black dashed line) and modelled (blue solid line) current speed (m/s) and direction (dir.) at the location of the Vectrino current meter.

Validation plots – Water Level

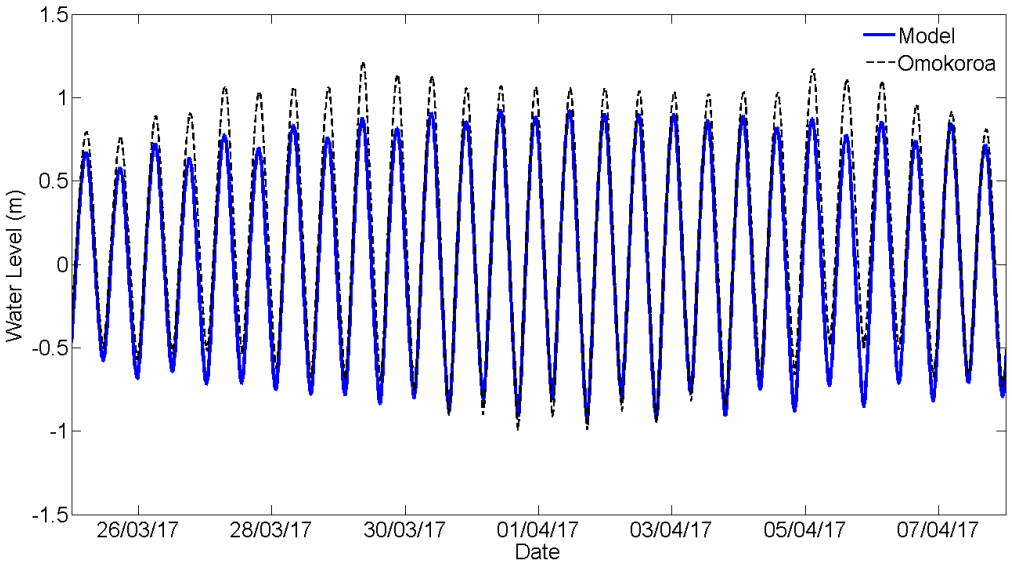

Figure D.16 Validation plot of measured (black dashed line) and modelled (blue solid line) water level (m) at Omokoroa tide gauge.

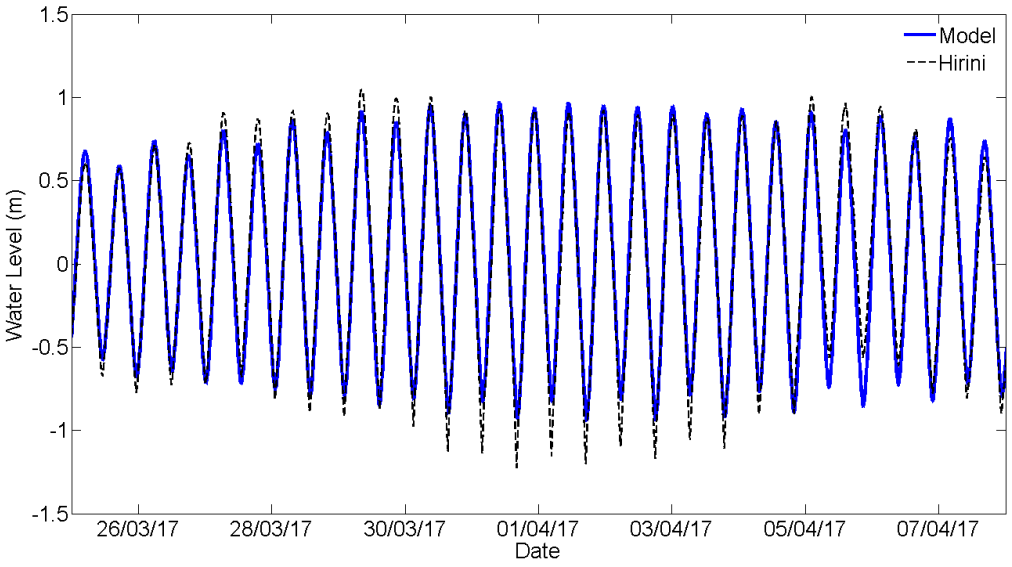

Figure D.17 Validation plot of measured (black dashed line) and modelled (blue solid line) water level (m) at Hirini tide gauge.

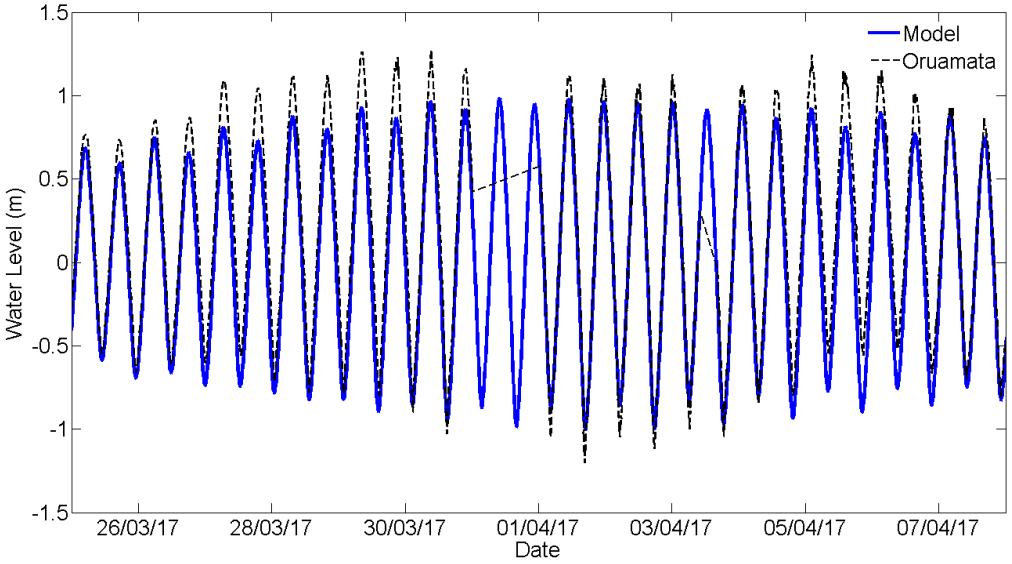

Figure D.18 Validation plot of measured (black dashed line) and modelled (blue solid line) water level (m) at Oruamata tide gauge.

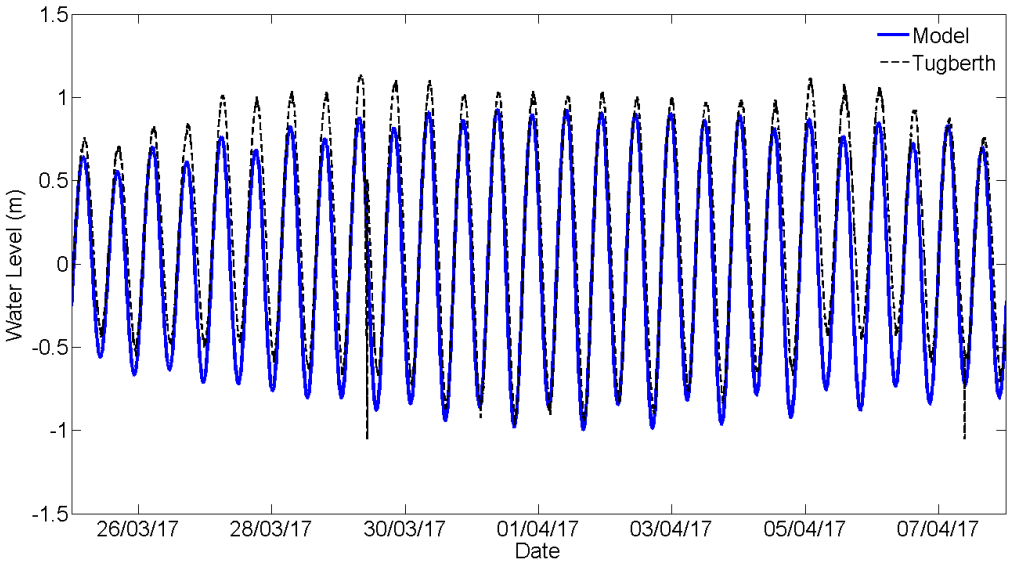

Figure D.19 Validation plot of measured (black dashed line) and modelled (blue solid line) water level (m) at Tugberth tide gauge.

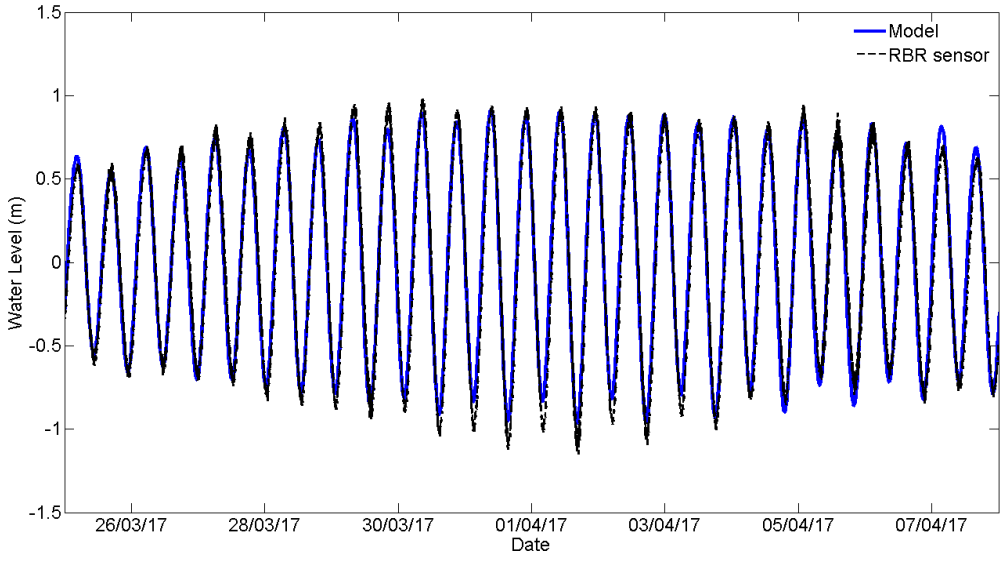

Figure D.20 Validation plot of measured (black dashed line) and modelled (blue solid line) water level (m) at the location of the RBR deployment.

REFERENCES

Abril, G., Borges, A.V., (2004). Carbon dioxide and methane emissions from estuaries. In: Tremblay, A., Varfalvy, L., Roehm, C., Garneau, M. (Eds.), Greenhouse Gases Emissions from Natural Environments and Hydroelectric Reservoirs: Fluxes and Processes. *Environmental science series*, 7, 187–207.

Allen, J. I., Somerfield, P. J., & Gilbert, F. J. (2007). Quantifying uncertainty in high-resolution coupled hydrodynamic-ecosystem models. *Journal of Marine Systems*, *64*(1-4), 3-14.

Anderson, D. M., Glibert, P. M., & Burkholder, J. M. (2002). Harmful algal blooms and eutrophication: nutrient sources, composition, and consequences. *Estuaries*, *25*(4), 704-726.

Bauer, J. E., Cai, W. J., Raymond, P. A., Bianchi, T. S., Hopkinson, C. S., & Regnier, P. A. (2013). The changing carbon cycle of the coastal ocean. *Nature*, *504*(7478), 61-70.

Beck, A. J., Kellum, A. A., Luek, J. L., & Cochran, M. A. (2016). Chemical flux associated with spatially and temporally variable submarine groundwater discharge, and chemical modification in the subterranean estuary at Gloucester Point, VA (USA). *Estuaries and coasts*, *39*(1), 1-12.

Beck, A.J., Rapaglia, J.P., Cochran, J.K. and Bokuniewicz, H.J., 2007. Radium mass-balance in Jamaica Bay, NY: Evidence for a substantial flux of submarine groundwater. *Marine Chemistry*, 106(3-4): 419-441.

Beck, A.J., Rapaglia, J.P., Cochran, J.K., Bokuniewicz, H.J. and Yang, S., 2008. Submarine groundwater discharge to Great South Bay, NY, estimated using Ra isotopes. *Marine Chemistry*, 109(3-4): 279-291.

Beck, A.J., Kellum, A.A., Luek, J.L. and Cochran, M.A., 2016. Chemical flux associated with spatially and temporally variable submarine groundwater discharge, and chemical modification in the subterranean Estuary at Gloucester Point, VA (USA). *Estuaries and Coasts*, 39(1), pp.1-12.

Beck, M. and Brumsack, H.J., 2012. Biogeochemical cycles in sediment and water column of the Wadden Sea: The example Spiekeroog Island in a regional context. *Ocean & coastal management*, 68, pp.102-113.

Beusen, A.H.W., Slomp, C.P. and Bouwman, A.F., 2013. Global land–ocean linkage: direct inputs of nitrogen to coastal waters via submarine groundwater discharge. *Environmental Research Letters*, 8(3), p.034035.

Burnett, W. C., Aggarwal, P. K., Aureli, A., Bokuniewicz, H., Cable, J. E., Charette, M. A., ... & Moore, W. S. (2006). Quantifying submarine groundwater discharge in the coastal zone via multiple methods. *Science of the total Environment*, *367*(2-3), 498-543.

Burnett, W. C., Bokuniewicz, H., Huettel, M., Moore, W. S., & Taniguchi, M. (2003). Groundwater and pore water inputs to the coastal zone. *Biogeochemistry*, *66*(1-2), 3-33.

Burnett, W. C., & Dulaiova, H. (2003). Estimating the dynamics of groundwater input into the coastal zone via continuous radon-222 measurements. Journal of Environmental Radioactivity, 69(1–2), 21-35.

Burnett, W.C. et al., 2006. Quantifying submarine groundwater discharge in the coastal zone via multiple methods. *Science of the Total Environment*, 367(2-3): 498-543.

Cai, W., McPhaden, M.J., Grimm, A.M. *et al.* Climate impacts of the El Niño–Southern Oscillation on South America. *Nat Rev Earth Environ* 1, 215–231 (2020).

Call, M., Maher, D. T., Santos, I. R., Ruiz-Halpern, S., Mangion, P., Sanders, C. J., ... & Eyre, B. D. (2015). Spatial and temporal variability of carbon dioxide and methane fluxes over semi-diurnal and spring–neap–spring timescales in a mangrove creek. *Geochimica et Cosmochimica Acta*, *150*, 211-225.

Call, M., Santos, I. R., Dittmar, T., de Rezende, C. E., Asp, N. E., & Maher, D. T. (2019). High pore-water derived CO2 and CH4 emissions from a macro-tidal mangrove creek in the Amazon region. *Geochimica et Cosmochimica Acta*, *247*, 106-120.

Charette, M. A., Buesseler, K. O., & Andrews, J. E. (2001). Utility of radium isotopes for evaluating the input and transport of groundwater-derived nitrogen to a Cape Cod estuary. *Limnology and Oceanography*, *46*(2), 465-470.

Charette, M. A., Buesseler, K. O., and Andrews, J. E.: Utility of radium isotopes for evaluating the input and transport of groundwater-derived nitrogen to a Cape Cod estuary, Limnol. Oceanogr., 46, 465–470, 2001

Charette, M. A., Henderson, P. B., Breier, C. F., & Liu, Q. (2013). Submarine groundwater discharge in a river-dominated Florida estuary. *Marine Chemistry*, *156*, 3-17.

Charette, M. A., W. S. Moore, and W. C. Burnett. "Uranium-and thorium-series nuclides as tracers of submarine groundwater discharge." *Radioactivity in the Environment* 13 (2008): 155-191.

Chiew, F. H., Piechota, T. C., Dracup, J. A., & McMahon, T. A. (1998). El Nino/Southern Oscillation and Australian rainfall, streamflow and drought: Links and potential for forecasting. *Journal of hydrology*, *204*(1-4), 138-149.

Childers, D. L., Boyer, J. N., Davis, S. E., Madden, C. J., Rudnick, D. T., & Sklar, F. H. (2006). Relating precipitation and water management to nutrient concentrations in the oligotrophic "upside-down" estuaries of the Florida Everglades. *Limnology and Oceanography*, *51*(1part2), 602-616.

Chislock, M. F., Doster, E., Zitomer, R. A., & Wilson, A. E. (2013). Eutrophication: causes, consequences, and controls in aquatic ecosystems. *Nature Education Knowledge*, *4*(4), 10.

Cho, H.M. and Kim, G., 2016. Determining groundwater Ra end-member values for the estimation of the magnitude of submarine groundwater discharge using Ra isotope tracers. *Geophysical Research Letters*, 43(8), pp.3865-3871.

Charette, M.A., Buesseler, K.O. and Andrews, J.E., 2001. Utility of radium isotopes for evaluating the input and transport of groundwater-derived nitrogen to a Cape Cod estuary. *Limnology and Oceanography*, 46(2): 465-470.

Charette, M.A. and Sholkovitz, E.R., 2002. Oxidative precipitation of groundwater-derived ferrous iron in the subterranean estuary of a coastal bay. *Geophysical Research Letters*, 29(10).

Charette, M.A., Moore, W.S. and Burnett, W.C., 2008. Uranium-and thorium-series nuclides as tracers of submarine groundwater discharge. *Radioactivity in the Environment*, 13, pp.155-191.

Charette, M.A., Henderson, P.B., Breier, C.F. and Liu, Q., 2013. Submarine groundwater discharge in a river-dominated Florida estuary. *Marine Chemistry*, 156(0): 3-17.

Cloern, J. E., Abreu, P. C., Carstensen, J., Chauvaud, L., Elmgren, R., Grall, J., ... & Xu, J. (2016). Human activities and climate variability drive fast-paced change across the world's estuarine–coastal ecosystems. Global Change Biology, 22(2), 513-529.

Conley, D. J., Kaas, H., Møhlenberg, F., Rasmussen, B., & Windolf, J. (2000). Characteristics of Danish estuaries. *Estuaries*, *23*(6), 820-837.

Corbett, D., Burnett, W., Cable, J.E. and Clark, S.B., 1998. A multiple approach to the determination of radon fluxes from sediments. *Journal of Radioanalytical and Nuclear Chemistry*, 236: 247-252.

Cucco, A., Umgiesser, G., Ferrarin, C., Perilli, A., Canu, D. M., & Solidoro, C. (2009). Eulerian and lagrangian transport time scales of a tidal active coastal basin. *Ecological Modelling*, *220*(7), 913-922.

Cussioli, M. C., Bryan, K. R., Pilditch, C. A., de Lange, W. P., & Bischof, K. (2019). Light penetration in a temperate meso-tidal lagoon: Implications for seagrass growth and dredging in Tauranga Harbour, New Zealand. Ocean & Coastal Management, 174, 25-37.

Cyronak, T.; Santos, I.R.; Erler, D.; Eyre, B.D. 2013. Groundwater and porewater as a major source of alkalinity to a fringing coral reef lagoon (Muri Lagoon, Cook Islands). *Biogeosciences*. 10(4):2467-2480.

Daly, C. J., Bryan, K.R., Gonzalez, M.R., Klein, A. H. F., Winter, C., (2014). Effect of selection and sequencing of representative wave conditions on process-based predictions of equilibrium embayed beach morphology. *Ocean Dynamics*. 64:863-877. DOI 10.1007/s10236-014-0730-9.

Davis, R. J. & Koop, K. 2006. Eutrophication in Australian rivers, reservoirs and estuaries – a southern hemisphere perspective on the science and its implications. Hydrobiologia, 559, 23-76.

de Weys, J., Santos, I.R. and Eyre, B.D. (2011) Linking groundwater discharge to severe estuarine acidification during a flood in a modified wetland. Environmental Science & Technology 45(8), 3310-3316.

Defne, Z., & Ganju, N. K. (2015). Quantifying the residence time and flushing characteristics of a shallow, back-barrier estuary: Application of hydrodynamic and particle tracking models. *Estuaries and Coasts*, *38*(5), 1719-1734.

Delhez, É. J., Deleersnijder, É., Mouchet, A., & Beckers, J. M. (2003). A note on the age of radioactive tracers. *Journal of marine systems*, *38*(3-4), 277-286.

Deltares. (2017) User Manual D-Water Quality (Version: 5.06), versatile water quality modelling in 1D, 2D or 3D systems including physical, (bio)chemical and biological processes. Deltares.

Deltares. (2018a). User Manual Delft3D-FLOW (Version: 3.15). Deltares.

Deser, C., Phillips, A. S., & Alexander, M. A. (2010). Twentieth century tropical sea surface temperature trends revisited. *Geophysical Research Letters*, *37*(10).

Devlin, M., Bricker, S. & Painting, S. (2011). Comparison of five methods for assessing impacts of nutrient enrichment using estuarine case studies. *Biogeochemistry.* 106, 177-205.

Dulaiova, H. and Burnett, W.C., 2008. Evaluation of the flushing rates of Apalachicola Bay, Florida via natural geochemical tracers. *Marine Chemistry*, 109(3-4): 395-408.

Dulaiova, H., Burnett, W. C., Wattayakorn, G., & Sojisuporn, P. (2006). Are groundwater inputs into river-dominated areas important? The Chao Phraya River—Gulf of Thailand. *Limnology and Oceanography*, *51*(5), 2232-2247.

Eller, K., Burnett, W., Fitzhugh, L. and Chanton, J., 2014. Radium sampling methods and residence times in St. Andrew Bay, Florida. *Estuaries and Coasts*, 37(1): 94-103.

Eyre, B., & Balls, P. (1999). A comparative study of nutrient behavior along the salinity gradient of tropical and temperate estuaries. *Estuaries*, *22*(2), 313-326.

Ferrarin, C., Rapaglia, J., Zaggia, L., Umgiesser, G., & Zuppi, G. M. (2008). Coincident application of a mass balance of radium and a hydrodynamic model for the seasonal quantification of groundwater flux into the Venice Lagoon, Italy. *Marine Chemistry*, *112*(3-4), 179-188.

Fong, C. R., & Fong, P. (2018). Nutrient fluctuations in marine systems: press versus pulse nutrient subsidies affect producer competition and diversity in estuaries and coral reefs. *Estuaries and coasts*, *41*(2), 421-429.

Fong, P., & Kennison, R. L. (2010). 10 Phase Shifts, Alternative Stable States, and the Status of Southern California Lagoons. *Coastal Lagoons: critical habitats of environmental change*, 227.

Ganju, N. K., Brush, M. J., Rashleigh, B., Aretxabaleta, A. L., Del Barrio, P., Grear, J. S., ... & Ralston, D. K. (2016). Progress and challenges in coupled hydrodynamic-ecological estuarine modeling. *Estuaries and Coasts*, *39*(2), 311-332.

Ganju, N. K., Jaffe, B. E., & Schoellhamer, D. H. (2011). Discontinuous hindcast simulations of estuarine bathymetric change: A case study from Suisun Bay, California. *Estuarine, Coastal and Shelf Science*, *93*(2), 142-150.

García-Alba, J., Bárcena, J. F., Ugarteburu, C., & García, A. (2019). Artificial neural networks as emulators of process-based models to analyse bathing water quality in estuaries. *Water research*, *150*, 283-295.

Garcia-Orellana, J., Rodellas, V., Tamborski, J., Diego-Feliu, M., van Beek, P., Weinstein, Y., ... & Scholten, J. (2021). Radium isotopes as submarine groundwater discharge (SGD) tracers: Review and recommendations. *Earth-Science Reviews*, 103681.

Garcia-Solsona, E., Garcia-Orellana, J., Masqué, P. and Dulaiova, H., 2008a. Uncertainties associated with 223Ra and 224Ra measurements in water via a Delayed Coincidence Counter (RaDeCC). *Marine Chemistry*, 109(3-4): 198-219.

Glantz, M. H., & Glantz, M. H. (2001). *Currents of change: impacts of El Niño and La Niña on climate and society*. Cambridge University Press.

Gleeson, J., Santos, I. R., Maher, D. T., & Golsby-Smith, L. (2013). Groundwater–surface water exchange in a mangrove tidal creek: Evidence from natural geochemical tracers and implications for nutrient budgets. Marine Chemistry, 156(0), 27-37.

Goldstein, E. B., Coco, G., & Plant, N. G. (2019). A review of machine learning applications to coastal sediment transport and morphodynamics. *Earth-science reviews*.

Gonneea, M.E., Morris, P.J., Dulaiova, H. and Charette, M.A., 2008. New perspectives on radium behavior within a subterranean estuary. *Marine Chemistry*, 109(3-4): 250-267.

González, F. U. T., Herrera-Silveira, J. A., & Aguirre-Macedo, M. L. (2008). Water quality variability and eutrophic trends in karstic tropical coastal lagoons of the Yucatán Peninsula. *Estuarine, Coastal and Shelf Science*, *76*(2), 418-430.

Gordon, N. D. (1986). The southern oscillation and New Zealand weather. *Monthly weather review*, *114*(2), 371-387.

Hall, D. R. (2013). Sensible Farming on Sensitive and Steep Land-A Catchment Management Approach in Tauranga Harbour. In Proceedings of the New Zealand Grassland Association (Vol. 75, pp. 33-38). New Zealand Grassland Association.

Hancock, N., Hume, T.M. and Swales, A., 2009. *Tauranga harbour sediment study: harbour bed sediments*. NIWA.

Heath, R. A. 1985 A review of the physical oceanography of the seas around New Zealand - 1982. *New Zealand Journal of Marine and Freshwater Research*, 19(1): 79-124.

Hougham, A. L., & Moran, S. B. (2007). Water mass ages of coastal ponds estimated using 223Ra and 224Ra as tracers. *Marine chemistry*, *105*(3-4), 194-207.

Howarth, R.W. and Marino, R., 2006. Nitrogen as the limiting nutrient for eutrophication in coastal marine ecosystems: evolving views over three decades. *Limnology and Oceanography*, 51(1part2), pp.364-376.

Hsieh, W. W., & Tang, B. (1998). Applying neural network models to prediction and data analysis in meteorology and oceanography. *Bulletin of the American Meteorological Society*, *79*(9), 1855-1870.

Hwang D. W., Lee Y. W. and Kim G., 2005. Large submarine groundwater discharge and benthic eutrophication in Bangdu Bay on volcanic Jeju Island, Korea. *Limnology and Oceanography,* 50, 1393–1403.

Hu C., Muller-Karger F. E. and Swarzenski P. W., 2006. Hurricanes, submarine groundwater discharge, and Florida's red tides. *Geophysical Research Letters*, 33, L11601.

IPCC, C. C. (2014). Mitigation of climate change. *Contribution of working group III to the fifth assessment report of the intergovernmental panel on climate change*.

Kim, G., & Hwang, D. W. (2002). Tidal pumping of groundwater into the coastal ocean revealed from submarine 222Rn and CH4 monitoring. *Geophysical Research Letters*, *29*(14), 23-1.

Kim, G., Lee, K.K., Park, K.S., Hwang, D.W. and Yang, H.S., 2003. Large submarine groundwater discharge (SGD) from a volcanic island. *Geophysical Research Letters*, 30(21).

Kim, G., Ryu, J.W., Yang, H.S., Yun, S.T., 2005. Submarine groundwater discharge (SGD) into the Yellow Sea revealed by Ra-228 and Ra-226 isotopes: implications for global silicate fluxes. *Earth Planet. Sci. Lett.* 237 (1–2), 156–166.

Kim, G., Ryu, J.W. and Hwang, D.W., 2008. Radium tracing of submarine groundwater discharge (SGD) and associated nutrient fluxes in a highly-permeable bed coastal zone, Korea. *Marine Chemistry*, 109(3), pp.307-317.

Kim, G., Kim, J.S. and Hwang, D.W., 2011. Submarine groundwater discharge from oceanic islands standing in oligotrophic oceans: Implications for global biological production and organic carbon fluxes. *Limnology and Oceanography*, 56(2), pp.673-682.

Kim, T.H., Kwon, E., Kim, I., Lee, S.A. and Kim, G., 2013. Dissolved organic matter in the subterranean estuary of a volcanic island, Jeju: Importance of dissolved organic nitrogen fluxes to the ocean. *Journal of Sea Research*, 78, pp.18-24.

Knee, K.L., Street, J.H., Grossman, E.E., Boehm, A.B. and Paytan, A., 2010. Nutrient inputs to the coastal ocean from submarine groundwater discharge in a groundwater-dominated system: relation to land use (Kona coast, Hawai'i, USA). *Limnology and Oceanography*, 55(3), p.1105.

Knee, K.L., Garcia-Solsona, E., Garcia-Orellana, J., Boehm, A.B. and Paytan, A., 2011. Using radium isotopes to characterize water ages and coastal mixing rates: A sensitivity analysis. *Limnology and Oceanography-Methods*, 9, pp.380-395.

Knee, K. and Paytan, A., 2011. 4.08 Submarine groundwater discharge: A source of nutrients, metals, and pollutants to the coastal ocean. *Treatise Estuar. Coast. Sci*, 4, pp.205-234.

Knee, K.L., Crook, E.D., Hench, J.L., Leichter, J.J. and Paytan, A., 2016. Assessment of Submarine Groundwater Discharge (SGD) as a Source of Dissolved Radium and Nutrients to Moorea (French Polynesia) Coastal Waters. *Estuaries and Coasts*, pp.1-18.

Kroeger, K.D., Swarzenski, P.W., Greenwood, W.J. and Reich, C., 2007. Submarine groundwater discharge to Tampa Bay: Nutrient fluxes and biogeochemistry of the coastal aquifer. *Marine Chemistry*, 104(1), pp.85-97.

Kwon, E.Y., Kim, G., Primeau, F., Moore, W.S., Cho, H.M., DeVries, T., Sarmiento, J.L., Charette, M.A. and Cho, Y.K., 2014. Global estimate of submarine groundwater discharge based on an observationally constrained radium isotope model. *Geophysical Research Letters*, 41(23), pp.8438-8444.

Lampman, G. G., Caraco, N. F., & Cole, J. J. (1999). Spatial and temporal patterns of nutrient concentration and export in the tidal Hudson River. *Estuaries*, *22*(2), 285-296.

Lehtiniemi, M., Engström-Öst, J., & Viitasalo, M. (2005). Turbidity decreases anti-predator behaviour in pike larvae, Esox lucius. *Environmental Biology of Fishes*, *73*(1), 1-8.

Lemagie, E. P., & Lerczak, J. A. (2015). A comparison of bulk estuarine turnover timescales to particle tracking timescales using a model of the Yaquina Bay Estuary. *Estuaries and coasts*, *38*(5), 1797-1814.

Liu, Q. et al., 2014. Effect of submarine groundwater discharge on the coastal ocean inorganic carbon cycle. *Limnology and Oceanography*, 59(5): 1529-1554.

Liu, Q., Dai, M., Chen, W., Huh, C. A., Wang, G., Li, Q., & Charette, M. A. (2012). How significant is submarine groundwater discharge and its associated dissolved inorganic carbon in a river-dominated shelf system? Biogeosciences, 9(5), 1777-1795.

Lorite-Herrera, M., Hiscock, K. and Jiménez-Espinosa, R., 2009. Distribution of dissolved inorganic and organic nitrogen in river water and groundwater in an agriculturally-dominated catchment, south-east Spain. *Water, Air, and Soil Pollution*, 198(1-4), pp.335-346.

Luek, J.L. and Beck, A.J., 2014. Radium budget of the York River estuary (VA, USA) dominated by submarine groundwater discharge with a seasonally variable groundwater end-member. *Marine Chemistry*, 165(0): 55-65.

Macklin, P. A., Santos, I. R., Maher, D. T., & Sanders, C. J. (2017). Mapping short-lived radium isotopes in estuarine residential canals (Gold Coast, Australia). Journal of Radioanalytical and Nuclear Chemistry, 313(2), 409-418.

McPhaden, M. J., Zebiak, S. E., & Glantz, M. H. (2006). ENSO as an integrating concept in earth science. *science*, *314*(5806), 1740-1745.

Michael, H.A., Charette, M.A. and Harvey, C.F., 2011. Patterns and variability of groundwater flow and radium activity at the coast: A case study from Waquoit Bay, Massachusetts. *Marine Chemistry*, 127(1–4): 100-114.

Michael, H. A., Mulligan, A. E., & Harvey, C. F. (2005). Seasonal oscillations in water exchange between aquifers and the coastal ocean. *Nature*, *436*(7054), 1145-1148.

Monsen, N.E., Cloern, J.E., Lucas, L.V. and Monismith, S.G., 2002. A comment on the use of flushing time, residence time, and age as transport time scales. *Limnology and Oceanography*, 47(5), pp.1545-1553.

Montaño, J., Coco, G., Antolínez, J. A., Beuzen, T., Bryan, K. R., Cagigal, L., ... & Idier, D. (2020). Blind testing of shoreline evolution models. *Scientific reports*, *10*(1), 1-10.

Moore, W. S. (1996). Using the radium quartet for evaluating groundwater input and water exchange in salt marshes. *Geochimica et Cosmochimica Acta*, *60*(23), 4645-4652.

Moore, W.S., 1996. Large groundwater inputs to coastal environments revealed by ^{226}Ra enrichments. *Nature*, 380: 612-614.

Moore, W. S. (1999). The subterranean estuary: a reaction zone of ground water and sea water. *Marine chemistry*, *65*(1-2), 111-125.

Moore, W.S., (2000)a. Ages of continental shelf waters determined from ^{223}Ra and ^{224}Ra. *Journal of Geophysical Research*, 105(C9): 117-122.

Moore, W. S. (2000)b. Determining coastal mixing rates using radium isotopes. *Continental Shelf Research*, *20*(15), 1993-2007.

Moore, W. S. (2006). Radium isotopes as tracers of submarine groundwater discharge in Sicily. *Continental Shelf Research*, *26*(7), 852-861.

Moore, W. S. (2006). The role of submarine groundwater discharge in coastal biogeochemistry. *Journal of Geochemical Exploration*, *88*(1-3), 389-393.

Moore, W.S., 2007. Seasonal distribution and flux of radium isotopes on the southeastern US continental shelf. *Journal of Geophysical Research: Oceans*, 112(C10).

Moore, W.S., 2010a. The effect of submarine groundwater discharge on the ocean. *Annual Review of Marine Science*, 2: 59-88.

Moore, W.S., 2010b. A reevaluation of submarine groundwater discharge along the southeastern coast of North America. *Global Biogeochemical Cycles*, 24(4): GB4005.

Moore, W.S. and Arnold, R., 1996. Measurement of ^{223}Ra and ^{224}Ra in coastal waters using a delayed coincidence counter. *Journal of Geophysical Research*, 101(C1): 1321-1329.

Moore, W. S., Beck, M., Riedel, T., Van Der Loeff, M. R., Dellwig, O., Shaw, T. J., .& Brumsack, H. J. (2011). Radium-based pore water fluxes of silica, alkalinity, manganese, DOC, and uranium: A decade of studies in the German Wadden Sea. *Geochimica et Cosmochimica Acta*, *75*(21), 6535-6555.

Moore, W.S., Blanton, J.O. and Joye, S.B., 2006. Estimates of flushing times, submarine groundwater discharge, and nutrient fluxes to Okatee Estuary, South Carolina. *Journal of Geophysical Research*, 111: C09006, doi:10.1029/2005JC003041.

Moore, W.S. and Reid, D.F., 1973. Extraction of radium from natural waters using manganese-impregnated acrylic fibers. *Journal of Geophysical Research*, 78: 8880-8886.

Moore, W.S. and Wilson, A.M., 2005. Advective flow through the upper continental shelf driven by storms, buoyancy, and submarine groundwater discharge. *Earth and Planetary Science Letters*, 235(3-4): 564-576.

Moosdorf, N., Stieglitz, T., Waska, H., Dürr, H.H. and Hartmann, J., 2015. Submarine groundwater discharge from tropical islands: a review. *Grundwasser*, 20(1), pp.53-67.

Mosley, M. P. (2000). Regional differences in the effects of El Niño and La Niña on low flows and floods. *Hydrological Sciences Journal*, *45*(2), 249-267.

Mullan, A. B. (1996). Non-linear effects of the Southern Oscillation in the New Zealand region. *Australian Meteorological Magazine*, *45*(2).

Mullan, A. B. (1998). Southern hemisphere sea-surface temperatures and their contemporary and lag association with New Zealand temperature and precipitation. *International Journal of Climatology: A Journal of the Royal Meteorological Society*, *18*(8), 817-840.

Nixon, S. W. (1995). Coastal marine eutrophication: A definition, social causes, and future concerns. *Ophelia,* 41, 199-219.

Olden, J. D., & Jackson, D. A. (2002). Illuminating the “black box”: a randomization approach for understanding variable contributions in artificial neural networks. *Ecological modelling*, *154*(1-2), 135-150.

Oliveira, J., Burnett, W. C., Mazzilli, B. P., Braga, E. S., Farias, L. A., Christoff, J., & Furtado, V. V. (2003). Reconnaissance of submarine groundwater discharge at Ubatuba coast, Brazil, using 222Rn as a natural tracer. *Journal of Environmental Radioactivity*, *69*(1-2), 37-52.

Paerl, H. W., Valdes, L. M., Peierls, B. L., Adolf, J. E., & Harding, L. J. W. (2006). Anthropogenic and climatic influences on the eutrophication of large estuarine ecosystems. *Limnology and Oceanography*, *51*(1part2), 448-462.

Park, S. 2004. *Aspects of mangrove distribution and abundance in Tauranga Harbour*. Report prepared by Stephen Park for Environment Bay of Plenty (Environmental Publication 2004/16).

Park, S.G., 2011. *Sea Lettuce and Nutrient Monitoring in Tauranga Harbour 1991-2010*. Report prepared for the Bay Plenty Regional Council (Environmental Publication 2011/05).

Pearl, H. W., Valdes, L. M. Peierls, B. L., Adolf, J. E. & Harding, L. W. (2006). Anthropogenic and climatic influences on the eutrophication of large estuarine ecosystems. *Limnol. Oceanogr.* 51 (1, part 2), 448-462.

Peterson, R.N. et al., 2008a. Radon and radium isotope assessment of submarine groundwater discharge in the Yellow River Delta, China. *Journal of Geophysical Research*, 113: C09021, doi:10.1029/2008JC004776.

Peterson, R.N., Burnett, W.C., Dimova, N. and Santos, I.R., 2009. Comparison of measurement methods for radium-226 on manganese-fiber. *Limnology and Oceanography: Methods*, 7: 196-205.

Peterson, R.N., Burnett, W.C., Glenn, C.R. and Johnson, A.G., 2009. Quantification of point-source groundwater discharges to the ocean from the shoreline of the Big Island, Hawaii. *Limnology and Oceanography*, 54(3), pp.890-904.

Peterson, R. N., Burnett, W. C., Taniguchi, M., Chen, J., Santos, I. R., & Ishitobi, T. (2008). Radon and radium isotope assessment of submarine groundwater discharge in the Yellow River delta, China. Journal of Geophysical Research: Oceans, 113(C9), C09021.

Peterson, R. N., Burnett, W. C., Taniguchi, M., Chen, J., Santos, I. R., & Misra, S. (2008). Determination of transport rates in the Yellow River–Bohai Sea mixing zone via natural geochemical tracers. *Continental Shelf Research*, *28*(19), 2700-2707.

Phlips, E. J., Badylak, S., Nelson, N. G., & Havens, K. E. (2020). Hurricanes, El Niño and harmful algal blooms in two sub-tropical Florida estuaries: Direct and indirect impacts. *Scientific reports*, *10*(1), 1-12.

Plant, N. G., Edwards, K. L., Kaihatu, J. M., Veeramony, J., Hsu, L., & Holland, K. T. (2009). The effect of bathymetric filtering on nearshore process model results. *Coastal Engineering*, *56*(4), 484-493.

Plew, D. R., Zeldis, J. R., Shankar, U., & Elliott, A. H. (2018). Using simple dilution models to predict New Zealand estuarine water quality. *Estuaries and coasts*, *41*(6), 1643-1659.

Povinec, P.P., Burnett, W.C., Beck, A., Bokuniewicz, H., Charette, M., Gonneea, M.E., Groening, M., Ishitobi, T., Kontar, E., Kwong, L.L.W. and Marie, D.E.P., 2012. Isotopic, geophysical and biogeochemical investigation of submarine groundwater discharge: IAEA-UNESCO intercomparison exercise at Mauritius Island. *Journal of Environmental Radioactivity*, 104, pp.24-45.

Power S, Haylock M, Colman R, Wang X, 2006. The Predictability of Interdecadal Changes in ENSO Activity and ENSO Teleconnections. *J. Climate*, 19, 4755–4771.

Ralston, D. K., Geyer, W. R., & Lerczak, J. A. (2010). Structure, variability, and salt flux in a strongly forced salt wedge estuary. *Journal of Geophysical Research: Oceans*, *115*(C6).

Ran, X., Bouwman, L., Yu, Z., Beusen, A., Chen, H., & Yao, Q. (2017). Nitrogen transport, transformation, and retention in the Three Gorges Reservoir: A mass balance approach. *Limnology and Oceanography*, *62*(5), 2323-2337.

Rapaglia, J., Ferrarin, C., Zaggia, L., Moore, W.S., Umgiesser, G., Garcia-Solsona, E., Garcia-Orellana, J. and Masqué, P., 2010. Investigation of residence time and groundwater flux in Venice Lagoon: comparing radium isotope and hydrodynamical models. *Journal of Environmental Radioactivity*, 101(7), pp.571-581.

Rasmussen, L. L. (2003). *Radium isotopes as tracers of coastal circulation pathways in the Mid-Atlantic Bight* (No. MIT/WHOI-2003-09). MASSACHUSETTS INST OF TECH CAMBRIDGE.

Reckhow, K. H. (1999). Water quality prediction and probability network models. *Canadian Journal of Fisheries and Aquatic Sciences*, *56*(7), 1150-1158.

Reichstein, M., Camps-Valls, G., Stevens, B., Jung, M., Denzler, J., & Carvalhais, N. (2019). Deep learning and process understanding for data-driven Earth system science. *Nature*, *566*(7743), 195-204.

Rodellas, V., Garcia-Orellana, J., Masqué, P., Feldman, M. and Weinstein, Y., 2015. Submarine groundwater discharge as a major source of nutrients to the Mediterranean Sea. *Proceedings of the National Academy of Sciences*, 112(13), pp.3926-3930.

Rodellas, V., Garcia-Orellana, J., Trezzi, G., Masqué, P., Stieglitz, T.C., Bokuniewicz, H., Cochran, J.K. and Berdalet, E., 2017. Using the radium quartet to quantify submarine groundwater discharge and porewater exchange. *Geochimica et Cosmochimica Acta*, 196, pp.58-73.

Romero, E., Garnier, J., Billen, G., Ramarson, A., Riou, P., & Le Gendre, R. (2019). Modeling the biogeochemical functioning of the Seine estuary and its coastal zone: Export, retention, and transformations. *Limnology and Oceanography*, *64*(3), 895-912.

Rosen, M.R. and White, P.A., 2001. Hydrochemistry of New Zealand's aquifers. *Groundwaters of New Zealand*, pp.77-110.

Roy A. Walters, Derek G. Goring & Rob G. Bell (2001) Ocean tides around New Zealand, New Zealand Journal of Marine and Freshwater Research, 35:3, 567-579, DOI: 10.1080/00288330.2001.9517023

Rueda, F., Moreno-Ostos, E., & Armengol, J. (2006). The residence time of river water in reservoirs. *Ecological Modelling*, *191*(2), 260-274.

Sadat-Noori, M., Santos, I. R., Tait, D. R., & Maher, D. T. (2016). Fresh meteoric versus recirculated saline groundwater nutrient inputs into a subtropical estuary. *Science of the total Environment*, *566*, 1440-1453.

Sadat-Noori, M., Santos, I.R., Tait, D.R., McMahon, A., Kadel, S. and Maher, D.T., 2016. Intermittently Closed and Open Lakes and/or Lagoons (ICOLLs) as groundwater-

dominated coastal systems: Evidence from seasonal radon observations. *Journal of Hydrology*, 535, pp.612-624.

Sadat-Noori, M., Santos, I. R., Tait, D. R., Reading, M. J., & Sanders, C. J. (2017). High porewater exchange in a mangrove-dominated estuary revealed from short-lived radium isotopes. *Journal of Hydrology*, *553*, 188-198.

Salinger, M. J., & Lefale, P. (2005). The occurrence and predictability of extreme events over the Southwest Pacific with particular reference to ENSO. In *Natural Disasters and Extreme Events in Agriculture* (pp. 39-49). Springer, Berlin, Heidelberg.

Salinger, M. J., & Mullan, A. B. (1999). New Zealand climate: temperature and precipitation variations and their links with atmospheric circulation 1930–1994. *International Journal of Climatology: A Journal of the Royal Meteorological Society*, *19*(10), 1049-1071.

Sandbach, S. D., Nicholas, A. P., Ashworth, P. J., Best, J. L., Keevil, C. E., Parsons, D. R., ... & Simpson, C. J. (2018). Hydrodynamic modelling of tidal-fluvial flows in a large river estuary. *Estuarine, Coastal and Shelf Science*, *212*, 176-188.

Sanford, L.P., Boicourt, W.C. and Rives, S.R., 1992. Model for estimating tidal flushing of small embayments. *Journal of Waterway, Port, Coastal, and Ocean Engineering*, 118(6), pp.635-654.

Santos, I. R., Burnett, W. C., Chanton, J., Dimova, N., & Peterson, R. N. (2009). Land or ocean?: Assessing the driving forces of submarine groundwater discharge at a coastal site in the Gulf of Mexico. *Journal of Geophysical Research: Oceans*, *114*(C4).

Santos, I.R., Burnett, W.C., Chanton, J., Mwashote, B., Suryaputra, I.G.N.A. and Dittmar, T., 2008. Nutrient biogeochemistry in a Gulf of Mexico subterranean estuary and groundwater-derived fluxes to the coastal ocean. *Limnology and Oceanography*, 53(2), p.705.

Santos, IR, Burnett, WC, Dittmar, T, Suryaputra, IGNA & Chanton, J 2009, 'Tidal pumping drives nutrient and dissolved organic matter dynamics in a Gulf of Mexico subterranean estuary', *Geochimica et Cosmochimica Acta*, vol. 73, no. 5, pp. 1325-1339.

Santos, I. R., Burnett, W. C., Misra, S., Suryaputra, I. G. N. A., Chanton, J. P., Dittmar, T., ... & Swarzenski, P. W. (2011). Uranium and barium cycling in a salt wedge subterranean estuary: the influence of tidal pumping. *Chemical Geology*, *287*(1-2), 114-123.

Santos, I.R.; Erler, D.; Tait, D.; Eyre, B.D. 2010. Breathing of a coral cay: Tracing tidally driven seawater recirculation in permeable coral reef sediments. *Journal of Geophysical Research*, 115: C12010.

Santos, I.R. and Eyre, B.D., 2011. Radon tracing of groundwater discharge into an Australian estuary surrounded by coastal acid sulphate soils. *Journal of Hydrology*, 396(3), pp.246-257.

Santos, I.R., Cook, P.L., Rogers, L., Weys, J.D. and Eyre, B.D., 2012. The "salt wedge pump": Convection-driven pore-water exchange as a source of dissolved organic and inorganic carbon and nitrogen to an estuary. *Limnology and Oceanography*, 57(5), pp.1415-1426.

Santos, I.R., de Weys, J., Tait, D.R. and Eyre, B.D., 2013. The contribution of groundwater discharge to nutrient exports from a coastal catchment: post-flood seepage increases estuarine N/P ratios. *Estuaries and Coasts*, 36(1), pp.56-73.

Santos, I.R., Bryan, K.R., Pilditch, C.A. and Tait, D.R., 2014. Influence of porewater exchange on nutrient dynamics in two New Zealand estuarine intertidal flats. *Marine Chemistry*, 167(0): 57-70.

Savage, C., Leavitt, P. R., & Elmgren, R. (2004). Distribution and retention of effluent nitrogen in surface sediments of a coastal bay. *Limnology and Oceanography*, *49*(5), 1503-1511.

Savage, C., Thrush, S. F., Lohrer, A. M., & Hewitt, J. E. (2012). Ecosystem services transcend boundaries: estuaries provide resource subsidies and influence functional diversity in coastal benthic communities. *PLoS One*, *7*(8).

Scavia, D., Field, J. C., Boesch, D. F., Buddemeier, R. W., Burkett, V., Cayan, D. R., ... & Reed, D. J. (2002). Climate change impacts on US coastal and marine ecosystems. *Estuaries*, *25*(2), 149-164.

Schindler, D. W. (2006). Recent advances in the understanding and management of eutrophication. *Limnology and oceanography*, *51*(1part2), 356-363.

Scully, M. E. (2016). Mixing of dissolved oxygen in Chesapeake Bay driven by the interaction between wind-driven circulation and estuarine bathymetry. *Journal of Geophysical Research: Oceans*, *121*(8), 5639-5654.

Seitzinger, S. P., Harrison, J. A., Dumont, E., Beusen, A. H., & Bouwman, A. F. (2005). Sources and delivery of carbon, nitrogen, and phosphorus to the coastal zone: An overview of Global Nutrient Export from Watersheds (NEWS) models and their application. *Global Biogeochemical Cycles*, *19*(4).

Sheldon, J. E., & Alber, M. (2002). A comparison of residence time calculations using simple compartment models of the Altamaha River Estuary, Georgia. *Estuaries*, *25*(6), 1304-1317.

Sheldon, J. E., & Burd, A. B. (2014). Alternating effects of climate drivers on Altamaha River discharge to coastal Georgia, USA. *Estuaries and coasts*, *37*(3), 772-788.

Slomp, C. P., & Van Cappellen, P. (2004). Nutrient inputs to the coastal ocean through submarine groundwater discharge: controls and potential impact. *Journal of Hydrology*, *295*(1-4), 64-86.

Smith, C.G. and Swarzenski, P.W., 2012. An investigation of submarine groundwater—borne nutrient fluxes to the west Florida shelf and recurrent harmful algal blooms. *Limnology and Oceanography*, 57(2), pp.471-485.

Smith, V. H., & Schindler, D. W. (2009). Eutrophication science: where do we go from here? *Trends in ecology & evolution*, *24*(4), 201-207.

Spiers, K. C., Healy, T. R., & Winter, C. (2009). Ebb-jet dynamics and transient eddy formation at Tauranga Harbour: implications for entrance channel shoaling. *Journal of coastal research*, 234-247.

Statham, P. J. (2012). Nutrients in estuaries—an overview and the potential impacts of climate change. *Science of the total environment*, *434*, 213-227.

Stewart, B. T., Bryan, K. R., Pilditch, C. A., & Santos, I. R. (2018). Submarine groundwater discharge estimates using radium isotopes and related nutrient inputs into Tauranga Harbour (New Zealand). *Estuaries and coasts*, *41*(2), 384-403.

Stewart, B.T., Santos, I.R., Tait, D.R., Macklin, P.A. and Maher, D.T., 2015. Submarine groundwater discharge and associated fluxes of alkalinity and dissolved carbon into Moreton Bay (Australia) estimated via radium isotopes. *Marine Chemistry*, 174, pp.112.

Stokes, D. J., Healy, T. R., & Cooke, P. J. (2010). Expansion dynamics of monospecific, temperate mangroves and sedimentation in two embayments of a barrier-enclosed lagoon, Tauranga Harbour, New Zealand. *Journal of Coastal Research*, 113-122.

Street, J.H., Knee, K.L., Grossman, E.E. and Paytan, A., 2008. Submarine groundwater discharge and nutrient addition to the coastal zone and coral reefs of leeward Hawai'i. *Marine Chemistry*, 109(3), pp.355-376.

Su, N., Burnett, W.C., MacIntyre, H.L., Liefer, J.D., Peterson, R.N. and Viso, R., 2014. Natural radon and radium isotopes for assessing groundwater discharge into Little Lagoon, AL: Implications for harmful algal blooms. *Estuaries and Coasts*, 37(4), pp.893-910.

Sutherland, J., Peet, A. H., & Soulsby, R. (2004). Evaluating the performance of morphological models. *Coastal engineering*, *51*(8-9), 917-939.

Swarzenski, P.W., 2007. U/Th series radionuclides as coastal groundwater tracers. *Chemical Reviews*, 107(2): 663-674.

Swarzenski, P.W., Reich, C., Kroeger, K.D. and Baskaran, M., 2007. Ra and Rn isotopes as natural tracers of submarine groundwater discharge in Tampa Bay, Florida. *Marine Chemistry*, 104(1), pp.69-84.

Taillardat, P., Willemsen, P., Marchand, C., Friess, D. A., Widory, D., Baudron, P., ... & Ziegler, A. D. (2018). Assessing the contribution of porewater discharge in carbon export and CO2 evasion in a mangrove tidal creek (Can Gio, Vietnam). *Journal of hydrology*, *563*, 303-318.

Tait, D.R., Santos, I.R., Erler, D.V., Befus, K.M., Cardenas, M.B. and Eyre, B.D., 2013. Estimating submarine groundwater discharge in a South Pacific coral reef lagoon using different radioisotope and geophysical approaches. *Marine Chemistry*, 156, pp.49-60.

Taniguchi, M. (2002). Tidal effects on submarine groundwater discharge into the ocean. *Geophysical Research Letters*, *29*(12), 2-1.

Taniguchi, M., Dulai, H., Burnett, K. M., Santos, I. R., Sugimoto, R., Stieglitz, T., ... & Burnett, W. (2019). Submarine Groundwater Discharge: Updates on its Measurement Techniques, Geophysical Drivers, Magnitudes and Effects. *Frontiers in Environmental Science*, *7*, 141.

Tay, H.W., Bryan, K.R., Pilditch, C.A., Park, S. and Hamilton, D.P., 2012. Variations in nutrient concentrations at different time scales in two shallow tidally dominated estuaries. *Marine and Freshwater Research*, 63(2), pp.95-109.

Tay, H.W., Bryan, K.R., de Lange, W.P. and Pilditch, C.A., 2013. The hydrodynamics of the southern basin of Tauranga Harbour. *New Zealand Journal of Marine and Freshwater Research*, 47(2), pp.249-274.

Thrush SF, Hewitt JE, Cummings VJ, Ellis JI, Hatton C, Lohrer, AM, Norkko A. 2004. Muddy waters: elevating sediment input to coastal and estuarine habitats. *Front Ecol Environ* 2:299–306.

Thrush, S. F., Coco, G., & Hewitt, J. E. (2008). Complex positive connections between functional groups are revealed by neural network analysis of ecological time series. *The American Naturalist*, *171*(5), 669-677.

Timmermann, A., An, S. I., Kug, J. S., Jin, F. F., Cai, W., Capotondi, A., ... & Stein, K. (2018). El Niño–southern oscillation complexity. *Nature*, *559*(7715), 535-545.

Tomasky-Holmes, G., Valiela, I. and Charette, M.A., 2013. Determination of water mass ages using radium isotopes as tracers: Implications for phytoplankton dynamics in estuaries. *Marine Chemistry*, 156, pp.18-26.

Maanen, B. V., Coco, G., Bryan, K. R., & Ruessink, B. G. (2010). The use of artificial neural networks to analyze and predict alongshore sediment transport. *Nonlinear Processes in Geophysics*, *17*(5), 395-404.

Vitousek, P. M., Aber, J. D., Howarth, R. W., Likens, G. E., Matson, P. A., Schindler, D. W., ... & Tilman, D. G. (1997). Human alteration of the global nitrogen cycle: sources and consequences. *Ecological applications*, *7*(3), 737-750.

Walters, R. A., Goring, D. G., & Bell, R. G. (2001). Ocean tides around New Zealand. *New Zealand Journal of Marine and Freshwater Research*, *35*(3), 567-579.

Wang, B., Wu, R., & Fu, X. (2000). Pacific–East Asian teleconnection: how does ENSO affect East Asian climate? *Journal of Climate*, *13*(9), 1517-1536.

Waska, H., Kim, S., Kim, G., Peterson, R.N. and Burnett, W.C., 2008. An efficient and simple method for measuring 226Ra using the scintillation cell in a delayed coincidence counting system (RaDeCC). *Journal of Environmental Radioactivity*, 99(12): 1859-1862.

Waska, H. and Kim, G., 2011. Submarine groundwater discharge (SGD) as a main nutrient source for benthic and water-column primary production in a large intertidal environment of the Yellow Sea. *Journal of Sea Research*, 65(1), pp.103-113.

Watson, H.M., 2016. Potential impacts of wharf extensions on the hydrodynamics of Stella Passage and upstream regions of Tauranga Harbour, New Zealand. MSc Thesis, University of Waikato.

White, P.A., 2005. *Future use of groundwater resources in the Bay of Plenty region*. Institute of Geological & Nuclear Sciences, Wairakei Research Centre.

White, P.A., Meilhac, C., Zemansky, G. and Kilgour, G., 2008. *Groundwater resource investigations of the Western Bay of Plenty area stage 1–conceptual geological and hydrological models and preliminary allocation assessment*. GNS Science consultancy report, 240, p.221.

Wilson, M., Meyers, S. D., & Luther, M. E. (2014). Synoptic volumetric variations and flushing of the Tampa Bay estuary. *Climate dynamics*, *42*(5-6), 1587-1594.

Yang, L. H., Bastow, J. L., Spence, K. O., & Wright, A. N. (2008). What can we learn from resource pulses. *Ecology*, *89*(3), 621-634.